General Disclaimer

One or more of the Following Statements may affect this Document

- This document has been reproduced from the best copy furnished by the organizational source. It is being released in the interest of making available as much information as possible.

- This document may contain data, which exceeds the sheet parameters. It was furnished in this condition by the organizational source and is the best copy available.

- This document may contain tone-on-tone or color graphs, charts and/or pictures, which have been reproduced in black and white.

- This document is paginated as submitted by the original source.

- Portions of this document are not fully legible due to the historical nature of some of the material. However, it is the best reproduction available from the original submission.
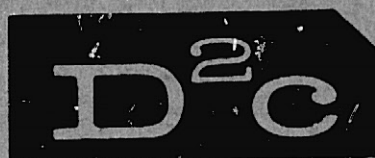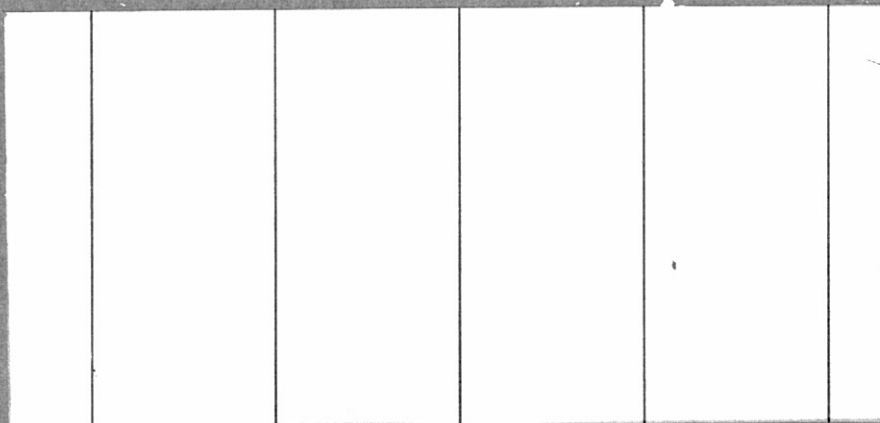
D²C

414 N. HALE   •   ESCONDIDO, CALIFORNIA 92025   •   (714) 741-0288

STUDY TO INVESTIGATE AND EVALUATE
MEANS OF OPTIMIZING THE RADAR FUNCTION
FOR THE SPACE SHUTTLE

For

NASA - Lyndon B. Johnson Space Center
Houston, Texas 77058

Prepared by
D^2C
414 North Hale Ave.
Escondido, CA 92025

Contract #NAS 9-14615

23 December, 1975

Glenn A. Walters
President, D^2C

1. Report No. 6	2. Government Accession No.	3. Recipient's Catalog No.

4. Title and Subtitle Interim report. "Optimize The Rendezvous Radar Function For The Space Shuttle	5. Report Date 23 December 75
	6. Performing Organization Code

7. Author(s)	8. Performing Organization Report No. #6

9. Performing Organization Name and Address	10. Work Unit No.
	11. Contract or Grant No. NAS9-14615

12. Sponsoring Agency Name and Address NASA-L.B.Johnson Space Center Houston, Texas 77058	13. Type of Report and Period Covered Final 5/16/75 to 12/15/75
	14. Sponsoring Agency Code

15. Supplementary Notes

16. Abstract This report summarizes the results of a study to define a radar and antenna system which best suits the space shuttle rendezvous requirements. The report treats antenna characteristics and antenna size trade-offs, fundamental sources of measurement errors inherent in the target itself, backscattering cross-section models of the target and three basic candidate radar types.

Antennas up to 1.5 meters in diameter can stow within specified installation constraints. A 1 meter diameter paraboloid and a folding, four slot backfeed on a two gimbal mount implemented for a spiral acquisition scan is recommended.

The candidate radar types discussed are (1) non-coherent pulse radar (2) coherent pulse radar and (3) pulse doppler radar with linear FM ranging. The radar type recommended is a pulse doppler with linear FM ranging.

17. Key Words (Suggested by Author(s)) Radar, Autotrack antenna, Measurement of Range, Range Rate, Angle and Angle Rate.	18. Distribution Statement

19. Security Classif. (of this report) Unclassified	20. Security Classif. (of this page) Unclassified	21. No. of Pages 315	22. Price*

*For sale by the National Technical Information Service, Springfield, Virginia 22151

JSC Form 1424 (rev. July 74)

NASA — JSC

Figure 2. Technical Report Standard Title Page

INTRODUCTION.

This is the final report of a study for "Optimizing
The Rendezvous Radar Function For The Space Shuttle";
Contract No. NAS 9-14615 for NASA, Lyndon B. Johnson Space
Center. The program has been expanded and will continue to
"Study To Investigate And Evaluate Means Of Integrating And
Optimizing The Combined Radar/Communication Function". This
final report, Volume I, summarizes the study efforts related
to optimizing the radar function. It is the sixth report
submitted during the contractural period and includes data
which otherwise would have been submitted as Progress Report
#6. Continuing efforts will be primarily directed towards
the integration and optimizing of the communication function.
A second final report, Volume II, will be submitted at the
end of the continuing study.

INDEX

FIGURE INDEX

FIGURE INDEX (continued)

TABLE INDEX

1.0 OBJECTIVE.

The objectives of the study to "Optimize the Rendezvous Radar Function for the Space Shuttle" were to perform conceptual design, performance analysis and trade-off studies leading to recommendation of a radar system which best suits the space shuttle rendezvous requirements.

Specific objectives of the study included:

- Preparation of detail block diagrams of candidate radar systems and a discussion of each.

- An evaluation of antenna types, angle tracking methods, scan program and allowable antenna size.

- An evaluation and ranking of candidate radar and antenna systems.

- A complete description including size, weight and power of the recommended system.

- Preparation of a recommended portion of the procurement specification pertaining to radar performance, including target model.

2.0 SUMMARY.

The study treated antenna characteristics and antenna size trade-offs, fundamental sources of measurement errors inherent to targets of interest, the backscattering cross-section model of the target and three basic candidate radar systems before recommending a total system.

The antenna study determined the maximum antenna aperture compatible with system constraints such as the physical dimensions of the stow installation, servo power demand and data rate requirements.

While reflectors of up to 1.5 meters in diameter can be stowed within the constraints of the shuttle installation, a 1 meter aperture was chosen from a standpoint of operational accuracy, reasonableness of servo power requirements and simplicity of installation.

Various radiation systems were considered such as the Cassegrain, reflector and feed, flat plate array, etc. A paraboloid fed with a folding backfeed provides optimum patterns, best mechanical packaging and design simplicity.

The most demanding operational function of the radar antenna is acquisition scan in the non-cooperative mode. Various scanning techniques were considered. It was found a spiral scan mechanization is optimum. Its geometry matches the geometrical requirements of a vector search. Furthermore the probability of early detection is enhanced.

The sources of error caused by scattering properties of the target itself and which are indistinguishable from the true target state by the radar include:

- Angular Scintillation (Glint)
- Range Scintillation
- Doppler (Velocity) Scintillation.

It was found that both angular scintillation and range scintillation can be an appreciable fraction of the target dimension. These effects can be significantly reduced, however, by the use of frequency agility. The doppler scintillation was found to be very small, less than 0.2 meters/sec for the class of targets considered.

The radar backscattering cross-section model of the target was taken at a mean of 1 square meter with Swerling Class 1 fluctuation characteristics. For purposes of computing the dynamic signal range the maximum target cross-section was taken at 100 square meters. Using the target/orbiter geometry of Mission 3-B the decorrelation time of the signal return from the target was estimated to be less than 10 seconds for target elements spaced 2 meters apart.

Three basic types of radars were analyzed:

- Non-coherent Pulse Radar
- Coherent Pulse Radar
- Pulse Doppler Radar With Linear FM Ranging.

A pulse doppler radar was recommended as a result of analysis and evaluation conducted.

The functional requirements for the radar used in this study and as defined by JSC are given in Table 2-1 and 2-2.

A comparison of system characteristics of the three radar types listed above are given in Table 2-3. A comparison

of measurement accuracy of the three radar types is given in Table 2-4 for the skin track mode and in Table 2-5 for the long range cooperative mode.

A summary of performance, system and physical characteristics of the recommended system is given in Table 2-6.

Since the range measurement accuracy involves several parameters a plot of random error was made as shown in Figure 2-1. Also shown on the figure is a specified accuracy 1% or 30 meters, 3σ at ranges between 30 meters and 19 km. The predicted area is well below that specified.

The discontinuity in the ranging error at 2 km range is due to changing the ranging scale factor from 10 Hz/meter to 1 Hz/meter at that point. It appears more favorable to operate at the higher scale factor for ranges less than 4 km as indicated on the figure.

TABLE 2-1

FUNCTIONAL REQUIREMENTS

The rendezvous radar shall provide range, range rate, angle, and angle
rate relative to passive or cooperative target for navigation during
the terminal phase of rendezvous. This information shall be supplied
to the G&N system and to the crew displays.

Nominally, star sensor tracking of the target will provide navigation
data for the last phasing, the coelliptic, and the TPI maneuvers. The
rendezvous radar shall have a beacon mode of operation capable of sup-
porting the above maneuvers. Performance requirements for the rendezvous
radar are described in the following paragraphs.

A. Parameter Measurements Limits

    1. Range*   19KM to 30M
    2. Range Rate $\pm$ 91 M/sec
    3. LOS Angle $\pm$ 40°
    4. LOS Angle Rate

        (a) acquisition   +4MR/sec
        (b) tracking $\pm$5deg/sec

*Data to be available at a range of 19 KM with a probability of detection
of .99 with a false alarm probability of 10^{-8}.

B. Parameter Measurements Accuracies (3 sigma)

Parameter	Random Error	Bias Error
Range		
R > 9 KM	91M	24M
R < 9KM	Greater of 0.01 R or 30 M	24M
Range Rate	0.3 M/sec	0.3 M/Sec
Angle	10 MR	< 3 degrees
Angle Rate	0.14 MR/sec	0.14 MR/sec

C. Data Acquisition and Convergence Time

    1. The maximum acquisition time after the radar has been designated
to the expected target direction shall be one minute.

    2. Range rate shall achieve the required accuracy within one minute
of radar acquisition and shall maintain that accuracy to a range of 30
meters. If range data is lost (after initial acquisition), the convergence
time for the range rate data after range reacquisition shall be no
greater than 10 seconds. During RCS braking, the radar range rate
shall not lag the true range rate by more than 2 seconds.

TABLE 2-1 (continued)

2

D. Target Definition

1. The target to be used configuration for items A, B and C shall have an average radar cross section of one square meter. (Swerling Case I). Frequency agility may be used to improve the detection capability of the radar.

TABLE 2-2   (Received 16 September 1975)

RENDEZVOUS RADAR REQUIREMENTS

PARAMETER	LIMITS	ACCURACIES (3 SIGMA)	
		RANDOM	BIAS
RANGE			
PASSIVE	19 KM TO 30 M	1% OR 3 OM	24 M
COOPERATIVE	560 KM TO 30 M		
RANGE RATE			
PASSIVE	-38 M/SEC + 7.5 M/SEC	0.3 M/SEC	0.3 M/SEC
COOPERATIVE	±91 M/SEC		
LOS ANGLE			
BOTH	± 40 DEG FUNCTION OF RANGE	10 MR	60 MR
LOS ANGLE RATE			
BOTH			
ACQUISITION	± 4 MR/SEC	0.14 MR/SEC	0.14 MR/SEC
TRACKING	± 5 DEG/SEC		

TABLE 2-3 SYSTEM CHARACTERISTICS OF CANDIDATE RADARS.

System	Method of range meas.	Method of Vel. Meas.	PRF	Pulsewidth	Freq. Agility	Transmitted power			
						Average, watts		Peak, watts	
						1m ant	0.5m ant	1m ant	0.5m ant
Noncoherent pulse	Time delay	Range Differencing	R<20km 3.7kHz	1.0&0.1μsec	None	25	166	6.8kw	45kw
			R>20km 214Hz		375mHz	5.4	33	1.5kw	8.9kw
Coherent pulse	Time delay	Doppler	R<20km 4.8kHz	1.0&0.1μsec	None	30	190	8.1kw	40kw
			R>20km 214Hz		375mHz	6	38	1.3kw	7.9kw
Pulse doppler	Linear FM	Doppler	4.8kHz& 25kHz dithered	104μsec and 20μsec	None	19	72	38	144
					375mHz	5	31	10	62

Notes:
1. Acquisition complete by time range closes to 19km for skin track.
2. Angular search region for skin track, 40° half angle cone.
3. Acquisition time 1 minute for probability of detection of 0.99.
4. For non-frequency agile case 2 angle scan frames/minute; frequency agile case 1 angle scan frame per minute.
5. Transmitted powers listed include 2 dB margin.

TABLE 2-4 MEASUREMENT ACCURACY OF CANDIDATE RADARS FOR SKIN TRACK MODE, 3σ

System	Range, meters		Velocity, m/sec		Angle, mRad		Angle rate, mRad/sec	
	Bias^2	Random	Bias^2	Random	Bias	Random	Bias	Random
Noncoherent pulse	—	$\dfrac{R\le 9km}{\sqrt{(.0003R)^2+(5.1)^2}}$ $\dfrac{R>9km}{\sqrt{(.0003R)^2+(25.2)^2}}$	—	$0.3\,(SNR>13dB)$	0.24	0.6	0.09	8.1
Coherent pulse	—	$\dfrac{R\le 9km}{\sqrt{(.0003R)^2+(5.1)^2}}$ $\dfrac{R>9km}{\sqrt{(.0003R)^2+(25.2)^2}}$	—	$\sqrt{(0.03)^2+(.006V)^2}$	0.24	0.6	0.09	8.1
Pulse doppler	—	$\dfrac{R\le 2km}{\sqrt{(.005R)^2+(.57)^2+(.085V)^2}}$ $\dfrac{R>2km}{\sqrt{(.005R)^2+(5.7)^2+(.85V)^2}}$	—	$\sqrt{(0.03)^2+(.006V)^2}$	0.24	0.6	0.09	8.1

Notes:

1. All values based on antenna size of 1 meter and use of frequency agility.
2. The large random angle rate error is principally due to glint assuming an 18 meter target.
3. Bias errors will occur in the form of data lag but it is assumed these can be removed by computation if required.
4. Angle accuracy does not include mechanical indexing error.

2.7

TABLE 2-5 MEASUREMENT ACCURACY OF CANDIDATE RADARS IN COOPERATIVE MODE
(R>20km), 3σ

System	Range, meters		Velocity, m/sec		Angle, mRad		Angle rate mRad/sec	
	Bias	Random	Bias	Random	Bias	Random	Bias	Random
Noncoherent pulse	–	30	–	0.23	0.24	0.34 (560km)	0.09	7.2(560km)
						0.01 (20km)		0.3(20km)
Coherent pulse	–	30	0.2	0.1	0.24	0.34 (560km)	0.09	7.2(560km)
						0.01 (20km)		0.3(20km)
Pulse doppler	–	$\sqrt{(.005R)^2+(68)^2}$ (560km)	0.2	0.1	0.24	0.17 (560km)	0.09	2.0(560km)
		$\sqrt{(.005R)^2+(21)^2}$ (20km)				0.01 (20km)		0.07(20km

Notes:

1. Bias errors will occur in the form of data lag but it is assumed these can be removed by computation if required.
2. Angle accuracy does not include mechanical indexing error.

PERFORMANCE CHARACTERISTICS

	Cooperative mode	Skin track mode
Operating range	560km to 30 m	19km to 30m
Target model	Transponder	$1m^2$ Swerling 1
Acquisition time	300 seconds	60 seconds
Probability of acquisition	0.99	0.99
False alarm time During acquisition)	10 minutes	10 minutes
Angular search sector	5° cone (half angle)	40° cone (half angle)
Relative velocity	±91 m/sec	−38,+7.5m/sec

Accuracy, 3σ

	Bias	Random		Bias	Random
Velocity, m/sec.	0.2	0.1m/sec		0	$(.03)^2+(.006V)^2$
Range, meters					
R≤2km	0	$(.005R)^2+(.57)^2$		0	$(.005R)^2+(.57)^2+(.085V)^2$
2km<R<20km	0	$(.005R)^2+(5.7)^2$		0	$(.005R)^2+(5.7)^2+(.85V)^2$
20km<R<560km	0	$(.005R)^2+(68)^2$			

	Bias	Random			Bias	Random
Angle, mr.	0.24	0.17	R=560km		0.24	0.6
		0.01	R=20km			
Angle rate, mr/sec	0.09	2.0	R=560km		0.09	8.1*
		0.07	R=20km			

*Principally due to glint.

TABLE 2-6 (Page 2 of 5 pages.)

S Y S T E M   C H A R A C T E R I S T I C S

	Cooperative Mode	Skin Track Mode
Carrier Frequency	15 GHz	15 GHz
Antenna		
Size	1 meter	1 meter
Beam width (2 way)	1.0 degrees	1.0 degrees
Gain	40.6 dB	40.6 dB
Scan program	Spiral, 10° cone	Spiral, 80° cone
Scan frame time	1 minute	1 minute
Max search rate		110 deg/sec
Max tracking rate	5 deg/sec	5 deg/sec
Transmitter		
PRF	20 to 30 (Dithered)	4.8 for acquisiti[on] 20 to 30 Dithered for track
Pulse width	25 to 17 n sec	
Duty cycle	50%	50%
Peak power	8.9 watts	8.9 watts
Average power	4.5 watts	4.5 watts
Frequency Agility Program		
Acquisition	none	6 frequencies 75 mHz. apart. dwell 1.5 m sec
Tracking	none	6 frequencies 75 mHz. apart. dwell 13 m sec
Frequency Modulation Program		
Deviation		
R< 2 km	20 mHz.	20 mHz.
R> 2 km	2 mHz.	2 mHz.
Time of Linear Sweep		
R< 20 km	13.3 m sec	13.3 m sec
R> 20 km	67 m sec	--
Time of retrace	0.5 m sec	0.5 m sec

TABLE 2-6 (Page 3 of 5 pages.)

	Cooperative Mode	Skin Track Mode
Doppler Scale Factor	100 Hz/m/sec	100 Hz/m/sec
Range Scale Factor		
R< 2 km	10 Hz/m	10 Hz/m
2 km< R< 20 km	1 Hz/m	1 Hz/m
20 km< R< 560 km	0.2Hz/m	---
Receiver Noise Temperature	1858°k	1858°k
Doppler Filter Bank		
Filter bandwidth	267 Hz	267 Hz
Effective number of filters (FFT implementation)	69	18
Frequency Tracking Filter bandwidth	267 Hz	267 Hz
Data Smoothing Time		
Velocity	2 seconds	2 seconds
Range	2 second	2 second
Angle	2 second	2 second
Angle Rate	2 second	2 second

TABLE 2-6 (Page 4 of 5 pages.)

P H Y S I C A L   C H A R A C T E R I S T I C S

Weight

Antenna Assembly	10.6 kg
Boom Assembly	5.1 kg
Electronics Assembly	4.8 kg
Total Weight	20.5 kg

Size

Antenna Assembly	40"dia. aperture
Boom Assembly	44" long
Electronics Assembly	25 x 17 x 18 cm

Power

Antenna Assembly

● Peak	100 watts
● Average during search	34 watts
● Average during track	13 watts

Boom Assembly   122 watts

Electronics Assembly

● During search	81 watts
● During track	71 watts

Total Power

● Peak	303 watts
● Average during search	237 watts
● Average during track	206 watts

TABLE 2-6 (Page 5 of 5 pages.)

ANTENNA CHARACTERISTICS

Frequency of operation	13.75 to 15.121gHz
Sum Pattern Characteristics (at 15gHz)	
Gain	41.6dB
Beamwidth, one-way	1.4 degrees
Minor lobe level below main lobe	17 dB
VSWR	2:1 max
Difference Pattern Characteristics (at 15gHz)	
Gain	37.5 dB
Beamwidth, one-way	1.1 degrees
Minor lobe level below main lobe	15 dB
VSWR	2:1 max
Transmitted Power Capability	100 watts peak or CW
Antenna Scan Coverage	
Azimuth	360°
Elevation	320°
Scan Coverage During Acquisition	40° half angle cone
Scan Frame Period	60 seconds
Frequency Response	1 Hz.

Figure 2-1 Range Measurement Accuracy of Pulse Doppler Radar
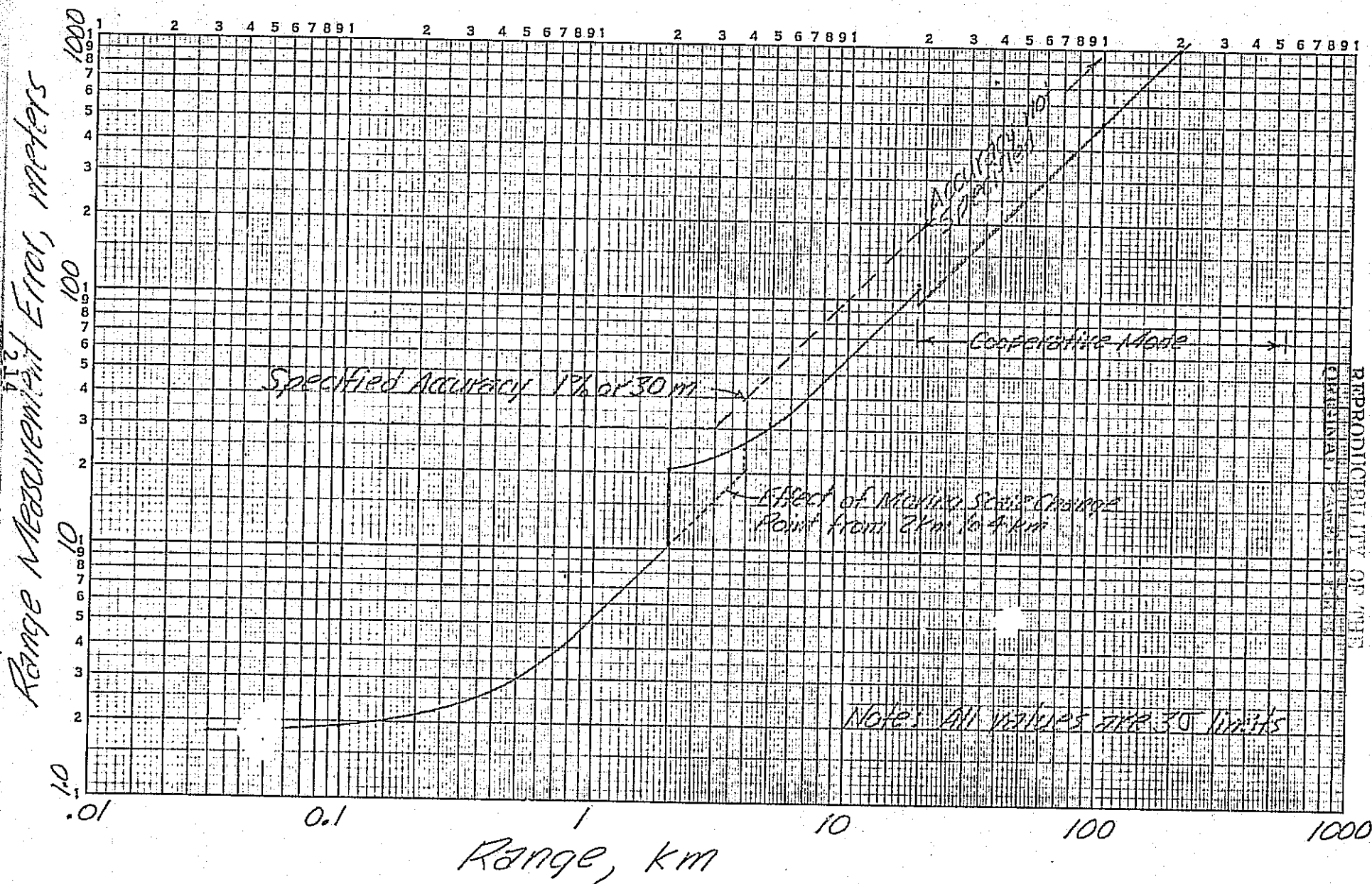
Figure 2-1 Range Measurement Accuracy of Pulse Doppler Radar

3.0 CONCLUSIONS AND RECOMMENDATIONS.

3.1 Antenna Type.

A mechanically scanned, 1 meter diameter parabolic reflector, illuminated with a four port monopulse, folding backfeed is recommended. A spiral scan mechanization is used for radar acquisition. Design features are:

1. The paraboloid and folding backfeed is a simple lightweight structure providing optimum pattern characteristics and maximum mechanical clearances.

2. The four slot backfeed with integral monopulse circuitry is simple, efficient and lightweight.

3. A spiral acquisition scan is well adapted to the geometry of a vectored search in terms of scan efficiency and probability of early detection.

4. If used with a single axis deploy/stow mechanization capable of deploying to two positions, one of which is parallel to the Z axis of the spacecraft, a spiral scan utilizing a spin axis can be implemented that minimizes scan power requirements.

5. Stow clearance is well in excess of the 3" all around.

3.2 Radar Type.

A pulse doppler, frequency agile radar with linear FM ranging is recommended for the space shuttle rendezvous function.

The rationale for selection of the recommended radar is summarized below:

- The average power is about the same as the other radar types considered but the peak power (twice the average power) is 2 orders of magnitude lower than the other radars considered.

- The relatively low peak transmitted power required minimizes breakdown problems and it can be provided by the communications TWT transmitter or by a solid state source.

- High velocity accuracy rather than high range accuracy is the driving requirement of the radar. The pulse doppler radar with FM ranging fits well with these requirements. (The pulse doppler radar inherently provides the most accurate velocity measurement of the systems considered.)

- The signal form of both the velocity intelligence and range intelligence is the same (frequency difference) which allows a common, time shared signal processor to be used for both velocity and range measurements.

3.3 PROBLEM AREAS.

Angle Rate Error.

The most difficult of the functional requirements of the radar to meet is the random error allowance for angle rate. The specified maximum error is 0.14 milliradians per second, 3σ. Considering antenna angle jitter due to thermal noise and glint from an 18 meter target, predicted values of the noise on the angle rate data output is about 8 milliradians per second.

3.4 Recommendations For Further Studies.

A. The angle rate accuracy requirement appears difficult to achieve considering angular scintillation of the target. Additional analysis is recommended of the entire target-antenna-receiver-servo tracking function.

B. A resonant analysis of the antenna structure and boom, including compliance of the spacecraft mount, should be performed.

C. Additional trade-off studies are recommended on the best type of servo motors to use for the antenna drive in the space environment.

D. Construction of a full scale, functional mock up of the recommended antenna is recommended.

4.0 RECOMMENDED PERFORMANCE SPECIFICATION FOR RENDEZVOUS RADAR.

4.1 PERFORMANCE REQUIREMENTS.

The radar shall automatically acquire the target, track and provide data outputs of relative velocity, range, line of sight (LOS) angle and LOS angle rate over the operating conditions listed below and the environmental conditions involved.

4.1.1. Range to Target.

The radar shall acquire the target and operate to the specified accuracy over a range of 30 meters to 19km in the skin track mode and 30 meters to 560km in the cooperative mode.

4.1.2. Relative Velocity.

The radar shall acquire the target and operate to specified accuracy over the following relative velocity limits.

Range Interval	Velocity Limits
30m to 10km	−20 m/sec to +7.5 m/sec
10km to 19km	−38 m/sec to +7.5 m/sec
19km to 560km (cooperative mode)	−91 m/sec to +91 m/sec

4.1.3. Acceleration.

The radar shall remain locked to the target during a series of RCS braking operations resulting in a maximum deceleration of 0.2 m/sec^2 for 20 seconds. The braking operations are separated

in time by 50 seconds. The braking operations occur at ranges to
the target of 9km to 30 meters. During RCS braking the measured
relative velocity shall not lag the true relative velocity by more
than 2 seconds.

4.1.4. LOS Angle.

The radar shall acquire, track and provide data over an
angular region bounded by a cone centered along the Z axis of the
orbiter with a half angle of 40° maximum. The LOS angle to the target
will be made available from the orbiter to the radar to assist in
initial acquisition. The uncertainty in the designated LOS angle
(Required angular search region) is as follows as a function of range
to the target.

Range	Required Search Region (Cone, half angle)
R < 13km	40°
13 < R< 19km	25°
19 < R< TBD	TBD
TBD < R< 560km	5°

4.1.5. LOS Angle Rate.

The maximum LOS angle rate shall be ±4 mRad/sec during
acquisition and ±5°/sec during tracking.

4.1.6. Target Model.

A mean radar backscattering cross-section of 1 square meter
shall be used for purposes of acquisition of the target in the skin
track mode. A Swerling Class 1 amplitude fluctuation model shall

be used. For purposes of acquisition the target echo decorrelation
time can be assumed to be 10 seconds. For purposes of computing
maximum signal return at close ranges the target shall be assumed
to have a mean cross-section of 100 square meters. The physical
size of the various targets vary from a cylindrical object 18 meters
long and 4 meters diameter to an irregularly shaped object 2 meters
in extent. Computations of angular scintillation effects (glint)
shall be based on the 18 meter cylindrical target.

4.1.7. Acquisition Time.

The radar shall search in angle for the target over the angles
specified in Paragraph 4.1.4., lock up the range and velocity
tracking loops and provide data to the required accuracy within
90 seconds of the start of the acquisition process for ranges less
than 19km and within 300 seconds for ranges greater than 19km.

4.1.8. False Alarm Rate.

During acquisition the false alarm rate may be selected as
required to achieve acquisition in the specified time, accounting
for disruption of the search pattern by false alarms. After
acquisition the data must be within the accuracy specified.

4.1.9. Data Smoothing Time.

The data smoothing time (equivalent of single section RC
low pass filter time constant) for all measured output data shall
not exceed 2 seconds.

4.1.10 Measurement Accuracy.

The accuracy of the radar measurements shall be within the values listed below over the operating conditions specified and data smoothing time given in Paragraph 4.1.9. All values listed are three sigma limits.

Measurement	Random Error	Bias Error
Range		
R<2km	5m+0.5% of Range	5m
2km<R<19km	10m+0.5% of Range	10m
19km<R<560km	30m+0.5% of Range	30m
Velocity	0.3m/sec	0.3m/sec
LOS Angle (Relative to deployed assembly mounting plate)	10mR	20mR
LOS Angle Rate		
•Skin track	10mR/sec	0.14mR/sec
•Cooperative		
R>20km	2mR/sec	0.14mR/sec
R<20km	0.14mR/sec	0.14mR/sec

4.1.11. OPERATING FREQUENCY.

The nominal operating frequency of the radar shall be 15gHz.

5.0 ANTENNA.

The common element controlling the performance of the combined radar/communication functions for the space shuttle is the antenna. Its characteristics, directly or indirectly, affect all evaluating criteria.

The antenna, as an electro-mechanical device, is unique by its encompassment of many enginerring specialties. Its design involves: microwave radiators and components, lightweight-low compliant structures, servo control and system analysis. All functions are interrelated. Operational requirements such as detection range as a function of the "power-aperture product", angle and angle rate are predicated upon the pattern beamwidth and monopulse tracking sensitivity. Data rate requirements are established by scanning rates and efficiency. The antenna is a major factor in determining system reliability, weight and cost.

5.1 ANTENNA GAIN.

The gain of a circular aperture antenna is:

$$G = \left[\frac{\pi D}{\lambda}\right]^2 f$$

or

$$G \propto D^2$$

where:

G = antenna gain

D = antenna aperture

λ = operational wavelength

f = efficiency

The maximum aperture possible, consistant with installation constraints and drive requirements is a design prerequisite. Related objectives are: good illumination efficiency, minimum beamwidth, reasonable side lobes, optimum monopulse patterns, Minimum transmission line losses and maximum scanning efficiency. Each design objective will be individually studied in the following sections of this report. First effort shall be directed to the further quantization of gain requirements.

5.1.1. RADAR RANGE EQUATION.

Radar range equation

$$R^4 = \frac{P\,G^2\,\lambda^2\,\sigma\,L_\varepsilon}{(4\eta)^3 K_b T_s B_n (S/N)} \quad \text{①}$$

where:

R = Range – m
P = Avg. power – watts
G = Antenna gain
λ = Wavelength – m
σ = Target's radar cross-section – m^2
L_ε = Summation of losses
K_b = Boltzmann's constant – 1.38×10^{-23} – Watts/Hz./K°
T_s = System noise temp.
B_n = Noise bandwidth
S/N = Signal to noise ratio

Under a given set condition ($R, \lambda, \sigma, L_\varepsilon$ & S/N requirements) the transmitter power proportionality is:

$$P \propto \frac{S/N}{G^2} \quad \text{②}$$

S/N relates to statistical assumptions of detection criteria and for a given set of conditions; example, a Swerling target type, a plot of S/N vs the number of pulses integrated has a slope such that:

$$S/N \propto n^{-.7} \quad \text{③}$$

$$n = \frac{\theta_x \theta_y \times PRF \times t_s \times \Delta R}{\Psi_x \Psi_y \quad R_s} \quad \text{④}$$

$$V_s = \Psi_x \Psi_y R \quad \text{⑤}$$

$$G = \frac{\pi^2 D^2}{\lambda^2} f \qquad G \propto D^2 \quad \text{⑥}$$

$$\theta_x = \frac{K\lambda}{D} \qquad \theta_x \propto D^{-1} \quad \text{⑦}$$

where:

θ_x = Pattern 1/2 pwr "X" beamwidth
θ_y = Pattern 1/2 pwr "Y" beamwidth
t_s = Time to search one frame – sec
PRF = Pulse repetition frequency
ΔR = Range gate width – m
R_s = Total range searched – m
Ψ_x = Ant. scan, x direction – deg
Ψ_y = Ant. scan, y direction – deg
V_s = Scan volumn – deg^2 – m
f = Efficiency factor
D = Radiator diameter – m
K = Constant

Substituting ⑤ in ④, fixing PRF, t_s and ΔR,

letting $\theta_x = \theta_y$ and substituting ⑦, ⑥, ④ and ③ into ② we have the following proportionality:

$$P \propto \frac{V_s^{.7}}{D^{2.6}} \quad \text{⑧}$$

5.1.2. COMMUNICATION LINK, GAIN EXPECTED.

In the baseline study a 12.5' diameter parabolic reflector is used on the TDRS, a 20" diameter Cassegrain radiation system on the shuttle orbiter. The calculated gains are 52.5 dBi and 35.5 dBi respectively. Recent measurements indicate that the gain of the 12.5' diameter parabolic antenna is up to 7 dB less than expected.

The characteristics of any optical device deteriorates as a function of physical errors due to manufacturing, mechanical loading and temperature changes, etc. If a given reflector is operated in increasing frequency, or similarly, if a reflector for a given frequency is increased in size, the gain at first increases as the square of the frequency or diameter, respectively, until the tolerance effect takes over and then a rapid deterioration takes place. For example, the realized gain, G_o, relative to the optimum gain, G, for an effective surface deviation, Δ, is related as follows:

$$\frac{G}{G_o} = e^{-\left[\frac{4\pi\Delta}{\lambda}\right]^2}$$

Reference: Mehdi Sarghamee, "Antenna Tolerance Theory"; IEEE, November 1967, Page 777.

Practical structures can be built and reasonably maintained to a tolerance of 1 part in 1,000. For a reflector 12.5' in diameter, cumulative errors up to .074" can be expected with a resulting loss from maximum of 6.06 dB. The gain of a 12.5' reflector operated at K_u-band (λ=.787") is:

$$G = 10 \log\left(\frac{\pi D}{\lambda}\right)^2 - 6.06 = 49.48 \text{dB (less aperture efficiency)}$$

Tolerance control achievable with standard shop practices are no longer adequate for antenna gains above 48dB. Furthermore minimum weight and environmental requirements tend to negate the effectiveness of high precision manufacturing techniques. Based upon previous experience and study this writer believes that the more vavorable values measured on existing hardware are representative of those that can be reasonable expected within the practicalities of the final system. (47.5 to 49.5 dB).

Furthermore, the illumination efficiency of a 20" diameter Cassegrain antenna can be expected to be approximately 45%, resulting in a net gain of 34.6 dB at 15 gHz. The realized loop gain of the communication link is 4 to 6 dB less than shown in existing budgets that are marginal in fulfilling operational requirements!

An offsetting factor, relative to the aforementioned antenna gain problem, is that the D^2C studies have indicated that the gain of the shuttle orbiter antenna can be substantially increased. Two factors are involved. The use of a point source feed and parabolic reflector is more efficient than the envisioned Cassegrain system. Furthermore the aperture diameter can be doubled (1 meter diameter) while retaining compatibility with shuttle installation constraints. The gain of the 1 meter diameter aperture increases to 41 dBi at 15 gHz. Comparative values of related characteristics such as orbiter transmitter power, link margins, etc. have been included in this study for the smaller and larger aperture antennas.

5.2 APPLICABLE ANTENNA TYPES.

A mechanically scanned antenna, as opposed to an electronically scanned antenna, is most applicable to the space shuttle task. It is basically less complex, more compatible with the space environment, has greater radiation efficiency (particularly at wide scanning angles), provides positive inertial erference data (a factor of particular importance when determining angular rate) and weighs less. Three types of radiating systems can be considered: a Cassegrain system, a point source fed parabolic reflector and a flat plate array. Comparative data is tabulated in Table 5.2-1. Values shown are typical.

The flat plate antenna is heavy because of its waveguide-array construction. The weight adds to its inertia which in turn requires excessively high servo power.

The Cassegrain antenna, in comparison with a point source fed paraboloid, exhibits, due to aperture shadowing by the hyperbolic sub-reflector, somewhat poorer pattern characteristics. It is heavier and correspondingly it requires a greater drive power. It is capable of providing a greater effective focal length for the same geometric depth than can the paraboloid. This improves its tracking sensitivity. This can be offset with a folding feed on the parabola. These factors will be discussed later.

The point source fed parabolic reflector offers the best overall performance, is cost effective and of minimum weight. Initial effort will be directed towards this design approach.

TABLE 5.2-1 COMPARISON OF CHARACTERISTICS OF THREE CANDIDATE
ANTENNAS.

	CASSEGRAIN	POINT FED PARABOLOID	FLAT PLATE
Non-minimal aperture	1 m	1 m	1 m
Gain	39.8 dB	41.3 dB	41.5 dB
BW	1.4°	1.4°	1.4°
ML	14	20	23
Weight	33	30	80
J_e	1.85	1.57 in-lb-sec^2	9.15 in-lb-sec^2
J_a	7.2	6.46 in-lb-sec^2	88 in-lb-sec^2
Peak servo power	90 watts	80 watts	1100 watts

5.3.1. MONOPULSE PATTERN; 1 METER PARABOLOID WITH BACKFEED.

The monopulse patterns are primarily a function of the F/D ratio and the spacing between elements of the backfeed. In Figure 5.3-9 typical dimensions for the aperture spacing of the four slot feed are shown. Element centers are equally spaced about the feed centerline axis. Using these values the squint angle as a function of the F/D ratio is: re:

Focal length	F/D ratio	Squint angle
33cm.	.33	1.15°
50cm.	.5	.7
72cm.	.72	.5

Monopulse patterns for F/D of .33 and .72 are shown in Figure 5.3-1. Note the greater slope for the pattern shape near null with the smaller quint angle.

Monopulse tracking sensitivity as a function of pattern crossover is shown in Figure 5.3-2. The optimum crossover is at a level of 1.1 dB corresponding to a squint angle of .423°. Based on the 1/2 inch spacing between the slot elements making up the array the optimum focal length would be 86cm. long, resulting in an F/D ratio of .86.

The error slope as a function of signal-to-noise ratio is shown in Figure 5.3-3 for squint angles of .5 and 1.15°. Note the greater the signal noise ratio, the greater the slope ratio. It is desirable to reduce the squint angle to the minimum value possible.

For a given focal length the spacing between elements can only be decreased by decreasing the physical size of the elements. In

that the electrical size cannot be decreased, a decrease in physical size requires the use of dialectic loading in the feed aperture. This aggravated the impedance match problem. Because of large bandwidths involved, the feasibility of this approach can only be determined through actual development.

The alternate is to increase the focal length. This can be accomplished with the folded feed design. For continuous rotation of the elevation motor an F/D of .5 is a maximum value. This reduces the error signal slope from a maximum value by approximately 1.1 dB.

$f/d = .33$

ANGLE OFF

$f/d = .72$

ANGLE OFF

FIG 5.3-1

CROSS OVER AT -.15 and -.5 db
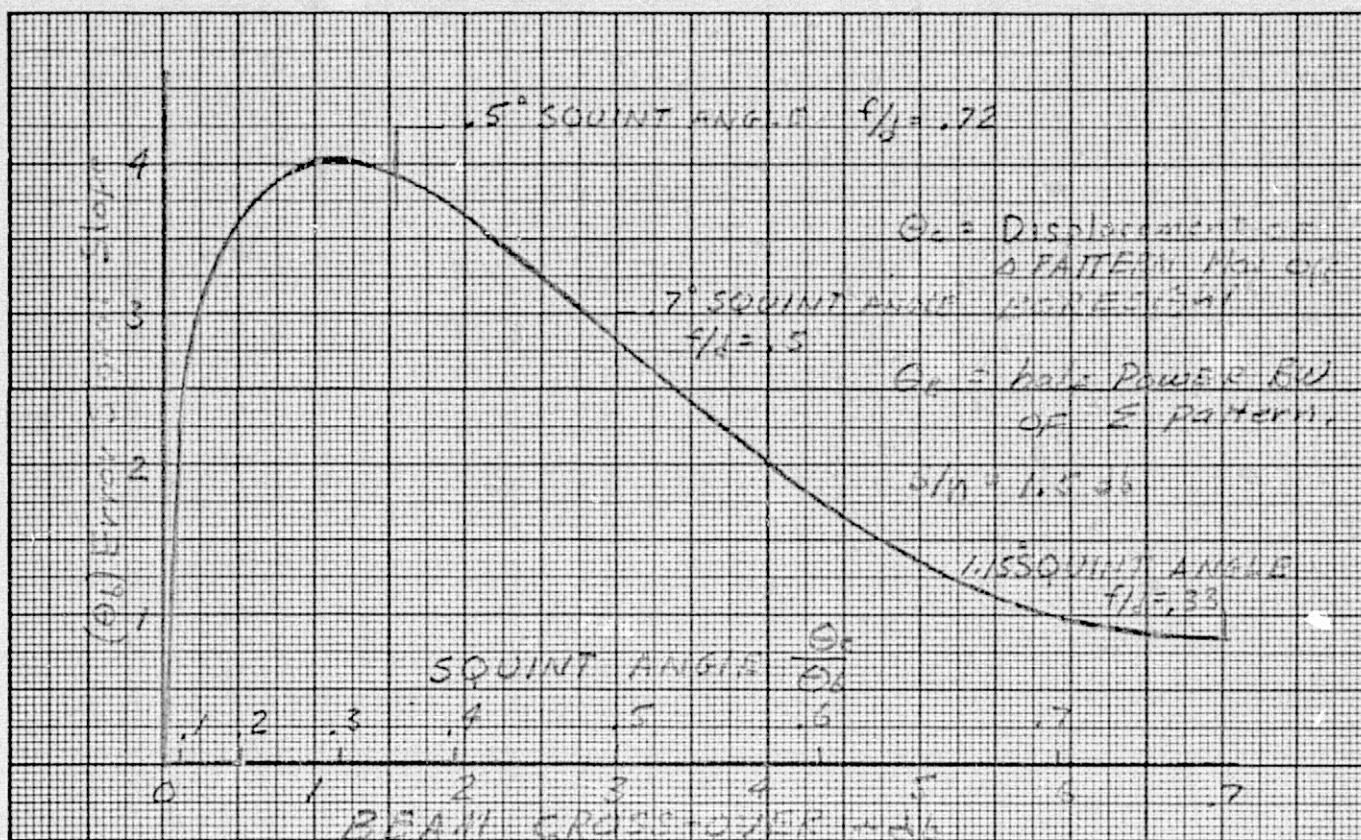
Fig 5.3-2 MONOPULSE TRACKING SENSITIVITY
as a function of
Δ PATTERN CROSS OVER
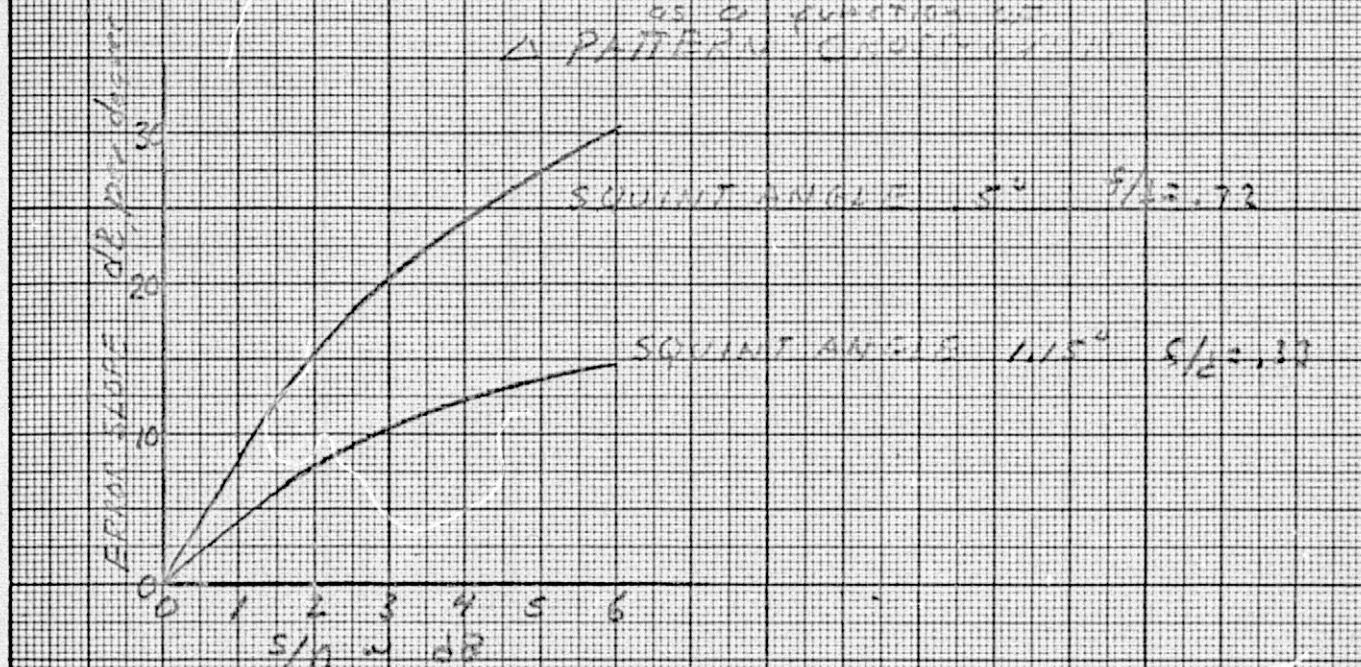
Fig 5.3-3 ERROR SLOPE vs S/N RATIO

5.3.2. COMPARISON OF PATTERN CHARACTERISTICS.

A relatively rigorous analytical program has been provided to NASA Houston to compute the pattern characteristics of the Cassegrain Antenna System. The results of this analytical study will be reported in a future report. In the interim period pattern characteristics of a Cassegrain Antenna can be based upon the results obtained from existing designs such as the rendezvous radar for the Apollo Lunar Missile and others. The pattern characteristics of various applicable type antennas are approximated in Table 5.3-1.

The tracking sensitivity is stated for a signal noise ratio of 1.5 and 7.5 dB. The 1.5 dB signal noise is referenced as a minimal value for consideration. The 7.5 dB signal noise ratio is chosen at equal gain pisition to compare the 50cm. Cassegrain system with the 100cm. short focal length point feed system. Because of the large offset angle required by the shorter focal length the tracking sensitivity at a signal noise ratio of 1.5 dB are approximately equal. However, at positions of equal gain, i.e., a 1.5 dB signal noise ratio for the 50cm. Cassegrain versus the 7.5 dB signal noise ratio for the 100cm. diameter reflector is improved by some 11 dB per degree.

It is apparent that the best results are obtained with a large reflector using the folded feed where a near uptimum F/D ratio can be employed.

TABLE 5.3-1   PATTERN CHARACTERISTICS OF APPLICABLE ANTENNAS.

ANTENNA	CASSEGRAIN		PARABOLOID WITH PRIMARY FEED	
			Fixed feed	Folded feed
Reflector – diameter	50 cm.	100 cm	100 cm.	100 cm.
F/D ratio	.9	.6	.33	.5
Gain (15gHz.,100% efficient)	37.91	43.9	43.9	43.9
Efficiency	45%	40%	45%	55%
Gain	34.4dB	39.8dB	41dB	41.3dB
Σ beamwidth	2.8°	1.4°	1.4°	1.4°
Δ beamwidth	2.2°	1.15°	1.39°	1.15°
Tracking sensitivity (1.15dB S/N)	6dB/°	16.5dB/°	6dB/°	16dB/°
Tracking sensitivity (7.5dB S/N)		33dB/°	17dB/°	33dB/°
Minor lobes	13dB	14dB	17dB	20dB

5.3.3. MONOPULSE BACKFEED.

A drawing of an applicable monopulse backfeed is shown in
Figure 5.3-4. Basically it is a Cutler type, (back feed)
four port feed in combination with a hybrid waveguide circuit
to provide an amplitude-amplitude monopulse capability.

The physical arrangement of the waveguide is shown in the lower
portion of Figure 5.3-4. The circuit is shown in the upper portion
of the diagram. Consider the operation of the equipment in the
receive mode. The signals are received at ports A,B,C and D.
The signal from port A is divided at Top Wall Coupler (1) into
2 equal parts and in-line and coupled-line circuit. The in-line
circuit passes without phase shift. The coupled-line undergoes
a -90° relative phase shift. In a similar manner the signal
received in port B is transmitted through a -90° phase shifter
and is equally divided at Top Wall Coupler #2 to a direct
circuit without further phase shift and coupled to the 2nd line
with a relative phase shift of -90°. Simultaneous reception
of the signal at port C is transmitted through a +90° phase
shift and then equally divided by Top Wall Coupler #1 to a
continuing circuit without phase shift and to a coupled circuit
with a relative -90° phase shift. Note: the original +90° and
the -90° phase shifts are self cancelling; i.e., signal received
at port C within the coupled line has no relative phase shift.
Along this specific line signals received from port A and
port C along transmission line A are now in phase ($A\angle 0 + C\angle 0$).
Signals received at port D are likewise equally divided through
Top Wall Coupler #2 to the direct line with no phase shift and
to a continuation of transmission line B with a phase shift
of -90°. Recall that the signal from port B had imposed upon
it a retardation in phase of -90°; therefore, signals arriving
from D and B along the continuation of transmission line B are
now in phase but carry a relative 90° phase lag; i.e.,
$B\angle -90° + D\angle -90°$. Continuing along this line these combined

signals are now equally divided to a continuing line and coupled
to a continuation of transmission line A through Side Wall
Coupler #3. The -90° phase shift carried by signals B and D
is now compensated for by the +90° phase shift introduced through
the Side Wall Coupler #3. These signals combine with signals A
and C to provide a sum-channel signal, i.e., (A+B+C+D). Signals
A+C along transmission line A couple through Side Wall Coupler #3
with a +90° phase shift to combine with signals B+D to form
(A+C) - (B+D) a ΔX signal. Correspondingly signals $A \angle -90° + C \angle +90°$
in a continuation of line C comgined with signals B+D from Side
Wall Coupler #4 to provide (C+D)-(A+B) a ΔY signal. Remaining
signals which couple into a continuation of line C form a cross-
coupled signal not related to the monopulsed tracking problem
and is matched into a resistive load. Continuation of channels
A, B and C provide a sum-signal, a ΔX difference signal and a
ΔY difference signal respectively. By reciprocity, the signal
entering the Σ channel are equally divided and transmitted in
phase from each of the four feed ports.

The physical arrangement of the waveguide components is shown in
the lower drawing of Figure 5.3-4. The drawing is self explanatory.

WAVEGUIDE CIRCUIT

$A\underline{/0°} + B\underline{/-180°} + C\underline{/+180°} + D\underline{/0°}$

Cross terms terminate in resistive load.

$B\underline{/-180°} + D\underline{/0°}$

—90° Top Wall Coupler (2)

$B\underline{/-90°} + D\underline{/-90°}$

$A\underline{/+90°} + C\underline{/90°} + B\underline{/+90°} + D\underline{/-90°}$
or
ΔX

$(A+C) - (B+D)$

+90° Side Wall Coupler (4)

Y

—90°

B

—90°

(3) Side Wall Coupler $\underline{+90°}$

$A\underline{/0°}\ C\underline{/0°}$

$A\underline{/0°} + B\underline{/0°} + C\underline{/0°} + D\underline{/0°}$
or

ΣT_x & R_x

X

A

4 PORT FEED

—90° Top Wall Coupler (1)

$A\underline{/-90°} + C\underline{/+90°}$

$A\underline{/-90°} + B\underline{/-90°} + C\underline{/+90°} + D\underline{/+90°}$
or
ΔY

$(C+D) - (A+B)$

C +90°

A+B+C+D
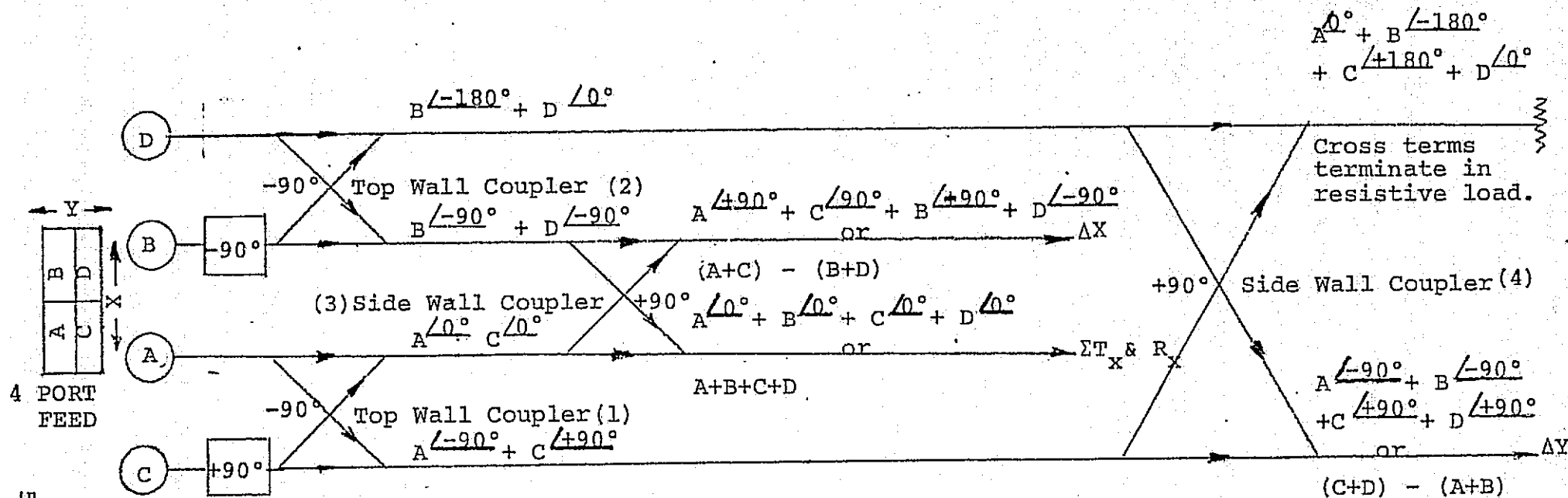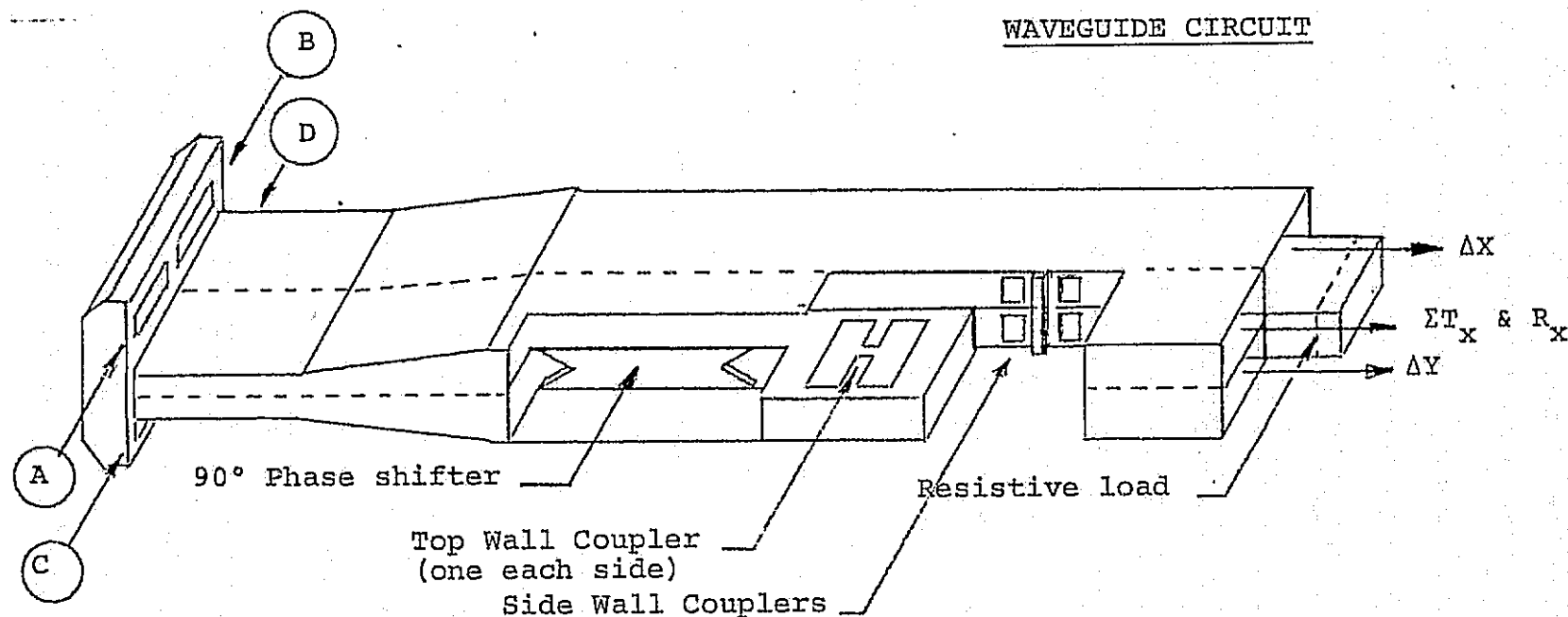
INTEGRATED HYBRID ARRANGEMENT

90° Phase shifter

Top Wall Coupler (one each side)

Side Wall Couplers

Resistive load

ΔX

ΣT_x & R_x

ΔY

FIGURE 5.3-4.   MONOPULSE BACKFEED

5.3.4.   DESIGN DETAILS; HYBRID COMPONENTS.

The design of short-slot hybrid end couplers for microwave
applications is well established. Characteristics of a typical
Side Wall Coupler are;

Manufacturer	Microwave Developments Laboratories, Inc.
Model #..............................	62 HS122
Waveguide............................	WR-62(.702"x.391"x.040")
Frequency............................	13.5 to 15.6GHz.
Coupling.............................	3db
Maximum output power unbalance	.25db
Minimum isolation	30db
Width	1.48"
Height	.045"
Length...............................	1.11" ± .003"

A typical Top Wall Coupler has similar characteristics. Example;

MDK Model	62HT82
Operating frequency.................	13.5 to 15.6GHz.
Output power unbalance..............	.25db
Isolation...........................	30db
Width...............................	.78"
Height..............................	.88"
Length..............................	1.25"

Assuming a reflector diameter of 1 meter and an $\frac{F}{D}$ ratio of 1/3,
the length of the feed is .33 meters (13.1"). Using WR-62
waveguide and considering a design frequency of 15GHz. we have;

$$\lambda_o = .7874"$$
$$\lambda_c = 1.244"$$
$$\lambda_g = 1.017"$$

The length of transmission line within the primary feed assembly can be assigned as follows;

Length of hybrids................ 2.36"
Length of half-height guide..... 1.017"
Length of taper................. 2.034"
Total........................... 5.411"
Length available for
phase shift..................... 7.689"

Relative phase shift of ± 90°, as required to correct the phase shift characteristics of the slot couplers, can be introduced in a number of ways. A preferred way is to change the width dimension of the guide over as long of a section of waveguide as possible. The greater the length used the better the bandwidth characteristics. Consider a 7" length.

Phase shift	Electrical length	$\lambda_{g'}$ prime	$\dfrac{\lambda_o}{\lambda_{g'}}$	λ_c	"b" guide width
+90°	$6.633\lambda_o$	.98"	.8034"	1.322"	.661"
0	$6.883\lambda_o$	1.017"	.774"	1.244"	.622"
−90°	$7.133\lambda_o$	1.0539"	.747"	1.184"	.592"

To achieve a +90° lead requires increasing the width of the waveguide by .039". To achieve a 90° lag in the waveguide requires decreasing the width of the waveguide by .030".

5.17

5.3.5. POLARIZATION TRANSFORMER.

Circular polarization is required for the communication mode of operation. Previous tests have indicated reflection losses of up to 4 dB if circular polarization is used in the radar mode. Companion studies have shown that 7 to 8 dB greater power is needed for the communication mode than for the radar mode; therefore, one could employ circular polarization for both the transmit and communication modes of operation. Not withstanding these factors, it is desirable to determine an optimum method of transforming the antenna's response to either linear or circular polarization.

A circularly polarized wave can be produced from two linear polarized waves of equal amplitude, in space quadrature and 90° out of phase. The transmission of a linear polarized wave is inherent to waveguide structures. The transformation of this linear polarized wave to circularly polarized is accomplished by dividing the linear polarized wave into two equal parts, arranged in space quadrature, i.e., the polarization vectors are normal, introduce a 90° relative phase lag re-combining to provide the desired circular polarization. There are two conventional ways of accomplishing this. One is within the waveguide circuitry, usually in the immediate vicinity of the primary feed. The second is by means of a space filter within the near field of the radiating antenna. In this particular case where four feeds are involved, the latter design is the simplest. Three techniques have been instrumented: a polarization grid in the immediate vicinity of the primary feed, a similar grid at the surface of the reflector and within the radome. In the first two techniques the grid assembly is rotated 45° to introduce a linear to circular polarization change. The latter technique has been used where a type of antenna structure is employed, usually having a large

aspect beam ratio, that is not conveniently adapted to the transmission or reception of circularly polarized waves; but, circular polarization is specified. In this case the grid is placed in the radome to provide the desired polarization transfer.

Polarization change introduced at the feed is the most convenient because of its relatively smaller size. This technique was used on the Mark II F-111 Radar Antenna. A modification of this design is suggested for this application.

A drawing of a polarization switch is shown in Figure 5.3.5. The polarization transformer consists of 3 wire (AWG #24) grids spaced $\lambda/4$ apart and oriented at 45° to the incident polarization vector. It is formed on a mica or ceramic substrait and mounts in two parts on a lever mechanism off the cap of the primary feed. In the position shown, the polarization transformer is not in the radiation path of the primary feed and linear polarization is provided. By pushing the lever linkage forward the polarization grids are rotated in front of the primary radiating apertures and circular polarization is produced. The mechanical motion can be initiated with a latching solenoid. For fail-safe operation it is spring loaded to the circular polarized position for stow and communication operation.

POLARIZATION GRID

CP LIN
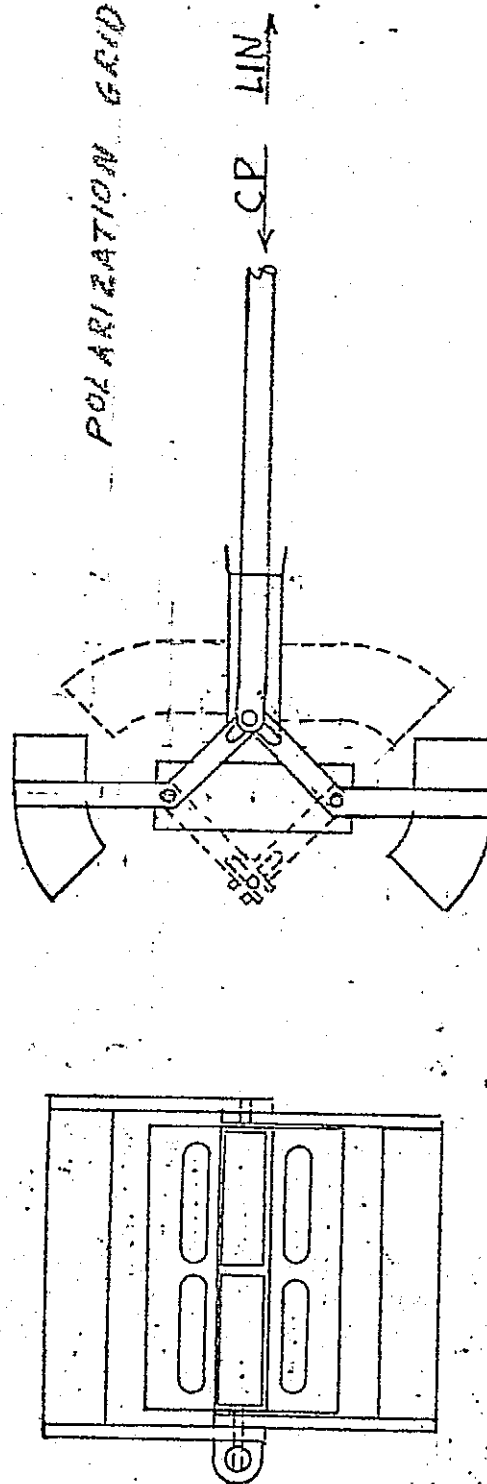
POLARIZATION SWITCH

FIG 5.3-5

5.20

The characteristics of a gridded polarization transformer
can be determined by considering a plane wave of amplitude $\vec{E}_1$
normally incident on a polarizing structure as shown below. The
polarizing structure has a width,L, and is constructed of a series
of wire grids oriented at an angle of 45° with the incident
polarization.
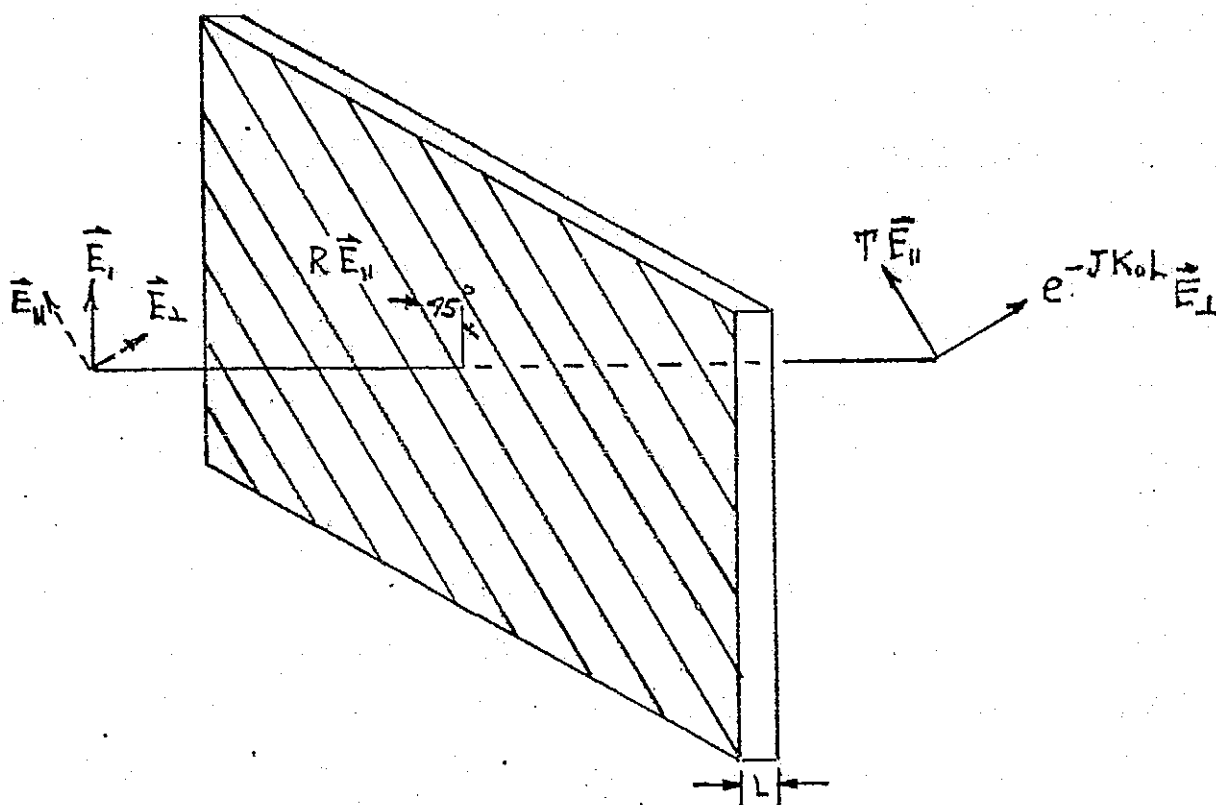
As indicated, the components of the incident field perpendicular
to the grids, $\vec{E}_\perp$, sees the grids as almost negligible capacitance
and is transmitted through the structure with essentially only a
phase shift of $k_o L$. The components of the incident field parallel
to the grids, $\vec{E}_{\parallel}$, on the other hand, sees the grids as appreciable

5.21

inductances and is reflected and transmitted through the structure with reflection coefficient R and transmission coefficient T. For use as a polarizer, the structure is constructed such that at the design frequency the structure is matched:

$$R = 0 \tag{1}$$

and the parallel and perpendicular field components transmitted through the grid are in time quadrature:

$$\angle T + k_o L = 90° \tag{2}$$

It is the purpose of this analysis to examine the effects of frequency variation on the reflection and polarization purity for two possible polarizing structures.
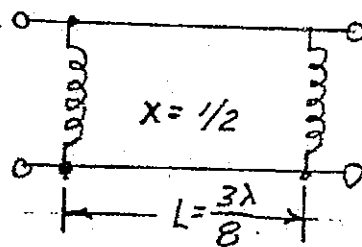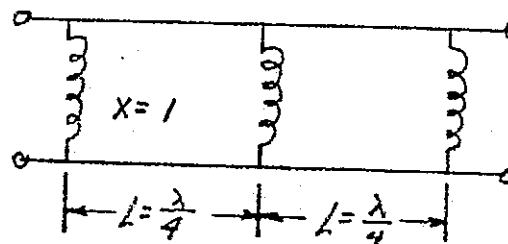
Two grid structure   Three grid structure

(All impedances normalized to Z_o=377 ohms.)

Shown above are the electrical equivalents of two grid and three grid structures which are satisfactory polarizers inasmuch as conditions (1) and (2) are satisfied at the design frequency. The two grid structure is made up of identical grids having inductive reactances equal to $Z_o/2$ spaced three eights of a wavelength apart. The three grid structure has double the reactance values with grid spacings of a quarter wavelength.

Results of calculations of the reflective properties of
the structures are exhibited in Figure 5.3.-7. The magnitude
of $\vec{E}_{\parallel}$ is .707 of the incident magnitude. The reflected field
from the grid is $R\vec{E}_{\parallel}$, and only .707 the magnitude of this
field appears as a component in the direction of the incident
field. It then follows that the reflection coefficient for the
incident polarization is R/2 and this quantity has been used to
calculate the VSWR in Figure 5.3-7.

The results of the calculation of the purity of the circular
polarization produced by the structure are presented in Figure 2.4-6.
When conditions (1) and (2) are not satisfied, the instantaneous
total field transmitted through the structure

$$\vec{E}_{total} = T\vec{E}_{\parallel} + e^{-jk_o L} E_{\perp} \tag{3}$$

will generally vary with polarization angle as the radius of an
ellipse. The ratio of the maximum to minimum value of the RMS
field strength gives a measure of the ellipticity and this ratio
is given in Figure 5.3-7 expressed in dB.

As can be seen in Figures 5.3-6 and 5.3-7, the three grid
structure has wider bandwidth than the two grid device. This
is to be expected since large shunt admittances are needed to
provide the required transmission phase shift in the two grid
case. The three grid structure, although somewhat more elaborate
to construct, requires only one half this grid admittance and is
thus inherently a more borad banded polarizer.

FREQUENCY BAND
LIMITS

2 GRID STRUCTURE

VSWR

DESIGN FREQUENCY

3 GRID STRUCTURE

1.5
1.4
1.3
1.2
1.1

13.5   14   14.5   15   15.5

FREQUENCY ~ GHz
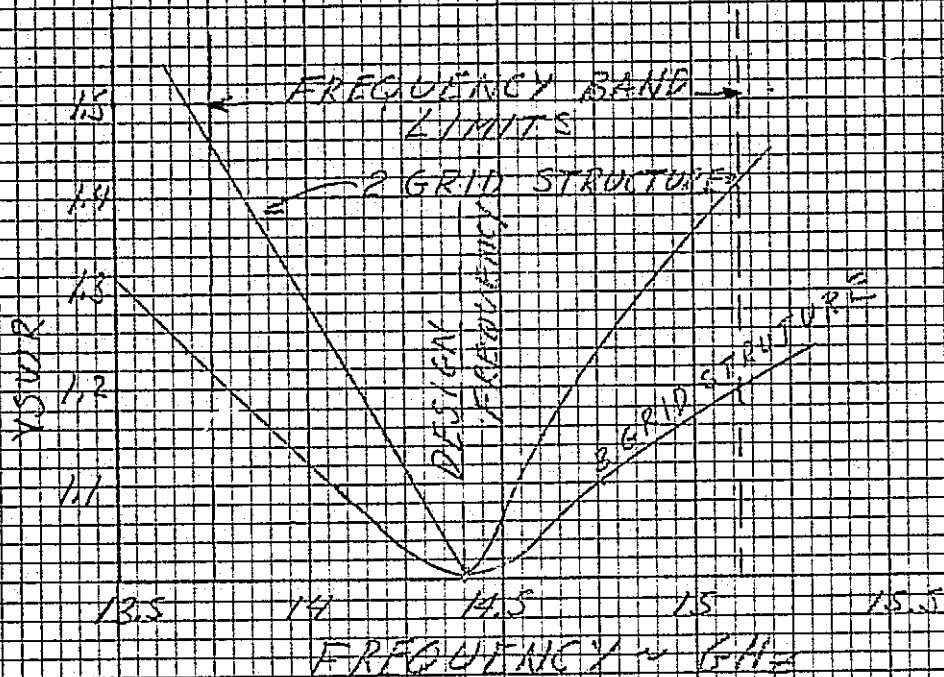
Fig 5.3-6   VSWR VS FREQ - POLARIZATION
TRANSFORMER.

ELLIPTICITY ~ dB

3
2
1
0

13.5   14   14.5   15   15.5

FREQUENCY ~ GHz
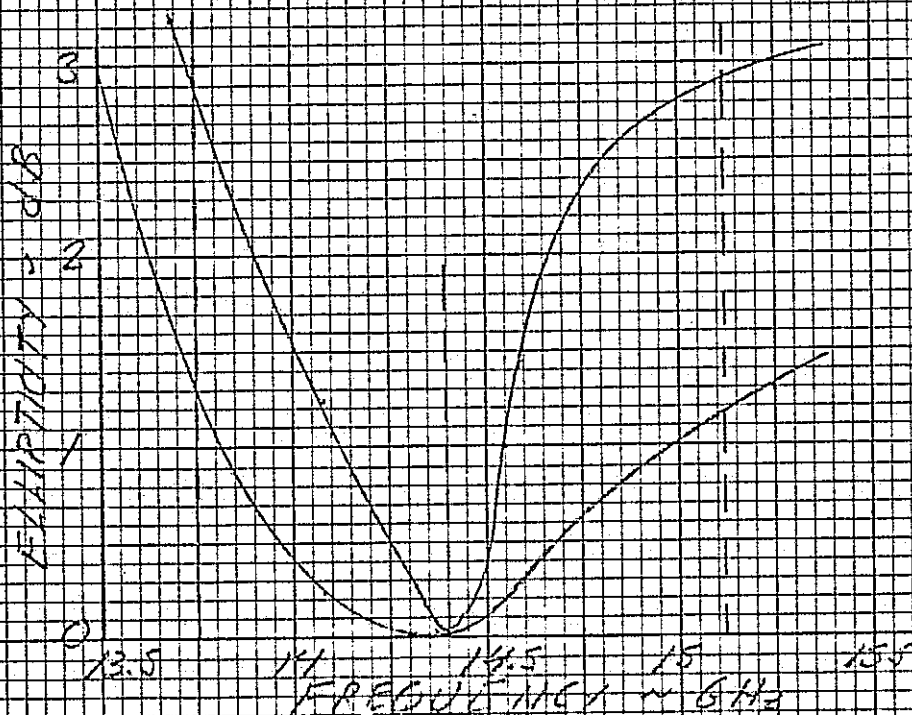
Fig 5.3-7   ELLIPTICITY VS FREQ POLARIZATION
TRANSFORMER

5.24

5.3.6. FOUR HORN FEED AND POLARIZER.

A four horn feed and polarizer is suggested as a design alternate to the previously described four port backfeed. A drawing of the alternate is shown in Figure 5.3-8.

Basically the feed is to illuminate a circular aperture with a monopulse pattern capable of providing either circular or linear polarization. Requirements for symmetry exist in the primary pattern, in both the individual and total dimensions of the primary feed and within a waveguide system capable of providing both linear and circular polarization. This can be accomplished with either circular or square transmission line and radiating apertures.

Referring to the central left-hand drawing of Figure 5.3-8, there is a cluster of four square horns making up the primary monopulse array. These are fed from WR62 waveguide through two angularly displaced quarterwave sections of waveguide. The first section is rotated 22.5° relative to the input guide. This rotates the polarization vector 22.5°. The next section is a similar section of waveguide except it rotates ±22.5° relative to the orientation of the first quarter wave section of waveguide. This rotates the polarization vector of the output wave to one of two positions, i.e., in alignment with or at 45° to the input polarization vector. In the first case the energy is transmitted through the square waveguide in the TE_{01} mode and linear polarization is radiated. In the second case the polarization vector is oriented at 45° to the axes of the square waveguide and both the TE_{01} and TE_{10} modes are excited. These two waves are of equal amplitude and in phase. If unperturbed a linear polarized wave would be radiated oriented at 45° relative to the elevation

POLARIZERS IN POSITIONS 1 OR 2.

REFLECTOR + FEED

NOTE FEED 1,2,3 OR 4 SECTIONS

DRIVE ± 45°

FIXED FLANGES

EACH λg/4

TO HYBRIDS

WR62

CHOKES

HORNS OR SQUARE WAVEGUIDES

± 22.5° FIXED

C.P.
± 45°
POLARIZATION SWITCH

SHOWN IN C.P. ROTATE 45° PER ARROWS FOR LINEAR
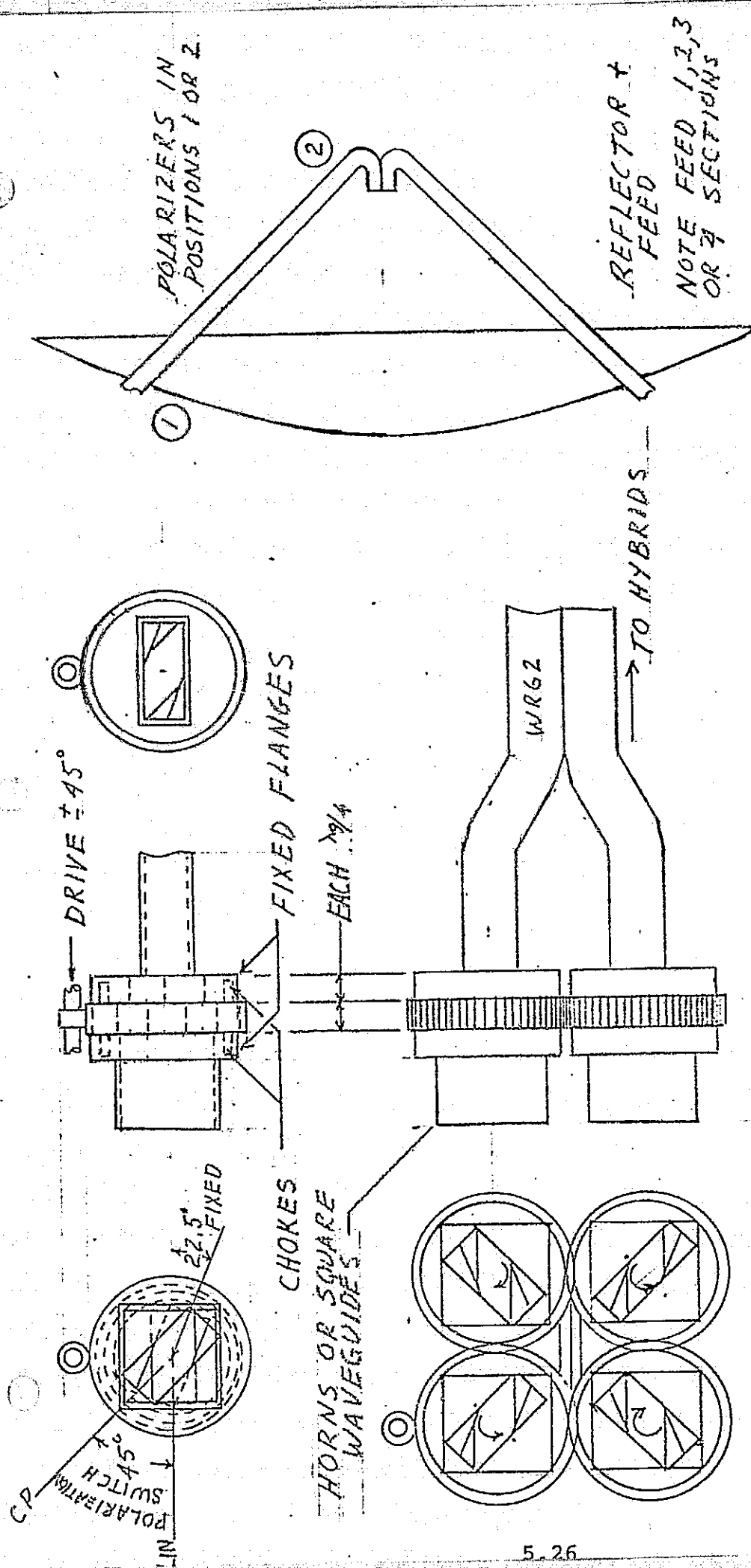
Fig 5.3-8 FOUR HORN FEED and POLARIZER

5.26

axis of the antenna. Circularly polarized energy is produced by
introducing a 90° phase shift between these two orthogonal waves.
This can be accomplished in one of two ways. A dielectric vane
can be introduced into one of the orthogonal axis of the square
waveguide of a proper dielectric constant, width and length to
provide a 90° phase differential in the orthogonal waves.
Alternately the dimensions of the square waveguide can be made
slightly rectangular, in the nammer previously discussed for
introducing the differential phase shift requirements in the
four port backfeed.

The second quarterwave section can be rotated a number of ways,
one of which is suggested in Figure 5.3-8. Bull gears are cut
into outer diameter of each quarter wave section to be rotated and
coupled together so as to rotate in accordance with the drawing.
In this arrangement adjacent sections rotate in counter directions.
To provide a single rotational sense to the circular polarization
(right hand circular polarization) **the relative** phase shift
between adjacent units are introduced in orthogonal axes. Non-
contacting wideband chokes have been used in adjacent sections
of polarization transformer. Torque requirements to change
polarization are minimal. While a solenoid drive can be used, a
motor drive is suggested.

The four output guides of WR62 from the four horn primary
feed must be routed to hybrids, such as described for the four
port backfeed or alternately any convenient combination of
appropriate microwave couplers. This feed and polarizer can be
used with either the Cassegrain or paraboloid reflector systems.
The four horns will generally be brought together so as to form
a minimum primary aperture. One possible arrangement of the
latter is shown in the right-hand drawing of Figure 5.3-8.

Considerable variability in package design exists. The polarizer
and its transformer, and for that matter, the hybrid circuitry,
can be mounted in a near focus position and three WR62 waveguides
used as a support tripod. Alternately polarizers and hybrids
can be mounted behind the reflector and the square waveguide used
in front of the reflector. The square waveguide can form a 1,
2 or 4 waveguide structural assembly for the primary feed. In
a practical sense a cluster arrangement of four waveguides is
preferred. From a servo standpoint the heavier parts of the system
can be mounted near to the scanning axes thereby reducing their
radius of gyration and the associate inertial loads.

5.3.7. FOLDED FEED.

        The microwave characteristics of the four port "Cutler
type" backfeed were described in Figure 3.3-4 of Section 5.3.3.
If this feed were mechanically arranged to fold back on itself
the F/D ratio can be increased. Pattern characteristics are
improved, additional volumn for the elevation drive assembly is
provided and the clearance between the antenna and other structures
is increased.

        A folded feed is shown in Figure 5.3-9. Mechanically, it
is a simple device consisting of a spring loaded hinge to
mechanically align and hold the feed against a mechanical stop.
This is the position the feed assumes when the antenna is operating
in its deployed position. When stowed it folds back against the
reflector. The folding motion can be actuated by one of several
methods. For example, a roller at the end of the feed can be
engaged by an appropriate pad off the payload or payload door to
fold the feed for stow. Alternately a size 8 motor can supply
power to stow and deploy the feed.

The waveguides are coupled at their end section by means of broadband, non-contacting chokes. They are cut into the broadside walls of the waveguide in a way that minimizes the radius of the fold circle, i.e., the chokes are alternated and arranged to minimize the chord to diameter spacing involved in hinge motion. In this way the hinge can be placed very close to the waveguide. This factor along with its relatively small size minimizes reflector shadow and associate pattern distortion.

Wall thickness of the waveguide in the vicinity of the choke has been increased from a nominal value of .1 centimeters (.040") to .150 centimeters (.060"). This has been accomplished by tapering the inner wall of the waveguide inward. This arrangement also makes it convenient to, as required, add mica windows on each side of the hinge section. These techniques are equally adaptable to the four horn "J" feed.

HINGE SPRING
LOADED AGAINST
STOP
FOLD LINE

STOP

HINGE AXIS

HINGE-CHOKE SECTION
FULL SCALE

Fig. 5.39 FOLDED FEED
DIMENTIONED IN CENTIMETERS

33.12 cm

FEED. 1cm = 2cm

FOLD

ROLLER

.95

3.81
.635
.635
.254

3.18

.95
.035
.035

.035
.115
.070
.150

CHOKE
SCALE 1cm = 1/2 cm

5.30
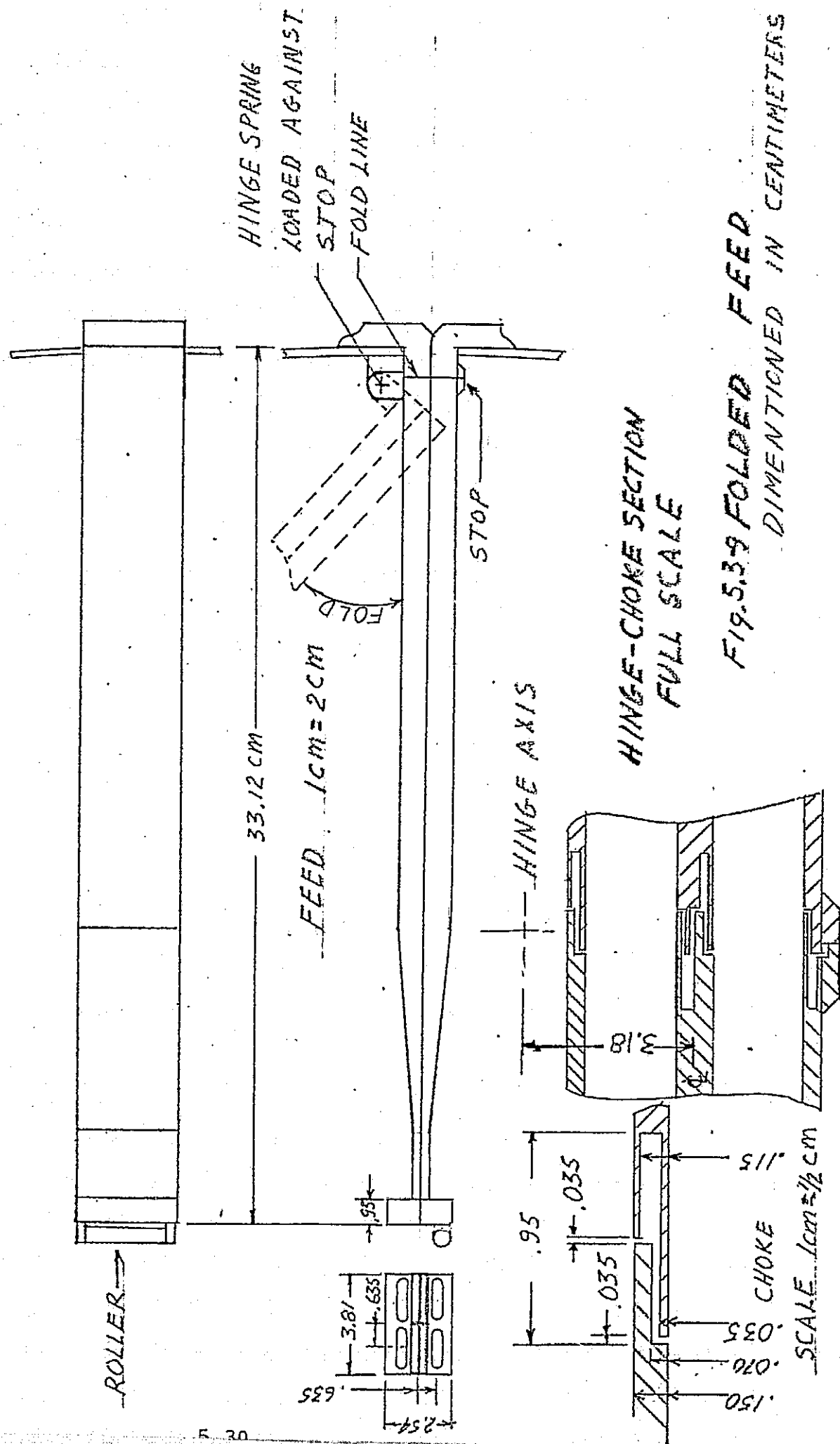
5.4   SCANNING EFFICIENCY.

The effective dwell time (t_d) on a target can be expressed:

$$t_d = f_s \frac{\Theta_x \Theta_y}{\Psi_x \Psi_y} \cdot t_f \qquad (1)$$

where:

f_s = scanning efficienty

Θ_x = half power beamwidth in x plane

Θ_y = half power beamwidth in y plane

Ψ_x = total scan angle in x plane

Ψ_y = total scan angle in y plane

t_f = total frame time

Geometric parameters and frame times are established by operational requirements. The maximization of (t_d) is accomplished by maximizing the scanning efficiency (f_s). (f_s) is composed of two parts:

$$f_s = (f_d)(f_g) \qquad (2)$$

where:

f_d = pulse density efficiency

f_g = geometric efficiency

and

$$f_d = \frac{\text{Minimum dwell time incurred}}{\text{Average dwell time utilized}} \qquad (3)$$

$$f_g = \frac{\text{Desired scan area to cover}}{\text{Actual scan area covered}} \qquad (4)$$

In the space shuttle application scanning efficiency is most critical during radar acquisition of non-cooperative targets. The detection capability of the receiver is proportional to the dwell time on target. Pertinent requirements are:

Scan areas, $\Psi_x\Psi_y$ .... 80x80° (circular)

Frame period (t_f)........ 60 seconds

BW, $\Theta_x\Theta_y$ .... 1°

The average dwell time (t_d) available is:

$$t_d = \frac{\cdot 1^2}{80^2} \cdot \frac{\pi}{4} \cdot 60 = .00736 \text{ seconds}$$

The mechanics of the scan mechanism involves periods of accelleration that prevent achieving this value. It is the minimum dwell time incurred relative to the average value available that is a measurement of scan efficiency.

5.4.1. WIGWAG SCAN; RECTANGULAR CROSS-SECTION.

A standard wig wag scan covers scan area (Ψ_x, Ψ_y) by sweeping in the Ψ_x direction with successive sweeps each displaced in the Ψ_y direction by approximately 70% of a beamwidth. The total number of sweep lines can then be calculated as

$$N_y = 1.3 \frac{\Psi_y}{\Theta_y}$$

where:
N_y = Number of line scans

1.3 = Beam overlap

Scan reversals are accomplished in a sinusoidal manner, i.e.:
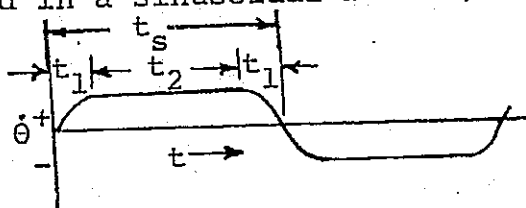
$$\Theta = A \sin \omega t \quad \text{⑦}$$

$$\dot\Theta = A \omega \cos \omega t \quad \text{⑧}$$

$$\ddot\Theta = -A \omega^2 \sin \omega t \quad \text{⑨}$$

where:
t_1 = 1/4 the period
t_2 = Period with constant velocity
Θ = Angle displacement
$\dot\Theta$ = Angle velocity
$\ddot\Theta$ = Angle accelleration
A = Maximum angle displacement
ω = $2\pi f$ where f= frequency

The frequency (f) relates to the frequency response capability of the drive system and establishes the time of scan reversal. $\Theta, \dot\Theta,$ and $\ddot\Theta$ can now be computed.

$$f = \frac{1}{4t_1} \qquad\qquad t_1 = \frac{1}{4f} \quad \text{⑩}$$

where:
t_s = period for one line scan.

$$2t_1 + t_2 = t_s \qquad\qquad t_2 = t_s - 2t_1 \quad \text{⑪}$$

$$\dot\Theta_m = A\omega \text{ but } A = \Theta \therefore \dot\Theta_m = 2\pi f\Theta \quad \text{⑫}$$

The total length of linear scan can also be calculated as:

$$L = \frac{A}{\Theta_y}/1.3 \quad \text{⑬}$$

where:
A = Total area scanned
$\Theta_y/1.3$ = Beamwidth step in y direction

or:

$$L = \frac{1.3}{\Theta_y} A = \frac{A N_y}{\Psi_y} \quad \text{(14)}$$

Further;

$$L = L_{lin} + L_{turn}$$

$$= \dot{\Theta}_m T_2 + \frac{2 N_y \dot{\Theta}_m}{2 \pi f}$$

$$L = \dot{\Theta}_m \left(T_2 + \frac{N_y}{\pi f} \right) \quad \text{(15)}$$

where:

L_{lin} = Total scan in linear sector

L_{turn} = Scan length while turning

T_2 = Σt_2 = Total time spent in linear mode.

A relationship also exists between the times involved.

$$t_f = T_2 + 2 N_y t_1 = T_2 + \frac{N_y}{2f}$$

where:

t_f = period to scan one complete frame.

or

$$T_2 = t_f - \frac{N_y}{2f} \quad \text{(16)}$$

Introducing equation (16) into equation (15) gives:

$$L = \dot{\Theta}_m \left[t_f - \frac{N_y}{f} \left(\frac{1}{2} - \frac{1}{\pi} \right) \right]$$

or

$$\dot{\Theta}_m = \frac{L}{t_f} \left(\frac{f}{f - 0.1817 \frac{N_y}{t_f}} \right) \quad \text{(17)}$$

and

$$\Theta = \frac{\dot{\Theta}_m}{2 \pi f} = \frac{L}{2 \pi t_f \left(f - 0.1817 \frac{N_y}{t_f} \right)} \quad \text{(18)}$$

The pulse density efficiency f_d may also be related to these general parameters by the equation;

$$f_d = \frac{1 / \dot{\Theta}_m}{1.3 \, t_f / L}$$

$$= \frac{L / t_f}{1.3 \, \dot{\Theta}_m}$$

$$f_d = \frac{\left(f - 0.1817 \frac{N_y}{t_f} \right)}{1.3 \, f} \quad \text{(19)}$$

$$f_d = \frac{f - .412}{1.3\ f}$$

The geometrical efficienty for this case is:

$$f_g = \frac{\pi}{4} = .7854$$

thus the total scan efficiency may be calculated as:

$$f_s = .6042\ \frac{f - .412}{f} \times 1.3$$

In practice the overlap does not, on the basis of a total frame period, detract from scanning efficiency. All time on target enhances detection probability. More realistically the scan efficiency can be expressed:

$$f_d = \frac{f - .412}{f} \qquad \text{and} \qquad f_s = \frac{\pi}{4} f_d$$

Calculated values are tabulated below: (30 second frame time)

f	.412	1	2	4	6	8	12
f_s	0	.462	.624	.704	.73	.75	.753

5.4.2. WIGWAG SCAN; CIRCULAR CROSS-SECTION.

A circular cross-section for the scan frame can be obtained with the same wigwag mechanization as used for a rectangular cross-section except that the angular amplitude (A_x) is sinusoidally changed on successive line scans through a half cycle. See below:
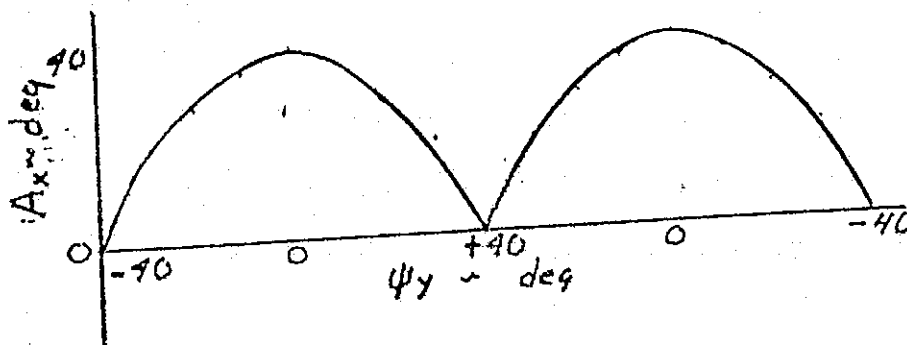
In this case:

$$f_s = f_d$$

appropriate values are tabulated below:

f	.412	1	2	4	6	8	12
f_f	0	.588	795	.90	.93	.955	.96

5.4.3. SPIRAL SCAN; CONSTANT ROTATIONAL SPEED

A spiral scan is produced by driving quadrature axes of a ractangle scan mechanism with sinusoidal signals of increasing amplitude and 90° out of phase; where:

$$x = a_x \cos \omega t \quad \textcircled{1}$$

$$y = a_y \sin \omega t \quad \textcircled{2}$$

Again using the values

$$\Theta_x = \Theta_y = 1.72°$$

$$\Psi_x = \Psi_y = 90° \text{ ie. } \pm 45°$$

$$t_f = 30 \text{ sec.}$$

Beam overlap = 1.3
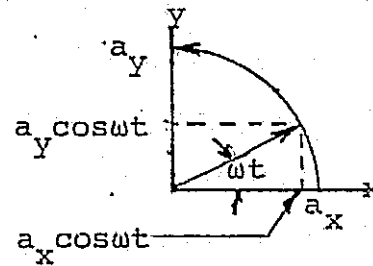
The number (n_t) of 2π rotations in a 45° spiraled area is:

$$n_t = \frac{45 \times 1.3}{1.72} = 34 \text{ and}$$

$$a_x = a_y = \frac{1.72}{1.3} \cdot \frac{34}{30} t \quad \textcircled{3}$$

$$\omega = 2\pi \cdot \frac{34}{30} \quad \textcircled{4}$$

The frequency responce is a constant ex.., f= <u>1.133 Hz.</u>

Further, the radius R equals:

$$R = \sqrt{x^2 + y^2} \text{ sub 1 \& 2} \qquad R = 2\pi \frac{34}{30} t \sqrt{\cos^2 \omega t + \sin^2 \omega t}$$

$$R = 2\pi \frac{34}{30} t \quad \textcircled{5}$$

The length of the spiral (L) is now computed:

$$L = \int_0^{68\pi} R d\Theta_\ell = \frac{1.72}{1.3} \frac{34}{30} + \int_0^{68\pi} d\Theta_\ell \quad \textcircled{6}$$

Where Θ_ℓ = the angle of travel as measured from the point of origin to the referenced point.

Also

$$\tan \Theta = \frac{y}{x} = \tan \omega t, \qquad \Theta = \omega t \quad \textcircled{7}$$

Substituting in 6

$$L = \frac{1.72}{1.3} \frac{34}{30} \omega \int_0^{30} tdt = \frac{1.72}{1.3} \frac{2\pi}{2} \frac{34}{30}^2 \left[t^2 \right]_0^{30}$$

$$L = \frac{1.72}{1.3} \pi \, 34^2 = \underline{4805°}$$

Note: As would be expected the total length of the scan travel is nearly the same as for the wig wag circular area scan (see 4.2.2.2.3)

The scanning efficiency of this system is calculated from:

$$\dot{Y}_{max} = a_y \omega \cos \omega t = \frac{1.72}{1.3} \cdot \frac{34}{30} \cdot 30 \cdot 2\pi \frac{34}{30} = 320.33 \, °/sec. \quad (8)$$

$$\tilde{Y} = \frac{L}{30} = \frac{4805}{30} = 160.167°/sec \quad (9)$$

$$f_s = f_d = \frac{160.167}{320.33} \times 1.3 = 65\%$$

Note: value 1.3 added in per previous note.

The scan geometry and operating constraints of the constant rotation speed conical scan mechanism establishes two important criteria.

1. The frequency response (f) of the drive system

    $f > 1.133$ Hz. (For $\Psi_x = \Psi_y = 90°, t_f = 30$ sec, $\theta_x = \theta_y = 1.7°, 1.3$ overlap)

2. The scanning efficiency is:

    $f_s = 65\%$

5.4.4.   SPIRAL SCAN: CONSTANT TANGENTIAL SPEED.

In the preceeding example the spiral scan mechanism was programmed with a constant rotation speed and the tangential velocity, due to the increasing radius of the scanning path, increases in proportion to the scan radius. The tangential velocity determines the beam overlap along the travel of the spiral. For maximum scanning efficiency it should be held constant. Unfortunately this is not possible , i.e., at zero radius the rotation speed is infinite. It is therefore necessary to establish some maximum value of $\dot\Theta$ that is consistant with the frequency response of the drive system and maintain that rotation velocity from the center of the scan out to that radius where the requirements for constant tangential velocity are accomplished with a decreasing value of rotational velocity. Basic relationships are:

$$R = K\Theta_\ell \quad \text{(1)} \qquad \Theta_\ell = \int \dot\Theta_\ell \, dt \quad \text{(2)}$$

$$x = R \cos \Theta_\ell = K \Theta_\ell \cos \Theta_\ell \quad \text{(3)} \qquad K = \frac{1.72}{(1.3)(2\pi)}$$

$$y = R \sin \Theta_\ell = K \Theta_\ell \sin \Theta_\ell \quad \text{(4)}$$

$$R\dot\Theta_t = \text{constant} = K\Theta_\ell\dot\Theta \quad \text{(5)}$$

where:

$$\dot\Theta_t = \text{tangential velocity.}$$

As previously stated $\dot\Theta$ must be some maximum value $(\dot\Theta_{max})$, related to frequency response of the system, from $\Theta_\ell=0$ to $\Theta_\ell=\Theta_{\ell 1}$. The frame (t_f) must be divided between these two scan programs.

$$t_f = \frac{\int_{\Theta_{\ell 1}}^{68\pi} K\Theta_\ell d\Theta_\ell}{K\,\Theta_\ell\dot\Theta_t} + \frac{\Theta_{\ell 1}}{2\pi f} \quad \text{(6)}$$

solving and entering fixed values in (6)

$$30 = \frac{1/2 K\Theta_\ell^2 \Big|_{\Theta_{\ell 1}}^{68\pi}}{K\Theta_{\ell 1} \cdot 2\pi f} + \frac{\Theta_{\ell 1}}{2\pi f} = \frac{1}{2\pi f}\left[\frac{1/2(68\pi)^2 - 1/2\Theta_{\ell 1}^2 + \Theta_{\ell 1}^2}{\Theta_{\ell 1}}\right]$$

$$\Theta_{\ell 1}^2 - 60(2\pi f)\Theta_{\ell 1} + 68\pi^2 = 0$$

$$\Theta_{\ell 1} = \frac{120\pi f \pm \sqrt{(120\pi f)^2 - 4 \times 68\pi^2}}{2}$$

Use negative value

$$\Theta_{\ell_1} = \pi(60f - \sqrt{3600f^2 - 68^2}) \tag{7}$$

Note:

$$f_{min} = 1.133 Hz.$$

The maximum tangential velocity occurs when Θ_{ℓ_1} is reached.

$$\dot{\Theta}_{max} = 2\pi Rf$$

Substituting (3) & value for K

$$\dot{\Theta}_{max} = \frac{2\pi \times 1.72 \Theta_{\ell_1} f}{(1.3)(2\pi)} = 1.32 \Theta_{\ell_1} f$$

The average velocity, refer equation (9), Section 5.4.3.

$$\dot{\hat{\Theta}} = 160.167°/sec$$

$$f_s = f_d = \frac{160.167}{1.320 \Theta_{\ell_1}} f1.3 = \frac{93.12 \times 1.3}{\Theta_{\ell_1} f} \tag{8}$$

Note: Factor 1.3 used per previous note

The following values can now be tabulated using equations (7) and (8) for appropriate values of f:

f	1.133	2	4	6	8	10
eff	.65	.912	98	.99	99.5	99.7

5.4.5. SUMMARY OF SCAN MECHANICS.

A plot of scanning efficiency as a function of drive system frequency response is shown in Figure 5.4-1. It is apparent that the best scanning efficiency can be achieved with a constant tangential speed, spiral scan.

A spiral scan is preferred during the radar rendezvous acquisition period. Its geometry matches the spacial geometry of the vectored search. The drive power associated with high scan rates involved is minimum. Scanning efficiency is improved by utilizing, to as great an extent as possible, a constant tangential speed program.

A wigwag scan is preferred for all other modes of operation; primarily, radar track, acquisition of the communication signal and tracking of the communication signal. This preference is based upon improved adaptation to servo control and is compatible with the reduced scan dynamics required. The error signals derived from the monopulse feed and associate hybrid circuitry are rectangularly oriented. The circular to rectangular coordinate transfer can be readily accomplished.

For future reference the analytical relationship between design parameters for the wigwag and spiral scan mechanizations are summarized in Figures 5.4-2 and 5.4-3.
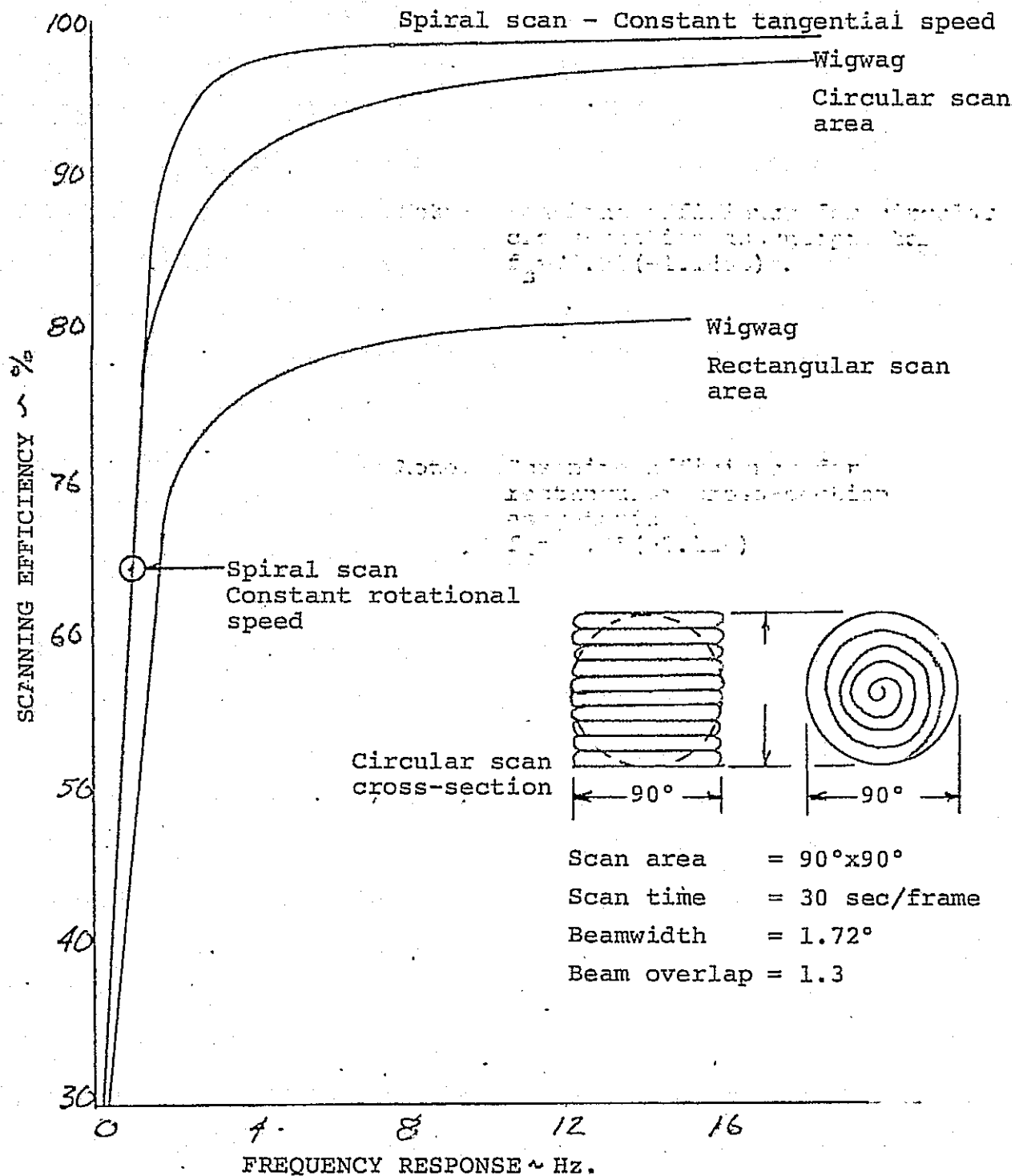
FIGURE 5.4-1   SCAN EFFICIENCIES VS FREQUENCY RESPONSES FOR VARIOUS MECHANIZATIONS.

A wig-wag or raster scan is accomplished by a cyclic motion in one direction (X) and a repetitive step function in the normal direction (Y). The X sweep is constant and equal to Ψ_x for rectangular scan coverage. The X sweep width can be programmed to vary in width as relative to (N_y) to cover a circular scan area. The step is the 2 way beamwidth ($BW_{2\ way}$) divided by the beam overlap, normally 1.3. A number of such steps (N_y) are required to cover the desired scan angle (Ψ_y).

$BW_{2way}/1.3$

$$N_y = 1.3\frac{\Psi_y}{\Theta_y}$$

$L = \Psi_x N_y$ (for rectangle)

$L = \frac{\pi}{4} \Psi_y N_y$ (for circle)

"X" dynamics

$$\dot{\Theta}_{x\ max} = \frac{L}{t_f} \left[\frac{f}{f - 0.1817\frac{N_y}{t_f}} \right]$$

$$\ddot{\Theta}_{x\ max} = \frac{\dot{\Theta}_{max}}{\omega} \qquad (\omega = 2\pi f)$$

$$\dddot{\Theta}_{x\ max} = \frac{\ddot{\Theta}_{max}}{\omega}$$

$$t_a = \frac{\pi\ \dot{\Theta}_{x\ max}}{2\ \ddot{\Theta}_{x\ max}}$$

"Y" dynamics

$$\Theta_{y\ max} = \frac{BW}{2.6}$$

$$\dot{\Theta}_{y\ max} = \Theta_{y\ max} \frac{\pi}{2\ t_a}$$

$$\ddot{\Theta}_{y\ max} = \Theta_{y\ max} \left[\frac{\pi}{2\ t_a} \right]^2$$
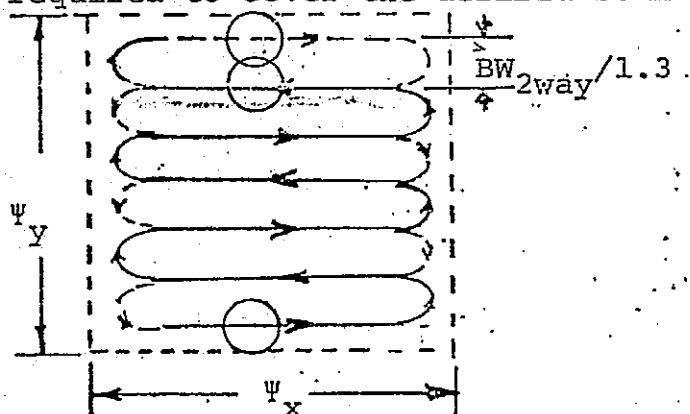
$\Psi_y =$ y scan angle, deg

$\Psi_x =$ x scan angle, deg

$BW_{2way} =$ 2 way beamwidth

N_y = number of y steps required to cover Ψ_y

L = total length of scan-deg

f = maximum frequency response of drive system, Hz.

t_f = fram time, sec.

$\dot{\Theta}_{x\ max}$ = maximum velocity of x scan - deg/sec.

Θ_x = angular travel along x during 1/2 reversal cycle, deg.

t_a = 1/2 period for end of scan reversal, sec.

$\Theta_{y\ max}$ = angular travel in y during reversal cycle-deg.

WIG WAG SCAN

FIGURE 5.4-2 5.43

The tangential velocity ($\dot{\Theta}_t$) determines the beam overlap along the travel of the spiral (Θ_ℓ). For maximum scanning efficiency it must be held constant. This is not possible; i.e., rotation speed ($\dot{\Theta}$) approaches ∞ as the radis (R) approaches 0. It is therefore necessary to establish some maximum value ($\dot{\Theta}_{max}$) of rotational velocity consistant with the frequency response of the drive system which is maintained out from the center to a radius where constant tangential velocity is maintained with decreasing values of rotational velocity.

BW$_2$ = 2 way beam width overlap = 1.3

Ψ = total nod angle

$N_t = \dfrac{1.3\Psi}{BW_2}$ = number of turns required for 1 frame
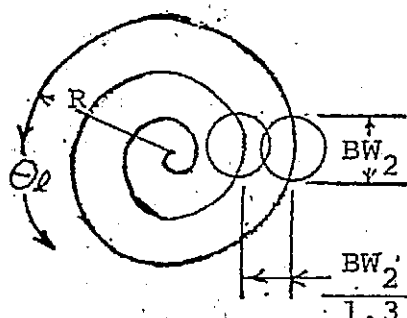
$L = \dfrac{BW}{1.3} \pi N_y^2$ deg.

$\Theta_{\ell 1} = ft_f - \sqrt{(ft_f)^2 - N_t^2}$ turns.

$f_{min} \geq \dfrac{N_t}{t_f}$ to achieve a spiral scan

$t_{d\,min} = \dfrac{1.3}{2\pi\Theta_{\ell 1} f}$ sec (1.3 = beam overlap) For R-Θ mechanism

$\dot{\Theta}_{max}$ = 360 f deg/sec (from 0 to $\Theta_{\ell 1}$)

$\ddot{\Theta}_{max}$ = 360 $f^2 (y - \dfrac{y^2}{2})$ where $y = 1 - \dfrac{\Theta_{\ell 1}}{\Theta_{\ell 1}+1}$

For x-y drive mechanism

$\dot{\Theta}_{\ell max} = \Theta_{\ell 1} \cdot \dfrac{BW}{1.3} \omega$ ($\omega = 2\pi f$)

$\ddot{\Theta}_{\ell max} = \dot{\Theta}_{\ell max} \omega$

L = total length of travel along spiral-deg

f = maximum frequency response of drive system, Hz.

t_f = frame time - sec.

$\Theta_{\ell 1}$ = the rotational angle (expressed as number of turns) along the spiral incurred at constant rotational velocity to the transition to constant tangential velocity

t_{dmin} = minimum dwell time

$\ddot{\Theta}_{max}$ = maximum rotational acceleration

$\dot{\Theta}_{\ell max}$ = max. x or y velocity required -deg/sec

$\ddot{\Theta}_{\ell max}$ = maximum x or y acceleration required - deg/sec^2

FIGURE 5.4.-3 SPIRAL SCAN, CONSTANT TANGENTIAL VELOCITY

5.5 MECHANICAL DESIGN.

The mounting arrangement, stow constraints, scan coverage, data rate requirements and design objectives relative to optimizing antenna gain, minizing power and weight, shape the mechanical design of the antenna. Requirements of immediate interest are:

Frame time......................	60 seconds.
Acquisition scan................	conical, 80° apex angle
Beamwidth.......................	1° (1m dia, 2 way; beamwidth a reference for analysis)
Beam overlap....................	1.3
Gimbal angle....................	2 perpendicular axes, continuous rotation
Gimbal rate (track).............	5°/sec
Gimbal acceleration (track)....	.04°/sec²
Gimbal angle position accuracy.	10 milliradians random
	60 milliradians bias
Gimbal angle rate accuracy.....	.14 milliradians/sec

A review of the above data indicates the dynamic requirements for the antenna are minimal during track. Servo power capabilities are determined by acquisition track dynamics which in turn relate to antenna size and weight. Plots of antenna characteristics versus reflector aperture are shown in Figures 5.5-1 and -2. This analysis has assumed a half gimbal for the trunnion mount and the use of 400 Hz 2φ servo motor and gear box drives. A near constant tangential speed, conical scan is implemented by sinusoidal wigwag in phase quadrature of the azimuth and elevation axes. Pertinent characteristics are:

> The antenna weight tends to be constant for small diameters due to the relative fixed weights assigned to the base mount and electronic, microwave, servo
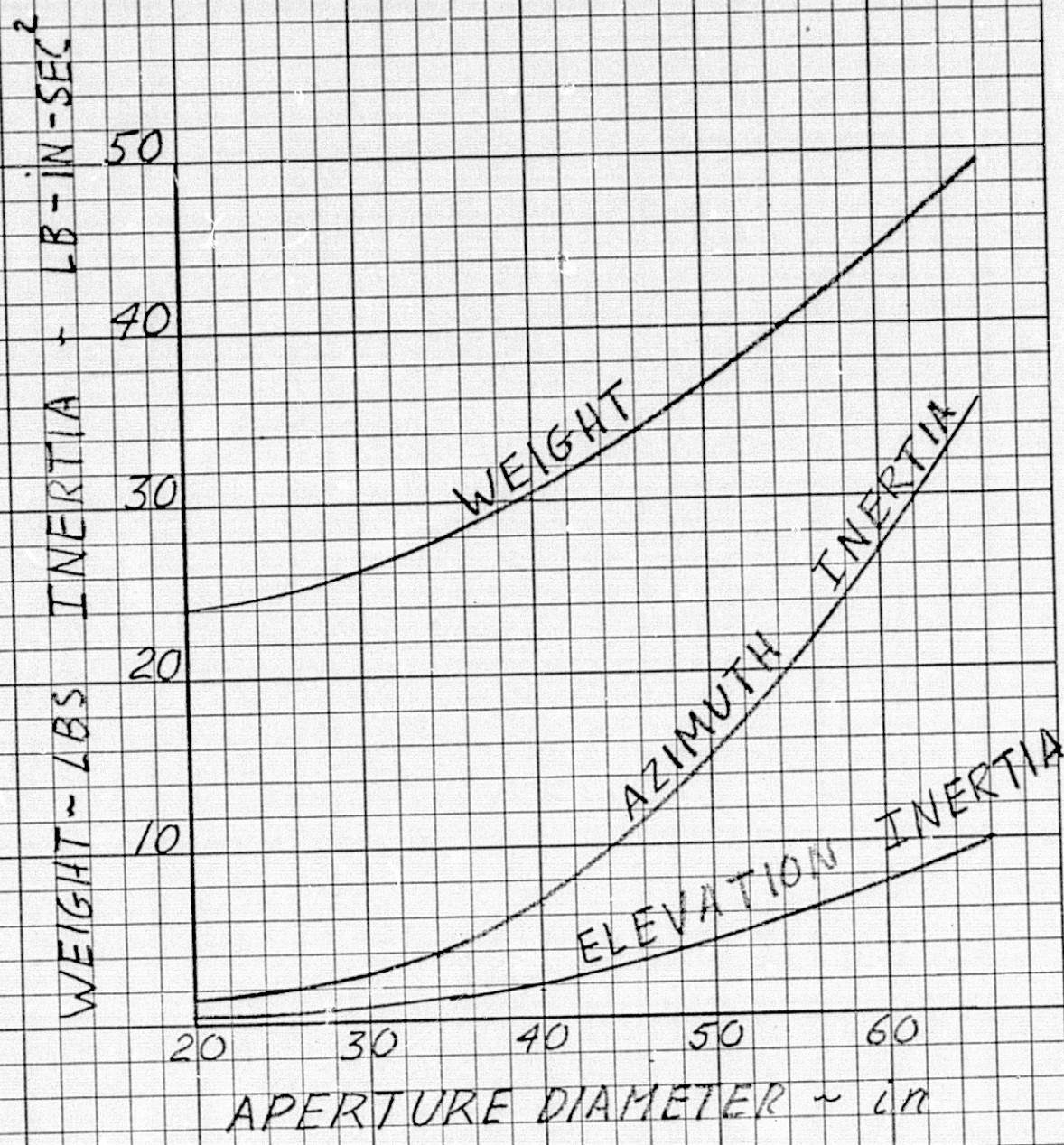
Fig 5.5-1 ANTENNA CHARACTERISTICS
VS
REFLECTOR APERTURE (1)
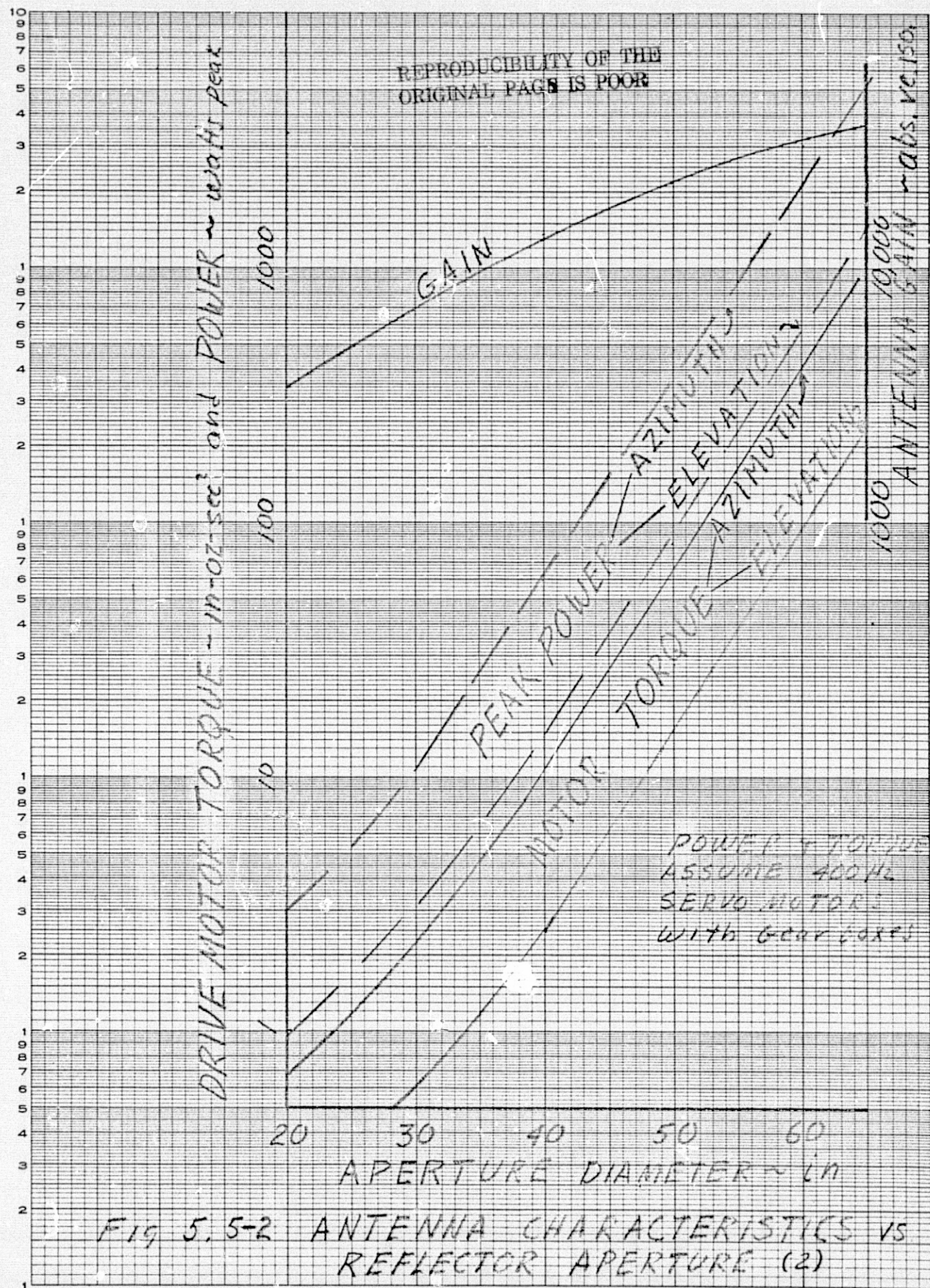
FIG 5.5-2 ANTENNA CHARACTERISTICS VS REFLECTOR APERTURE (2)

and gyro components. As the diameter (d) is increased the weight increases, primarily due to increased weight associated with the trunnion gimbal and drive power requirements.

Inertial loads around the elevation and azimuth axes tend to increase slowly for small diameters and more rapidly for larger diameters. The aximuth inertia increases more repidly than the elevation inertia. The microwave, servo and electronic components have fixed weights and mount near the center of rotation. Inertia associated with these components remains relatively constant. Inertia associated with the reflector and elevation gimbal increase as d^4. For larger reflector diameters the latter factor has a larger influence on total inertia.

The aximuth inertia increases faster than the elevation inertia because of the inertia of the elevation drive assembly and support gimbal. Both its weight and radius of gyration are functions of the reflector diameter and the resulting aximuth inertia to drive this load increases approximately as d^3.

The elevation and azimuth drive motor torques increase exponentially. Torque is proportional to a number of factors that all increase as a function of the reflector diameter; primarily:

$$T \propto \dot{\theta} \times \ddot{\theta} J$$

As the diameter is increased the beamwidth increases and the number of scan rotations per frame period is increased proportionally. The rotational speed (f) must be increased

As the diameter is increased the beamwidth increases and the number of scan rotations per frame period is increased to provide for the additional scan cycles. This in turn increases $\dot{\theta}$. As previously discussed J increases. The resulting torque is shown graphically in Figure 5.5-2.

Drive power requirements are directly related to torque and speed requirements.

Antenna gain increases as the square of the diameter. This is included in Figure 5.5-2 and provides a reference, so to speak, for value received (antenna gain) as a function of cost (drive power).

In the above curves the motor torque is based upon the use of a 400 Hz two phase servo motor and gearbox. Alternately, a DC brushless, torque motor can be used. Torque motor output requirements as a function of reflector aperture are shown in Figure 5.5-3. As a first estimate a DC torque motor is capable of driving a maximum size reflector of 40 to 45 inches in diameter. Under such conditions the drive motor is approximately 10" in diameter and dissapates 150 watts.

5.5.1. INSTALLATION CONSTRAINTS.

The antenna stows between the payload and payload doors from frames X=579 to 669. Refer Figure 5.5-4. A minimum clearance of 3" is to be maintained between the antenna assembly and the payload doors. The minimum clearance from the payload doors is, at this writing, under study. It shall be either 2" or 3". The antenna is to be stowed in the Z and Y positions where the aforementioned clearance can be maintained while providing the maximum volume possible for the antenna assembly. Note how the inner and outer mold lines fair in as they come forward; i.e., approach X=579. It is evident that the stowed antenna should be moved aft as far as possible to make use of the greater installation depth available. The limit here is the manipulator assembly centered at frame X=679.5.

FIG. 5.5-3. DRIVE PRESSURE VS. REACTOR
APERTURE

APERTURE DIAMETER — IN

3" Clearance for Payload

2"or3" Clearance for Payload Doors

Largest Payload → R=90"

Inner Mold Line

Outer Mold Line

⅛ Scale

Fig 5.5-4 INSTALLATION CONSTRAINTS
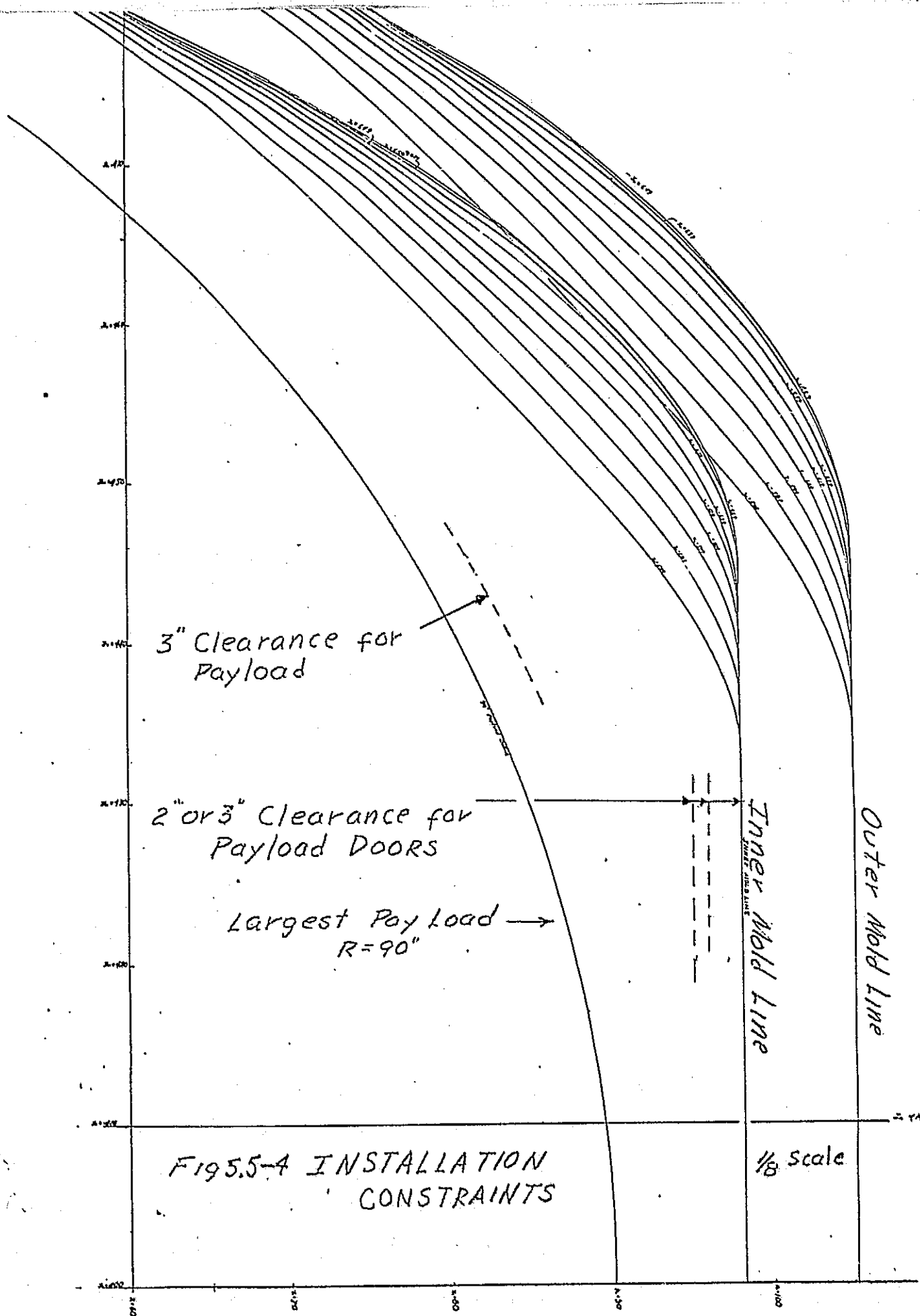
The antenna must be forward of the manipulator by the radius of the
reflector plus clearance. For example, a 40" diameter reflector
is centered on frame X=649.

A layout study was made to determine the relation between
diameter depth of a cylindrical volume capable of fitting within
defined constraints. The results are graphically shown in Figure 5.5-5.
The center of volume is located at:

>   X=649 (held fixed for this study)
>   Y=82 .to 90"
>   Z=446.5" to 449"

The maximum depth available for the antenna is 12.8" to 13.8",
depending upon the use of a 2" or 3" clearance from the payload
doors. This is the most restrictive dimension and is the basis
of a design approach utilizing a folded feed. This is discussed
in greater detail in other portions of the report.

The cylindrical volume must contain the trunnion gimbal,
elevation drive and the rotary joint-slip ring assemblies. A
favored position for the reflector is a mounting wherein the
center of gravity of the reflector assembly is located in the
center of volume of the clearance sphere and the rear side of
the reflector extends out of the cylindrical volume so as to fit
within the inner curve of the payload doors. This places the
feed on the payload side of the reflector. In the fore and aft
direction the reflector curves away from the cylindrical doors
so as to provide room for those microwave and servo components
that mount on the back of the reflector.

Another variable in mounting relates to the stow position
of the elevation axis. If it is normal to the x axis then the
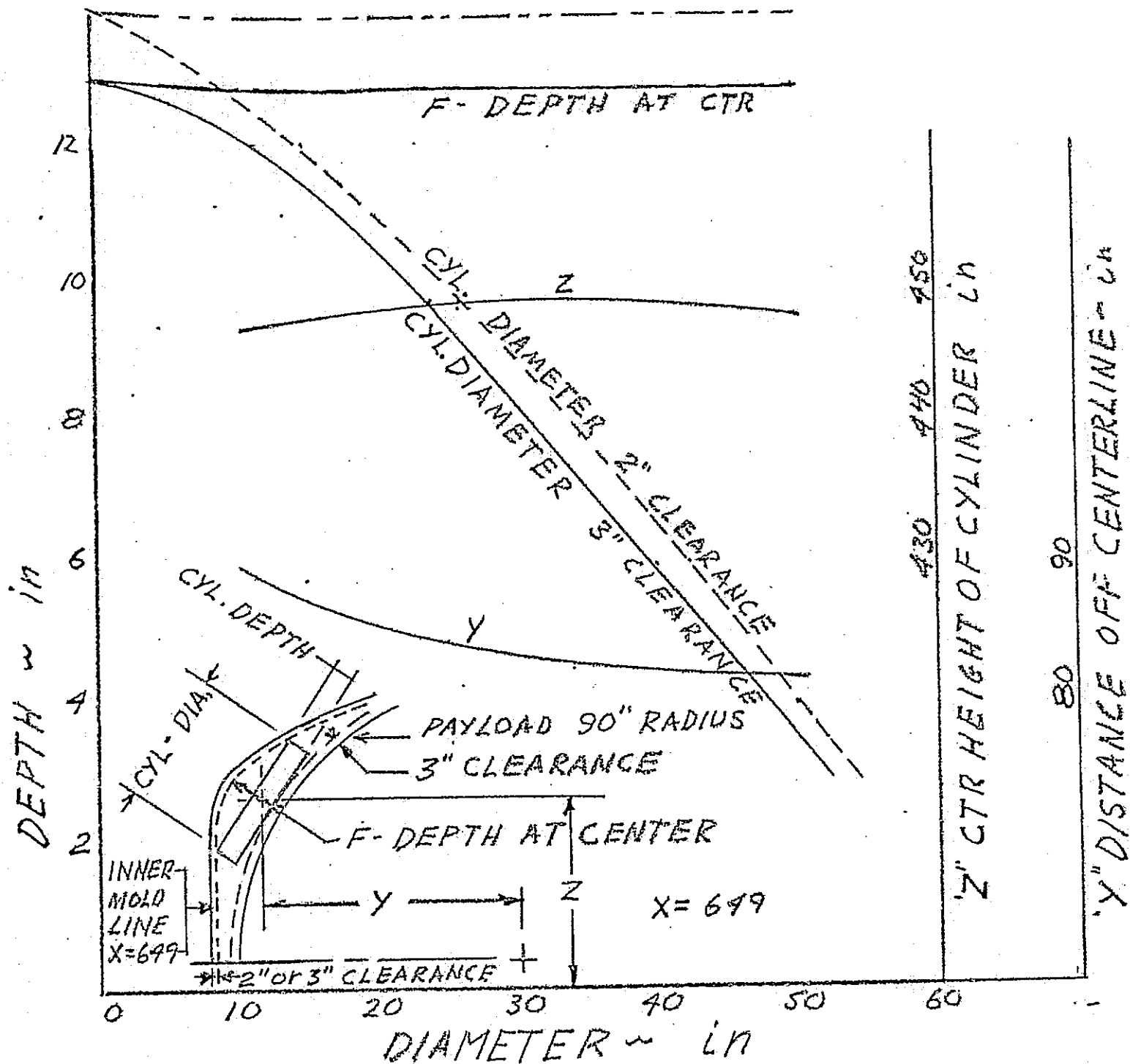
Fig 5.5-5 STOW VOLUME AVAILABLE FOR RADIATOR

trunnion mount, elevation drive assembly and rotary joint-slip ring assembly lies in a critical clearance area. This is avoided by rotating the slew position of the elevation axis towards parallelism with the x axis.

It is apparent that a number of factors influence the size of the radiating system that can be stowed within the designated installation area; primarily:

The 2" versus 3" clearance requirement relative to the payload door.

The stow position of the elevation axis relative to parallelism with the x axis.

The use of a fixed or folded feed.

The orientation of the antenna in the stowed position.

In using the fixed feed a minimal acceptable focal length is used resulting in an F/D ratio of .33. With a folded feed an F/D of .5 was used. Under these conditions the end of the feed clears the trunnion gimbal and the elevation axis can be continually rotated. A longer focal length can be used if the elevation motion is limited to approximately ±165°. The use of a longer focal length does not modify the dimensions of the maximum available aperture. The maximum antenna aperture as a function of applicable design parameters are listed in Table 5.5-1.

TABLE 5.5-1   MAXIMUM ANTENNA APERTURE AS A FUNCTION OF APPLICABLE
              DESIGN PARAMETERS.

Type of feed	Focal Length	Payload door clearance	Elevation axis ll or ⊥ to x axis	Stow orientation of feed	Maximum aperture
Fixed	11.5	3"	⊥	outboard	34" dia.
"	11.5	3"	ll	"	#34
"	13	2"	⊥	"	40"
"	13.	2"	ll	"	#40
Folded	25	3"	⊥	"	50
"	30	3"	ll	"	60
"	21	2"	⊥	"	53
"	32	2"	ll	"	63
"	20	3"	⊥	inboard	39
"	22	3"	ll	"	42
"	19	2"	⊥	"	41
"	21	2"	ll	"	45

#Note diameter limited by minimum acceptable focal length considerations.

5.5.2. ANTENNA ORIENTATION –SPACECRAFT COORDINATE INTERFACE.

For presentation of data it is necessary to determine the angular position and inertial rates of the antenna's line-of-sight (boresight axis) referenced to the spacecraft coordinates (x,y and z). The angular position of the boresight axis relative to the x,yand z axes of the spacecraft is measured in terms of two angles:

> μ – angular displacement from the z axis in plane yz; equivalent to the aximuth axis as measured to the port and starboard of the z axis.

> ν – angular displacement from the x axis to the line of sight; equivalent to the co-elevation angle referenced to the x axis.

This system of coordinates is the same functionally as described in baseline documents.

The system of coordinates chosen for the antenna reference system is as shown in FIgure 5.5-6 The boresight line-of-sight is described in terms of seven rotations, three angles which can be driven and four fixed angles. The three rotational angles are:

> Deployment axis – Ψ; function – deployment & stow positioning.
> Shaft axis – Θ; function – azimuth or spin scanning.
> Trunion axis – ϕ; function – elevation or nod scanning.

The four fixed angles involved in the mechanization of the antenna system are:

> α – angular displacement of the deployment axis from the x axis in the xy plane.
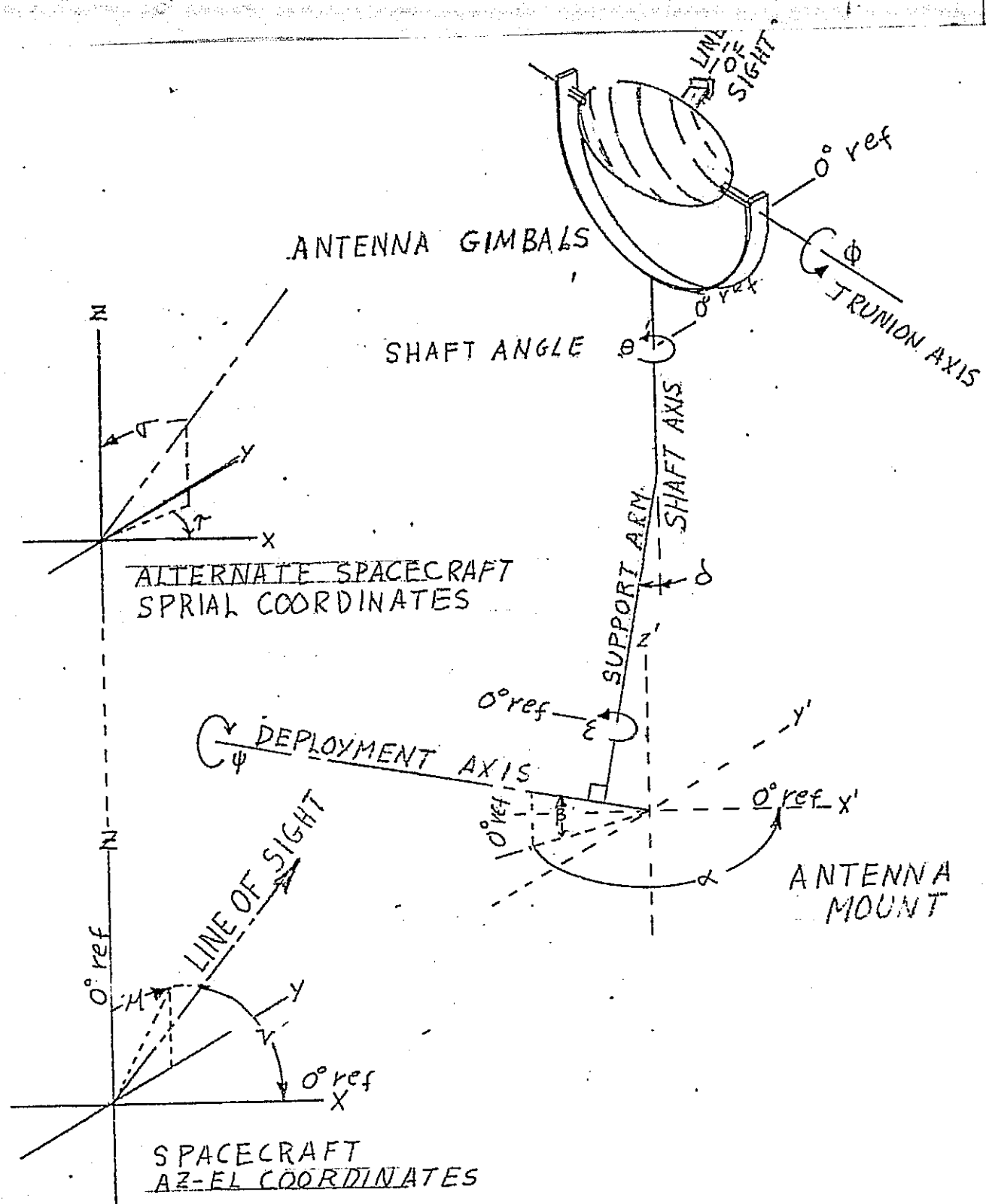
FIG. 5.5-6 COORDINATE REFERENCES

β — angular displacement of the deployment axis above and below the xy plane (positive angle above xy plane)

δ — angular displacement of the shaft axis relative to its support arm axis.

ϵ — rotational position of the support arm $\epsilon=0$ when δmax lies in the plane formed by the support arm and the deployment axis.

In the baseline system, Ψ is fixed at one of two positions, i.e., either stow or operate. Furthermore, during operation, the shaft axis is parallel to the x axis of the spacecraft. Translation from Θ and ϕ to μ and ν is direct, i.e., $\Theta=\mu$, $\phi=\nu$

In another system, when the antenna initiates a conical scan for acquisition, the shaft axis is made parallel to the z axis of the spacecraft and the transformation to μ and ν is simple. It will be shown later if the spacecraft coordinate system is made complimentary to the antenna's circular coordinate system, the translation is direct.

During track operation if the antenna is rotated in Ψ around the deployment axis, the translation of boresight angle into μ and ν then involves Θ, ϕ, and Ψ. The purpose of the latter motion is to avoid the requirement for tracking through a scanning pole.

In addition, it is necessary to translate antenna gimbal inertial rates $\dot{\Theta}$ and $\dot{\phi}$ into corresponding rates $\dot{\mu}$ and $\dot{\nu}$ relative to spacecraft coordinates.

5.5.2.1 LINE-OF-SIGHT ORIENTATION.

A matrix rotation is employed to determine the position of the antenna boresight axis with respect to the spacecraft coordinates. Define the unit vector $\begin{bmatrix} 1 \\ 0 \\ 0 \end{bmatrix}$ as the boresight axis position in the trunion coordinate system, and $\overline{X}$ as the boresight axis unit vector in the spacecraft coordinate system. In transforming the boresight axis position in the trunion coordinates to the spacecraft coordinates, the following matrix rotation equation must be satisfied:

$$\overline{X} = \begin{bmatrix} C\alpha & -S\alpha & 0 \\ S\alpha & C\alpha & 0 \\ 0 & 0 & 1 \end{bmatrix} \begin{bmatrix} 1 & 0 & 0 \\ 0 & C\beta & -S\beta \\ 0 & S\beta & C\beta \end{bmatrix} \begin{bmatrix} C\psi & 0 & S\psi \\ 0 & 1 & 0 \\ -S\psi & 0 & C\psi \end{bmatrix} \begin{bmatrix} 1 & 0 & 0 \\ 0 & C\varepsilon & -S\varepsilon \\ 0 & S\varepsilon & C\varepsilon \end{bmatrix} \begin{bmatrix} C\delta & -S\delta & 0 \\ S\delta & C\delta & 0 \\ 0 & 0 & 1 \end{bmatrix} \begin{bmatrix} 1 & 0 & 0 \\ 0 & C\theta & -S\theta \\ 0 & S\theta & C\theta \end{bmatrix} \begin{bmatrix} C\phi & 0 & S\phi \\ 0 & 1 & 0 \\ -S\phi & 0 & C\phi \end{bmatrix} \begin{bmatrix} 1 \\ 0 \\ 0 \end{bmatrix}$$

In the matrix rotation equation, the ϕ matrix denotes a rotation of the parabolic reflector through an angle ϕ around the trunion axis (y axis) in the trunion coordinate system; θ matrix denotes a rotation of the yoke assembly through an angle θ around the shaft axis (x axis) in the shaft coordinate system, δ matrix denotes a rotation of the shaft axis through an angle δ in the plane formed by the support arm and deployment axis in the shaft coordinate system; ε matrix denotes a rotation of the shaft and arm assembly through an angle ε around the support arm in the arm shaft coordinate system; ψ matrix denotes a rotation of the shaft axis through an angle ψ around the deployment axis in the deployment axis coordinate system; β matrix denotes the rotation of the deployment axis through an angle β relative to the x-y plane of the spacecraft coordinate system; α matrix denotes a rotation of the deployment axis through an angle α around the z axis of the spacecraft coordinate system.

5.5.2.2   BASELINE SYSTEM.

In the baseline system, α, β, δ and ε are fixed, and a single deployment position is chosen such that the shaft axis is parallel with the x axis. Under this condition, with proper choice of zero reference and ignoring parallax, the following relationships hold:

$$\mu = \Theta = 0$$
$$\nu = \phi = 0$$

when the antenna boresight axis is parallel to the x axis and pointing in the negative direction.

$$\mu = \Theta = 0$$
$$\nu = \phi = 90°$$

when the antenna boresight axis is parallel to the z axis and pointing in the positive direction.

5.5.2.3. CONICAL SCAN SYSTEM.

In this system, α, β, δ and ε are again fixed. The antenna is rotated about the deployment axis such that the shaft axis is parallel to the z axis. The components of the boresight axis as measured in the spacecraft coordinate system are again

$$\overline{X} = \begin{bmatrix} x \\ y \\ z \end{bmatrix} = \begin{bmatrix} 1 & 0 & 0 \\ 0 & C\mu & S\mu \\ 0 & S\mu & C\mu \end{bmatrix} \begin{bmatrix} C\nu & 0 & S\nu \\ 0 & 1 & 0 \\ -S\nu & 0 & C\nu \end{bmatrix} \begin{bmatrix} -1 \\ 0 \\ 0 \end{bmatrix} = \begin{bmatrix} -C\nu \\ S\mu S\nu \\ C\mu S\nu \end{bmatrix}$$

To obtain the correct orientation of the shaft axis (parallel to the z axis) and the proper reference for the shaft rotation θ requires the rotation matrix.

$$\begin{bmatrix} 0 & 0 & 1 \\ 0 & -1 & 0 \\ 1 & 0 & 0 \end{bmatrix}$$

Therefore, the boresight axis in antenna coordinates must be equal the spacecraft coordinates, or

$$\begin{bmatrix} 0 & 0 & 1 \\ 0 & -1 & 0 \\ 1 & 0 & 0 \end{bmatrix} \begin{bmatrix} 1 & 0 & 0 \\ 0 & C\theta & -S\theta \\ 0 & S\theta & C\theta \end{bmatrix} \begin{bmatrix} C\phi & 0 & S\phi \\ 0 & 1 & 0 \\ -S\phi & 0 & C\phi \end{bmatrix} \begin{bmatrix} 1 \\ 0 \\ 0 \end{bmatrix} = \begin{bmatrix} x \\ y \\ z \end{bmatrix} = \begin{bmatrix} 1 & 0 & 0 \\ 0 & C\mu & S\mu \\ 0 & -S\mu & C\mu \end{bmatrix} \begin{bmatrix} C\nu & 0 & S\nu \\ 0 & 1 & 0 \\ -S\nu & 0 & C\nu \end{bmatrix} \begin{bmatrix} -1 \\ 0 \\ 0 \end{bmatrix}$$

$$\begin{bmatrix} 0 & S\theta & C\theta \\ 0 & -C\theta & S\theta \\ 1 & 0 & 0 \end{bmatrix} \begin{bmatrix} C\phi \\ 0 \\ -S\phi \end{bmatrix} = \begin{bmatrix} 1 & 0 & 0 \\ 0 & C\mu & S\mu \\ 0 & -S\mu & C\mu \end{bmatrix} \begin{bmatrix} -C\nu \\ 0 \\ S\nu \end{bmatrix}$$

$$\begin{bmatrix} -C\theta S\phi \\ -S\theta S\phi \\ C\phi \end{bmatrix} = \begin{bmatrix} -C\nu \\ S\mu S\nu \\ C\mu S\nu \end{bmatrix}$$

Expanding the matrix rotation equation through matrix multiplications, the beam axis position in the spacecraft coordinate system is obtained as follows:

$$X = C\alpha C\delta C\phi C\Psi - C\alpha S\delta S\theta S\phi C\Psi + C\alpha S\epsilon C\delta C\phi S\Psi - C\alpha S\epsilon S\delta S\theta S\phi S\Psi$$
$$- C\alpha C\epsilon C\theta S\phi S\Psi - S\alpha C\beta C\epsilon S\delta C\phi - S\alpha C\beta C\epsilon C\delta S\theta S\phi$$
$$- S\alpha C\beta S\epsilon C\theta C\phi - S\alpha S\beta C\delta C\phi S\Psi + S\alpha S\beta S\delta S\theta S\phi S\Psi$$
$$+ S\alpha S\beta S\epsilon C\delta \ C\phi C\Psi - S\alpha S\beta S\epsilon S\delta S\theta S\phi C\Psi$$
$$- S\alpha S\beta C\epsilon C\theta S\phi C\Psi$$

$$Y = S\alpha C\epsilon C\phi C\Psi - S\alpha S\delta S\theta S\phi C\Psi + S\alpha S\epsilon C\delta \ C\phi S\Psi - S\alpha S\epsilon S\delta S\theta S\phi S\Psi$$
$$- S\alpha C\epsilon \ C\theta S\phi S\Psi + C\alpha C\beta C\epsilon S\delta \ C\phi + C\alpha C\beta C\epsilon C\delta S\theta S\phi$$
$$C\alpha C\beta S\epsilon C\theta C\phi + C\alpha S\beta C\delta C\phi S\Psi - C\alpha S\beta S\delta S\theta S\phi S\Psi$$
$$- C\alpha S\beta S\epsilon C\delta \ C\phi C\Psi + C\alpha S\beta S\epsilon S\delta S\theta S\phi C\Psi + C\alpha S\beta C\epsilon C\theta S\phi C\Psi$$

$$Z = S\beta C\epsilon S\delta C\phi + S\beta C\epsilon C\delta \ S\theta S\phi + S\beta S\epsilon C\theta C\phi - C\beta C\delta C\phi S\Psi$$
$$+ C\beta S\delta S\theta S\phi S\Psi + C\beta S\epsilon C\delta C\phi C\Psi - C\beta S\epsilon S\delta S\theta S\phi C\Psi$$
$$- C\beta C\epsilon C\theta S\phi C\Psi$$

where x, y, z are the vectorial components of the beam axis in the spacecraft coordinate system. $\overline{X}$ is a unitary vector, that is $x^2+y^2+z^2=1$,

and $x = \text{Cos } \nu$

$\quad , \ y = \text{Sin } \mu \ \text{Sin } \nu$

$\quad \quad z = \text{Cos } \mu \ \text{Sin } \nu.$

or $\begin{bmatrix} x \\ y \\ z \end{bmatrix} = \boxed{\overline{X}} = \begin{bmatrix} C\nu \\ S\mu \ S\nu \\ C\mu \ S\nu \end{bmatrix}$

These equations can then be solved in either direction, that is, find θ and ϕ in terms of μ and ν or find μ and ν in terms of θ and ϕ:

$$\theta = \text{Tan}^{-1}(-\text{Sin } \mu \tan \nu)$$
$$\phi = \text{Cos}^{-1}(\text{Cos } \mu \text{ Sin } \nu)$$
$$\text{or} \quad \nu = \text{Cos}^{-1}(\text{Cos } \theta \text{ Sin } \phi)$$
$$\mu = \text{Tan}^{-1}(-\text{Sin } \theta \tan \phi)$$

5.5.3. DEPLOY/STOW MECHANIZATION.

Studies to optimize the gimbal design are subject to a number of constraints; primarily:

(1) The antenna system, including associate electronic assembly, must stow within the volume between the payload and the payload door and between frames X=579 to X=669, with a minimum clearance of 3" from the surface of the largest payload (90") radius and 2" to all other structures. It must be recognized that there is presently a revaluation of clearance requirements that may require a minimum clearance of 3" all around.

(2) The antenna must deploy to a position forward from the leading edge of the door and outboard of the fuselage. The mechanical clearance of 3" is to be maintained.

The gimbal mechanics are analytically reviewed in the previous section of this report. The mathematical relationship between angular motions of the gimbal assembly relative to the spacecraft coordinance system were developed for the general case. The general equations are quite involved. The vector position of the antenna relative to the specefraft involve trigonometrical functions of three pairs of angles related to the antenna structure. If the antenna is oriented such that its azimuth and elevation axes are aligned with the axes of the spacecraft, the trigonometrical terms involving two angle pairs related to the antenna structure are eliminated. Furthermore, if the coordinate system of the antenna and the spacecraft are made similar, the angular relationships

become direct. There are three arrangements where the shaft axis of the deployed antenna is parallel to the X, Y or Z axis of the spacecraft that provides a direct angular relationship.

The shaft axis parallel to the Y axis of the spacecraft is referenced in the baseline study. The deployed antenna is shadowed by the spacecraft fuselage, wing structure or payload door structure. The use of two antennas on the port and starboard system eliminate the fuselage shadow. The need for dual antennas is inherent to the installation configuration.

A gimbal system, as described in the baseline study, can be modified to accomodate a parabolic reflector 1 meter in diameter. Reference Figure 5.5-7. The radiating system consists of 1 meter diameter paraboloid having a 33cm. focal length ($\frac{f}{d}$ = .33) illuminated by a 4 port "Cutler Type" backfeed.

As previously described, the hybrid waveguide circuitry required to process the 4 receiving signals to Σ, Δ El and ΔAz monopulse signals are integral to the feed structure. In addition, the polarizer is a wire grid assembly mounted in front of the slot radiating apertures. These two design factors reduce complexity, associate component loss and the size and weight associated with using catalog equivalents. Other factors pertinent in this design are:

(1) The antenna attaches to the existing mounting interface, X=589, Y=100, Z=425. Deploy axis is parallel to the "Z" axis.

(2) The gimbal assembly is to be mounted as far aft as possible, but clear the remote manipulator by 2". The purpose of going aft is to obtain the
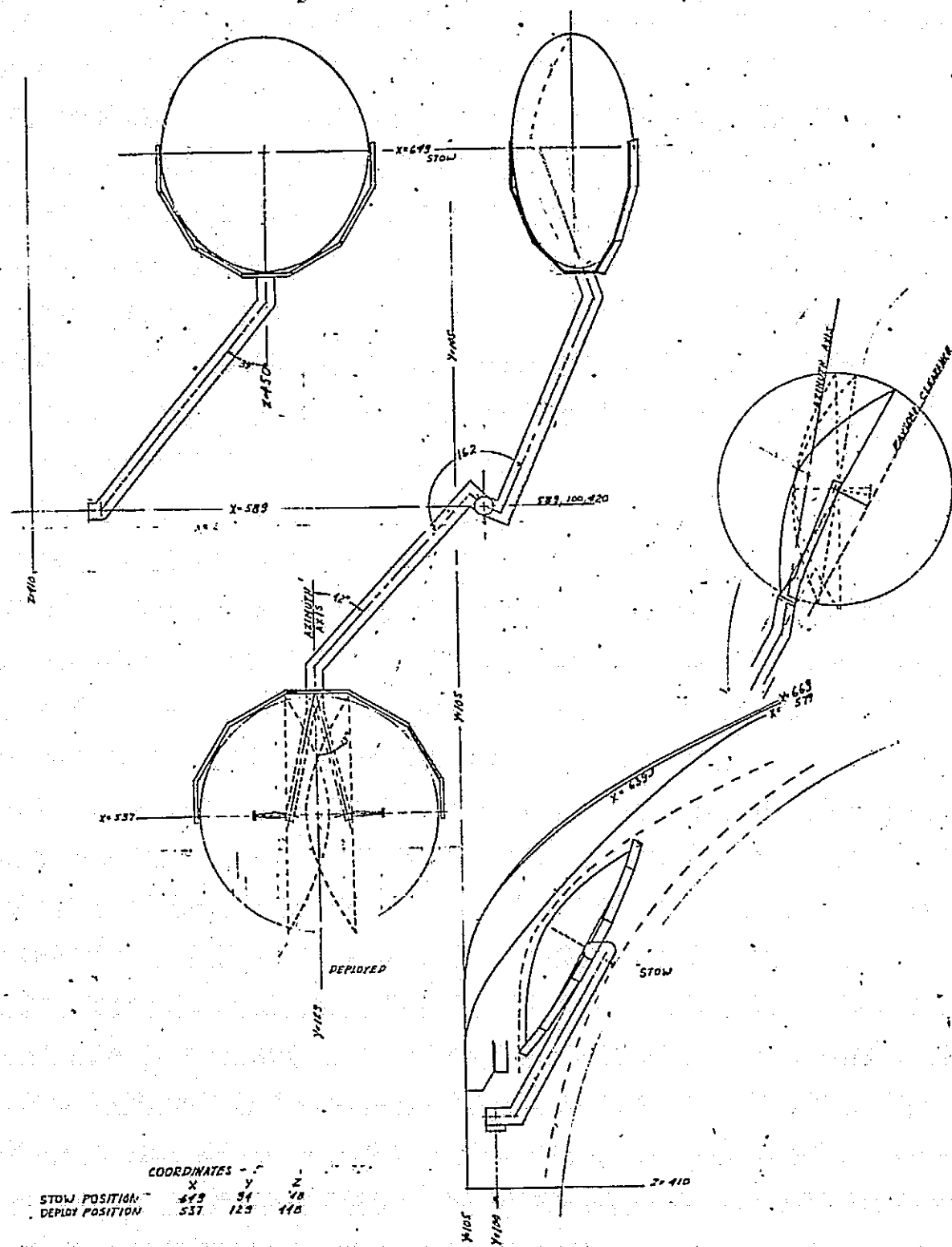
COORDINATES

	X	Y	Z
STOW POSITION	619	94	48
DEPLOY POSITION	537	123	118

maximum spacing possible between the payload and
the closed payload doors.

(3) The antenna is to be mounted at a height "Z"
that provides a maximum spacing between the
payload and the payload doors.

(4) There is adequate room for all electrical components
associated with the antenna's radiating structures;
such as pre-amps, mixers, rate integrating syros,
etc. They mount across the reflector's rear surface,
parallel to the "Y" axis and away from the reflector's
center line.

(5) The mounting structure for the antenna must have the
maximum offset angle possible in the XY plane. It
is this angle, in combination with the translation
offset available, that determines the separation
between the antenna structure and the spacecraft
fuselage when the antenna is in its deployed
position.

A gimbal study, refer Figure 5.5-7, indicates the following
arrangement is optimum for the stow and deployment of a 1 meter
diameter parabolic antenna.

POSITION	COORDINATES – CENTER OF PARABOLA FACE		
	X	Y	Z
Stow	649	94	448
Deploy	537	129	448

An alternate installation geometry for the antenna is described in Figure 5.5-8. In this design the axis of rotation for the deploy/stow mechanism is rotated to an optimum position such that the azimuth axis can be deployed to a position where it is parallel to either the "Z" or "Y" axis. Design factors 1 through 4 previously mentioned apply. Factor 5 is applicable but modified by the requirement for 2 deployed positions. A gimbal study indicated the following arrangement is optimum.

A projection of the deploy/stow rotation axis into the "Y" plane lies 23.5 degrees off parallel from the "Y" axis in a clockwise direction when viewed from above the spacecraft. Furthermore, it is 58.5 degrees off parallel from the "Z" axis.

POSITION	X	Y	Z
Stow	649	91	454
Deploy parallel to "Z" axis	600.5	130	480
Deploy parallel to "Y" axis	531.8	133	445

A difficulty is encountered with either of the aforementioned gimbal arrangements. In the stowed position, where the elevation axis tends to lie parallel to the "Z" axis, the elevation drive system, rotary joints, slip ring assemblies and gimbal structure lies in a critical clearance area. There are 5 solutions to the problem.

(1) The reflector can be made smaller in the azimuth plane; approximately 92cms.

(2) The elevation drive can be made remote from this critical area and the elevation motion coupled from

FIGURE 5.5.-8   INSTALLATION GEOMETRY OF THE ANTENNA.

the elevation gearbox output shaft to the elevation
axis through a steel tape drive. Angular alignment
can be maintained by means of a non-slip perforated
or lined steel tape.

(3) The elevation drive can be offset in the forward
     direction. This aggravates the unbalance problem.
     This factor is of secondary importance; but does
     aggrevate the "on earth" testing.

(4) Eliminate the fixed feed and use a folding type
     feed. A simple technique for accomplishing this
     is described in Section 5.3.6. This approach has
     several advantages in that the depth of the stowed
     gimbal and antenna assembly is no longer a function
     of a focal length requirement. The folded feed
     design can provide:

     (a) A larger reflector assembly approximately
          1.2m. in diameter.

     (b) Improved radiation characteristics. A longer
          focal length provides improved monopulse
          pattern characteristics.

     (c) Additional clearance for the gimbal system.
          Example: to provide a 3" clearance from the
          doors rather than the present 2".

     (d) Any combination of the above.

(5) Change the gimbal arrangement such that the elevation
     axis is rotated off parallel from the "Z" axis. This
     allows room for the elevation drive assembly.

The first, second and third approaches are undesirable and
deemed unnecessary. concepts 2 and 4 are discussed in other
sections.

A third arrangement for the antenna utilizing design approach
five is shown in Figure 5.5-9. Design factors 1 through 5
previously mentioned were observed. In the first and second design
approaches described, a parallel arrangement between antenna axes
and the spacecraft's axes during deployment of the antenna were
maintained. In this design approach the stow configuration is made
as simple as possible and the antenna rotated to a best deploy
position relative to minimizing shadow effects during both communication
and radar operation. Minimal considerations ere given to the relative
alignment of axes between the antenna and the spacecraft. This
design approach accepts the need for a mini-computer to convert
measured gimbal angles and rates into spacecraft coordinates.
Conversion requirements are discussed in Section 5.5.4.

Referring to Figure 5.5-9 it is noted that in the stow
position the shaft angle extends upward 45° off the "X" axis and
11° inboard from the "Y" axis. The gimbal system is rotated
providing adequate room for the elevation drive and indicator
assembly. Adequate area for the rate gyros and microwave components
is provided on the back of the reflector in the designated areas.
The elevation rotary joint and slip ring assembly mounts opposite
from the elevation drive system. The reflector assembly mounts
in a half gimbal, which in turn connects through the azimuth drive
assembly to the base mount. The azimuth drive contains the
motor-tack, synchro, gearbos, rotary joint and slip ring assemblies.
The base mount is a box structure suitable for containing
electronic hardware such as transmitter, etc. The deploy/stow
axis is parallel to the "Z" axis of the spacecraft. Pertinent
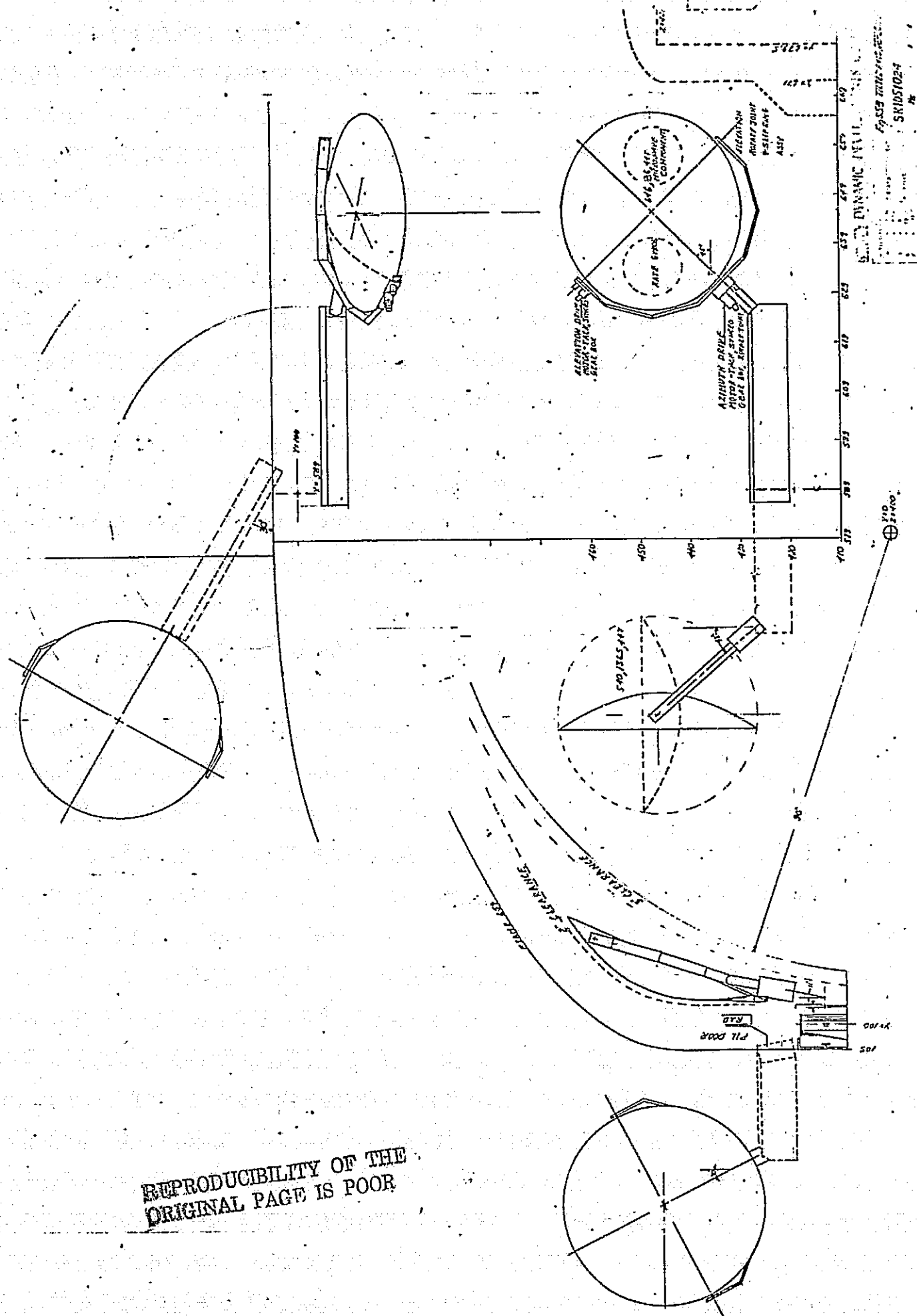
positional data is tabulated below:

POSITION	X	Y	Z
Stow	646	86	447
Deploy	540	136.5	447

Two gimbal antenna systems, capable of 4π steradian
scanning, encounter scan poles. As the antenna tracks to its pole
position the dynamics required by the outer gimbal become unaccept-
ably high. This pole exists whenever the target being tracked
becomes coaxial with the outer gimbal's scanning axis. Where less
than hemispherical coverage is required this condition can be
avoided by aligning the shaft axis along the scan horizon. In
this case, the scanning pole can be avoided. For the radar application
this requires that the shaft axis be displaced off parallel from
the "Z" axis by an angle greater than 45°.

In the communication mode of operation greater than
hemispherical coverage is required. A scanning pole exists;
for example, with the antenna scan mechanism of Figure 5.5-7
when the TDRS lies dead ahead of the space shuttle. This places
the target's line-of-sight coaxial with the shaft (or azimuth axis)
of the antenna. This condition can be avoided one of two ways.
The space shuttle can be maneuvered prior to reaching the scan
pole. Or alternately, when the antenna is within, say 3° of its
pole, the deploy/stow axis and therefore the shaft angle of the
antenna can be rotated back from the primary deploy position by 7°.
If later this 2nd position is approached to an offset of less than
3° the antenna will return to the primary stow position. This is
a scheduled function introduced occasionally as may be required.
The logic involved is simple. In practice this problem is only
encountered during communication tracking and angular position and
rate are not required. The correction need not be implemented.

When the antenna shaft is rotated out of the XY plane, as encountered with the deploy/stow mechanization of Figure 5.5-9 and conical scan is accomplished by a phase quadrature sinusoidal wigwag motion of the shaft and trunnion motions, the dynamics of the shaft axis are increased. The vectored position of the target to be acquired during acquisition search tends to lie along the Z axis of the spacecraft. It is the projection of this shaft angle along a line normal to the Z axis that determines the scan's angular amplitude along that line. If the shaft axis is canted, a greater angular motion of the shaft axis is required to produce a given change in its projected angle. Requirements for greater amplitude demand a correspondingly greater velocity and acceleration capability with an associate increase in servo power. In conclusion, from a standpoint of power conservation, it is desirable to have the deployed shaft axis lie in the XY plane.

A fourth arrangement for the deploy/stow mechanization is shown in Figure 5.5-10. In this case a folded feed is employed. In the deployed position the shaft axis lies in the XY plane but is not parallel to the Y axis. The angular orientation is convenient from a standpoint of optimizing the stow clearances and provides optimum scan coverage in the deploy position. In this example the clearance between the payload door and the antenna has been increased to 3". In fact, there is more than adequate clearance around the total antenna assembly in the stowed position. Furthermore, with the folded feed, a long focal length parabola can be used. In the example shown the focal length is some 28" and provides an optimum monopulse pattern. The feed does not clear the trunnion gimbal if the antenna is allowed to rotate a full 360°. It should be noted in the case where the feed approaches the gimbal interference the antenna is looking back into its own shadow, the shadow of the payload doors and the spacecraft wing section. A reduction in focal length to an F/D=.5 eliminates the interference

ANT STOWED - TOP VIEW

ANT STOWED - SIDE VIEW

Y=82

X=649

Z=456

TRUNNION DRIVE

SHAFT DRIVE

Z=420

TX/RX ELECTRONICS
4 X 8 X 24

ANT DEPLOYED
SHAFT DRIVE AT STOW POSITION

FWD EDGE OF DOOR

X=589

Y=100

X=535

ANT DEPLOYED
SHAFT DRIVE POSITIONED WITH
FEED & REFLECTOR PARALLEL TO Z AXIS

OML 649

IML 649
3.00 CLEARANCE TO IML 649

3.00 CLEARANCE TO 90.00 R

9.00 R

Y=130

Z=456

FEED IN STOWED
POSITION

Z=400

Y=82

Y=100

Z=420

148°

5:75

and has minimal change in pattern characteristics.

Because of the angular displacement of the shaft axis off the Y axis a mini-computer is required to compute angular position and rate relative to spacecraft coordinates.

5.6 MICROPROCESSOR PROGRAM TO COMPUTE ANTENNA BORESIGHT POSITION IN SPACECRAFT COORDINATES.

The antenna configuration shown in Figure 5.2-9 is not aligned, in its deployed position, with the coordinates of the spacecraft. As a result the transfer of boresight position in terms of gimbal angles and fixed angular orientation of the shaft axis relative to the spacecraft requires the use of a microprocessor and fixed software program to correct gimbal angles to spacecraft coordinates.

Given ϕ, Θ — antenna gimbal angles

Ψ, β, α — constants of the antenna support.

Method:

Each coordinate system is rotated to align with the coordinates of the successive coordinate system. Start with the vectors of the spacecraft coordinates (X,Y,Z).
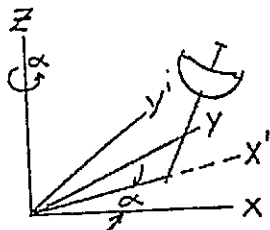
(1) Rotate antenna base structure about Z by an angle α to bring the X axis under the support arm. $\alpha = 30°$
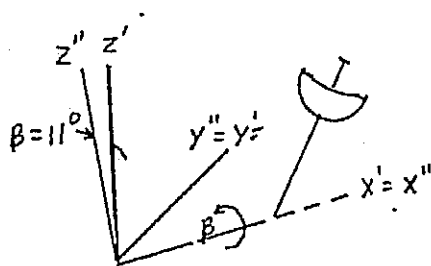
(2) The antenna support arm (shaft axis) is canted by an angle β from the base structure (spacecraft z). This cant is in the plane $y^1 z$. Rotate around x^1 by the angle β. $\beta = 11°$
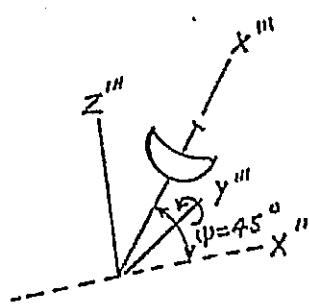
The shaft axis is also at an angle Ψ to the base structure. Ψ is contained within the X" `Z" plane. Rotate X" around the Y" axis by the angle Ψ. $\Psi=45°$.

Two more rotations are required. First the new coordinate system X''', Y''', Z''' must be rotated about X''' with the antenna shaft axis (θ). And finally, a rotation about Y'''' to align X_a with the antenna boresight. This can be best expressed in analytical terms with rotation matrices.

Rotate around an arbitrary X axis to map Y and Z into Y' and Z'. The sketch below provides the following relations.

$$X = X'$$
$$Y = Y' \cos\theta - Z' \sin\theta$$
$$Z = Y' \sin\theta + Z' \cos\theta$$

5.78
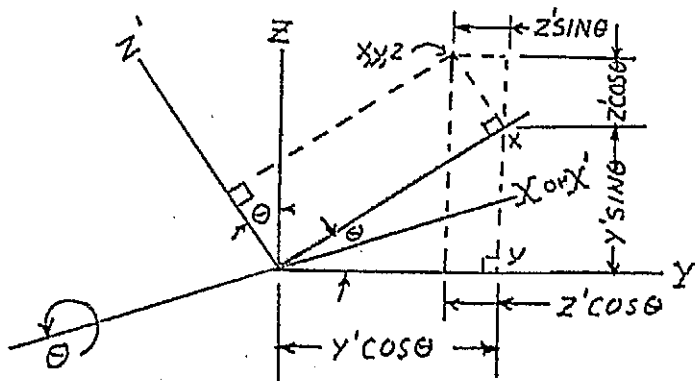
Matrix algebra provides a convenient way of writing these three equations.

$$[x \; y \; z] = \begin{bmatrix} 1 & 0 & 0 \\ 0 & c\Theta & -s\Theta \\ 0 & s\Theta & co\Theta \end{bmatrix} \begin{bmatrix} x' \\ y' \\ z' \end{bmatrix} \qquad \text{where:} \quad \begin{matrix} c = \text{cosine} \\ s = \text{sine} \\ t = \text{tangent} \end{matrix}$$

A multiplication of matricies provides:

$$\begin{bmatrix} 1 \cdot x' + 0 \cdot y' + 0 \cdot z' \\ 0 \cdot x' + c\Theta \cdot y' - s\Theta \cdot z' \\ 0 \cdot x' + s\Theta \cdot y' + c\Theta \cdot z' \end{bmatrix}$$

The rotational matricies take a form

for rotation around X
(as above)
$$\begin{bmatrix} 1 & 0 & 0 \\ 0 & c\Theta & -s\Theta \\ 0 & s\Theta & c\Theta \end{bmatrix}$$

for rotation around Y
$$\begin{bmatrix} c\Theta & 0 & \Theta \\ 0 & 1 & 0 \\ -s\Theta & 0 & c\Theta \end{bmatrix}$$

for rotation around Z
$$\begin{bmatrix} c\Theta & -s\Theta & 0 \\ s\Theta & c\Theta & 0 \\ 0 & 0 & 1 \end{bmatrix}$$

Referring to the original presentation relative to the rotation of spacecraft coordinates and successive rotating the vectors as discussed provides the following matrix equations.

5.79

$$
\begin{bmatrix} x \\ y \\ z \end{bmatrix} = \begin{bmatrix} c\alpha & -s\alpha & 0 \\ s\alpha & c\alpha & 0 \\ 0 & 0 & 1 \end{bmatrix} \begin{bmatrix} 1 & 0 & 0 \\ 0 & c\beta & -s\beta \\ 0 & s\beta & c\beta \end{bmatrix} \quad \text{continued below}
$$

(1) rotate around Z
$\alpha = 30°$

(2) rotate around X
$\beta = 11°$

$$
\begin{bmatrix} c\Psi & 0 & s\Psi \\ 0 & 1 & 0 \\ -s\Psi & 0 & c\Psi \end{bmatrix} \begin{bmatrix} 1 & 0 & 0 \\ 0 & c\Theta & -s\Theta \\ 0 & s\Theta & c\Theta \end{bmatrix} \quad \text{continued below}
$$

(3) rotate around Y
$\Psi = 45°$

(4) rotate around X varible
shaft angle Θ.

$$
\begin{bmatrix} c\phi & 0 & s\phi \\ 0 & 1 & 0 \\ -s\phi & 0 & c\phi \end{bmatrix} \quad X \quad \begin{bmatrix} x_a \\ y_a \\ z_a \end{bmatrix}
$$

(5) rotate around Y
varible Trunion angle ϕ

(6) unit vector along antenna
boresight can only be
1,0,0.

A somewhat tedious multiplication of the above matricies yields

$$
\begin{bmatrix} x \\ y \\ z \end{bmatrix} = \begin{bmatrix} A \cos\alpha & - c \sin\alpha \\ A \sin\alpha & + c \cos\alpha \\ \sin\beta \sin\Theta \sin\phi & + B \cos\beta \end{bmatrix}
$$

where: $A = -s\Psi \, c\Theta \, s\phi + c\Psi \, c\phi$

$B = -s\Psi \quad c\phi - c\Psi \, c\Theta \, s\phi$

$C = \quad c\beta \, s\Theta \, s\phi - B \, s\beta$

To simplify, substitute fixed values, i.e.,

$$\alpha = 30°$$
$$\beta = 11°$$
$$\Psi = 45°$$

then

$$A = .7071(\cos\phi - D)$$
$$B = -.7071(\cos\Psi + D)$$
$$C = .9816E - .1908B$$
$$D = \cos\theta \sin\phi$$
$$E = \sin\theta \sin\phi$$

and

$$x = .866A - .5C$$
$$y = .5 A + .866 C$$
$$z = .1908 E + .9816 B$$

The solution is quite easily implemented with a microprocessor of moderate speed. Specialized digital hardware can be implemented to convert ϕ and θ to spacecraft coordinates x,y,z or μ,υ where:

$$x = \cos \upsilon$$
$$y = \sin \mu \sin\upsilon$$
$$z = \cos \mu \sin\upsilon$$

Sines and cosines can be done by a "table look-up". Multiplication can be accomplished in a few microseconds.

To illustrate, a program has been written for D^2C desk-top calculator, a Compucorp #326. The program solves for x,y,z. The coding is included here, Figure 2.3.4., only to indicate the relative number of stops required for this computation. A microprocessor program can be executed in a few milliseconds.

TABLE 5.6-1   PROGRAM TO COMPUTE ANTENNA BORESIGHT POSITION INTO
              SPACECRAFT COORDINATES.

COMPUCORP #326   KEYSTROKES

1   .9816
f9 input   x
ss ϕ RCL 9
cos   -
Sto 1   [
f cos $^{-1}$ .1908
sin   x
Sto 2   RCL 6
z   ]
f 9 input   =
ss (θ)   Sto 7   (C)
cos   .866
Sto 3   x
f cos-1   RCL 5
sin   -
Sto 4   [
RCL 3   .5
x   x
RCL 2   RCL 7
=   ]
Sto 8   (D)   = output
RCL 2   ss   (X)
x   .5
RCL 4   x
=   RCL 5
Sto 9   (E)   +
.7071   [
Ch 5   .866
x   x
[RCL 7
RCL 1   ] output
+   =
RCL 8   ss   (Y)
]   .1908
=   x
Sto 6   (B)   RCL 9
.7071   +
x   [
[.9816
RCL 8   x
Ch5   RCL 6
+   ]
RCL 1   = output
]   ss   (Z)
=   Jmp
Sto 5   (A)   ss

5.82

5.7 DRIVE POWER REQUIREMENTS.

Drive power requirements for the antenna's gimbal system relate to loads in terms of inertia, friction unbalance and dynamic requirements in terms of angular motion, velocity and acceleration for the load. Weight and inertia estimates for the gimbal system are tabulated in Table 5.7-1. In summary:

Total antenna weight...................... 13.5 Kg (30lbs.)

Elevation inertia $\frac{WR_g}{g}$, J_{El} .... 1.57 in lbs.sec^2

Azimuth inertia $J_{Az}^{\#1}$ .... 6.46 in lbs.sec^2

Boom inertia $J_B^{\#1}$ .... 150 in lbs.sec^2

#1. Exclusive of drive motor inertia.

Peak dynamic requirements for the antenna gimbal mechanics are required during the acquisition scan. The following conditions apply:

Search volume (Ψ).................... 40° conical scan
Frame time (t_f)..................... 60 seconds
Beamwidth, one way .... 1.4°
Beamwidth, two way .... 1°
Beam overlap 1.3
Number of scan rotations 52

Consistent with both search and track modes of operation, good scan mechanism is accomplished with a recto-linear drive system. Spiral scan is accomplished by sinusoidal Wig-wag of two

Table 5.7-1. WEIGHT AND INERTIA ESTIMATE.

ITEM	WEIGHT IN POUNDS	(W) Kg.	RADIUS OF GYRATION (R_g) " El.	Az.	W R_g^2 in²-lbs. El.	Az.
Reflector, 1 m.	3	1.36	13	13	507	507
Central structure	1	.45	2	12	4	144
Feed	.4	.182	7	7	20	20
Feed drive	.25	.114	4	4	4	4
Polarizer	.25	.114	14	14	49	49
Polarizer drive	.25	.114	4	4	4	4
Waveguide on reflector	.2	.091	2	8	.8	12.8
Mixers and IF preamps	.66	.3	2	6	.8	7.2
Circulator	.3	.136	2	6	1.2	10
Δ channel switch	.54	.27	2	4	4.?	16
Frequency multiplier	.33	,15	2	8	1.3	21
Rotary joint and slip rings	.5	.227	.5	21	.1	220
Rate gyros	2	.91	2	4	8	32
Misc. wiring, connectors, etc.	2.27	1.03	1	8	2.27	145
Elevation assembly	12	5.45			606.5	1052
Azimuth gimbal	1.65	.75		14		323
Azimuth waveguide	.28	.13		8		18
Elevation drive	2.2	1		22		1065
Rotary joint and slip rings	.65	.29		1		.65
Misc. wiring, connectors, etc.	.22	.1		13		37
Azimuth assembly	5	2.27				2496
Gimbal assembly	17	7.73				
Base	2	.91				
Azimuth drive	5	2.27				
Electronic box	2.3	1.04				
Electronics		2.2				
Misc.	2.5	1.14				
Total weight	32	14.54				

Note moment of inertia around the deploy/stow axis = 150 lb-in sec^2

perpendicular gimbal axes in phase quadrature at linearly increasing amplitudes starting at the center (θ=0) to the maximum value (θ=40°). For maximum scan efficiency it is desired to scan the antenna at constant tangential velocity; however, this requires an infinite velocity at θ=0. As previously discussed, the practical solution is to scan the antenna at a maximum rate possible consistent with the gimbal structure and/or drive power limitations and then at a value $\theta = \theta l_1$ continue scanning at a constant tangential velocity through a scheduled decrease in rotational rate. With a constant tangential velocity the dwell time on target is held constant and maximum scanning efficiency is accomplished. In the central area, where the tangential rate is slower than desired, excessive dwell time is used. Fortunately this is in an area where the probability of detection is greatest. Pertinent relationships were summarized in Section 5.4 and summarized in Figures 5.4-2 & 5.4-3. The starting position for constant tangential velocity is:

$$\theta l_1 = ft_f - \sqrt{(ft_f)^2 - N_t}$$

The drive motor torque rating relates to θ_{ℓ_i} as follows:

$$\dot{\theta}_{max} = \frac{\theta_{\ell_1} \omega}{1.3} \qquad \omega = 2\pi f$$

$$\ddot{\theta}_{max} = \frac{\theta_{\ell_1} \omega^2}{1.3} \qquad 1.3 = \text{Beam overlap.}$$

The dynamic requirements must be matched through a gear transfer to the dynamic characteristics of an appropriate motor. Consider a 4 pole, 400 Hz. 2 phase servo motor having a synchronous speed of 12,000 rpm and a nominal working speed of

5,000 rpm. The gear ratio (G) matches these working

$$T = \frac{\ddot{\Theta}J}{G}$$

$$G = \frac{m_s}{\dot{\Theta}} \qquad\qquad G = \text{gear ratio}$$

$$T = \frac{\dot{\Theta}\ddot{\Theta}J}{m_s e} \qquad\qquad m_s = \text{working motor speed} = 3\times10^4 \text{deg/sec}$$

$$e = \text{transfer efficiency, i.e.,}$$
$$\text{friction loss} = .85$$

for $J = 6.46$ in-lb sec.^{2} or 103.36 in-oz sec^2

$$T = \left(\frac{\Theta_{\ell_1}}{1.3}\omega\right)\left(\frac{\Theta_{\ell_1}}{1.3}\omega^2\right)\left(\frac{103.36}{57.3\times 3\times10^4\times.85}\right)$$

$$T = \overset{\#1}{.01039} \; \Theta_{\ell_1}{}^2 \; f^3 \quad 0z\text{-in.}$$

#1. Exclusive of drive motor inertia.

For a chosen drive motor speed, torque is directly related to servo power requirements. Recall that the scanning efficiency and therefore the detection range of the radar is improved as a function of the antenna's frequency response. It is necessary to quantitize these effects. The scanning efficiency (f_g) is defined as:

$$f_s = \frac{\text{minimum dwell time during scan}}{\text{average time on target}} = \frac{t_d \text{ min}}{t_d \text{ avg}}$$

$$t_d \text{ avg} = \frac{60\times1.3}{\pi 52^2} = .00918 \text{ sec.}$$

where 60 = frame time
        52 = number of revolutions

$$t_d \text{min} = \frac{1.3}{2\pi f \Theta_{\ell_1}}$$

The detection range of the radar system is a function of the scanning efficiency. This can most easily be analyzed in terms of a pulse radar system; however, such analysis is applicable to all other types. In the range (R) equation

$$R^4 \; \alpha \; \frac{1}{S/N}$$

For a given set of conditions, a plot of signal-to-noise ratio (S/N) vs the number of pulses (n) integrated for various target types (Swerling, etc.) has a slope such that

$$S/N \; \alpha \; n^{-\,.7}$$

and

$$n \; \alpha \; t_d \text{ and } f_s \qquad t_d = \text{dwell time}$$

thus

$$R \; \alpha \; n^{.7/4} = n^{.175} \text{ Pwr.}$$

Pertinent data relative to choosing frequency responses of space shuttle antenna is shown in Table 5.7-2.

Graphical comparison of pertinent data to choose antenna frequency response is plotted in Figure 5.7-1. The maximum drive motor torque required is reasonably flat between f= 1.1 to 1.3 Hz. Choosing the upper value results in:

Antenna maximum rotational rate..... 1.3 rps
Maximum drive torque................ (azimuth≈9 oz-in)
Scanning efficiency 87.5%
Realized detection range............ 98.5% of maximum available.

TABLE 5.7-2. DATA PERTINENT TO CHOOSING FREQUENCY RESPONSE.

f	.867	1	1.2	1.4	1.5	1.6	1.8	2	∞	H_z
Θ_{ℓ_1}	52	30.07	22.2	18.03	16.54	15.3	13.34	11.85	0	revolutions
t_d min	.0046	.00688	.00777	.0082	.00834	.00845	.00862	.00873	.00918	sec
E_s	50.1	74.9	84.6	89.3	90.8	92.0	93.9	95.1	100	%
T_{AZ}	18.3	9.39	8.85	9.27	9.59	9.96	10.78	11.67		
$\dfrac{R}{R\ max}$	88.5	95	97.3	98.3	98.5	99	99.2	99.5	100%	%

RECOMMENDED OPERATION

1   12   14   16   18   2
FREQUENCY ~ Hz

18   50   60   70   80   90   100
SCAN EFFICIENCY   %

1   12   14   16   18   2
FREQUENCY ~ Hz

50   60   70   80   90   100
SCAN EFFICIENCY

FIG 5.7-1   GRAPHICAL COMPARISON OF
PERTINENT DATA TO CHOOSE
ANTENNA FREQUENCY RESPONSE
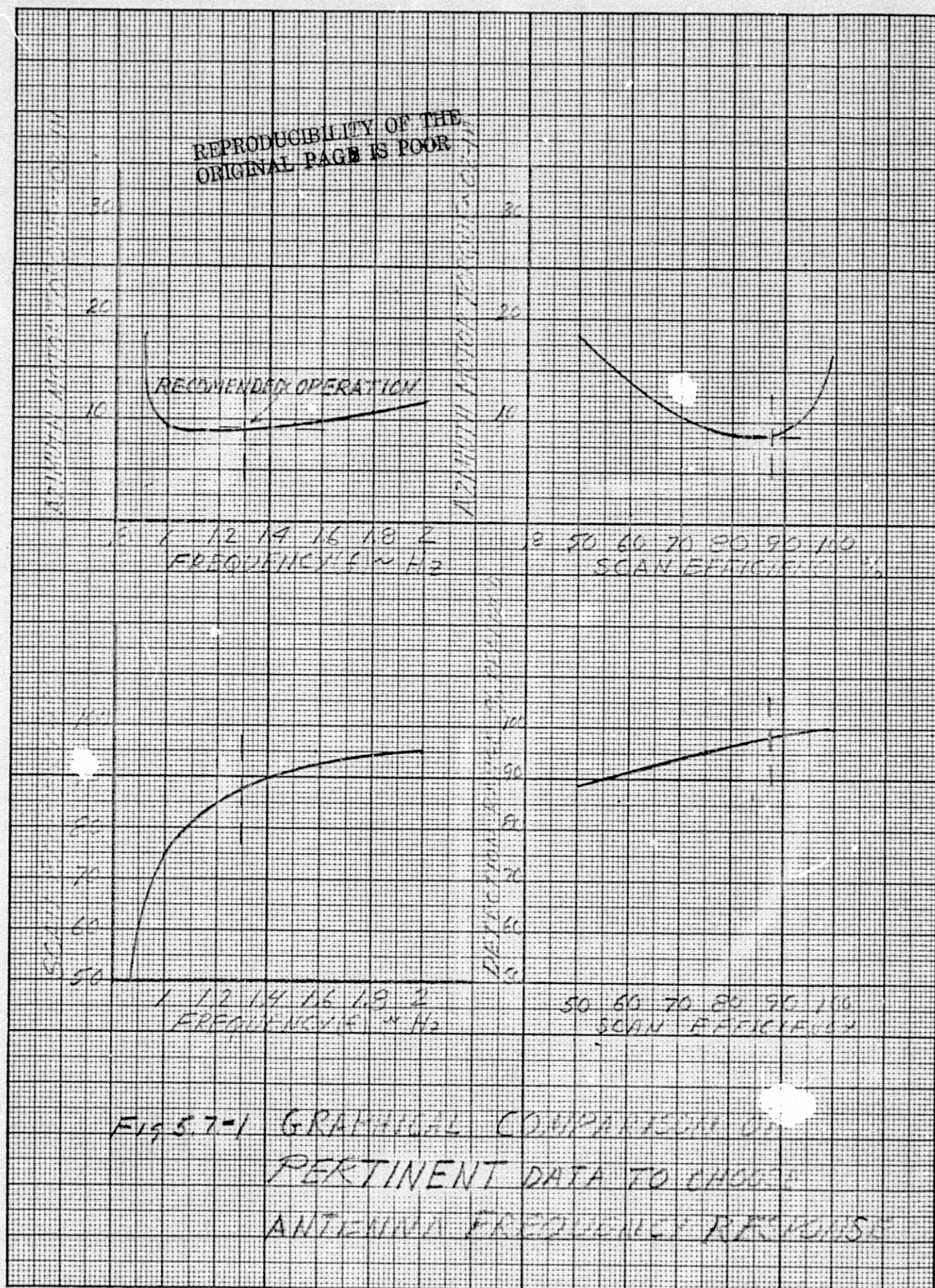
At $f = 1.3$ Hz., $\theta_{\ell_1} = 19.86$ revolutions and

$$\theta = 15.27 \text{ degrees}$$
$$\dot{\theta} = \theta\omega = 124.8°/\text{sec}$$
$$\ddot{\theta} = \theta\omega^2 = 1019.4°/\text{sec}^2$$

These maximum values only occur at 19.86 scan revolutions, or a 15.27 degree scan angle, from the scan axis. Dynamic requirements increase from the start of the scan to these maximum values and then decrease for scan angles greater than 22.2°. Pertinent data is summarized in the table 5.7-3 and graphically presented in Figure 5.7-2. As a result:

Drive motor	Peak torque	Average torque
Elevation	2.19 oz-in	1.36 oz-in
Azimuth	9 oz-in	5.59 oz-in

Servo component characteristics are summarized in Table 5.7-4. Size 18 servo motors are used in both azimuth and elevation; however, the former is longer than the latter. Identical gear boxes and synchros are used on each axis.

Value for torque during the radar acquisition scan are valid for the antenna configuration of 5.5-7 where the axis of the vectored radar acquisition scan lies along the "Z" axis and therefore perpendicular to the azimuth (shaft) axis of the gimbal antenna. This condition does not exist, for example, with the antenna configuration of 5.5-9 In this case the inner or elevation gimbal can be oriented to an optimum alignment and the maximum torque involved is the value previously calculated. The antenna's azimuth axis, in its deployed position, is displaced from the "Z" axis by approximately 30°. The increased angular displacement around to shaft axis to provide for the project angle acan increases the azimuth motor torque to 18 oz-in. This is acceptable to the antenna operation but does represent an increase in peak servo power required.

TABLE 5.7-3.. SCAN DYNAMICS.

Relationship	For $\theta=0°$ to 15.27	For $\theta=15.27$ to 40°
	$\omega =8.168$ rad/sec	$\omega =8.168$ to 3.19 rad/sec
	$f =1.3$ Hz.	$f =1.3$ to .508 Hz.
$\dot{\theta} = \theta\omega$	$\dot{\theta} =0$ to 124.7°/sec	$\dot{\theta} =124.7°/sec.$ constant
$\ddot{\theta} = \theta\omega^2$	$\ddot{\theta} =0$ to 1019°/sec^2	$\ddot{\theta} =1019$ to 398/sec^2
$G = \dfrac{3000}{\dot{\theta}max}$	$G =240$	$G = 240$
$T^* = \dfrac{\ddot{\theta}J}{85} \times \dfrac{16}{57.3}$	$T_e=0-2.19$ oz-in	$T_e=2.19$ to .856 oz-in
	$T_a=0-9$ oz-in	$T_a=9$ to 3.52 oz-in

* Exclusive of drive motor inertia.

Fig 5.7-2 AQUISITION SCAN PROGRAM

CONDITIONS
FRAME TIME = 1 SEC
SCAN 80 CONICAL
ANT - 1 m PARABOLOID
$J_{EL} = 1.57$ in-lbs-sec^2
$J_{AZ} = 6.46$ in-lbs-sec^2

TANGENTIAL VELOCITY

AZIMUTH DRIVE MOTOR TORQUE
Avg $T_{AZ} = 5.59$ oz-in

SCAN TIME

ELEVATION DRIVE MOTOR TORQUE
Avg $T_{EL} = 1.36$ oz-in

MOTOR TORQUE - OZ-INCHES

TANGENTIAL VELOCITY ~ deg/sec

SCAN TIME ~ sec

SCAN ANGLE ~ deg off AXIS

5.92
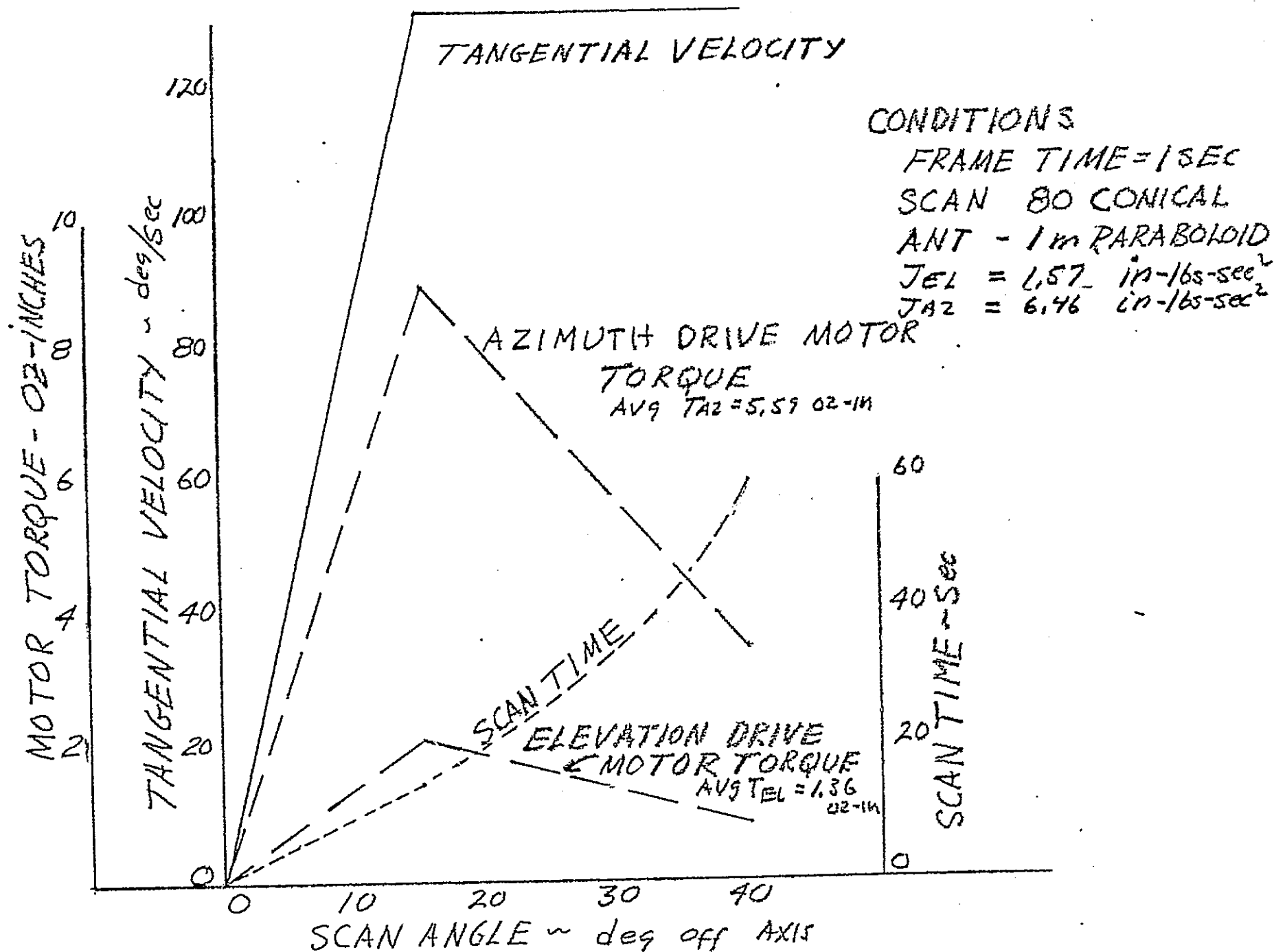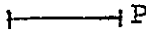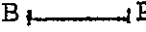
TABLE 5.7-4. AZIMUTH AND ELEVATION DRIVE COMPONENTS.

	Elevation drive motor	Azimuth drive motor
Peak torque	2.19 oz-in	9 oz-in
Avg. torque during acquisition.(60 sec)	1.36 oz-in	5.59 oz-in
Motor tach size	1.75"dia.x3.38	1.75" dia.x 4.5
Weight	1 lb.	2 lbs.
Motor peak power	30 watts	80 watts
Motor avg. power (acquisition 60 sec.)	19 watts	50 watts
Tach power	1.5 watts	1.5 watts
Synchro size	.8" dia.x1.68"	.8" dia.x1.68"
weight	2 oz.	2 oz.
power	1.5 watts	1.5 watts

Gearbox ratio 315:1

gears P-pinion,B-bull	P	B⊢——⊣P		B⊢——⊣P		B
ratio		39		8		10
no. teeth	22	89	18	144	18	180
pitch	96	96	96	96	72	72
diameter	.229"	.927"	.1875"	1.5"	.25"	2.5"

Sub assembly weight	2.2 lbs.	5 lbs.

5.7.1 SPIRAL SCAN USING A SPIN AXIS.

An Alternate scan technique can be considered wherein the
spiral scan is accomplished with a rotary drive around the shaft
axis in combination with an increasing tilt (trunnion angle) off
the spin axis. Drive dynamics, in terms of accelleration and
torque requirements during acquisition scan are drastically
reduced. Utilizingthe same dynamics as discussed in the previous
paragraphs; primarily:

Frame time.......................	60 seconds
Maximum rotational speed........	$\dot{\theta} = 125°/sec$
Beamwidth........................	1° (two-way)
Beam overlap....................	1.3
Number of revolutions (N).......	50

The first step is to determine appropriate values for
accelleration and frequency response. During the tracking phase
of operation the maximum velocities and accellerations involved
are:

$$\dot{\theta} = 5°/sec$$
$$\ddot{\theta} = .04°/sec^2$$

During the acquisition scan the velocity requirements can be
established. The elevation axis must move a total of 40° during
the frame time of 60 seconds, i.e., an average velocity of .67°/sec.
The maximum azimuth spin rate is 125°/sec . A choice of accelleration
requirements is somewhat arbitrary. The most stringent requirement
exists during the transition to track lock-on. The objective is
to reduce this transition time to a minimum within the practicalities
of the servo system. The related factor is the frequency response
of the servo system. This is most critical in the azimuth axis

where the higher rates and inertia are involved.

A plot of the time to the first overshoot and the shaft axis torque as a function of frequency response is shown in Figure 5.7-3. All things considered it would appear that a 1 second period to the first overshoot is a reasonable compromise, i.e.,:

$$\omega = 1$$
$$f = .16 \text{ Hz}$$

A comparison of the torque requirements for the spin drive (R,θ) and the rectilinear drives (x,y) are listed in Table 5.7-4. Torque requirements and the associate drive power requirements are substantially reduced. This method of drive involves a companion decision; primarily, the deploy/stow mechanism must be of the type shown in Figure 5.5-8. With this mechanization the shaft axis of the deployed antenna can be made parallel to the z axis of the spacecraft.

Fig. 5.7.3 AQUISITION TO TRACK TRANSITION DYNAMICS

SHAFT AXIS TORQUE

TIME TO FIRST OVERSHOOT

FREQUENCY RESPONSE ~ Hz

TIME TO 1st OVERSHOOT - SEC, TORQUE ~ IN-lbs x10⁻¹
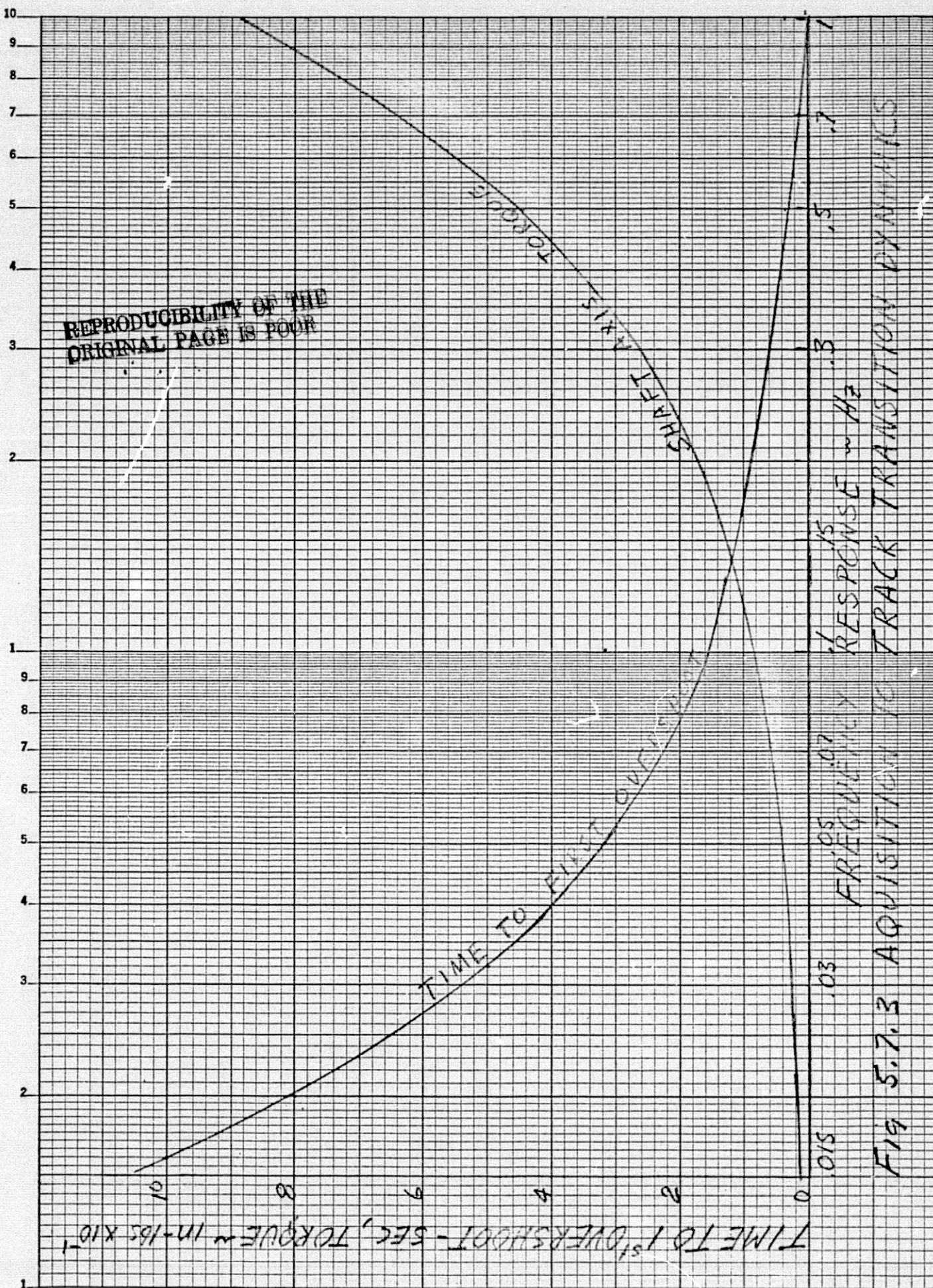
TABLE 5.7-4   COMPARISON OF TORQUE REQUIREMENTS FOR R,Θ and X,Y DRIVES.

	R,Θ spiral coordinates	X,Y rectilinear coordinates
f	.16 Hz	1.3 Hz
$\dot{\Theta}_{el}$	.67°/sec	125°/sec
$\ddot{\Theta}_{el}$	.67°/sec^2	1019.4°/sec^2
T_{el} (inertia only)	.018 in-lb.	27.93 in-lbs.
$\dot{\Theta}_{az}$	125°/sec	125°/sec
$\ddot{\Theta}_{az}$	125°/sec^2	1019.4°/sec^2
$\dot{T}_{az}$ (inertia only)	14.1 in-lbs	115 in-lbs

5.7.2. DYNAMICS AT THE SCAN POLES.

It has been stated that the rotational rates demanded of the shaft axis increase as the target being tracked approaches a scan pole. The geometry involved is shown below:
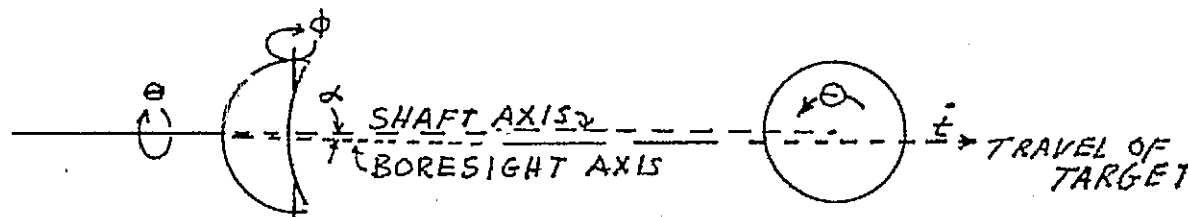
The target, at some velocity $(\dot{t})$, is passing over the antenna near the projection of its shaft axis. At zenith it is off the projection of the shaft axis by an angle α. As it continues it travels from the left-hand side of the zenith position to the right-hand side the shaft axis (θ) must rotate 180°. For small angles:

$$\dot{\theta}_{max} = \frac{\dot{t}}{\tan\alpha} \approx \frac{1}{\alpha} \qquad\qquad \dot{\theta}_{max} = \text{maximum shaft angle rate}$$

It is apparent that for $\alpha=0$, $\dot{\theta}_{max}=\infty$. More realistically however, there is a finite value involved relative to the practicalities involved. The maximum target velocities involved are:

During acquisition $\quad \dot{t} = \pm\ 4$ mv sec (.23°/sec)

During track $\qquad\qquad \dot{t} = 5°/sec$

A plot of $\dot{\theta}_{max}$ vs α for these two maximum values are shown in Figure 5.7-4. The shaft axis of the antenna can rotate at 125°/sec, adequate for full tracking capability up to 4 mv (.23°) and 40 mv (2.3°) for maximum target rates encountered in acquisition

FIG. 5.7-4 SHAFT ANGLE RATE vs TRACKING ANGLE OFF SHAFT AXIS

TRACKING ANGLE = OFF SHAFT AXIS

REF TO MAXIMUM RATE INC. VELOCITY DE 5/sec

REF TO SHAFT ANGLE RATE VELOCITY

MAXIMUM ACQUISITION VELOCITY

SHAFT ANGLE RATE ~ deg/sec
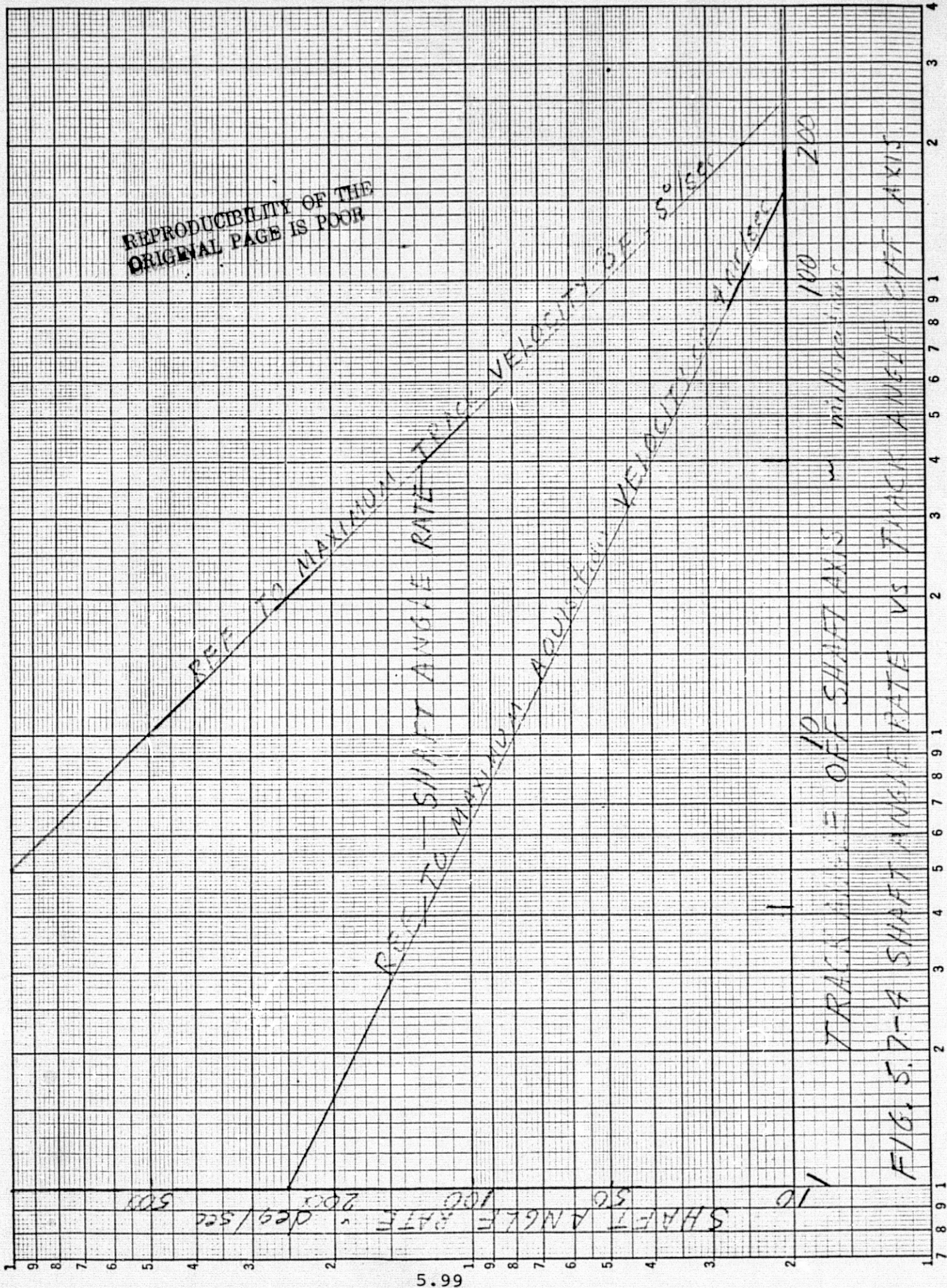
and track reapectively. The .23° offset is acceptable in the
lock-on budget, i.e., well under a half beamwidth. The track
situation can be avoided by instrumenting the stow/deploy
mechanization as discussed elsewhere in this report.

5.8 GIMBAL DESIGN.

A sketch showing the gimbal arrangement for the space shuttle antenna is shown in Figure 5.8-1. The gimbal and its antenna mount on the shaft axis off the antenna base assembly. The major sub-assemblies consist of: shaft axis drive, the trunnion gimbal, the trunnion drive, the reflector and feed and the components mounted on the rear of the reflector.

The shaft (azimuth) and trunnion (elevation) drives are of similar design. They consist of a size 18 motor with integral size 8 tach coupled to the respective axes through a 240:1, four stage, spur gear reduction. Refer Table 5.7-4. In each case the output gear is 2.5" in diameter. The RF rotary joint and slip ring assembly pass through this gear. In addition the position sensor, a snychro, mounts coaxial to the rotary axis.

Transmitter power from the electronic assembly mounted within the base mount is routed through waveguide to the shaft axis rotary joint, along one side of the trunnion gimbal, through the trunnion elevation joint to the circulator and/or diplexor, hybrid waveguide circuitry and finally radiated from the primary feed. The reflector, a composit carbon-epoxy construction, mounts within the trunnion gimbal. It is supported by a support bracket that spand the trunnion gimbal. This same support bracket supports the various components that are mounted on the back of the reflector.

Components consist of such items as the circulator, diplexers, mixers, hybrids , frequency multiplier, trunnion axis gyro, feed deploy and polarizor drive mechanisms. These components vary in detail; however, for the purposes of this study we have assumed that individual assemblies will be used with waveguide inputs and outputs. This tends to present a "largest package requirement". It is noted

WAVEGUIDE ASSY
TRUNNION AXIS TO CIRCULATOR

WAVEGUIDE ASSY
SHAFT DRIVE AXIS TO TRUNNION AXIS

POLARIZER DRIVE MOTOR
(SEE DETAIL)

CIRCULATOR

FEED DEPLOY MOTOR
(SEE DETAIL)

SHAFT DRIVE
GEAR BOX

MOTOR/TACH

SHAFT AXIS

POSITION SENSOR

SLIP RING &
ROTARY JOINT ASSY

GYRO

TRUNNION YOKE

TRUNNION AXIS SLIP RING
& ROTARY JOINT ASSY

PARAMP

MIXER

FREQUENCY MULTIPLIER

IF PREAMP

REFLECTOR

TRUNNION DRIVE MOTOR/TACH

TRUNNION DRIVE GEAR BOX

TRUNNION GIMBAL POSITION SENSOR

MOTOR

FEED DEPLOYED

FEED RETRACTED

WORM GEAR DRIVE

FEED DEPLOY DRIVE DETAIL
(FULL SIZE)

REFLECTOR SUPPORT

PUSH ROD

SPRING

CIRCULAR

LINEAR

DRIVE PIN

MOTOR

REFLECTOR

POLARIZER DRIVE DETAIL
(FULL SIZE)

Fig 5.8-1

DYNAMIC DEVELOPMENT CORP

SPACE SHUTTLE ANTENNA

SKIO51026

that there is more than adequate room available. All such
components are mounted near the center of a rotation to minimize
the effective R_g and therefore the load inertia presented to the
drive system.

Details of the feed deploy and polarizer drive mechanizations
are shown at the right hand side of Figure 5.8-1. Two phase drive
motors and gear boxes are suggested.

5.9   SERVO CONTROL SYSTEM.

The servo electronics contains amplifiers which drive the
antenna shaft and trunnion axis servo motors and the gyro torquer
coils.   The servo electronics, in conjunction with the antenna
components and radar receiver, forms inner and outer closed servo
loops for each axis.   The inner, or stabilization loop, keeps the
antenna boresight axis fixed in inertial space in the presence
of spacecraft motions.   The outer, or tracking loop, keeps the
antenna boresight on the target using tracking error signals from
the receiver.   In lieu of this outer or tracking loop, it is also
possible to drive the antennas from the spacecraft or from a
slew/search/scan computer.   A functional block diagram of the
antenna servo control system is shown in Figure 5.9-1.

All antenna positioning and tracking is accomplished by
repositioning
function to follow the gyro repositioning to maintain the gyro-pick
offs as close as possible to zero.

In addition, the Gyro Torquing signals are sampled by two
Velocity filters, one for Shaft and one for Trunnion, to obtain
an indication of commanded LOS angular rate.   This angular rate
can be derived from the designation or slew inputs, or as during
target tracking from the receiver angle error channels.

5.9.1.   SEARCH PROCEDURE.

The initial search coordinates for the rendezvous target
are generated in the spacecraft computer.   The coordinates are
transmitted to the guidance computer and this system then initiates
a slew to this system followed by commands to the control system

Fig 5.9-1 SERVO DESIGN, FUNCTIONAL DIAGRAM

to initiate the vectored search for the target. The resulting acquisition scan consists of a spiral search centered on the computed vector position of the target and extending as necessary to the 3σ limits of $\pm 40°$. See below.
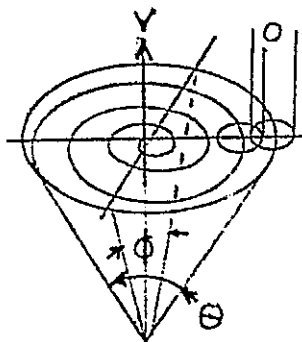
V= computed vector to target

O= 1.3 overlap in radially displaced beams

$$\dot{\theta} = A_t \sin 2\pi f_t$$
$$\dot{\phi} = A_t \cos 2\pi f_t$$

The spiral scan is formed by a sinusoidal wigwag of $\theta + \phi$, spaced 90° in phase and of increasing amplitude with a 1° beamwidth and 1.3 overlap between radially displaced beams, 52 revolutions are required to scan a 1 m. dia. aperture antenna (1° two-way beamwidth) over an 80° apex angle conical section. The speed of rotation is modified, to as great an extent as possible, to provide a constant tangential velocity. In actual practice the central area is scanned at constant rotational speed, 468°/sec or 1.3 revolutions per second, out to an angle of $\pm 15.3°$ from the central axis and then the speed of rotation is linearly decreased to 183°/sec or .508 revolutions persecond thereby maintaining constant tangential velocity out to the scan limit of $\pm 40°$. The frame period is 60 seconds. The constant tangential rate provides constant dwell time on target intercepts, improving scanning efficiency and related detection capability. A_t, the amplitude of the wigwag motion, is varied with time to provide a constant spacing between radial sweeps. f_t, the frequency of the wigwag cycle, is held constant at 1.3 Hz. from center to $A_t = 15.3°$, and then is decreased to provide the aforementioned constant tangential velocity.

Upon detection of the target, the position of the antenna at the time of detection (as measured by the position of the integrating rate gyros) is recorded in the memory of the guidance computer, and at the same time, the rate command to the gyro torquers from the guidance computer is removed. The integrating rate gyro is now essentially a one degree of freedom, free gyro which will control the drive motors to keep the antenna continually pointing to the same location in space. If the target detection is not reconfirmed, another rotation is made at the fixed value of A_t and if not confirmed this second time the acquisition search is continued. Upon confirmation the target position data is updated and the acquisition scan is transferred to the lock-on mode.

5.9.2. LOCK-ON AND TRACK.

Once the target has been detected and the antenna brought to a stop (in inertial space) with the boresight capture angle of the antenna, the autotrack command loop is closed. When this outer loop is closed, the two rate-integrating gyros provide line-of-sight space stabilization for the antenna. The residual tracking signals provide line-of-sight angle rate measurements. The outer servo loop has been designed to function equally well using boresight measurement errors determined from cooperative (transponder of communication systems), from non-cooperative (radar) systems, and from target enhanced systems.

5.9.3. SERVO COMPONENTS.

Two rate-integrating gyros provide line-of-sight space stabilization and enable line-of-sight angle rate measurements. The trunnion gyro is mounted on the reflector support structure behind the reflector and is oriented to monitor motion about the

trunnion axis. The spin axis gyro is not mounted on the reflector but on the trunnion gimbal. This mounting arrangement simplifies the coordinate transformations required to control the system. Again it is oriented to monitor azimuth motion.

The antenna shaft and trunnion positioning is accomplished by two phase 400 Hz servo motors driving through 240:1 gear drive systems. To obtain more stable servo operation, tachometers are attached to the motor output shafts. These tachometers tend to linearize the drive motors and allow considerably higher outputs of the drive system without encountering stability problems.

The line-of-sight error to the target is detected by the antenna using a four slot backfeed-parabola reflector antenna arranged in a monopulse configuration. If the antenna is aligned with the target line-of-sight, the return energy is equally received by each of the four slots. If the antenna is not directly in line, the amplitudes of energy received by the four slots are not equal. The received signals are processed through the monopulse comparator to develop the required sum and difference tracking signals. If the line-of-sight is directly above or below the transponder, a negative or positive θ coordinate pointing error is generated. Similarly, with the line-of-sight on either side of the transponder, a ϕ coordinate pointing error is generated. The received signal, processed for monopulse operation, contains three information channels: The ϕ (trunnion) channel, the θ (shaft) channel and the Sum (reference) channel. The θ channel input is the difference in received energy between the vertically adjacent feedhorns $(A+B)-(C+D)$. The ϕ channel input is the difference in received energy between the horizontally adjacent feedhorns $(A+D)-(B+C)$. The Sum channel input is the sum of the received energy of all four feedhorns $(A+B+C+D)$.

The functional design of the system is shown in Figure 5.9-1. The actual servo design loops are shown in Figure 5.9-2.
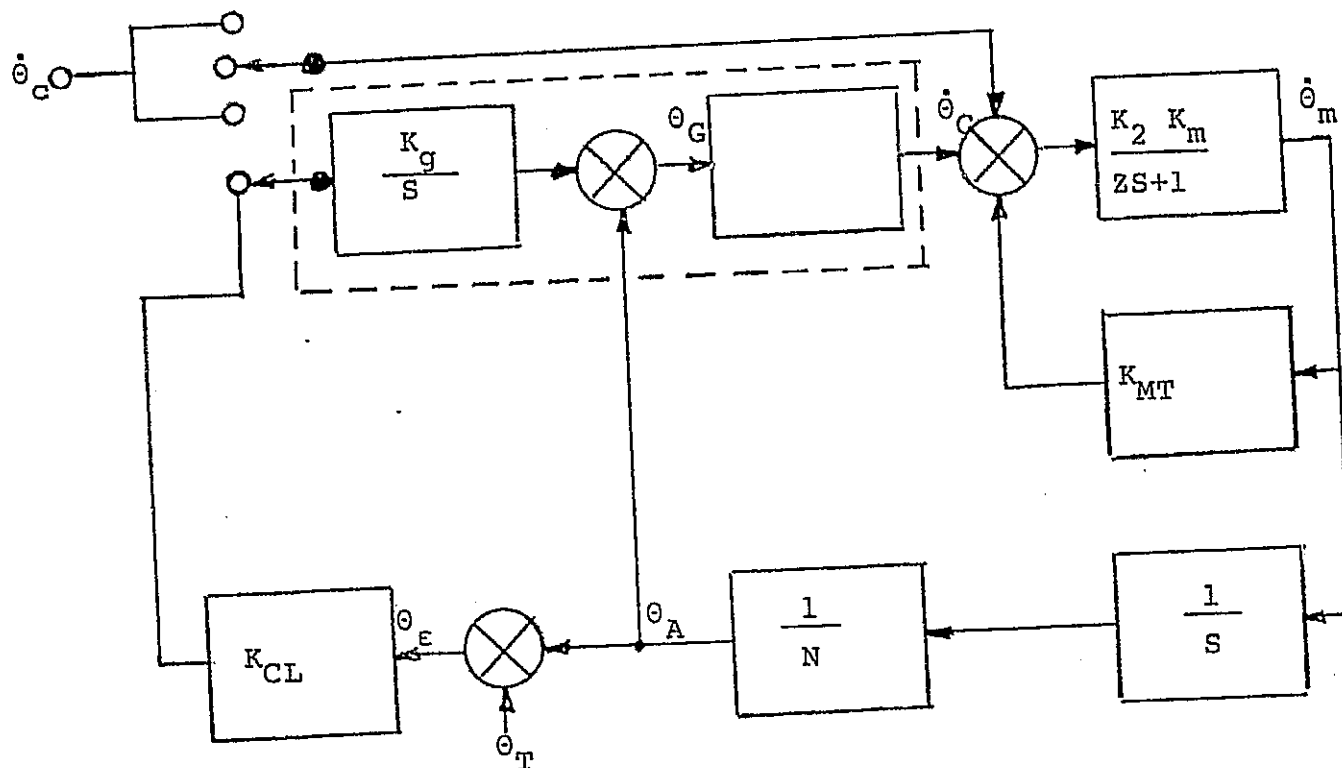
FIGURE 5.9-2

SINGLE AXIS STABILIZATION DIAGRAM

where: K_G = gyro torquer scale factor

K_{GO} = gyro output scale factor

K_2 = motor amplifier gain

Z = motor time constant

K_M = motor scale factor

N = gear ratio (=240)

K_{CL} = closed loop scale factor.

Two separate stabilization conditions must be met with the antenna drive systems. These are:

(1) During search, the loop gain must be such that a maximum of .5° error may exist when the system is driving at its maximum rate of 125°/sec, thus:

$$K_v = \frac{(125)(240)}{0.5} = 60,000 \text{ sec}^{-1}$$

(2) During track, the maximum error allowed is 10 mrad at the maximum rate (spacecraft) of 5°/sec (=.0873 rad/sec).

$$K_v = \frac{(.0873)(240)}{.01} = 2,095 \text{ sec}^{-1}$$

Therefore, the critical design point would be during the search mode if the total loop gain were to be derived from the gyro stabilization loop inputs. However, in order to lower the loop gains and provide a more reasonable loop during scan, a feed forward loop is put around the gyro during search/scan. Thus the gyro will still represent the desired location of the antenna, the motor drive will be commanded by the feed forward input and any errors in the system will be detected and corrected by the gyro. Thus the closed loop gyro stabilization loop will be designed to easily satisfy the tracking requirements instead of the search requirements.

5.9.3.1. TRUNNION DRIVE SERVO DESIGN.

The design constants associated with the trunnion system are (all reflected to motor):

Moment of inertia, J............... $.000511$ oz-in sec^2

No load speed, ω_{max} .... 1257 sec^{-1} = 12000 RPM

Motor stall torque, T_M .... 2.6 oz-in

Motor time constant, τ .... $\frac{J}{T_M}\omega_M = .247$ sec

Tachometer FB scale, K_{MT} .... $K_{MT}^M = .9$

The trunnion closed loop drive system is shown in Figure 5.9-3.
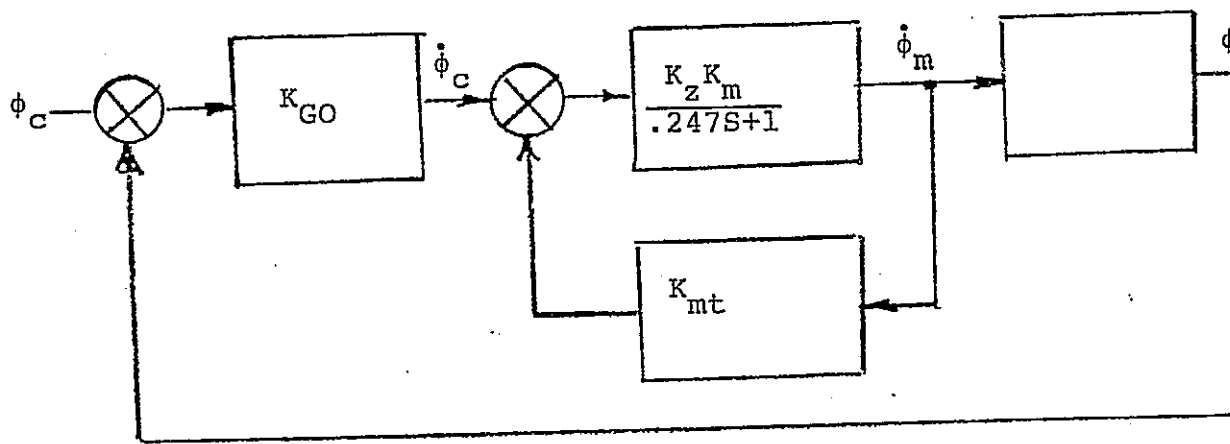
where:

$$K_T = \frac{K_2 K_m K_{GO}}{1 + .9 K_2 K_m} = K_{V_{min}}$$

and τ is arbitrarily chosen to be

$$\bar{\tau}_i = \frac{.247}{1 + .9 K_2 K_m} = .05$$

thus

$$K_2 K_m = 4.4$$

let $K_{V_{min}} = 5000$

then $K_{GO} = 5636°/\text{sec}/\text{deg}$

where

$\omega = 20.4$ rad/sec

$\zeta = .49$

5.9.3.2. SHAFT DRIVE SERVO DESIGN.

The design constants associated with the shaft drive system are (again all reflected to the motor):

$$J = .00208 \text{ oz-in sec}^2$$

$$\omega_{max} = 1257 \text{ sec}^{-1} = 12000 \text{ RPM}$$

$$T_m = 10.5 \text{ oz-in}$$

$$\tilde{L} = \frac{.00208}{10.5} \times 1257 = .249 \text{ sec}$$

$$K_{MT} = .9$$

Again by making the choice of K_V minimum of 5000 sec^{-1}, the natural frequency and damping of the shaft drive system are:

$$\omega = 20.4 \text{ rad/sec}$$
$$\zeta = .49$$

5.9.3.3. NATURAL FREQUENCY OF THE SYSTEM.

Although the natural frequency of the system is near 8 Hz the drive systems for both the trunnion and shaft systems contain practically no structural limitations. With the shaft system, the gyro is mounted on the trunnion gimbal only 6" from the shaft axis. The trunnion gyro is similarly well mounted structurally, being placed on the channel section only 20 inches from the drive. It is felt that the minimum K_V chosen to remove the spacecraft rotations can easily be increased with little probability of encountering structural feedback problems or their attendant servo problems.

5.9.3.4. ERROR ANALYSIS OF DRIVE SYSTEMS.

The maximum error of the pointing system may be obtained

by considering all error sources and then statistically combining them. The error sources are:

<div style="margin-left: 2em;">

Gyro drift rate 15°/hour........   .0042°/sec

.073 mr/sec

Spacecraft drift 5°/sec.........   87.3 mr/sec

Glint error rate................   8 mR/sec

</div>

The total of these is (considering these as non-correlated):

87.7 mr/sec

which when divided by the K_V used gives:

Error = 4.2 mR.

5.10 DESIGN OPTIMIZATION.

In a study of this type the antenna designer directs his first efforts towards developing a maximum size aperture. The ligic path for determining aperture size in this application is outlined in Figure 5.10-1. Controlling constraints are first listed relative to installation clearances in stow, antenna implementation and desired servo poser limits. A layout study based on the listed criteria indicated that the largest size reflector is 85 cm (34") in diameter.

The original constraints are then reviewed and new logic paths chosen. If only 2" of clearance were provided between the antenna structure and the payload door the antenna aperture increases to 1 m diameter. While this reflector provides increased gain it is not an optimum design from a standpoint of monopulse tracking sensitivity. A larger focal length is desired.

An alternate logic path is available wherein the 3" clearance to the payload/door is retained but a folded feed is utilized. This can also provide a 1 m diameter aperture with the desired gain increase, optimum monopulse pattern characteristics and more than adequate clearance. Rectilinear scanning of a larger antenna during acquisition requires excessive servo power, particularly around the shaft axis. To provide a meaningful increase in aperture requires that the rectilinear (xy) acquisition scan be abandoned and an R-θ scan implemented. This within itself allows the aperture diameter to be increased to 1.25 m. Again if the clearance to the payload door is reduced to 2" the aperture can be increased to 1.35 meters.

In the above arrangement the elevation drive motor and gimbal assembly occupies a critical clearance area. Rotation of the elevation axis towards the y axis provides increased clearance. This can be partially accomplished with a single axis deploy/stow mechanism but

Start constraints
1. 3" clearance in stow,
   all around.
2. Fixed feed.
3. x-y rectilinear drives.
4. Servo power less than 100 watts.

86 m (34" diameter aperture)

Use folding feed   Reduce clearance to payload
                    door to 2"

Use R-θ coordinates   1m(40") aperture   1m(40") aperture
deploy 11 to Z axis   (drive power limited)   (clearance limited)

+----------------------+
| Features |
| 1. Best patterns |
| 2. Can use R,θ or |
| xy drives |
| 3. More than adequate|
| clearance |
+----------------------+

1.25m(50") aperture

Two axis deploy/stow   Reduce clearance to payload
                        door to 2"

                                    1.35m(53") aperture
                                    (clearance limited)

                        Reduce clearance to payload
                        door to 2"

1.52(60") aperture   1.6m(63") aperture
(clearance limited)   (clearance limited)

FIGURE 5.10-1 LOGIC PATH FOR APERTURE SIZE.

5.115

for substantial improvement it is required that a two axis deploy/ stow mechanism be used. This increases the reflector diameter to 1.52 meters. Again if one decreases the clearance to the payload doors to 2" the largest size possible reflector can be employed, i.e., 1.6 meters in diameter.

It is evident that a sufficiently large aperture can be stowed within the constraints of the spacecraft and still maintain a 3" clearance all around. In summary:

1. A spiral acquisition scan is best adapted to the geometry of the vectored search in terms of scan efficiency and early detection probability.

2. The folded feed design is simple, reliable in operation, provides optimum patterns and maximum mechanical clearance.

3. A R-θ scan mechanization provides the required servo responce with minimum drive power. If used two deploy positions are required, one near parallel to the z axis of the spacecraft.

4. The maximum size aperture without implementing step 3 is 1 m in diameter. The constraint is drive power. Implementing 3 allows the reflector diameter to increase to 1.25 m.

6.1.   TARGET GENERATED ERRORS IN ANGLE, RANGE AND VELOCITY.

As part of the conceptual design of the Rendezvous Radar an investigation was made of fundamental sources of radar measurement error inherent to the target itself. A summary of the results of this investigation is included in this section.

Of particular interest during this investigation were those factors which influence the accuracy of the velocity measurement. A comparison was made of the performance of coherent and noncoherent methods of determining target velocity from the standpoint of target induced errors.

Certain errors in radar measurements of target state are generated by the target itself. These errors, which are indistinguishable from the true target state by the radar, include:

> Angular scintillation (glint)
> Range scintillation
> Doppler (velocity) scintillation.

This group of errors is caused by distortion of the expected spherical phase front of the echo signal by vector combining of the reflected signals from several reflecting surfaces on the target.

6.1.1.   ANGULAR SCINTILLATION (Glint).

The magnitude of the angular scintillation, or glint, is related to the size of the target and relative amplitude

and phase of the reflected signal from major scattering elements. The magnitude of the glint varies rapidly with aspect angle of the target as a result of a strong phase dependence.

An estimate of the magnitude and distribution function of the angular scintillation for typical targets for the Rendezvous Radar will be developed in this section. A simplified, two-reflector model which lends itself to hand calculation will be considered first. Following this, measured data on aircraft targets will be examined and a mathematical model will be adopted which fits the measured data. The mathematical model will be examined for applicability to the type of targets of interest to the Rendezvous Radar.

The simplified two-reflector model shown in Figure 6.1-1 was suggested by Mr. J. Griffin of the Johnson Space Center during early discussions. It consists of two point reflectors separated by 60 feet (18.3 meters).
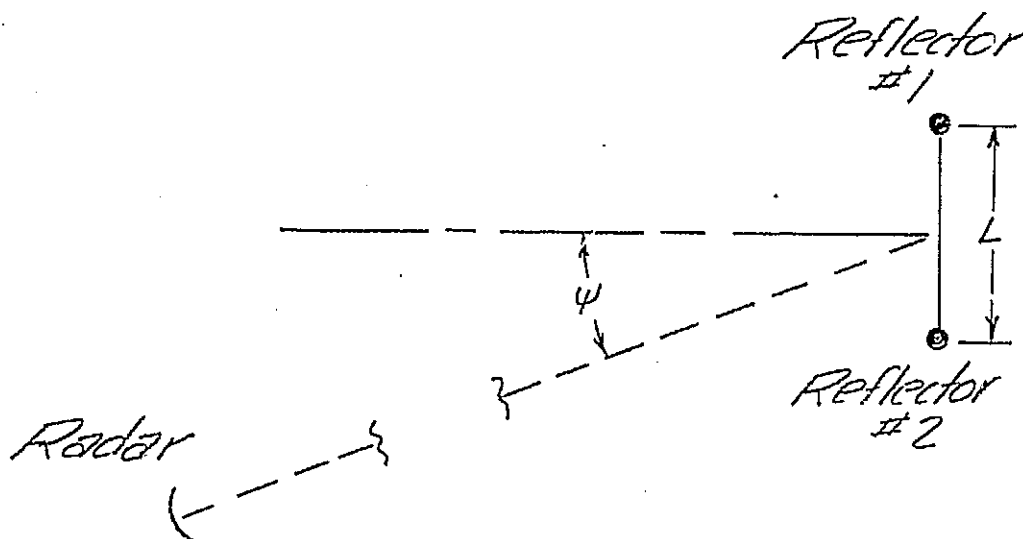
FIGURE
6.1 -1 . GEOMETRY OF TWO-REFLECTOR TARGET.

Although this is a highly simplified model it is roughly representative
of the Large Space Telescope and Large Space X-ray Telescope which
are potential targets for the Rendezvous Radar. Both of these space
vehicles have flat solar panels on one end of a long cylinder and
structure at the other end which would appear to also result in a
large radar return.

Following the work of Howard[1] the apparent location of this dual
source target can be expressed in terms of the error,E, from the
midpoint of the target as follows:

$$E = \frac{L \cos \psi}{2} \; \frac{1 - a^2}{1 + a^2 + 2a \cos(\phi + L \sin \psi)}$$

where:

L = the spacing between the two reflecting points.

Ψ = the viewing angle measured from a line perpendicular to the
line connecting the two reflectors.

a = the ratio of amplitudes of the signals from the two scatterers.

ϕ = the relative phase of the two signals as seen by the radar.

1   Howard, D.D.,"Radar Target Angular Scintillation in Tracking and
    Guidance Systems...."; Proceedings of the National Electronics
    Conference, Vol. 15, 1959.

A plot of the error in apparent location of a 18.3 meter dual source target viewed broadside by the radar is given in Figure 6.1-2 as a function of relative phase and amplitude of the two reflected signals. The figure illustrates the well known fact that the magnitude of the angular scintillation can exceed the physical dimensions of the target. Another pertinent observation is that the peak displacement occurs at 180° of relative phase, which coincides with minimums of the amplitude function of the net return signal.

Turning now to some measured characteristics of glint from aircraft targets, an excellent series of measurements on aircraft models by Mensa[1] at the Naval Missile Center leads to an empirical model for glint. Mensa's measurements were made on two different aircraft targets, both scaled 5.7:1. The lengths of the models were about 2 meters. A 10 MHz. CW illumination source was used.

His test results indicated the error in the phase front varied sharply with aspect angle. The sharp excursions always coincided with a minimum in the amplitude recording. The angular position error corresponding to the wave front error often exceeded 2 to 3 times the extent of the target.

Perhaps of most significance in his study was the finding that for both targets the amplitude of the glint as a function of aspect angle closely followed a normal distribution between the 10 and 90 percentiles. The standard deviation was approximately equal to one half of the target extent.

The normal distribution function for amplitude of glint for aircraft type targets has also been reported by Dunn and Howard[2,3] as a result of analysis of flight test data. Their analysis indicates the standard deviation of the angle error is equal to about 0.3 times the extent of the target for a side view of an aircraft, and also for a nose-on

1. Mensa, D.L. "Scintillation Characteristics of Aircraft Targets", Naval Missile Center Publication TP-71-13, 26 March, 1971.

2. Dunn, J.H. and Howard, D.D. "Radar Target Amplitude, Angle and Doppler Scintillation...", IEEE Transactions MTT No.9, September 1968.

3. Skolnik, M.I., The Radar Handbook, Chapter 28 (Dunn and Howard).

174 Meters at 180°

Radar Looking Broadside at Two Reflectors Separated 18.3 Meters

a = Amplitude Ratio

Radar

L = 18.3m

a = 0.9

a = 0.5

End of Target

Midpoint

(Vertical axis: Apparent Displacement From Center, Meters — 0, 4, 8, 12, 16, 20, 24, 28, 32, 36, 40, 44, 48)

(Horizontal axis: Relative Phase, Degrees — 0, 30, 60, 90, 120, 150, 180, 210, 240, 270, 300, 330, 360)
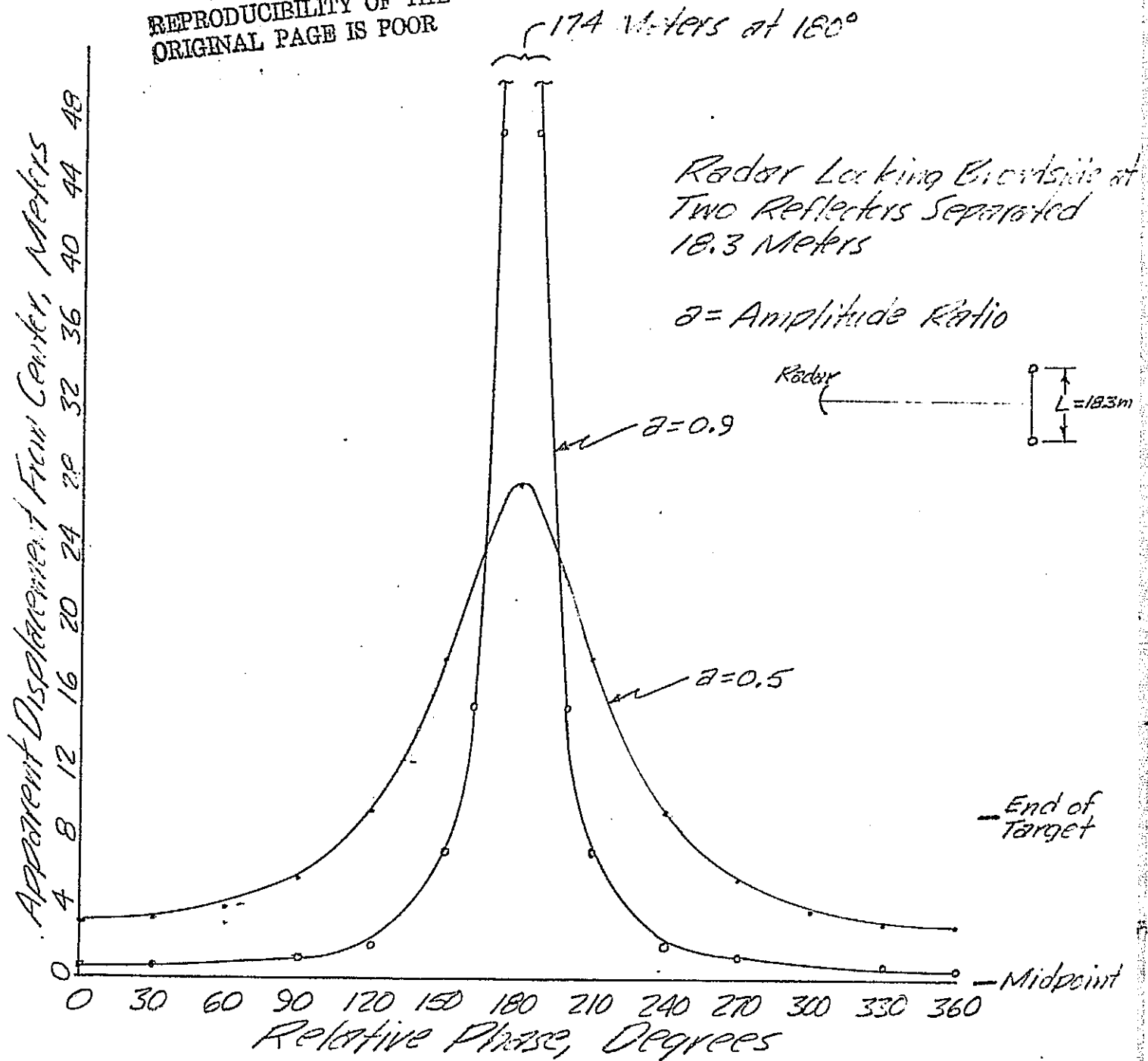
Fig. 6.1-2 Error in Apparent Location of Dual Reflector Target as a Function of Relative Phase and Amplitude of the Two Reflected Signals

view if the aircraft has outboard engines or wing tanks. The standard deviation of angle error decreases to 0.1 times the extent of the target for a nose-on view of a single engine aircraft without wing tanks.

For the purposes of the Rendezvous Radar study two models will be considered; the two-reflector (or dumbbell) model with glint shown in Figure 6.1-2, and a multiple reflector model with a normal distribution function for glint with a standard deviation equal to 0.5 times the extent of the target.

The previous discussion on angle noise, or glint, assumed that the distance between the target and radar was very large compared to the extent of the target. As the radar closes towards the target the antenna subtends a larger portion of phase front and the distorted region becomes averaged with regions of lesser distortion. The larger and closer the target the more averaging over the range of phase fronts takes place.

It has been found[1] that when the target subtends an angle greater than 0.25 times the radar antenna beamwidth that the RMS target angle noise is significantly reduced. Under these conditions the angular error is limited to a few tenths of the antenna beamwidth. In the case of the 18.3 meter long target discussed previously and an antenna beamwidth of about 2.7 degrees (50 cm diameter antenna),the target subtends one fourth of the beamwidth at a range of 157 meters. Thus, at ranges greater than about 157 meters the models for glint developed above apply. At ranges less than about 157 meters the glint decreases to a fraction of the antenna beamwidth. At these short ranges, however, the antenna can track various points on the target, eg. one end or the other so that all that can really be ascertained is that the antenna pointing angle contains some portion of the target.

The magnitude of the angular scintillation is a direct function of the relative phase and amplitude of the reflected signals from various scattering surfaces on the target. Consequently,it can be altered by

1. Dunn, J.D. and Howard, D.D., Loc Cit.
1.   , J. .   ,   .6..6

changing either the relative amplitude or phase of the reflected signals. A number of independent samples of the angle of arrival can then be averaged within the passband of the antenna pointing servos to reduce the angle scintillation.

For a general complex target a change in polarization, e.g. vertical to horizontal, will change the relative amplitude of the reflected signals. Thus, by changing polarization pulse-to-pulse some averaging of glint can be achieved. However, in the case of targets which have symmetrical scattering surfaces to both polarizations changing polarization will not have a significant effect.

The relative phase of the reflected signals from various scattering surfaces can be altered by changing the carrier frequency of the radar from pulse-to-pulse. The effectiveness of frequency agility in modifying the glint function is dependent on the extent of the target in the range direction and the amount of frequency change from pulse-to-pulse. It should be noted that if we look broadside at the two-reflector model previously discussed, the distances from the radar to the two targets are exactly the same and frequency agility will not modify the glint characteristics. It is interesting to note that polarization agility would still be effective in changing glint characteristics with equal ranges.

For the general case where the target exhibits a range depth, Lind[1] has shown that complete decorrelation of the glint between two pulses occurs if the frequency change between the pulses is greater than a critical difference frequency Δf_c where

$$\Delta f_c = \frac{C}{2D}$$

where C is the velocity of light and D is the range depth of the target. In the case of the 18.3 meter, two-reflector target viewed slightly off of head-on (the glint is zero head-on), the range depth

1. Lind, G. "Reduction of Radar Tracking Errors with Frequency Agility", IEEE Transactions AES-4 No.3, May 1968.

is about 18.3 meters and the critical frequency is 8.2MHz. If the target
is viewed slightly off of broadside the depth of the target in the
range direction becomes small and the critical frequency becomes
much higher due to the inverse relationship between critical frequency
and depth.

The 18.3 meter separation between reflectors is equivalent to 915
wavelengths at a carrier frequency of 15 GHz. The angular separation
between nulls of the amplitude pattern of the composite signal, and hence
between glint regions, is less than a degree for this large spacing.
A frequency change of 420MHz. (critical frequency) is required to
decorrelate the glint from pulse-to-pulse when viewing the 18.3 meter
target 1 degree from broadside.

The decrease in spectral density of the glint at zero frequency is
shown by Lind to be, in the limit, approximately equal to the frequency
agility bandwidth divided by two times the critical frequency. The
limit requirement is for the PRF to be much larger than the original
glint bandwidth, a condition which will likely apply for space vehicle
targets. The tracking error reduces by the square root of the decrease
in spectral density of the glint at zero frequency.

In summary, frequency agility can effectively be used to reduce angular
scintillation as long as the scintillation arises from scatterers
distributed in the range dimension as well as in the angular dimension
of the target. In the case of the 18.3 meter two-reflector target
viewed near head-on a total agility bandwidth of 300MHz. results in a
decrease in glint spectral density by a factor of

$$\frac{300}{2(8.2)} = 18.4$$

which corresponds to a reduction in rms angular pointing error by about

$$\sqrt{18.4} = 4.3.$$

Viewing the same target near broadside with the same frequency agility

bandwidth, the reduction in glint spectral density is a factor of

$$\frac{300}{2(420)} = 0.36$$

or in effect, no significant improvement.

It may be noted from Figure 6.1-2 that the displacement error is one sided. Consequently, the effect of averaging the error over 360° of relative phase by frequency agility is to create a displacement bias error. For the case of the 18.3 meter two-reflector target and a ratio of the amplitude of the two reflected signals equal to 0.5, the average displacement is equal to about 9 meters.

The subject of frequency agility will be treated in detail later in this study.

6.1.2. Target Generated Range Errors.

Range scintillation errors arise from a mechanism similar to that described above for angle scintillation. As in angle scintillation, the target generated range errors can exceed the extent of the target.

Range scintillation has been treated by Cross and Evans[1] who show that the target induced range errors are related to the slope of the phase (with respect to frequency) added to the transmitted spectrum by the target. Since the error slope is essentially constant over the transmitted spectrum an actual time shift of the return occurs. This shift and accompanying range measurement error can not be distinguished from actual target motion by standard range processors used in either pulse or FM/CW radars.

Cross and Evans derive expressions for the phase of the target modulating function and for the slope of this function which yields the range

1. Cross, D.G. and Evans, J.E., Target Generated Range Errors, IEEE International Radar Conference, April 1975.

error. The form of these equations is identical to those derived by Howard[1] for angle scintillation. In particular, for the case of the two-reflector target previously considered, the expression for range error expressed in terms of a time error Δt is

$$\Delta t = \frac{t_o}{2} \frac{1-a^2}{1+a^2+2a \cos(\omega_c t_o)}$$

where t_o = Target length in range direction expressed in time.

a = Relative amplitude ratio of the two reflected signals.

ω_c = Carrier frequency.

$\omega_c t_o$ = Relative phase of the two reflected signals.

A plot of the range error as a function of the relative phase between the two reflected signals from a two-reflector target is reproduced below.
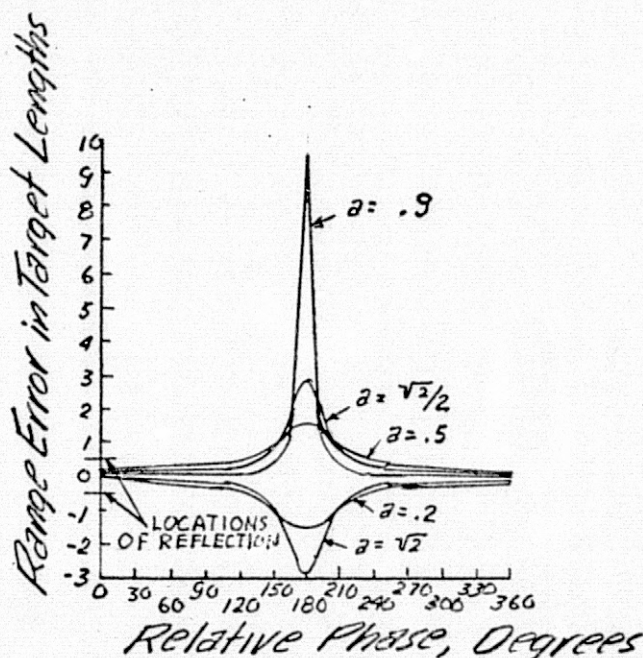
FIGURE
6.1-3   Range Error VS Relative Phase for Two-Reflector Target.
          (After Cross and Evans)

1.   Howard, D.D., Loc Cit.

It may be noted that Figures 6.1-2 and 6.1-3 represent the same function, the only difference being that Figure 6.1-2 is plotted in terms of actual displacement. Thus, for the case of the target being viewed head-on, the range error may also be read off of Figure 6.1-2.

It is reasonable to assume that the range error for more complex targets will follow the same normal error distribution function as found for glint. It follows also that the standard deviation will be approximately equal to one half of the target extent in the range direction.

As in the case of angular scintillation, the effects of range scintillation can be reduced by using pulse-to-pulse frequency agility and averaging the range measurement over several pulses. Once again, since the amplitude ratio does not change significantly with frequency agility, the range error is one sided and when averaged over all relative phase, a range bias error is generated. For the case of the 18.3 meter target viewed head-on and with amplitude ratio equal to 0.5 the range bias error is about 9 meters.

An important consequence of range scintillation as applied to the Rendezvous Radar is that the range data will be noisy. The magnitude of the noise is given by the range error developed above. The bandwidth of the noise is a function of the rate of change of aspect angle.

To gain some insight into the apparant range rate due to the time rate of change of the range scintillation, the rate of change of the relative phase, $\omega_c t_o$, between the reflected signals for the two-reflector target was computed for an assumed angular rate, and the corresponding range rate was determined using range error data of Figure 6.1-2.

The two-way time delay, t_o, of the farthest reflector relative to the near reflector is

$$t_o = \frac{2L \sin\psi'}{c}$$

where

L = Length of the target.

Ψ' = Aspect angle measured from a normal to the boresight axis.

c = Velocity of light.

then,

$$\omega_c t_o = \frac{2L\omega_c}{c} \sin\Psi' = \frac{4\pi L}{\lambda} \sin\Psi'$$

and,

$$\frac{d(\omega_c t_o)}{dt} = \frac{4\pi L}{\lambda} \frac{d(\sin\Psi)}{d\Psi} \frac{d\Psi'}{dt} = \frac{4\pi L}{\lambda} \cos\Psi \frac{d\Psi'}{dt}$$

Assuming an aspect angle Ψ' of 45° and a change of aspect angle (rotation of the vehicle) of 0.01 radians per second, the rate of change of relative phase is $0.089 \frac{L}{\lambda}$ radians per second. For the case of the 18.3 meter target and an operating frequency of 15GHz. (λ=2cm) the rate of change of relative phase is 82 rad/sec or 4,700 degrees per second.

Referring now to Figure 6.1-2 and assuming an amplitude ratio of 0.5 a maximum slope of about 0.4 meters per degree of relative phase is noted. The maximum apparent range rate due to range scintillation for the conditions assumed is then (4700°/sec)(0.4m/°) = 1870m/sec.

This extremely high range rate for a relatively low physical rate is a consequence of the large number of wavelengths between the two reflectors. A potential advantage of this situation is that time averaging of the range data can be achieved with relatively short time constants.

6.1.-3 Target Generated Doppler Errors.

In the previous section it was shown that the target generated range
errors result in extremely high apparent range rates. If velocity
information were to be extracted by examining range rate, the resulting
data would have very high short term errors. The question then arises,
are there similar mechanisms which give rise to errors in the doppler
measurements of a complex target?

Following Dunn and Howard[1] it can be shown that the distortion of the
phase front which gives rise to the angular scintillation (glint)
also gives rise to doppler scintillation.

As the aspect of the target changes slightly the distortion region
of the phase front may rotate past the radar and cause a rapid phase
change. The rate of this change is equivalent to frequency. The
frequency term generated appears as a noise or modulation on the
average doppler frequency if the target is moving.

The doppler modulation may be determined by differentiating the phase
deviation from that of a point souce target with respect to time
as follows:

$$f(t) = \frac{d\phi}{dt}$$

where

f(t) is the instantaneous frequency.

$\frac{d\phi(t)}{dt}$ is the time rate of change of the phase deviation as seen
by the radar.

Since the doppler scintillation arises from the same fundamental
mechanism as yields the angular scintillation measured or calculated
angular scintillation parameters can be used to compute the spectrum
of the doppler scintillation as follows[2]

1,2. Dunn, J.H. and Howard, D.D. Loc Cit.

$$\rho(f) = \frac{\lambda}{(2\pi)^2 \sigma_t \sigma_{ang}} K_o \left(\frac{(f-f_d)\lambda}{4\pi \sigma_t \sigma_{ang}} \right)$$

where

$p(f)$ = Probability density distribution of doppler signal.

λ = RF wavelength.

σ_t = Standard deviation of aspect angle rate.

σ_{ang} = Standard deviation of angular scintillation in linear units measured at the target.

f_d = Average doppler frequency.

K_o = Modified Hankel function.

For comparison purposes the amount of doppler modulation for the simple model of two reflectors separated by 18 meters as considered previously will be computed. The resulting value for velocity perturbation will be compared with the errors which would result by determining velocity through differentiating the measured range data for the same target model.

The instantaneous pseudo doppler frequency is obtained by differentiating the phase deviation from that of a point source with respect to time. This is most readily accomplished as follows

$$f(t) = \frac{d\phi}{dt} = \frac{d\phi}{d\psi} 2 \frac{d\psi}{dt}$$

where Ψ is the aspect angle defined in Figure 6.1-1. The factor of 2 comes about since the change in aspect angle affects both the incident path and the reflected path between the reflectors and the radar.

The function $\frac{d\Phi}{d\Psi}$ is the phase front distortion as a function of target aspect angle, Ψ. This has previously been shown to be equivalent to the linear angle error which is equal to

$$\frac{d\phi}{d\psi} = \frac{L \cos\psi}{2} \frac{1-a^2}{1+a^2+2a\cos(\phi + L\sin\psi)}$$

For our purposes the expression above for the error in linear units at the target is converted to dimensionless units of radians of phase per radian of aspect angle as follows

$$\frac{d\bar{\phi}}{d\psi} = \frac{2\pi}{\lambda} \frac{d\bar{\phi}}{d\psi}\bigg|_{Linear}$$

Considering the 18.3 meter two-reflector model, an aspect angle, Ψ, of 45° and an amplitude ratio of 0.5, the peak linear error is about 19 meters and the value of the dimensionless error for a carrier frequency of 15GHz (λ=2cm) is 6000.

Assuming as before a change in aspect angle of 0.01 radians per second, the maximum pseudo doppler frequency is

$$f(t) = \frac{d\bar{\phi}}{d\psi} 2 \frac{d\psi}{dt} = 6000 (2)(0.01) = 120 \text{ radians/sec.}$$
$$= 19 \text{ Hz.}$$

At a carrier frequency of 15GHz., a 19 Hz. doppler frequency represents a velocity of about 0.19 meters/second

We conclude, therefore, that the quality of the velocity data obtained from doppler measurements of a complex target is far superior to that obtained by differentiating measured range data.

.6.2 PERFORMANCE ANALYSIS OF NON-COHERENT PULSE RADAR.

A candidate non-coherent pulse radar, scaled to the requirements of the Rendezvous Radar, is described in this section. A summary of characteristics of the radar are given in Table 6.2-1. A functional block diagram of the radar is given in Figure 6.2-1.

Range to the target is determined by measuring the time delay between the transmitted and received pulse. Velocity information is obtained by determining the rate of change of range data. The short term quality of the velocity data is generally not as good as obtained by doppler processing of the received signal. However, the non-coherent pulse system has the advantage of simplicity and ability to provide unambiguous range to any desired value.

6.2.1. AMBIGUITY CONSIDERATIONS.

The ambiguity function for a periodic pulse train with pulse width τ spaced Δ seconds and with N received pulses integrated is: [1]

$$\chi(T,\phi) = e^{jn\pi\phi\Delta} \, \chi_V(T-n\Delta,\phi) \, \frac{\sin(N-|n|)\pi\phi\Delta}{N\sin\pi\phi\Delta} \quad |T-n\Delta| \le \tau$$

$$= 0 \quad \text{elsewhere}$$

$$n = -(N-1), \cdots 0, \cdots N-1$$

where $\chi_V(T,\phi)$ is the ambiguity function of the single pulse

$$\chi_V(T,\phi) = \text{rect}\left(\frac{T}{2\tau}\right) e^{j\pi\phi T} \, \frac{\tau-|T|}{\tau} \, \frac{\sin\pi\phi(\tau-|T|)}{\pi\phi(\tau-|T|)}$$

where $T =$ difference between time signal is received and time to which filter is matched

$$= \frac{2}{c}(R_r - R_m)$$

$\phi =$ difference between received doppler frequency and doppler frequency to which filter is matched.

$$= \frac{2}{\lambda}(V_r - V_m)$$

A sketch of this function as given by Nathanson[2] is shown in Figure. 6.2-2.

1. Skolnik, M.I.;Radar Handbook
2. Nathanson, F.E.;Radar Design Principles
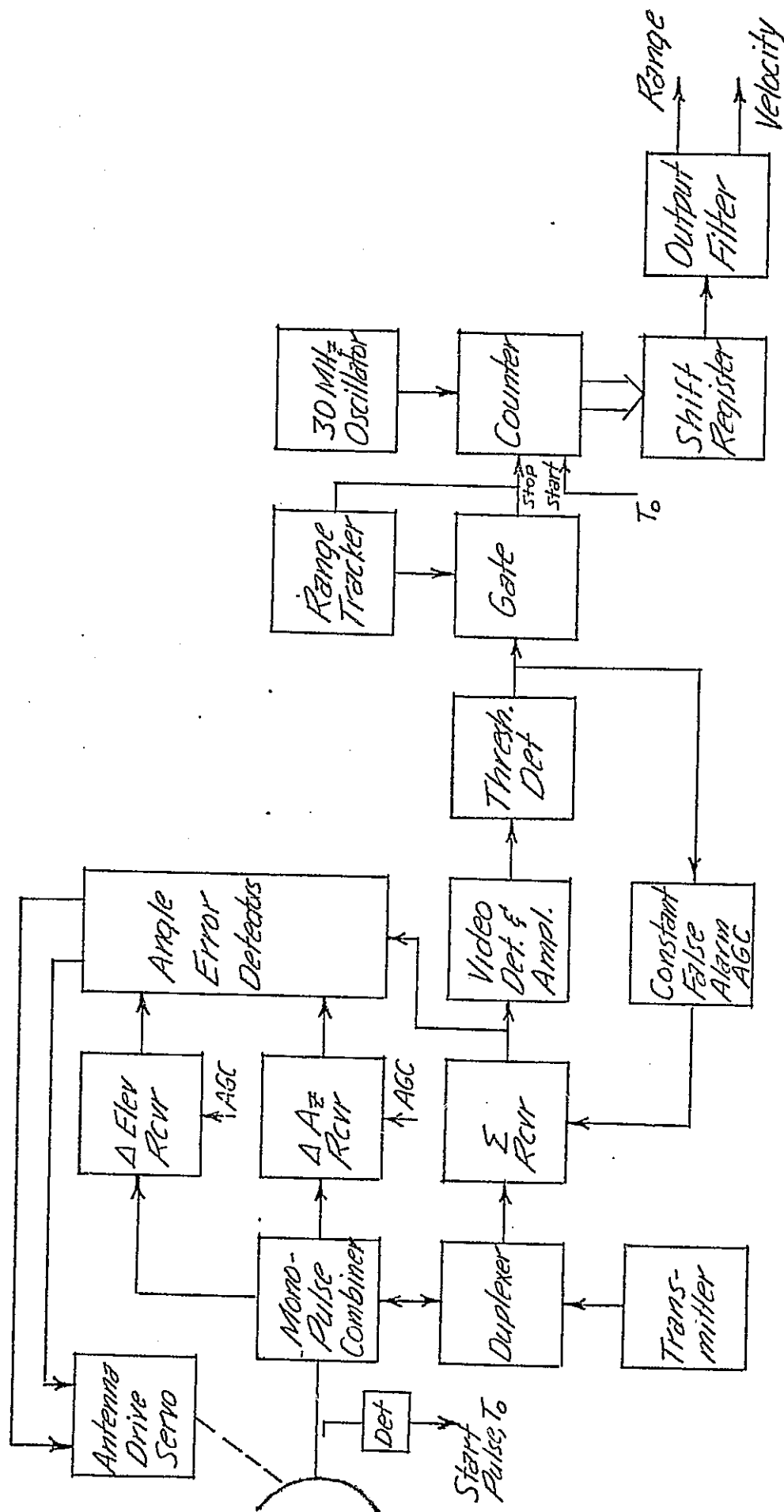
Figure 6.2-1 Functional Block Diagram of Noncoherent Pulse Radar

TABLE 6.2.-1.   CHARACTERISTICS OF CANDIDATE NON-COHERENT PULSE RADAR

PERFORMANCE CHARACTERISTICS

Detection range (P_d=0.99,Swerling I, $1m^2$ target)...   19km

Acquisition time.................................   60 sec

Angular search coverage ....   80° cone

Accuracy, 3σ (at maximum range)

	Bias	Random
Angle track	0.24 mR	0.1 mR
Angle rate	0.09 mR/sec	1.3 mR/sec
Range	(lag error)	29.7 m
Velocity	(lag error)	0.3 m/sec

SYSTEM CHARACTERISTICS

Frequency of operation..................   15 gHz.

Antenna

    Size...............................   1 m diameter

    Beamwidth (two-way) ....   1.0 degrees

    Gain ....   41.7 db

    Scan program ....   spiral

Transmitter

    Pulsewidth

        Range >9 km 1μsec

        Range <9 km 0.1μsec

    Peak power* ....   8.9 kw

    PRF ....   3.7 kHz

    Average power*   5.4 watts

Transmitted frequency ....   Frequency agile

    Number of discrete frequencies ...   6

    Frequency separation ....   75mHz.

    Total agility bandwidth ....   375mHz.

Receiver noise temperature ....   1758°K

Receiver noise bandwidth

    Range >9 km ....   750kHz.

    Range <9 km ....   7.5mHz.

* with 2dB margin.
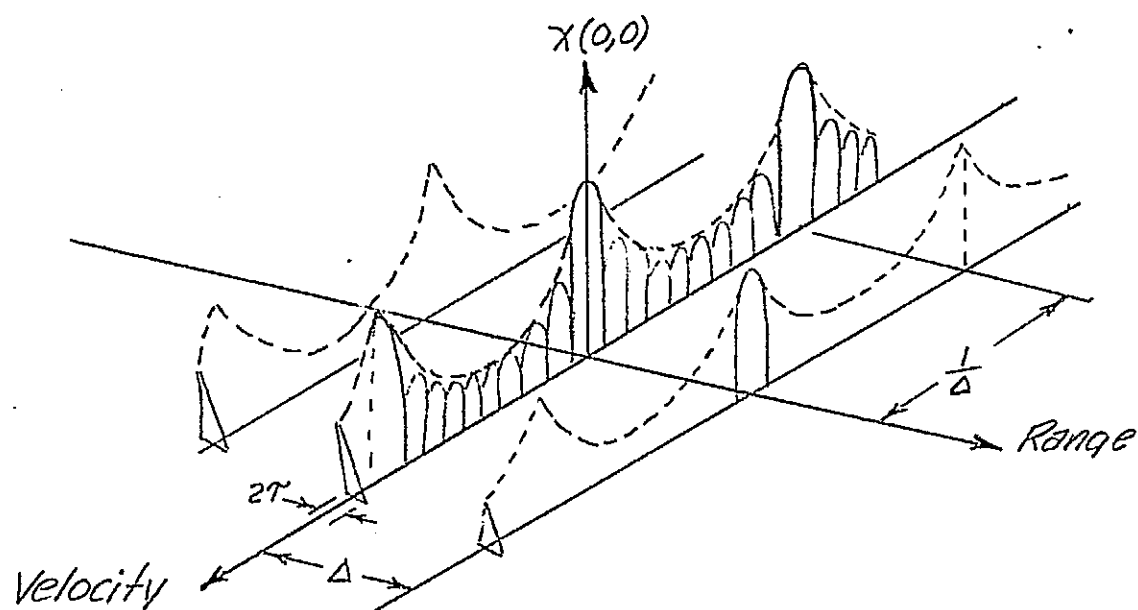
Figure 6.2-2 Ambiguity Diagram For Uniform Pulse Train. (After Nathanson)

The ambiguity diagram shows regions of range ambiguities spaced in time equal to the interpulse interval. Velocity ambiguity peaks occur at doppler frequencies spaced by the reciprocal of the interpulse interval. The velocity ambiguity characteristics will be treated in a later section discussing doppler processing.

Since there is complete absence of time ambiguities in the region between transmitted pulses, unambiguious range measurements can be achieved by making the interpulse period as long as required.

Another item of interest is the range resolution which can be provided by the radar. The ambiguity function in the range coordinate is of the form:

$$\text{rect} \left(\frac{T}{2\tau} \right) \frac{\tau - |T|}{\tau}$$

(In other words it is of the form $\frac{\tau - |T|}{\tau}$ over the time interval $|T| \leq \tau$ and zero elsewhere.) This defines a triangle shaped function with a width at the base equal to two times the pulse width, τ. The range resolution, or the ability of the radar to distinguish between 2 targets closely spaced in range, is then equal to the two way range equivalent of the pulse width, or

$$\text{Range Resolution} = \frac{c\tau}{2} .$$

The specified maximum operating range for the Rendezvous Radar in the skin track mode is 19km. To assure acquiring the target prior to reaching 19km, allowing 60 seconds for acquisition, and assuming the relative velocity is 45m/sec.,a maximum range of 21.7km is indicated. If the radar output were not used until the actual range closed to this value the pulse repetition interval could be made equal to the time equivalent of this two way range. If knowledge of the relative range to within a few km is not available an inspection of the ambiguity diagram indicates that the radar would read a range of 10km should the target be detected at 21.7+10 or 31.7km.

Modulation methods such as pulse-to-pulse frequency agility avoid this situation by in effect frequency taging each return pulse with a given transmitter pulse. For a simple non-coherent pulse radar it is customary to set the PRF about a factor of two lower than that value which corresponds to the maximum range.

We will treat two cases in this study. The first assumes that approximate knowledge of the target range is available so that an unambiguous range interval of 22km can be used. The second assumes no a priori knowledge of target range and an unambiguous range interval of 40km. In the first case the pulse repetition frequency (PRF) is 6.8KHz. and in the second case it is 3.7KHz.

6.2.2. TARGET AMPLITUDE FLUCTUATION MODEL.

A Swerling Class 1 fluctuation model has been specified as a
baseline for the Rendezvous Radar Study. This model applies
to targets characterized by a number of independent scattering
surfaces of about equal echoing area. The assumption is also
made, in the case of a pulse radar, that the echo pulses are
correlated pulse-to-pulse during the time target but that the
fluctuations are independent scan-to-scan. In our case the
time between antenna scans while searching for the target will
likely be between 15 seconds and 60 seconds.

The question then becomes, is there sufficient relative
angular motion between the target and the radar to result in
a decorrelation time of the echo signal of 15 to 60 seconds
or less? In absence of information on the angular rates of
the target itself about its own axis we examined the relative
motions between the orbiter and the target for the nominal
mission 3-B. Figure 5.5-2 of a JSC reference document entitled
"Rendezvous" was used as a reference. The angle and angular
rate between the radar and the target for this mission is
plotted in Figure 6.2-3. The data points are in 1 minute
increments.
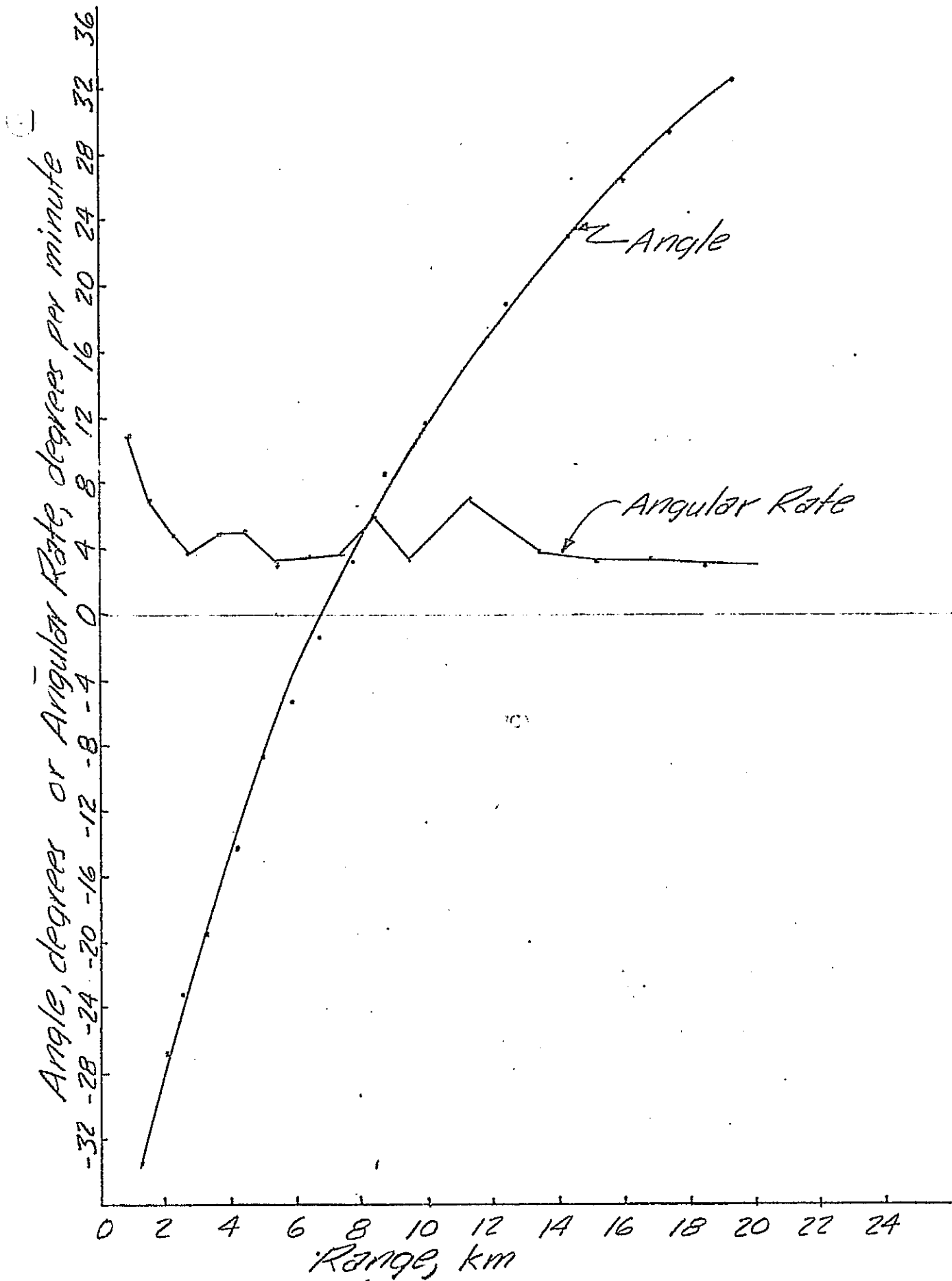
FIGURE 6.2-3 *Angle and Angle Rate vs. Range, Mission 3-B*

Referring to Figure 6.2-3 we note that the angular rates near the maximum radar range is greater than 2.8 degrees per minute or 0.047 degrees per second. Assuming that zero angle corresponds to viewing the target broadside, the change in path length from one end of the target to the other in the first 1 minute period (19.3 to 17.6km) is about 0.042L where L is the length of the target in meters. The rate of change may also be expressed $0.042\frac{L}{\lambda}$ wavelengths/min. The net reflected signal from the two ends of the target will essentially decorrelate as the path difference changes $\lambda/2$. The decorrelation time, T_c, for the conditions assumed is then

$$T_c = \frac{\lambda \; 60}{2(0.042)L} \quad seconds$$

which for the case of operation at 15GHz. (λ=0.02m) becomes

$$T_c = \frac{14.3}{L} \quad seconds.$$

In the 15 second minimum scan period, target elements spaced 0.95 meters will decorrelate between scans. Therefore, the assumption of independence of the amplitude fluctuations between scans is valid for mission 3-B for targets several meters in length.

6.2.3. EFFECTS OF FREQUENCY AGILITY ON TARGET FLUCTUATION MODEL.

One means of achieving a greater number of independent samples in a given period of time is to alter the phase relationship between the signals reflected by the various scattering elements of the target on a pulse to pulse basis. This can be accomplished by changing the transmitted frequency from pulse-to-pulse. If complete decorrelation between pulses can be achieved, Swerling Case 2 detection characteristics can be used for a target previously considered Case 1.

The benefit of pulse-to-pulse decorrelation in reducing the signal-to-noise ratio for a given probability of detection is a function of the single scan probability of detection desired, as illustrated in Figure 6.2-4. For single scan probabilities below 30% Swerling 1 characteristics are more favorable. For a single scan probability of 90%, the signal-to-noise ratio required for acquisition is reduced about 8db by pulse-to-pulse decorrelation.

Figure 6.2-4
Single Scan Detection Probability
vs. Signal to Noise Ratio

$n' = 10^6$
Swerling 1 Target — — —
Swerling 2 Target ———

N=300   N=30   N=300   N=30

N = Number Pulses Integrated

Signal to Noise Ratio, dB

Single Scan Detection Probability, %
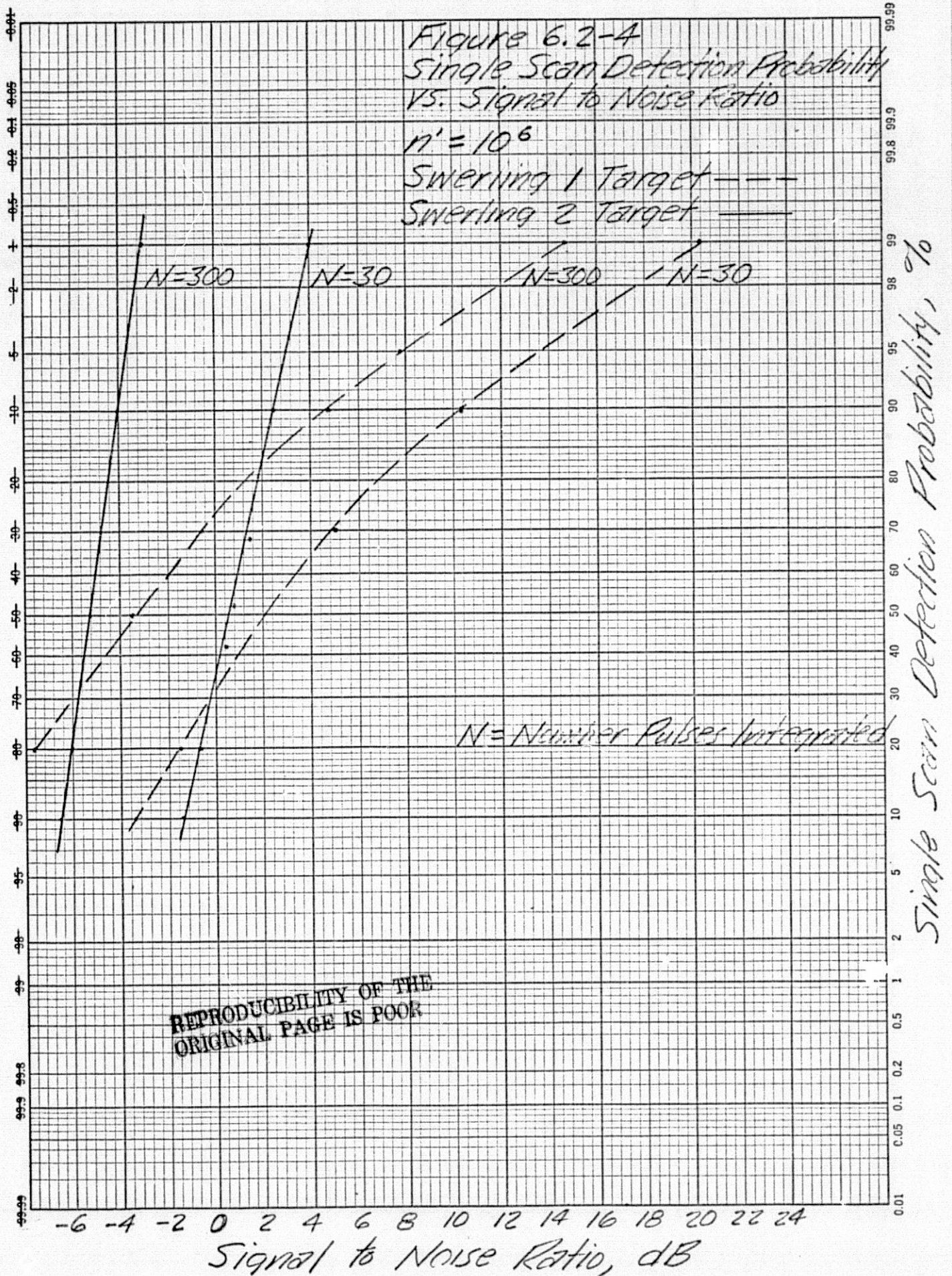
The amount of frequency change required to achieve decorrelation was treated earlier while discussing reduction of angular scintillation by frequency agility. It was shown that decorrelation occurs when the frequency change between pulses is greater than a critical difference frequency Δf_c

$$\Delta f_c = \frac{c}{2D}$$

where c is the velocity of light and D is the depth of the target (scattering elements) in the range direction.

A listing of potential targets for the Rendezvous Radar given in a series of sheets entitled "Automated Payload" were examined to determine a representative minimum physical size target. The majority of the small satellite targets are 4 to 5 meters in size although a few, such as the High Altitude Explorer and the GRAVSAT, have smallest dimensions between 1 and 2 meters.

For purposes of preliminary sizing of the amount of frequency agility required, a minimum target dimension in the range direction of 2 meters will be assumed. The critical difference frequency, Δf_c, is then 75MHz.

Barton[1] has developed an empirical relationship between the number of independent signal samples n_e, and the reduction in a term he refers to as fluctuation loss, L_f. (the difference in average signal-to-noise ratio required for a given probability of detection for a fluctuating target and for a steady target).

$$10 \log G(n_e) = \left(1 - \frac{1}{n_e}\right) 10 \log L_f(1)$$

where $G(n_e)$ = frequency agility gain

$L_f(1)$ = fluctuation loss for single frequency system

The number of independent samples is related to the total frequency bandwidth, ΔF, and critical frequency Δf_c as follows:

$$n_e = 1 + \frac{\Delta F}{\Delta f_c} \quad .$$

A plot of the reduction in signal-to-noise ratio required for detection, or frequency agility gain, relative to that required for a Swerling 1 target is given in Figure 6.2-5 as a

1. Barton, D.K.;"Simple Proceedures for Radar Detection Calculations" IEEE Transactions AES5 No.5, Sept. 1969.

D²C

Figure 6.2-5.
Frequency Agility Gain
vs Number of Independent
Samples
$n' = 10^6$

$P_D = 0.99$ (Single scan)

Swerling 2 Limit

$P_D = 0.90$

$P_D = 0.79$

$P_D = 0.68$

$P_D = 0.54$

Frequency Agility Gain, dB

Number of Independent Samples
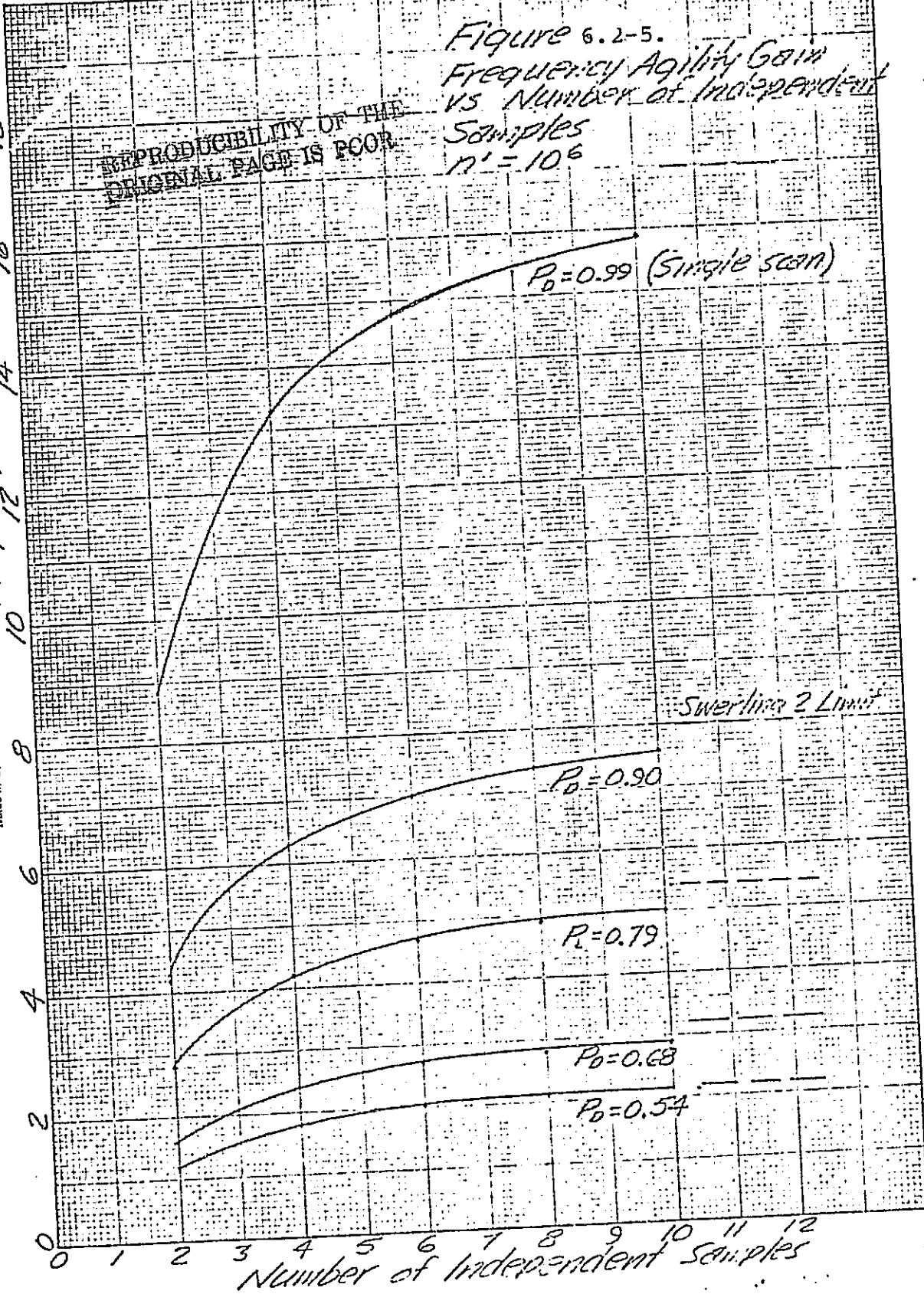
function of the number of independent frequency samples provided. Also shown on the figure is the Swerling 2 limit, or the maximum gain which can be achieved with complete independence pulse-to-pulse for the total number of pulses received.

A brief examination of Figure 6.2-5 indicates that the greatest gain is obtained from the first few independent samples. The improvement for a number of samples above about six is quite slow. In our case , six independent samples, corresponds to six frequency positions and a total frequency agility bandwidth of

$$\Delta f = (n_e-1)\Delta f_c = (6-1)75 = 375\text{MHz}.$$

6.2.4 RANGE EQUATION.

The various parameters affecting radar performance are placed in perspective by the radar range equation. A general form of the range equation, useful for comparison of candidate radar types, can be written in terms of the ratio of received energy, E_r, to noise density, N_o, as follows:

$$\frac{E_r}{N_0} = \frac{P_t G^2 \lambda^2 \sigma}{(4\pi)^3 R^4 k T_s L}$$

where;

P_t = Transmitted power

G = Antenna gain (assuming the same antenna is used for transmit and receive)

λ = Wavelength of radiation

σ = Radar cross section of target

R = Range

K = Boltzman's constant

T_s = System noise temperature

L = Losses

The general form of the radar range equation is adapted to the non-coherent pulse radar by noting that the transmitted energy per pulse is the peak transmitted power times the pulse width and the energy received per pulse is equal to the peak received power times the pulse width. Then the range equation may be written

$$\frac{E_r}{N_0} = \frac{P_t \tau}{N_0} = \frac{P_t \tau G^2 \lambda^2 \sigma}{(4\pi)^3 R^4 k T_s L}$$

The commonly used detection criterion is based on the signal-to-noise ratio defined as the ratio of the peak received signal power to the noise power in the bandwidth, B.

$$SNR = \frac{P_r}{N_O B} \ .$$

then:

$$SNR = \frac{P_t G^2 \lambda^2 \sigma}{(4\pi)^3 R^4 k T_s B L}$$

6.2.5 TARGET ACQUISITION.

6.2.5.1 ANTENNA SCAN PARAMETERS.

The signal-to-noise ratio required for acquisition is a
function of the amplitude fluctuation characteristics of the
target, the number of pulses received during the antenna
scan past the target and the allowable false alarm rate.
The number of pulses received is a function of the PRF,
antenna beamwidth and antenna scan characteristics.

The antenna scan options are to cover the required 80°
conical sector once in the 60 second allowable acquisition
time or to scan at a higher rate and obtain two or more looks
at the target in the 60 second period. The higher scan
rates result in less time on target per scan which results
in a lower probability of detection. However, an offsetting
factor is that the required probability of detection per
scan to obtain a given cumulative probability of detection
also decreases with the number of scans.

The probability of detection per scan P_d required for a given
cumulative probability of detection P_c, for a given number
of sweeps, n, in the acquisition interval is given by

$$P_c = 1-(1-P_d)^n$$

To achieve a cumulative detection probability of detection
of 0.99 the required detection probability per scan is given
below as a function of the number of scans in the acquisition
interval.

n	P_d
1	0.99
2	0.90
3	0.79
4	0.68

In order to optimize the overall radar system the antenna
gain, beamwidth and scan rate will be treated as variable
parameters at this time. The antenna gain and beamwidth
are a function of antenna size. Three different size
antennas will be considered along with various scan rates as
listed in Table 6.2-2. The time on target and the number of
pulses received as the antenna scans by the target are also
indicated in the Table.

The antenna sizes and scan rates are representative of possible
values for the Rendezvous Radar. The antenna scan rates are

Antenna Size, meters	Gain, db	Two-way Beamwidth, Deg.	Search Frames in 60 sec.	Scan Rate Deg/sec	Dwell time, milliseconds	Number of Pulses Received	
						PRF=3.7KHz	PRF=6.8KHz
1.5	45.2	0.66	1	170	3.9	14	26
			2	374	1.8	6	12
1.0	41.7	1.0	1	111	8.9	32	60
			2	227	4.4	16	29
0.5	35.7	2.0	1	55	36.0	133	244
			2	111	17.8	65	121
			3	165	12.0	44	81
			4	220	9.0	33	61

Table 6.2-2. ANTENNA AND SCAN PARAMETERS

based on a spiral scan program discussed in Section 5.2. The maximum scan rates indicated are for the constant angular velocity phase of the scan, which is the outer portion of the scan envelope. Near the center of the search area the scan rates are lower.

A maximum of 2 scan frames were considered in the 60 second acquisition interval for the 1.0 and 1.5 meter antennas to limit the angular scan rate required to reasonable values.

6.2.5.2 DETECTION STATISTICS.

The signal-to-noise ratio required for a given probability of detection of a Swerling Class 1 target with a given number of pulses available for non-coherent integration is conveniently obtained from Fehlner's treatment of Marcum's and Swerling's data on detection.[1] The detection data is referenced to a false alarm number which in turn is related to the false alarm time. The false alarm time is defined as the time during which the probability is 0.5 that there will not be a false alarm.

In view of the maximum search time of 60 seconds, a reasonable false alarm time is about 600 seconds. This will result in only a momentary halt in the antenna scan with a probability of 0.5 once every 10 search intervals. During tracking only those false alarms which occur within the range gate are important and these are filtered by the range tracking loop. The false alarm time will be optimized later in the study.

Fehlner defines the false alarm number as the number of independent opportunities for a false alarm in the false alarm time. It is related to false alarm time, t_f, as follows:

$$n' = \frac{t_f (PRF) \; G}{mN}$$

where;

G = number of range gates (of width τ) per range sweep
m = number of pulses integrated coherently ($m > 1$)
N = number of pulses integrated incoherently ($N > 1$)

If range gating is not used the number of effective range gates of width τ in the interpulse interval $\frac{1}{PRF}$ is $\frac{1}{\tau (PRF)}$

and for this case, $(PRF)G = \frac{1}{\tau}$ and $n' = \frac{t_f}{mN\tau}$

1. Fehlner, L.F.; "Target Detection by Pulsed Radar", John Hopkins University Report TG451.

Considering the use of range gates we may express the false alarm number in terms of the ratio, α, of the range gate on time t_g, to the interpulse period, $\frac{1}{PRF}$, as

$$n' = \frac{t_f \, \alpha}{mN\tau}$$

For the incoherent radar case m=1 and

$$n' = \frac{t_f \alpha}{N\tau}$$

For the case of the 6.8 KHz. PRF the range gate is on approximately for the entire interpulse period and $\alpha=1$. For the case of the 3.7 KHz. PRF the range gate is on for 22km or 147 µsec out of the 270 µsec interpulse period and $\alpha=0.55$.

An investigation was made to determine if it is more efficient, in terms of signal-to-noise ratio required, to use a range gate equal in width to the range interval to be searched or to search in range with a narrow range gate at the same time as the angle search is in process.

If a priori range information is available to an accuracy of ±2km as indicated for mission 3-B then it is more efficient to use a 4km range gate to capture all of the received pulses while minimizing the opportunities for false alarm. The benefit of using a 4km wide range gate rather than a 22km wide gate amounts to about 0.4db at a 90% single scan probability for a Swerling 1 target.

If a priori range information is not available and the 22km interval is searched by a 4km wide range gate, the number of pulses available for integration is reduced by a factor of 22/4. The signal-to-noise ratio required for acquisition of a Swerling 1 target is about 3.6db greater for the swept 4km gate than for a "wide open" gate 22km wide.

Consequently, we will assume that for acquisition the range gate is equal in width to the range interval to be searched.

For comparison and sizing purposes a pulse width of 1µsec will be used to compute the false alarm number. Variations up to a factor of 5 from the 1µsec value will result in less than 0.5db change in the computed value of signal-to-noise ratio required for acquisition.

A plot of the signal-to-noise ratio required for acquisition for a Swerling 1 target as a function of the number of scan frames in the 60 second acquisition interval is given in Figure 6.2-6.A

Figure 6.2-6
Signal to Noise Ratio Required
for Acquisition vs. Number
of Scan Frames in 60 sec
Acquisition Interval
Swerling 1 Target
False Alarm Time 10 Minutes

PRF
6.8 kHz −−−−−
3.7 kHz ———

1.5 m Diameter Antenna

1.0 m Diameter

0.5 m Diameter

Signal to Noise Ratio, dB

Number of Scan Frames

Form No. 642—10 Squares to Inch
AMERICAN PAD & PAPER CO., HOLYOKE, MASS.
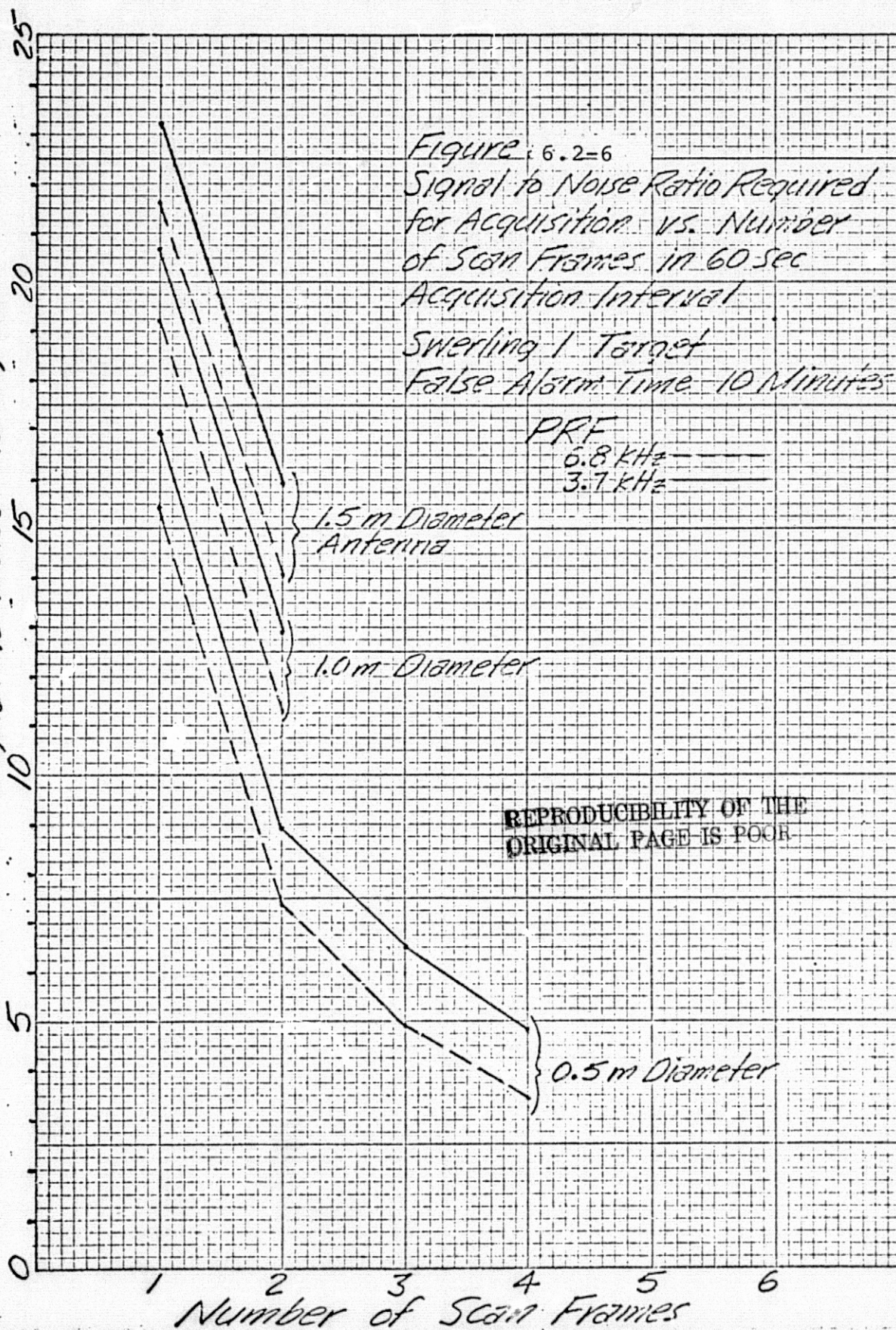
similar plot for the same target with 6-step frequency
agility is given in Figure 6.2-7.

Since the pulses are essentially uncorrelated pulse-to-
pulse when frequency agility is used the signal-to-noise
ratio required is essentially independent of the number of
scan frames in the 60 second interval.

6.2.6 TRANSMITTER AND RECEIVER PARAMETERS.

Having established the signal-to-noise ratio required for
a 0.99 probability of detection in a 60 second interval for
various radar conditions, we will next determine the
transmitter and receiver characteristics which are required
to acquire the $1m^2$ target before the range closes to 19km.
Considering the maximum velocity of 45m/sec and an acquisition
time of 60 seconds, the acquisition process must start at
21.7km.

The range equation discussed previously will be referenced
in the following discussion. It is repeated for reference
below.

$$SNR = \frac{P_t G^2 \lambda^2 \sigma}{(4\pi)^3 R^4 k T_s B L}$$

Values for the parameters L, B and T_s are established in
the following paragraphs. The other parameters are either
given or are to be determined.

6.2.6.1. LOSSES.

The general loss term L, will be defined to include the
following:

$$L = L_m L_s L_f$$

where;
L_m = Microwave loss in transmit path.
L_s = Beam Scanning loss.
L_f = Filter missmatch loss.

6.34

Figure 6.2-7
Signal to Noise Ratio Required
For Acquisition vs Number
of Scan Frames in 60 sec
Acquisition Interval
Six Step Frequency Agility
False Alarm Time 10 Minutes

PRF
6.8 kHz ----
3.7 kHz ——
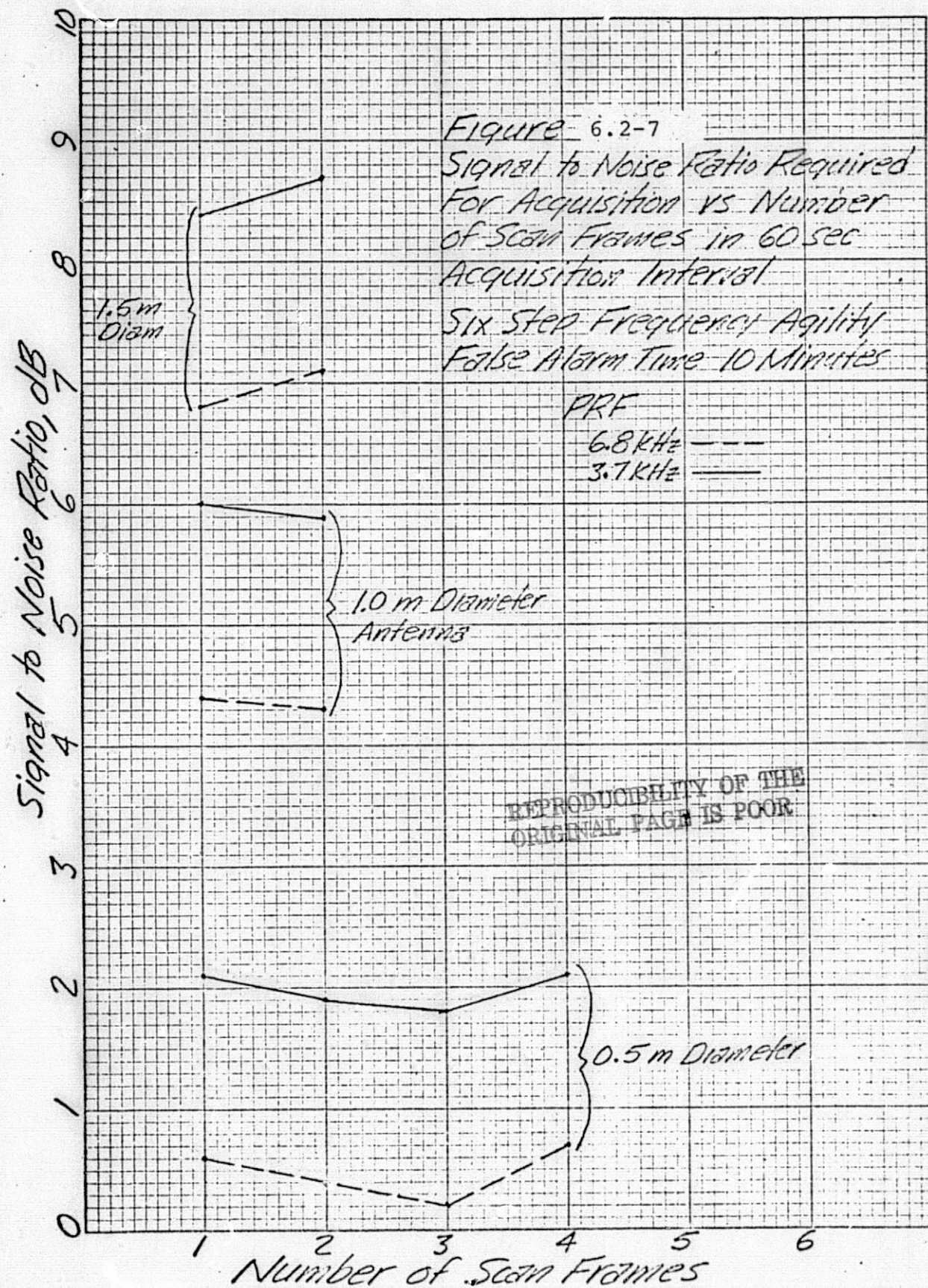
The total loss in the transmit path, L_m, is estimated to be about 1.6 dB. The loss in the receive path is estimated at 1.5 dB.

The beam scanning loss, L_s, pertains to the fact that the signal is not received at full amplitude except at the peak of the beam as the beam scans past the target, whereas in computing signal-to-noise required for acquisition we assumed the pulses integrated were all the same amplitude.

Typical values for beam scanning loss given in the literature is 1.6 dB for each scan dimension or a total of 3.2 dB for a two dimensional scan. These values are based on the use of 1-way beamwidths in determining time on target and scan spacing. In this study 2-way beamwidths are used throughout. An integration over the two-way power pattern of a uniformly illuminated circular aperture between the two-way half power points indicates an average scanning loss of 1.0 dB. Using a 30% overlap of successive scans the loss in the cross scan dimension is equal to 0.55 dB. The total scan loss is then equal to 1.55 dB.

The maximum signal-to-noise ratio, SNR, occurs when the receiver bandwidth is matched to the pulsewidth. However, to minimize complexity in the receiver the matched filter is usually approximated by a passive circuit. In particular, using two synchronously tuned stages as an IF filter the filter mismatch loss, L_f, is about 0.56 dB for the optimum 3 dB bandwidth time product of 0.61.[1] The noise bandwidth for this filter is a factor of 1.22 times the 3 dB bandwidth.

For a given pulsewidth, τ, the 3 dB bandwidth should then be equal to $\dfrac{0.61}{\tau}$ Hz. The noise bandwidth, B_n, for this filter is a factor of 1.22 times the 3 dB bandwidth or $\dfrac{0.75}{\tau}$ Hz.

6.2.6.2. SYSTEM NOISE TEMPERATURE, T_s.

The system noise temperature, T_s, may be expressed:

$$T_s = T_a + T_r + LT_e$$

where:

T_a = Antenna noise temperature.
T_r = Transmission line noise temperature = $T(L-1)$.
T = Thermal temperature.
L = Transmission line loss factor.
T_e = Receiver noise temperature = $T_o(NF-1)$.
T_o = Reference temperature = 290°K.
NF = Receiver noise figure.

1. Skolnik, M.I.; Introduction to Radar Systems.

The antenna temperature due to cosmic radiation looking into space is about 2.7°K.

The physical temperature of the transmission line will be assumed to be 290°K which with the receive path loss of 1.5dB yields a transmission line noise temperature of 119°K.

The receiver will be assumed to be a microwave mixer type without RF amplification for preliminary sizing purposes. Using a balanced Schottky diode type mixer a noise figure of about 7.0db can be realized at any given frequency from 9.3GHz. to 16GHz. The equivalent receiver noise temperature is then 1160°K.

The root system noise temperature becomes

$$T_s = 2.7 + 119 + 1636 = 1758°K$$

6.2.7. TRANSMIT ENERGY REQUIRED FOR ACQUISITION.

The transmitted energy per pulse required to achieve a given signal-to-noise ratio is computed in Table 6.2-3.

The substitution $F_n = \dfrac{0.75}{\tau}$ is made in the radar range equation to relate the receiver noise bandwidth, B_n, to pulsewidth, τ. This assumes the use of a two stage synchronous filter as discussed previously. The transmitted energy per pulse can then be written:

$$P_t \tau = \frac{(SNR)\ (4\pi)^3 R^4 KT_s (0.75)L}{G^2 \lambda^2 \sigma}$$

where the symbols are as defined previously.

The result of the calculation in Table 6.2-3.

$$P_t \tau = 47.0 + 10\log(SNR) - 20\log G \text{ dB W sec}$$

6.2.7.1 AVERAGE TRANSMITTED POWER REQUIRED FOR ACQUISITION.

The amount of transmitted energy per pulse required for acquisition is found by substituting the value for antenna gain given in Table 6.2-2 into the expression for transmitted energy per pulse given in Table 6.2-3 along with the value

$$D^2C$$

$$P_t\tau = \frac{(SNR)(4\pi)^3 R^4 kT_s(0.75) L_m L_s L_f}{G^2 \lambda^2 \sigma}$$

Symbol	Parameter	Value	Value in db
SNR	Signal-to-noise ratio		10 log(SNR)
$(4\pi)^3(0.75)$		1500	31.8
R^4	$(Range)^4$	$(21.7\times10^3 m)^4$	173.6
K	Boltzmann's Constant		-228.6
T_s	System Noise Temperature	1758°K	32.4
L_m	Microwave loss in transmit path	1.6 dB	1.6
L_s	Scan loss	1.6db	1.6
L_f	Filter Missmatch loss	0.6db	0.6
G^2	$(Antenna\ Gain)^2$	G^2	-20 log G
λ^2	$(Wavelength)^2$	$2\times10^{-2} m$	34.0
σ	Radar cross section	$1m^2$	0

$P_t\tau$ (Peak Transmit Power)(Pulse width)   47.0+10log(SNR)- 20 log G

Table 6.2-3   COMPUTATION OF TRANSMITTED ENERGY PER PULSE FOR
                INCOHERENT PULSE RADAR.

of signal-to-noise ratio required for acquisition from
Figures 6.2-6 and 6.2-7.

The average transmitted power required for acquisition
is obtained by multiplying the required transmitted eneray
per pulse by the pulse repetition frequency. The average
transmitted power required for acquisition of a $1m^2$ Swerling
1 target is given in Figure 6.2.-8 as a function of antenna
size and the number of scan frames in the 60 second acquisition
interval.

The corresponding value of average transmitted power for the
case of six-step frequency agility is given in Figure
6.2.-9. The average power required in this case is
essentially independent of the number of scan frames in the
60 second interval since the pulses are uncorrelated pulse-
to-pulse.

The use of frequency agility has two important benefits.
First, the average transmitted power required for acquisition
is substantially lowered. Secondly, it is not necessary to
program more than 1 scan frame in the acquisition interval.
The later factor translates into lower weight and power
consumption of the antenna drive mechanism.

Figure 6.2-8
Average Transmitted Power
Required for Acquisition vs.
Number of Scan Frames in
60 Sec Acquisition Interval
Swerling 1 Target
False Alarm Time = 10 Minutes
PRF
6.8 KHz ------
3.7 KHz ———

REPRODUCIBILITY OF THE
ORIGINAL PAGE IS POOR

Figure 6.2-9
Average Transmitted Power
Required for Acquisition vs.
Number of Scan Frames in
60 Sec Acquisition Interval

Six Step Frequency Agility
False Alarm Time = 10 Minutes

PRF
6.8 kHz ----
3.7 kHz ——

0.5 m Diameter

1.0 m Diameter Antenna

1.5 m Diameter Antenna

Average Transmitted Power, Watts

Number of Scan Frames

6.2.8. RANGE TRACKING ACCURACY.

The range tracking errors may be grouped into deterministic errors, which are fixed for a given set of operating parameters; fixed random errors, which are random but relatively constant over the period of time the radar is in use; and fluctuation errors which have periods of a few seconds or less. A tabulation of range tracking errors is given in Table 6.2-4. A brief discussion of these errors is given in the following paragraphs. The error in the range tracker itself is assumed negligible for signal-to-noise ratios above unity due to digital implementation of the tracking loop.

The net long term, or bias error, is the sum of the deterministic error and the fixed random error. For pulse widths of 1μsec or less the maximum error (deterministic plus 3σ fixed random) is equal to 48.5 meters. However, if the lag error is removed by computation the net bias error is about 25.5m 3σ which is near the 24m specified maximum value.

The fluctuating error is dominated by target induced range errors. The net 3σ fluctuating error considering a 18.2 m target at 30° aspect is about 15m. This is half of the allowable error of 30 m.

6.2.8.1. VELOCITY LAG.

The range data is filtered by the equivalent of a low pass filter with a time constant of 0.5 seconds. The resulting lag error for a steady velocity of is equal to 0.5 (velocity). This error can be removed by computation since velocity and time constant are known.

6.2.8.2. CLOCK FREQUENCY.

The basic timing reference for the radar is a 30 MHz. crystal controlled clock. An accuracy of about 0.01%, 1σ is adequate for this application.

6.2.8.3. START PULSE STABILITY.

A "start" pulse is generated to start the time measuring interval by detecting the leading edge of the transmitted RF pulse. The variation in delay between the transmitted pulse and generation of the start pulse is less than ± 2 nsec. Assuming a uniform distribution of error the 1σ value is about 1.2 nsec or 0.18 meters.

ERROR SOURCE	Deterministic error	1σ error value, meters	
		Fixed random	Fluctuating
Velocity lag*	0.5 V		
Clock frequency (0.01%)		.0001 R	
Start pulse stability		0.2	
Propagation delay in receiver pulsewidth= 0.1,1.0, μsec.		0.83,8.3,	
Gating and threshold delay		0.1	
Calibration		0.3	
Quantization			0.05
Range tracker jitter μsec pulsewidth,SNR=3db			
Target induced range errors** (18.2m target,30°aspect)			4.6
Total RSS 1σ error	0.5 V	$\sqrt{(.0001R)^2+(.91)^2}$ $\sqrt{(.0001R)^2+(8.4)^2}$	4.7

* Error may be removed by computation.

** Error may be reduced to 1.4 meters, 1 σ, using frequency agility.

$$\text{Net error} = 0.5V+\sqrt{(.0001R)^2+(4.8)^2} \qquad R\leq 9km$$
$$\text{Net error} = 0.5V+\sqrt{(.0001R)^2+(1.7)^2} \qquad R\leq 9km,\text{Freq. agile}$$
$$\text{Net error} = 0.5V+\sqrt{(.0001R)^2+(9.8)^2} \qquad R\geq 9km$$
$$\text{Net error} = 0.5V+\sqrt{(.0001R)^2+(8.4)^2} \qquad R\geq 9km,\text{Freq. agile}$$

TABLE 6.2-4   RANGE TRACKING ERROR

6.2.8.4. PROPAGATION DELAY IN RECEIVER.

The signal propagation through the microwave and electronic portions of the receiver will amount to several hundred nanoseconds. However, the nominal delay can be removed in calibration and only the variation over temperature and aging constitutes an error. We have assumed, to minimize matching loss, that the dominant filter are two synchronously tuned stages. Considering cases of pulsewidths of 0.1 and 1.0 the corresponding receiver noise bandwidth will be about 7.5 mHz. and 0.75 mHz. respectively. The time delay through each stage is approximately equal to the reciprocal of the bandwidth of each stage, which is approximately a factor of $\sqrt{2}$ greater than the net resultant bandwidth. The net delay through the receiver is then about 0.19 μsec and 1.9 μsec corresponding to the bandwidths of 7.5 and 0.75 respectively.

Assuming the use of an attenuator pad type of AGC to hold the signal level relatively constant, the variation in delay can be held to about ±5%. Taking this as a maximum value with a uniform error distribution the 1σ value is about 2.9%. The propagation delay in terms of range is then 0.83m and 8.3m for the bandwidths of 7.5 and 0.75 mHz. respectively.

6.2.8.5. GATING DELAY STABILITY.

Variation in the propagation delay of the signal through the range gate and counter start/stop circuitry are sources of error. The nominal delay through these circuits will typically be about 10ηsec with a variation of less than ±3ηsec maximum. Assuming a uniform distribution of error the 1σ value is 1.7ηsec or about 0.12 meters.

6.2.8.6. CALIBRATION.

We estimate that a calibration of the range measurement portion of the radar can be made to an accuracy of ±0.5 meters at any range to 19km. Assuming a uniform distribution of error, the 1σ value is about 0.3 meters.

6.2.8.7. QUANTIZATION.

A 30 mHz. crystal controlled clock is used as the basic timing reference for the radar. One clock cycle is then 3.33×10^{-8} seconds which is equivalent to 5 meters of range.

The RMS value of the quantization error for asynchronous counting of a pulse train is related to the sample value and number of samples as follows:

$$\text{RMS error} = \frac{\text{Sample value}}{\sqrt{6}\ \sqrt{\text{Number of samples}}}.$$

In our case the sample value is 5 meters. The number of samples for a half second accumulation time at a PRF of 3.7 KHz. is 1850. The RMS error is then 0.05 meters.

6.2.8.8. RANGE TRACKER JITTER.

For purposes of system sizing and comparisons, a split-gate range tracker will be assumed. This type of tracker is approximately matched to the received signal when the receiver bandwidth is selected to optimize signal-to-noise ratio. Other tracker configurations such as a leading edge tracker which can yield better accuracy but requires wider receiver bandwidths, will be treated later in the study.

Barton[1] has developed expressions for the one sigma value of the random error or noise at the output of a split-gate range tracker, σ_r, as follows:

$$\sigma_r = \frac{\tau}{K_r \sqrt{(SNR)\dfrac{(PRF)}{B_r}}} \qquad\qquad (SNR > 1)$$

where;

τ = Pulse width.

K_r = Error slope factor = 2.5 when gate width and bandwidth is matched to pulse width.

SNR = Signal-to-noise ratio.

PRF = Pulse repetition frequency.

B_r = Bandwidth of range tracking loop.

The bandwidth of the range tracking loop can be relatively long for the skin track mode due to the moderate dynamics involved. The bandwidth must be sufficiently high to prevent the tracker from lagging off of the pulse during target-radar dynamics and to prevent excessive lag error in the data.

Since the lag error can be removed from the range data by computation, a time constant of 0.5 seconds which restricts the lag to a small fraction of the 1μsec pulse width was chosen.

1. Barton, Loc Cit.

The 1σ value of the fluctuating component of range error due to themal noise is plotted in Figure 6.2.-10 as a function of signal-to-noise ratio and pulse width. A PRF of 3.7KHz. was used.

6.2.8.9. TARGET INDUCED RANGE ERRORS.

The subject of target induced range errors was discussed in Section 6.1.   The 1σ value of the range fluctuations due to target effects is equal to about one half of the target depth in the range direction. For the 18.2 meter target at a 30° aspect the range fluctuations will be about 4.6 m,1σ.

This error can be reduced by a factor of about 3.4 using pulse-to-pulse frequency agility with a total bandwidth of 375 Hz.

6.2.9.   ACCURACY OF THE VELOCITY MEASUREMENT.

Relative velocity is determined in the non-coherent pulse radar by taking range differences per unit time. Since we have assumed a digital range tracking mechanization, the velocity data can be obtained by implementing a digital filter. The filter would consist of a near perfect differentiator followed by a low pass filter. The filter would be of the form:

$$H(S) = \frac{S}{(1+\tau_f S)}$$

where;

τ_f is the time constant of the low pass filter.

The response of the range tracker will also be approximated by a low pass filter having a time constant $\tau_t = 0.5$ seconds as discussed previously.

The transfer function of the tracker plus differentiator plus low pass filter may then be expressed as:

$$H(S) = \frac{S}{(1+\tau_t S)(1+\tau_f S)} ,$$

For the case of a constant range rate of V meters per second the output of t output of the filter can be expressed:

$$F_o(S) = \frac{V}{S^2} \frac{S}{(1+\tau_t S)(1+\tau_f S)} ,$$

which in the time domain is equal to:

$$f_o(t) = V [1 + \frac{1}{\tau_t - \tau_f}(\tau_t e^{-\frac{t}{\tau_t}} - \tau_f e^{-t/\tau_f})]$$

Figure 6.2-10
Fluctuation Error of Split-
Gate Range-Tracker vs Signal
to Noise Ratio

Tracker Bandwidth = 0.32 Hz
PRF = 3.7 kHz

Pulse Width $\tau = 5 \mu sec$

$\tau = 1 \mu sec$

$\tau = 0.1 \mu sec$

Note: The fluctuation error
given for SNR < 3 dB is
larger than actual since
the tracker bandwidth
decreases at low SNR

1σ Fluctuation Error, meters (vertical axis)

Signal to Noise Ratio, dB (horizontal axis: -6 -4 -2 0 2 4 6 8 10 12 14 16 18 20)
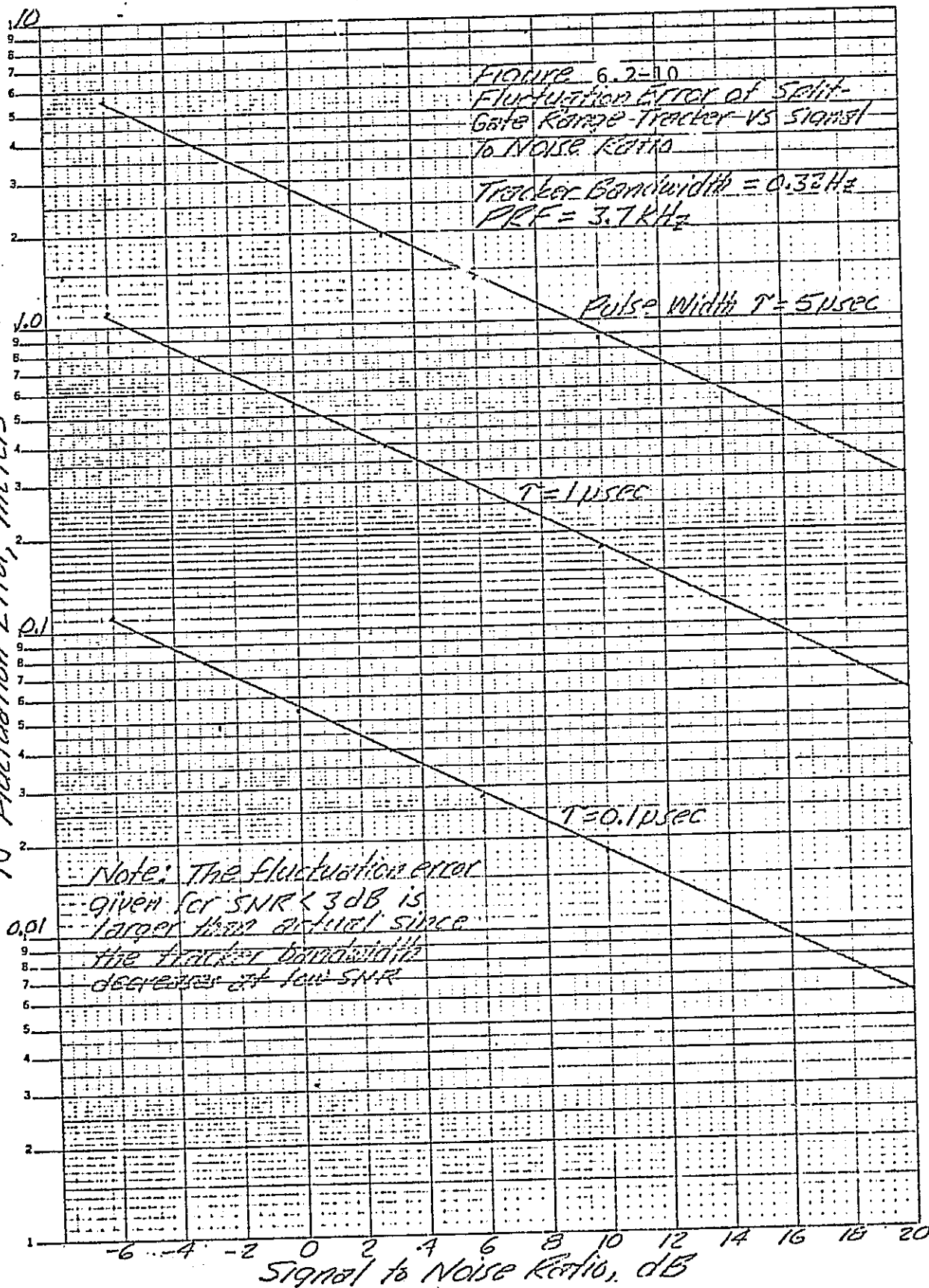
In the steady state $(t >> \tau)$ the output is a steady signal of amplitude V meters per second as desired.

For the case of a constant relative acceleration between the target and the radar of A meters/sec^2, the output of the filter becomes:

$$F_0(S) = \frac{A}{S^3} \frac{S}{(1+\tau_T S)(1+\tau_F S)}$$

which in the time domain is:

$$f_0(t) = A\left[t - \tau_T - \tau_F - \frac{1}{\tau_T - \tau_F}\left(\tau_F^2 e^{-t/\tau_F} - \tau_T^2 e^{-t/\tau_T}\right)\right]$$

In the steady state $(t >> \tau)$ the output becomes:

$$f_0(t)_{ss} = A\left[t - (\tau_T + \tau_F)\right]$$

Thus, for the case of changing velocity at a constant rate the output will lag the input by $(\tau_t + \tau_f)$ seconds.

Item C.2 of the Functional Requirements for the Rendezvous Radar specifies that "the radar range rate shall not lag the true range rate by more than 2 seconds." Since the range tracker time is about 0.5 seconds the time constant of the low pass velocity filter should be less than 1.5 seconds. A value of 1.0 second will be used for preliminary computation purposes.

The error in the velocity measurement can be expressed as a steady term plus a fluctuating error component.

The steady error will be proportional to the range error plus the error in the differentiating process. The latter error is negligible for the digital mechanization. The steady error is also very low because all except the fluctuating errors and the error in the clock frequency listed in Table 6.2-4 are slowly varying errors (constants) which drop out in the differentiation process. The steady velocity error will then be about 0.01% of the velocity.

Considering the fluctuating component of the velocity error we will treat first the fluctuating error due to tracker jitter due to thermal noise. We define a range spectral density, $W_r(W)$, which exists prior to the effective filter in the range tracker. $W_r(\omega)$ is essentially flat over the frequency region of interest or $W_r(\omega) = W_r$. Then, the total noise at the velocity output port is:

$$N = W_r \int_0^\infty \frac{\omega^2}{[1+(0.5\omega)^2][1+(1.0\omega)^2]} \, d\omega \; .$$

This integral was evaluated by numerical means with a result of

$$N = 1.85 \, W_r \; .$$

The range noise spectral density, W_r, at the input to the tracker low pass filter is equal to

$$W_r = \frac{\sigma_r^2 \, \tau_t}{1.57} \qquad\qquad m^2/radian$$

where σ_r is the RMS range noise at the couput of the range tracker low pass filter and the factor of 1.57 relates to the ratio of effective noise bandwidth to 3db bandwidth of a single section low pass filter.

For a value for the time constant of range tracker filter of 0.5 seconds and a time constant of 1.0 seconds for the low pass filter following the differentiator, the total noise power at the velocity output port of the filter is:

$$N = \frac{1.85 \, \sigma_r^2 \, 0.5}{1.57} = 0.59 \, \sigma_r^2$$

The RMS or 1σ value of the noise is $\sqrt{N} = 0.77\sigma_r$.

To maintain the velocity noise below a 1σ value of 0.1m/sec as specified (0.3m/sec,3σ), the range noise must not exceed 0.13 meters, 1σ. Referring to Figure 6.2-10 and considering only thermal noise we see that for pulse width of 1μsec a signal-to-noise ratio of 13db is required to achieve this low value.

The largest contributer to noise on the velocity output will be due to target induced range noise. This subject was discussed in Section 6.1   where it was shown that extremely high apparent range rates can be generated due to very small changes in target aspect.

Considering the 18.2 meter target with two dominant reflecting surfaces on either end with a ratio of effective scattering area of 0.5 and a relative change in aspect angle of 2.8°/min at an aspect angle of 30° as discussed previously for mission 3-B, a maximum range rate of about 122m/sec is indicated. The rate of this variation will be about 0.87Hz. This rate will be attenuated by a factor of about 5 by the velocity filter network to about 24 m/sec.

An appreciable reduction in the target induced noise can be obtained by the use of frequency agility. By using the six step frequency agility and a PRF of 3.7KHz. the lowest frequency component of the range noise will be increased to 617Hz. A 617Hz. variation will be attenuated approximately a factor of 4000 by the velocity filter network. The 122m/sec peak velocity noise would then be reduced to about 0.03 m/sec.

6.2.10 ANGLE TRACKING ACCURACY.

The accuracy of the angle track of the target can be expressed in terms of bias errors and fluctuating errors. The former may be caused by offsets in the positioning servo and phase errors in the antenna feed lines, in the monopulse combiner and in post combiner circuits. Fluctuating errors may be caused by receiver noise and glint of the target.

The allowable error (3σ) in line-of-sight angle (LOS) is 60 milliradians (3.4°) bias error and 10 milliradians (0.57°) random error. The allowable error (3σ) in LOS angle rate is o.14 mR/sec (0.008°/sec) bias and 0.14 mR/sec random. We note that with the narrow beam antennas contemplated that the allowable bias angle error is well off the main lobe of the antenna. Further, the allowable angular rate error is extremely small.

6.2.10.1 BIAS ANGLE TRACKING ERRORS.

The tracking error introduced by phase errors in the monopulse combiner process and antenna feeds has been analyzed by Dunn and Howard[1] who give the following expression:

$$\epsilon_\Theta \approx \frac{1}{2K} \, \Psi \, \tan \phi$$

where

ϵ_Θ = Error in pointing angle

K = Gain constant

Ψ = Pre-combiner phase error (assumed small)

ϕ = Post-combiner phase error

The gain constant K relates the output of the phase sensitive detector to small angular displacements from boresight for a given

1. Dunn, J.H. and Howard, D.D. "Precision Tracking with Monopulse Radar" Electronics, April 22, 1960.

signal amplitude. Barton[1] has shown that the error slope for typical monopulse antennas is equal to 1.57 times the maximum voltage of the sum channel per beamwidth error. In Dunn and Howards equation then, assuming unity max reference voltage, the value of K is equal to 1.57 divided by the beamwidth.

The error equation may then be written in terms of the antenna beamwidth, α, as follows

$$\varepsilon_\theta \approx \frac{\alpha\Psi \ \tan\phi}{3.14}$$

Typical monopulse combiners at K_u band, such as those built by MDL, have phase errors of about 5° over a 10% bandwidth. Allowing an additional 5° of phase error in the feeds a total pre-combiner error of 10° will be assumed. The post-combiner phase error, principally that associated with the IF amplifier can be maintained less than 10° over the range of input signal levels.

The net bias error is then computed to be 0.24 milliradians (0.014°) for the 1 meter diameter antenna and 0.48 milliradians (0.028°) for the 0.5 meter antenna. These values are two orders of magnitude better than the 60 milliradian allowable bias error. We conclude that the phase match tolerances can be appreciably larger than those assumed and still meet the angle accuracy requirements.

6.2.10.2 FLUCTUATING ANGLE TRACKING ERROR.

The fluctuating error due to receiver noise in a monopulse tracking system has been treated by Barton who gives the following

1. Barton, D.K. Radar System Analysis.

expression:

$$\sigma_t = \frac{\alpha}{K_m \sqrt{\dfrac{SNR\ B\tau f_r}{C\ \beta}}}$$

where

σ_t = RMS antenna pointing error

K_m = Slope of monopulse error

SNR = Signal-to-noise ratio in bandwidth B

τ = Pulsewidth

f_r = Pulse repition frequency

β = Antenna servo bandwidth

α = Antenna beamwidth

$C = \dfrac{1+SNR}{SNR}$

The parameter C takes into account the fact that both the reference and the signal input to the phase sensitive detectors are noisy and that the output signal-to-noise ratio of the detector is reduced from the input signal-to-noise ratio of the difference channel by the facter $\dfrac{1+SNR}{SNR}$ where SNR is the signal-to-noise ratio in the sum channel.

Barton shows that the error slope, K_m, is equal to 1.57 for typical monopulse antennas. The servo bandwidth must be optimized for best tracking performance with minimum random error or noise. For preliminary sizing purposes a value of 1Hz. for the 1 meter antenna and 0.5 Hz for the 0.5 meter diameter

antenna, which are indicated from search requirements, will be used. The bandwidth can be changed during the tracking mode if required to optimize tracking.

The resulting RMS noise for the two antennas is tabulated below. The signal-to-noise ratio used is that obtained at about 19km range which is about 2.3 dB greater than at 21.7 km where acquisition must begin. The IF noise bandwidth was taken as 0.75 mHz., the pulsewidth at 1μsec and the PRF at 3.7 kHz.

Antenna size, m	Beamwidth one-way, Rad	SNR dB	IF noise BW, mHz.	Servo noise BW, Hz.	RMS tracking noise, mR
0.5	0.049	4.3	0.75	0.79	0.38
1.0	0.024	8.3	0.75	1.57	0.15

The tracking data is smoothed with a time constant of 2 seconds which has an equivalent bandwidth of 0.08 Hz. The RMS tracking noise on the data is then reduced by the square root of the ratio of data smoothing bandwidth to servo bandwidth or to 0.12 mR for the 0.5 m antenna and 0.034 mR for the 1.0 meter antenna. The 3σ values are 0.36 mR and 0.1 mR for the 0.5 and the 1.0 meter antennas respectively.

Angular scintillation (glint) of the target also contributes to the random tracking error. As reported in Section 6.1 of this report, test data on aircraft models and on aircraft in flight indicates that the standard deviation of the glint error is between 0.3 and 0.5 times the target extent. In the case of the 18 meter target, and assuming an aircraft-like scattering properties rather than the dumbbell model also treated in Section 6.1, the

RMS glint is about 9 meters. At ranges less than 2.7 km the tracking error due to glint exceeds the 3.3 mR RMS allowed random error.

The use of frequency agility can reduce angular scintillation as long as the scintillation arises from scatterers distributed in the range dimension as well as in the angular dimension.

Lind[1] shows that the decrease in spectral density of the glint at zero frequency is approximately equal to the frequency agility bandwidth divided by 2 times the critical frequency. The critical frequency, Δf_c, as discussed in Section 6.1 is equal to

$$\Delta f_c = \frac{c}{2D}$$

where c is the velocity of light and D is the range depth of the target.

The reduction in tracking error by frequency agility is the square root of the reduction in spectral density as given below:

$$\text{Reduction} = \sqrt{\frac{\beta D}{c}}$$

where β is the frequency agility bandwidth.

The 18 meter target has a radius of about two meters. In the case of this target viewed broadside (which appears to be the condition for Mission 3-B at a range of about 7 km), D=2 meters.

With the 375 mHz. frequency agility bandwidth previously considered for acquisition the reduction in tracking error with frequency agility is a factor of 1.6.

1. Lind, G. "Reduction of Radar Tracking Errors with Frequency Agility", IEEE Transactions AES-4 No.3, May 1968.

At a range of 2.7 km for Mission 3-B the target is viewed at an angle about 20 degrees from broadside and D becomes equal to about 6.5 meters and the reduction in tracking error is about a factor of 2.9. At 1 km range the viewing angle is about 32 degrees from broadside and the reduction in tracking error is about 3.8.

A plot of the RMS angle tracking noise due to glint for the 18 meter target and Mission 3-B is shown in Figure 6.2-11 for the frequency agile and non-frequency agile cases. It is noted that there is a significant reduction in the tracking noise due to glint when frequency agility is used, particularly when the target is viewed at an angle off of broadside.

We will next estimate the spectral characteristics of the glint.

The 18 meter target viewed near broadside passes through glint cycles about every 0.04° of aspect angle change for dominant reflectors on either end and at a slower rate for reflectors nearer the center. At a maximum LOS rate of about 0.2° per second indicated for Mission 3-B, a maximum angular scintillation rate of about 5 Hz. can be expected without frequency agility. The glint spectral density, assuming a flat response to the maximum frequency of 5 Hz. and for the RMS value of 6.2 mR, indicated in Figure 4-3 for a 1 km range, is $7.7 \times 10^{-6} \mathrm{Rad}^2/\mathrm{Hz}$. Using 375 mHz. bandwidth frequency agility, the spectral density is reduced about a factor of 14 to about $5.5 \times 10^{-7} \mathrm{Rad}^2/\mathrm{Hz}$.

The 1 Hz. servo bandwidth associated with the 1 meter antenna will then result in tracking noise due to glint equal to about 0.93 mR RMS. The 0.5 Hz. servo bandwidth of the 0.5 meter antenna yield tracking noise of 0.66 mR RMS.

18 meter target
Random Scatterer Model
Mission 3-B

Note: For the case
of glint frequencies
low relative to servo bandwidth

Allowable Random Error

RMS Glint
Without Frequency Agility

Broadside Aspect

RMS Glint
With 375 MHz Frequency
Agility
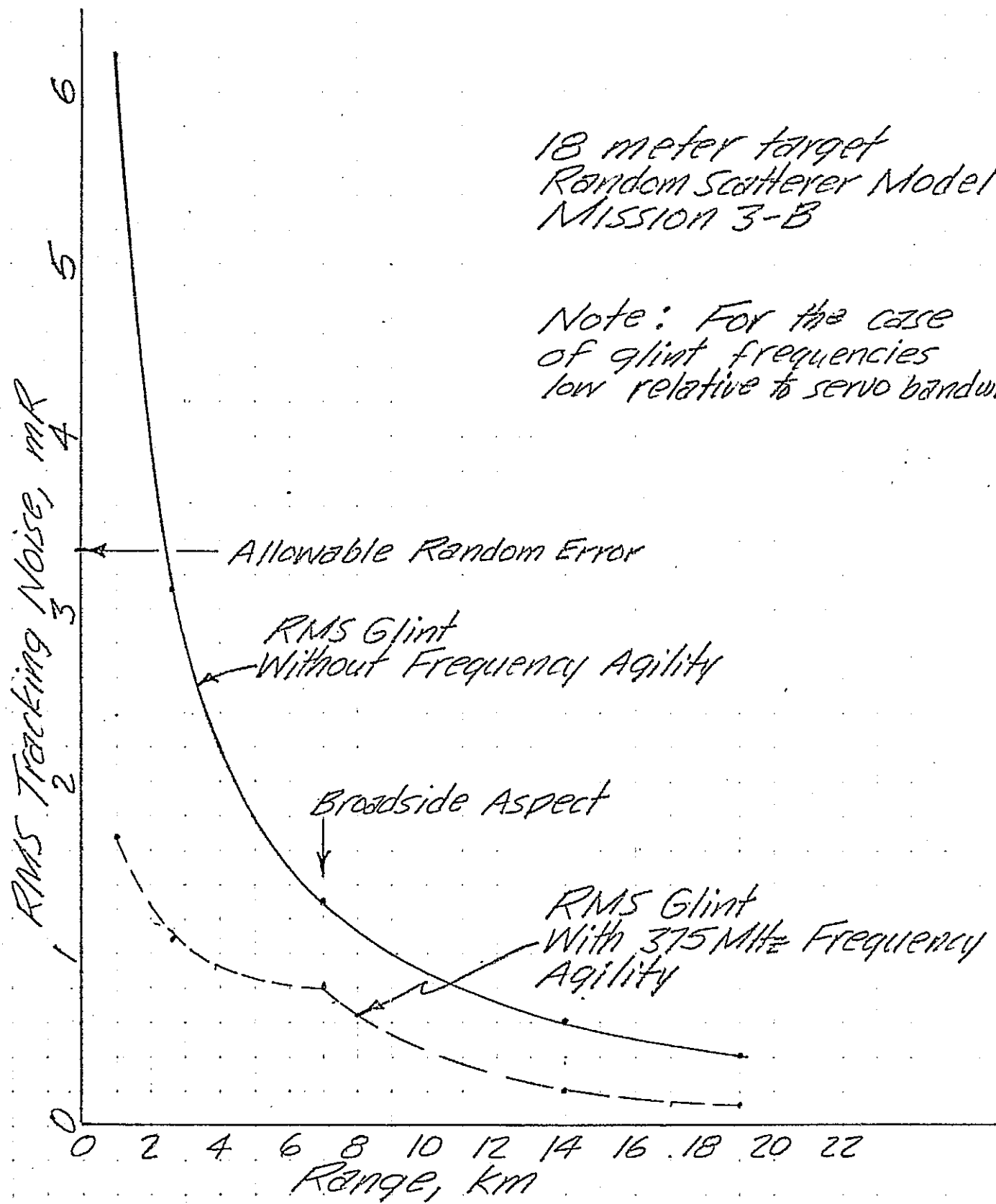
Figure 6.2.11 Tracking Noise Due To
Glint with and without Frequency Agility

In addition, if the angle data is smoothed with a time constant of 2 seconds (0.08 Hz. bandwidth) the RMS noise on the angle readout for either antenna will be 0.2 mR RMS or 0.6 mR, 3σ.

6.2.11 ANGLE RATE ACCURACY.

The error in the angular rate measurement includes errors contributed by the rate gyro, dynamic response of the tracking system and noise due to differentiation of antenna positioning noise caused by thermal noise and glint.

Angular rates up to 5 degrees per second as specified can be measured with an accuracy of .005 degrees per second or about 0.09 milliradians/sec., using a good quality rate gyro. The standoff error is also about this same value. The rate errors due to dynamic response of the servo is a function of the angular acceleration of the target. This error will not be treated in this study due to lack of information on the parameters involved.

The response of the rate measuring device to antenna jitter due to thermal noise and glint is treated next. The parameters involved in rate response to antenna jitter are shown below.

$$W \longrightarrow \boxed{\frac{1}{1+.32S}} \longrightarrow \boxed{S} \longrightarrow \boxed{\frac{1}{1+2S}} \longrightarrow N$$

Angle Noise Density · Antenna Servo · Rate Gyro · Data Smoothing · Output Noise
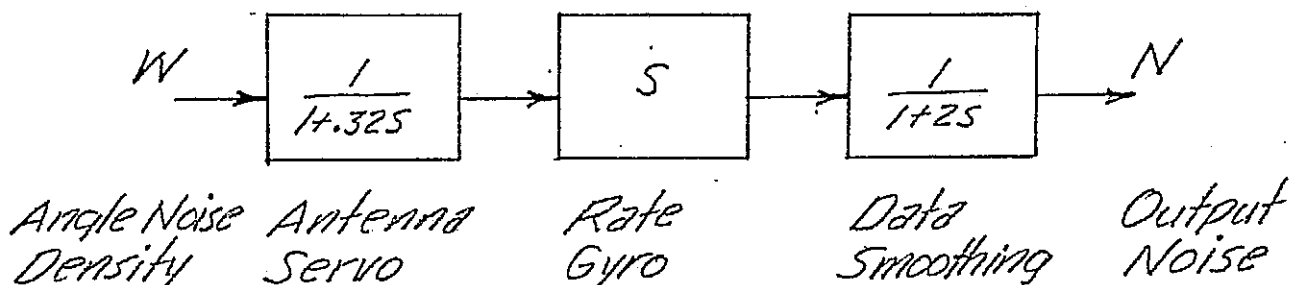
Carrying out the operations indicated above, the mean square noise on the rate output, N, can be expressed in the case of the 0.5 meter antenna

$$N = W(\omega) \int_0^\infty \frac{w^2}{[1+(.32w)^2][1+(2w)^2]} \, dw$$

carrying out the indicated integration by numerical means we find

$$N = 1.03 W(w) \, .$$

For the 1.0 meter antenna the relationship is

$$N = 2.12 W(w) \, .$$

The density function in the case of antenna jitter due to thermal noise is developed from the previous expression

$$\sigma_t = \frac{\alpha}{K_m \sqrt{\dfrac{SNR \ B\tau f_r}{c\beta}}}$$

to be equal to

$$W(w) = \frac{2\pi\alpha^2 C}{k_m^2 (SNR) B\tau f_r} \ Rad^2/Rad$$

In the case of the 0.5 meter antenna W(w) is computed to be 1.12×10^{-6} Rad^2/Rad and for the 1.0 meter antenna case it is 9×10^{-8} Rad^2/Rad.

The resultant RMS noise on the angle rate output in the case of the 0.5 meter antenna is then computed as follows:

$$\alpha_{rn} = \sqrt{(1.03)(1.12 \times 10^{-6})} = 1.07 \times 10^{-3} \text{Rad/sec}$$

In the case of the 1.0 meter antenna the RMS angle rate noise due to thermal noise is 4.4×10^{-4} Rad/sec.

Considering next the effects of glint on the rate output, we use the expression previously determined for the angular noise density due to glint, $5.5 \times 10^{-7} \text{Rad}^2/\text{Hz}$., and compute the resultant noise on the angle rate output as above. The result for the case of the 0.5 meter antenna is

$$\sigma_{rg} = \sqrt{(1.03)(2\pi 5.5 \times 10^{-7})} = 1.9 \times 10^{-3} \text{Rad/sec}$$

and for the 1.0 meter antenna the RMS angle rate noise due to glint is equal to 2.7×10^{-3} Rad/sec.

The 3σ values of the angle rate noise are tabulated below.

Antenna size	Angle rate noise, mRad/sec., 3σ	
	Due to thermal noise at 19km	Due to glint
0.5 m	3.2	5.7
1.0 m	1.3	8.1

We note that the maximum error due to thermal noise occurs at maximum range whereas the maximum noise due to glint occurs at shorter ranges. The angle rate noise in either event is predicted to be substantially larger than the specified value of 0.14mR/sec, 3σ.

The total random angle rate error is the RSS of these values and the rate gyro error of about 0.09 mR/sec.

6.3. ANALYSIS OF COHERENT PULSE RADAR.

A candidate coherent pulse radar scaled to the requirements of the rendezvous radar is described in this section. A summary of characteristics of the radar is given in Table 6.3-1 A functional block diagram of the radar is given in Figure 6.3-1

The range to the target is determined by measuring the time delay between the transmitted and receive pulse in the same manner as described for the non-coherent pulse radar. The relative velocity between the radar and the target is determined by extracting and measuring the doppler shift on the received signal.

6.3-1 AMBIGUITY CONSIDERATIONS.

The ambiguity diagram for a uniform pulse train was discussed in Progress Report #2. The diagram is shown again for reference in Figure 6.3-2.

Velocity ambiguity peaks occur for doppler frequencies spaced by the PRF = $(\frac{1}{\Delta})$. The ambiguity function is of the form $\frac{\sin N\pi\phi\Delta}{N\sin\pi\phi\Delta}$ along the velocity axis where N is the number of pulses integrated and ϕ is the difference between the received doppler frequency and the doppler frequency to which the filter is matched.

For the number of pulses integrated, N, equal to 16 or greater, as is the case with both the 0.5 and 1.0 meter antennas and a PRF of 3.7 KHz., the amplitude of the first sidelobe is about 15.7 db below the main lobe.

It is apparent from the ambiguity diagram that to avoid the possibility of tracking the wrong doppler peak the PRF should be higher than the greatest spread in doppler frequencies, considering both opening and closing velocities.

TABLE 6.3-1   CHARACTERISTICS OF CANDIDATE COHERENT PULSE RADAR

PERFORMANCE CHARACTERISTICS

Detection range (P_D=0.99, Swerling I, 1 m^2 target)...... 19km
Velocity capability .... -20 to +46 m/sec
Acquisition time .... 60 sec
Angular search coverage .... 80° cone
Accuracy, 3σ at maximum range

	Bias	Random
Angle track	0.24 mR	0.1 mR
Angle rate	0.09 mR/sec	1.3 mR/sec
Range	(lag error)	29.7 m
Velocity	(lag error)	$\sqrt{(.03^2+(.006V)^2}$

SYSTEM CHARACTERISTICS

Operating frequency .... 15 gHz.
Antenna
    Size .... 1 m diameter
    Beamwidth (two way) .... 1.0 degrees
    Gain .... 41.7 dB
    Scan program .... spiral

TRANSMITTER[1]

A.   During angle and range acquisition.
    Pulsewidth .... 1.0 usec
    PRF[2] .... 4.8 kHz.
    Peak power .... 1.3 kw
    Average power .... 6 watts

1.   A margin of 2 dB has been applied to transmitted power.
2.   Changed to 4.8 kHz due to revised velocity limits.

6.62

TABLE 6.3.-1. (continued)

Transmitted frequency..........................Frequency agile

      Number of discrete frequencies 6

      Frequency separation .... 75 mHz.

      Total agility bandwidth................ 375 mHz.

B. During velocity acquisition and target tracking.

      Pulsewidth

           Range <9km......................... 1.0μsec

           Range <9km......................... 0.1μsec

      PRF.....................................4.8 kHz.

      Peak power............................. 1.3 kw

      Average power.......................... 6 watts

      Transmitted frequency.................. Frequency agile

Receiver noise temperature................... 1758°K

Receiver noise bandwidth

      Range >9km .... 750 kHz.

      Range <9km............................. 7.5 mHz.

Doppler tracking filter width............... 200 Hz.

Figure 6.3-1   Functional Block Diagram of Coherent Pulse Radar
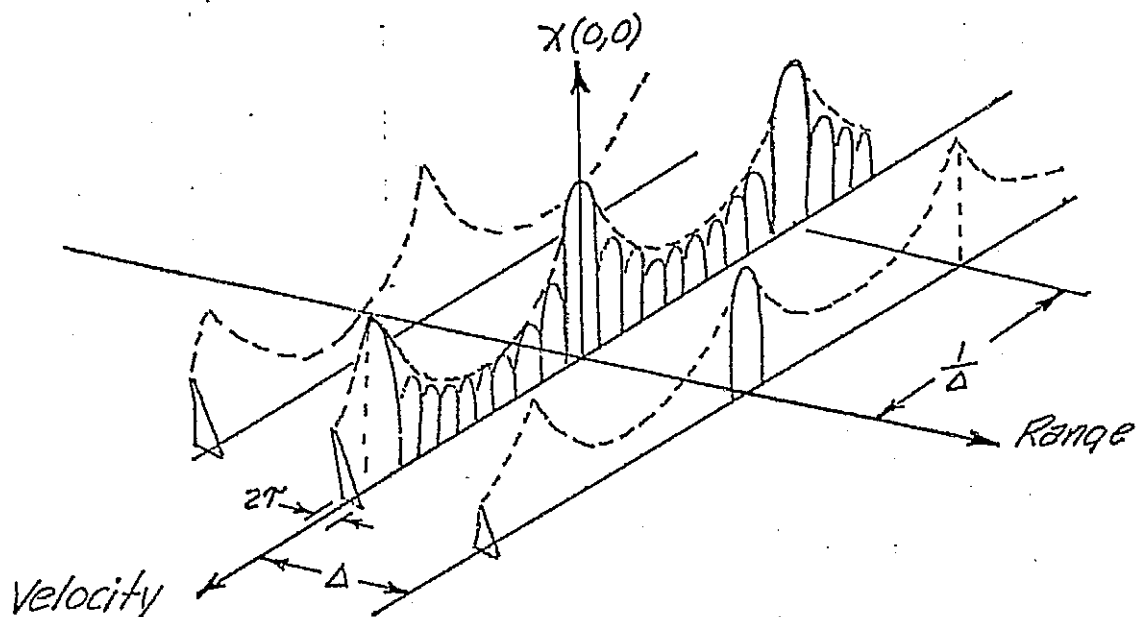
Figure 6.3-2 Ambiguity Diagram For Uniform Pulse Train. (After Nathanson)

The maximum velocity for the rendezvous radar in the skin track mode has been specified by JSC as ±150 fps or ±46 m/sec.[1] Plots of allowable range velocity envelopes to avoid range and velocity ambiguities at transmitted frequencies of 10, 15 and 30GHz. are given in Figure 6.3-3 along with the specified operating envelope.

Also shown in the figure is the nominal range-velocity profile for mission 3B. The range and velocity uncertainties for that mission are also shown for the maximum specified operating range of 19 km.

It may be observed from the figure that even without allowances for a dead band beyond the upper limits of range and velocity, that it is not possible to obtain unambiguous range and velocity data over the limits specified at the favored operating frequency of 15 GHz.

There is the possibility that the maximum opening velocity will not be as high as the maximum closing velocity. The profile of mission 3B, for example, indicates a closing velocity for most of the rendezvous. If we assume a maximum closing velocity of 46 m/sec as specified, but a maximum opening velocity of 20 m/sec the doppler frequency spread is 6.6 KHz. In this event a PRF of 6.8 KHz. can be used as discussed for the non-coherent pulse radar. This results in unambiguous range information to 22 km and unambiguous velocity information over the velocity range +46 m/sec to -20 m/sec.

6.3.2. METHOD OF RESOLVING RANGE AMBIGUITIES.

In the event that the total velocity spread is too large to allow unambiguous operation at maximum range, methods exist to resolve the ambiguities as discussed in the following paragraphs.

It is apparent from the ambiguity diagram for a periodic pulse train, Figure 6.3-2 that the range and doppler ambiguities

1. The velocity range was later modified to -38m/sec to +7.5m/sec.

Figure 6.3-3
Range-Velocity Profiles
Velocity May be Either Opening or Closing

6.67
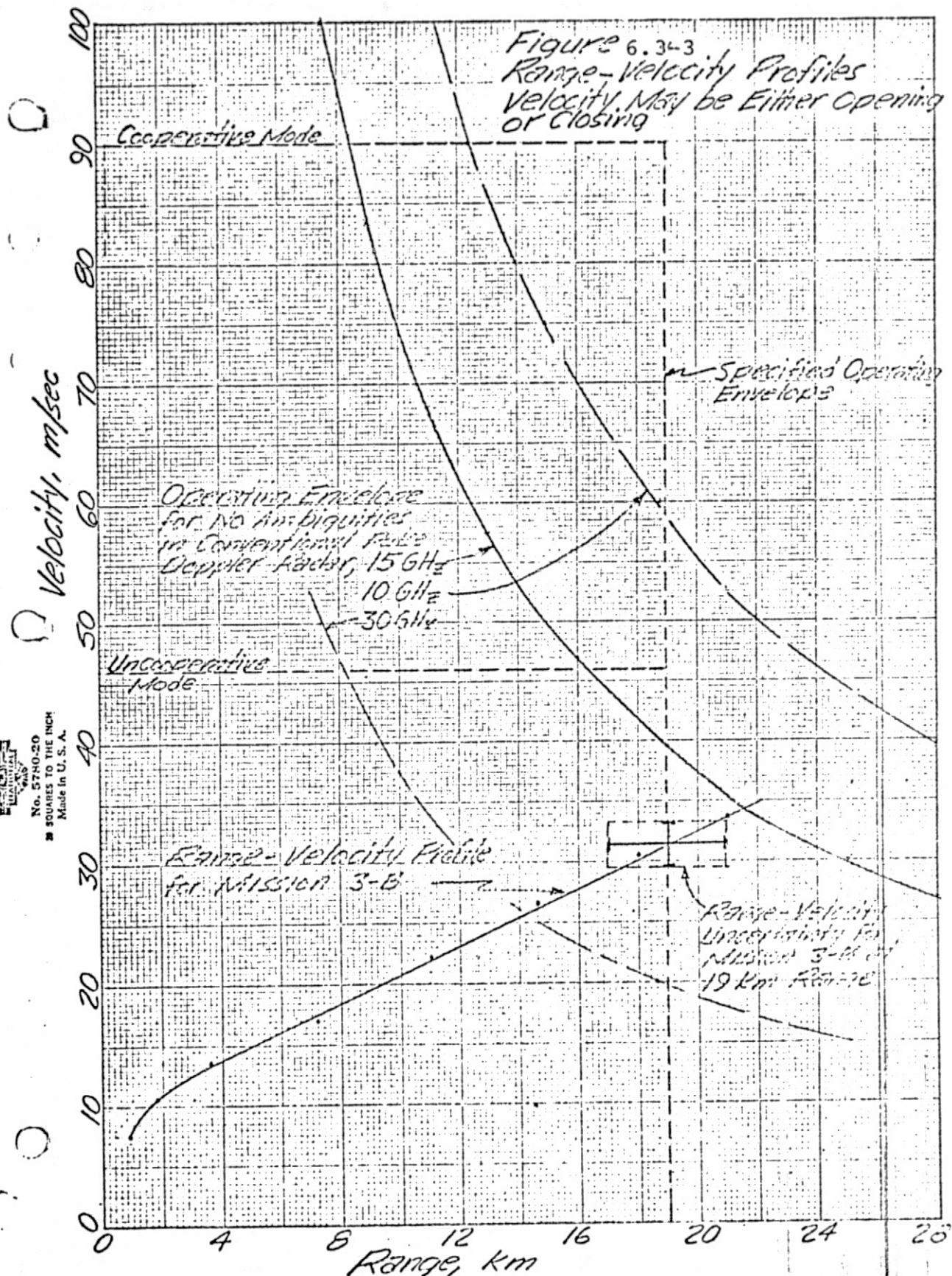
are a result of the equal spacing of identical transmitted pulses. Two commonly used approaches can be taken to expand the non-ambiguous range-velocity region. The first is to sequentially transmit multiple fixed values of PRF and resolve the range ambiguities in data processing. The second is to use a random PRF which in effect smears all but the central ambiguity peak into a broad area, allowing the ambiguity to be resolved through amplitude discrimination.

The multiple discrete PRF approach is the easier to implement of the two and it will be used for reference purposes in this study. A dual sequential PRF system uses two values of PRF switched to resolve range ambiguities. The two PRFs are chosen to have a common sub-multiple frequency and a ratio of highest PRF to lowest of m_1/m_2, where m_1 and m_2 are integers. The maximum unambiguous range may then be expressed[1]:

$$R_{unamb.} = \frac{m_2 \, C}{PRF_{min} \, 2}$$

In our case to avoid velocity ambiguities over a ±46 m/sec velocity interval the minimum PRF must be twice the doppler frequency or $PRF = 2 \left(\frac{2V}{\lambda}\right) = 9.2$ KHz. at a transmitted frequency of 15 GHz. To provide a margin to facilitate filtering, a PRF of 10KHz will be selected. The parameter m_2 becomes equal to 1.47. Since m_2 must be an integer its value will be 2 and the unambiguous range becomes equal to 30 kn. The two values of PRF are then:

$$PRF_2 = 2 \, \alpha = 10 \text{ KHz.}$$
$$PRF_1 = 3 \, \alpha = 15 \text{ KHz.}$$

where α is a parameter used for convenience in calculating the value of PRF_1 given PRF_2.

1. Skolnik, M.I. Radar Handbook

In this dual PRF system the initial angular search for the target would be conducted with a PRF of 10 KHz. After acquisition and stop of the antenna scan the range tracker would be allowed to search the 15 km range associated with the 10 KHz. PRF, lock on, and measure a range which we will call R'. The measured range can either be equal to the true range or equal to the true range minus 15 km.

The PRF is then changed to 15 KHz and the range gate is positioned in the various positions tabulated below and a test is made for signal presence.

R'	Gate positions for 15 KHz. PRF		Signal presence		True range
	G_1	G_2	G_1	G_2	
<10 km	R'	–	✓		R'
<10 km	–	$R +5km$		✓	$R' +15km$
>10 km	$R' -10km$	–	✓		R'
>10 km	–	$R -5km$		✓	$R' +15km$

The true range is then determined by noting which gate the signal appeared in as indicated in the table.

After resolving the range ambiguity the PRF is switched back to the 10 KHz. mode and range tracking proceeds. A digital implementation of the range tracker is assumed so that the 15 km offset can be readily switched in to the data registers. When the measured range approaches 15 km the PRF is switched to 15 KHz. to avoid eclipsing the return signal by the transmit interval. When the measured range decreases below 15 km the PRF is switched back to 10 KHz.

6.3.3. TARGET ACQUISITION.

Three conditions will be considered during initial acquisition. (1) That the velocity range is -20 to +46 m/sec and the target range is known within an uncertainty of ±2 km so that a PRF of 6.8 KHz. may be used. (2) That we have the same velocity range but no a-priori information so that a PRF of 3.7 KHz. must be used for initial acquisition and switch to 6.8 KHz. for tracking. (3) That the velocity range is ±46 m/sec and a dual PRF mode is used with a PRF of 10 KHz. and 15 KHz.

In conditions (1) and (2) the acquisition characte 'stics and average power required for acquisition are the same as previously established for the non-coherent radar with a PRF of 3.7 KHz. or 6.8 KHz. We note also that since there is only one pulse "in flight" within the range interval of interest (22 km) that pulse-to-pulse frequency agility can be used just as in the case of the non-coherent radar previously discussed. The only complication, as discussed later, is that the frequency agility program results in a spreading of doppler frequency which complicates acquisition and tracking of the doppler signal

Considering the third case of the dual PRF of 10 and 15 KHz. we note that we can not use frequency agility when the target signal return time may be greater than the interpulse period. The reason being that the local oscillator is normally switched to the new frequency when the next pulse is transmitted and the retain signal from the first pulse would then not be recognized.

In order to take advantage of the benefits of frequency agility a lower PRF could be used for initial acquisition and range determination and then the PRF increased to 10 and 15 KHz. as required. This sequence would be as follows:

Conduct the initial angular search at a PRF of either 6.8 or 3.7 KHz. depending if a-priori range information is, or is not available. Frequency agility would be used. This search program is the same as discussed for the non-coherent radar and the acquisition parameters developed previously apply.

After initial acquisition and stop of the antenna scan, the range tracker is allowed to search for and acquire the signal. At the lower 3.7 KHz. PRF the tracker can search through the entire interpulse region moving 1 range gate width per pulse in about 0.073 seconds assuming a range gate width of 1 μ sec.

Allowing a dwell time of 10 pulses per range position, the total range search time is about 0.8 seconds. Now having the true target range contained in the tracking register the PRF can be increased to 10 KHz. to provide unambiguous velocity information. A switch would be made to 15 KHz for a short period when required to avoid eclipsing.

Having knowledge of target range the local oscillator signal can be programmed for the proper frequency to correspond to the transmitted pulse being received.

6.3.3.1. DOPPLER FREQUENCY SEARCH AND ACQUISITION.

The amount of power in the carrier term, P_c, or central line, which will be processed by the doppler tracker, is related to the peak power of the received pulse train, P_r, as follows:

$$P_c = P_r T^2 (PRF)^2$$

where T is the pulse width.

Assuming the use of 2 synchronously tuned IF stages as before, the noise bandwidth, B, is equal to $\frac{0.75}{T}$ and the signal to noise ratio at IF as previously developed for the non-coherent pulse radar is $SNR/_{if} = \frac{P_r T}{0.75 N_0}$ where N_0 is the noise density. The peak signal to noise density ratio becomes

$$\frac{P_r}{N_0} = SNR/_{if} \left(\frac{0.75}{T}\right)$$

Finally, the carrier to noise density ratio can be expressed:

$$\frac{P_c}{N_0} = SNR/_{if} (0.75) T (PRF)^2$$

The doppler tracker is fed from the range gated IF signal. Consequently, the amount of noise power is reduced by the duty ratio of the range gate acting on the noise, D_n. Assuming a range gate equal to the pulse width, $D_n = T (PRF)$.

The signal to noise ratio within the doppler tracking filter having an effective noise bandwidth, B_t, can then be expressed:

$$SNR/_{tracker} = \frac{P_c}{N_0 B_t D_n} = SNR/_{if} \frac{(0.75) PRF}{B_t}$$

6.3.3.2. SELECTION OF DOPPLER FILTER WIDTH.

The optimum doppler tracking filter width is a function of the acceleration to be tracked, closed tracking loop bandwidth, allowable doppler search time and IF signal-to-noise ratio available.

Considering first the acceleration to be tracked, at maximum range (19 km) for mission 3-B the rate of change of velocity is only about 0.1 fps or 0.03 m/sec. During the braking sequence commencing at about 7.5 km range the velocity is decremented in 5 fps steps. Using a value of $\Delta V = $ ___ 10 fps/sec^2 or 3.05 m/sec^2 the rate of change of doppler frequency is 305 Hz./sec.

The doppler tracking loop can be implemented with a rather fast closed loop time constant, 0.05 to 0.1 seconds is typical, to allow tracking during each ΔV step. The velocity data can be smoothed later to the extent required.

A first order tracking loop with a transfer function of the form $\dfrac{1}{1 + T S}$ with $T = 0.1$ seconds will be assumed. Since accurate velocity data is apparently not required during the actual velocity step a second order loop is not required.

The loop will then track the frequency change during the step with a lag (in the steady state) of 30.5 Hz. To maintain track during the step the one sided tracking filter bandwidth should be 30.5 Hz. or 61 Hz. total.

By the time the range has decreased to 7.5 km the signal-to-noise ratio in the IF bandwidth has increased by about 18 db from its value at initial angle acquisition beginning at about 22km. This results in a high signal-to-noise ratio in the doppler tracker during the time of maximum acceleration. The signal-

6.73

to-noise ratio within the tracking filter which is required for good tracking performance is about 3 db.

Considering next doppler tracker acquisition and operation at maximum range, the rate of change of doppler frequency is extremely small, about 3 Hz /sec. The choice of doppler tracking filter width in this region is dictated by signal-to-noise ratio and acquisition considerations.

The probability of acquisition per doppler search cycle will be a function of the fluctuation rate of the target return. From considerations of rate of change of relative target aspect angle for mission 3-B as discussed previously it appears that targets 3 meters in length or greater will decorrelate in about 5 seconds for a fixed transmit frequency. Therefore it is reasonable to select the doppler search period to be about this value since little benefit is gained in searching at a higher rate.

Adopting a 5 second search rate we can determine the appropriate doppler filter width to cover the ±46 m/sec. velocity or ±4.6 KHz doppler frequency band in the interval. If we assume the tracking filter is made up of a dual section RC filter as will be discussed in a later section the equivalent time constant of the filter, T_f, is equal to:

$$T_f = \frac{1}{4 f_r}$$

where f_r is the one sided noise bandwidth, which in turn is equal to 1.22 times the 3db corner frequency of the dual section filter.

The 3 db filter width, B, is then selected such that the dwell time on any frequency is equal to T_f when the filter is swept over the 9.2 KHz. doppler range in 5 seconds. This criterion results

6.74

in a two-sided, 3 db doppler filter width, B, of 28 Hz.

Using this value for 3 db bandwidth the noise bandwidth, B_t, is 34 Hz. The signal-to-noise ratio in the tracking bandwidth is related to the signal-to-noise ratio in the IF bandwidth as follows:

$$\frac{SNR/_{tracker}}{SNR/_{if}} = \frac{0.75\ (PRF)}{B_t} \quad \begin{array}{l} = 19\ db\ for\ PRF = 3.7\ KHz. \\ = 21.8\ db\ for\ PRF = 6.8\ KHz. \end{array}$$

6.3.3.3. DOPPLER SIGNAL ACQUISITION.

Assuming the frequency search time equal to the target decorrelation time for the case of a fixed transmitter frequency the doppler acquisition problem involves Swerling case 1 statistics (an independent look each data sample) with a single pulse integrated. Allowing 2 sweep intervals at 90% probability of acquisition per sweep a signal-to-noise ratio of about 21 db in the doppler tracker bandwidth is required. This corresponds to a signal-to-noise ratio at IF of 2 db at a PRF of 3.7 KHz. and -0.8db at a PRF of 6.8 KHz. This is appreciably less than required for initial angle and range acquisition.

The SNR required for initial acquisition, as given in Section 6.2 is as follows for 2 angular search frames in 60 seconds.

Antenna size	PRF	SNR required for acquisition
0.5m	3.7 KHz.	9 db
0.5m	6.8 KHz.	7.5 db
1.0m	3.7 KHz.	13 db
1.0m	6.8 KHz.	11.3 db

We conclude that initial angle acquisition is the driving requirement with respect to signal-to-noise ratio required, rather than doppler acquisition and tracking.

6.75

Considering next the use of frequency agility, the doppler frequency spread due an agility bandwidth of 375 MHz. is 2.5%. To accomodate the resulting doppler frequency spread of 115 Hz. at a velocity of 46 m/sec, the doppler tracking filter bandwidth should be at least 115 Hz. A filter bandwidth of 200 Hz. was selected to decrease acquisition time as discussed later.

Rather than calculate the signal-to-noise ratio required for acquisition for a signal spectrum of this type, some measured data was examined. For a Gaussian shaped doppler signal spectrum with a half power bandwidth of 100 Hz and a 100 Hz. tracking filter searching at a rate of 1.6 KHz /sec, a signal-to-noise ratio of 4 db is required to achieve an acquisition probability of 0.90 per scan. The total doppler frequency range, ±4.6 KHz., could be searched in 5.8 seconds at the 1.6 KHz./sec rate. The search rate can be increased by using a wider tracking filter width at a corresponding loss in signal-to-noise ratio. A filter width of 200 Hz. for example allows a search rate of 2.8 KHz./sec to be used which corresponds to a search time of 3.3 sec per frame.

A 4 dB SNR in the doppler tracking bandwidth corresponds to a -6.6dB signal-to-noise ratio in the IF bandwidth at a PRF of 3.7 Hz. and -9.2 db at a PRF of 6.8 KHz.

For comparison purposes the signal-to-noise ratio required for initial angle acquisition using frequency agility is tabulated below: (see Section 6.2)

Antenna size	PRF	SNR required
0.5m	3.7 KHZ.	2.1 db
0.5m	6.8 KHz.	0.6 db
1.0m	3.7 KHz.	6.0 db
1.0m	6.8 KHz.	4.4 db

It is apparent that initial angle acquisition is again the driving requirement so far as sizing the system parameters which affect signal-to-noise ratio rather than doppler frequency acquisition and tracking. Therefore, the transmitted power requirements developed for the non-coherent pulse radar in Section 6.2 also apply to the coherent pulse radar as discussed in this section.

6.3.4. DOPPLER FREQUENCY MEASUREMENT.

A block diagram of a candidate doppler frequency tracker is given in Figure 6.3-4. The signal at the output of the IF amplifier is converted to audio (zero IF frequency) by mixing with a quadrature signal at the IF frequency which is coherent with the transmitted frequency. The conversion to audio frequency facillitates filtering of the signal to avoid the doppler shifted signals associated with other spectral lines. The conversion to audio is done in quadrature to preserve the sign sense of the velocity data. The quadrature signals are applied to a single sideband modulator where they are mixed with quadrature signals generated by the tracking loop. One pair of mixed signals is used to operate the acquisition circuit. The other pair is summed, which effectively cancels one sideband of the mixing process. The single sideband error signal is equal to a fixed loop reference frequency, F_c, which can be any convenient frequency above the maximum doppler frequency, plus the tracker error frequency. This signal is mixed in quadrature with the reference frequency and the resulting quadrature components of the error frequency are filtered and limited and applied to a discriminator. The low pass filters form the doppler tracking filter. Either an up pulse or a down pulse is generated each cycle of the error frequency depending if the error frequency plus reference frequency is above or below the reference frequency. The discriminator
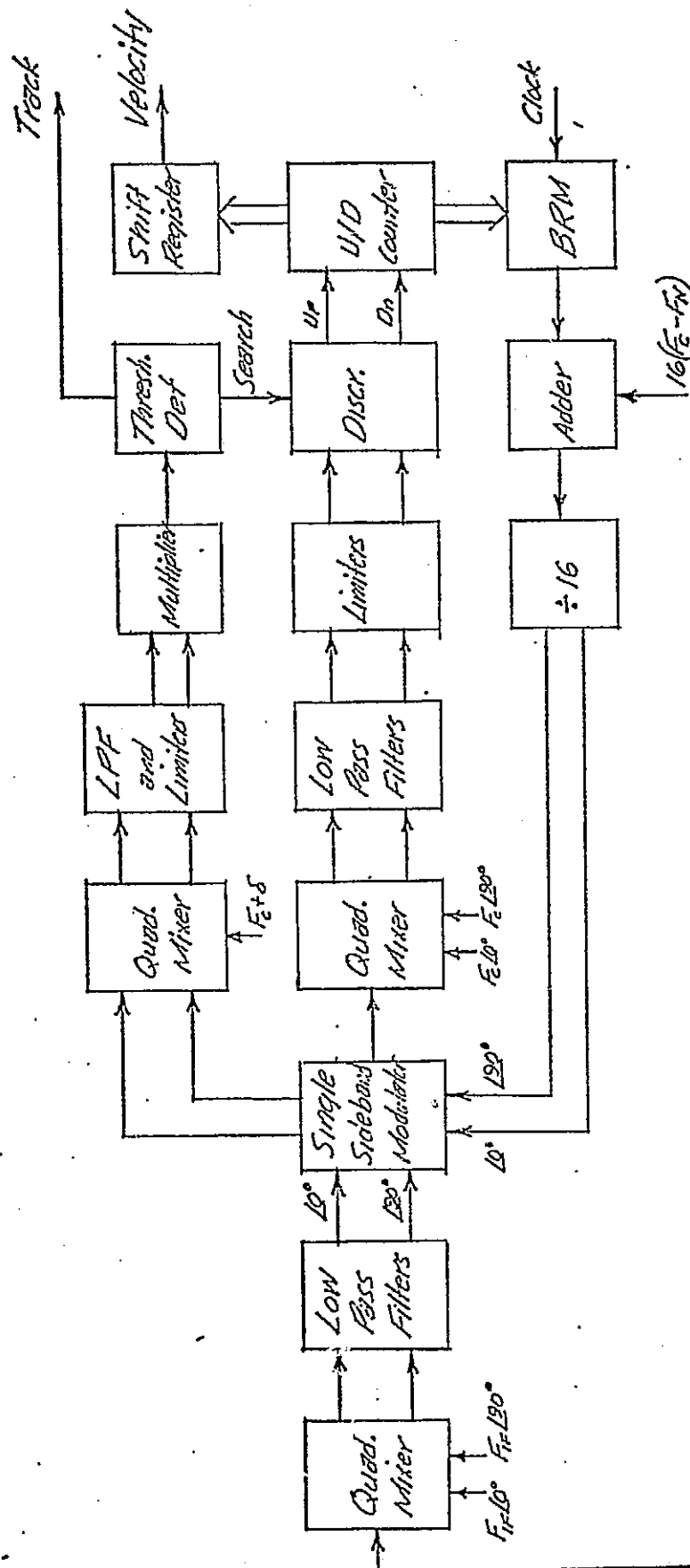
Figure 6.3-4. Candidate Frequency Tracker

output is applied to an up/down counter which counts up or down depending on the sense of the error frequency.

The output of the up/down counter controls a binary rate multiplier, BRM, which operates on the clock frequency. The BRM generates a frequency which, after adding in an offset frequency and debunching, is applied to the simgle sideband modulator to close the tracking loop. To avoid the complication of determining sign sense the loop is offset with a frequency equal to the maximum expected negative doppler frequency, F_n.

The parallel binary signal at the output of the up/down counter is transferred into a shift register. The doppler frequency measurement is then shifted out to a display upon command.

Signal search and acquisition is achieved by applying a clock signal to the discriminator which causes it to generate up pulses which are used by the up/down counter to generate a frequency sweep. The frequency transitions back to the lower sweep limit when the counter overflows.

Signal acquisition is based on a correlation process in the two acquisition channels. If noise alone is present the signals in the two channels are uncorrelated and the average value at the multiplier output is zero. If signal is present the multipler output has a net positive average value which is sensed by the threshold detector when the signal-to-noise ratio reaches a preset value (about 3 db). Upon sensing the presence of a signal the frequency search is halted and doppler tracking is initiated.

6.3.5. ACCURACY OF MEASUREMENT OF DOPPLER FREQUENCY.

The accuracy of measurement of the average doppler frequency will be better than 1 Hz. (0.01 m/sec) with the digitally implemented frequency tracker described above. This accuracy value was obtained from examination of test data on similar frequency trackers and under conditions of doppler spectrum widths up to the tracking filter bandwidth and signal-to-noise ratios as low as 3 db.

In the case where frequency agility is not used, the central doppler line has a very small bandwidth after mixing with the coherent source and the fluctuation error of the frequency tracker is mainly a function of the tracker bandwidth and signal-to-noise ratio. For this case the rms value of noise at the tracker output, σ_T, is approximated by the expression

$$\sigma_T = \left[\frac{.078B \ (1+\frac{1}{S/N})^2}{T \ (1 + S/N)^{1/2}} \right]^{1/2}$$

where B = tracking filter bandwidth
   T = averaging time
   S/N = signal-to-noise ratio

Considering operation at the maximum range, the signal-to-noise ratio available at angle acquisition varies from about 9 to 13 db depending on PRF and antenna size. Using the 9 db value and a tracking filter width of 200 Hz. with a 2 second data smoothing time the rms value of the noise at the tracker output after smoothing is 1.8 Hz. This is equivalent to a rms velocity fluctuation of 0.018 m/sec.

The noise at the output of the frequency tracker for the case of frequency agility is a complex function of the fluctuation

characteristics of the target. This comes about since the discrete doppler spectrum will peak at various frequencies depending on what carrier frequency yields the highest target return at a given instant of time.

A maximum value for this variation is equal to the extent of the doppler spreading due to frequency agility. This is equal to ± 1.25% of the center doppler frequency for the 375 MHz frequency agility bandwidth considered previously. However, this is clearly an extreme case requiring the return from the first or last agility positions to be at least an order of magnitude larger than from any other frequency agility step over the 2 second allowed averaging time.

A more reasonable model would be a linear variation from zero at one side of the spectrum to a maximum at the other. The tracking position for this case, assuming a tracking filter wider than the doppler spectrum, is about 0.47 times the half spectrum width, displaced from the center of the spectral band. In our case it amounts to about 0.6% of the center doppler frequency. This will be taken as a 3σ value. The 1σ value of fluctuation noise for the maximum velocity of 46 m/sec is then 9.2 Hz. which is equivalent to 0.09 m/sec.

Another approach to determining the fluctuating component of the error is to approximate the discrete doppler spectrum by a continuous doppler spectrum of the same bandwidth. For the case of signal-to-noise ratios greater than 10 db the tracker noise for the continuous Gaussian doppler spectrum case given by the expression:

$$\sigma_T = \left[\frac{0.78}{T} \ \frac{B_i}{B} \ \sqrt{B^2 + B_i^2} \right]^{1/2}$$

where T = averaging time
B_i = doppler spectrum bandwidth
B = tracking filter bandwidth

6.81

Taking a 2 second averaging time (time constant) corresponding to the 2 second allowable dynamic lag in velocity data, a doppler spectrum width of 115 Hz. and a tracking filter bandwidth of 200 Hz. the RMS noise is 2.3 Hz. The equivalent RMS velocity noise is 0.023 m/sec.

As would be expected this approach results in a smaller value of noise than the former method since the high frequency spectral components are filtered by the 2 second filter. The more conservative 0.006V m/sec value will be used for this study.

6.4. ANALYSIS OF PULSE DOPPLER RADAR WITH FM RANGING.

A candidate high duty ratio pulse doppler radar with FM ranging is described in this section. A summary of characteristics of the radar is given in Table 6.4-1. A functional block diagram is given in Figure 6.4.-1.

The duty ratio of the radar is approximately 0.5. The transmitter is operated in a fixed frequency mode during initial acquisition then switched to an alternating fixed frequency and linear frequency modulated mode as illustrated in Figure 6.4-1. Velocity is measured during the fixed frequency mode and range is measured during the FM period.

During the velocity measuring mode the difference between the transmitted and received frequencies is related to velocity through the doppler relationship,

$$f_d = \frac{2V}{\lambda}$$

During ranging the difference between the received and transmitted frequencies is equal to the doppler shift plus a frequency proportional to range as follows:

$$F = f_d + f_R = \frac{2V}{\lambda} + \frac{S2R}{c}$$

where

> V = velocity
>
> λ = Wavelength of radiation
>
> S = Slope of linear frequency modulation
>
> R = Range
>
> c = Velocity of light

Range is determined after subtracting off the doppler shift obtained during the velocity measuring mode.
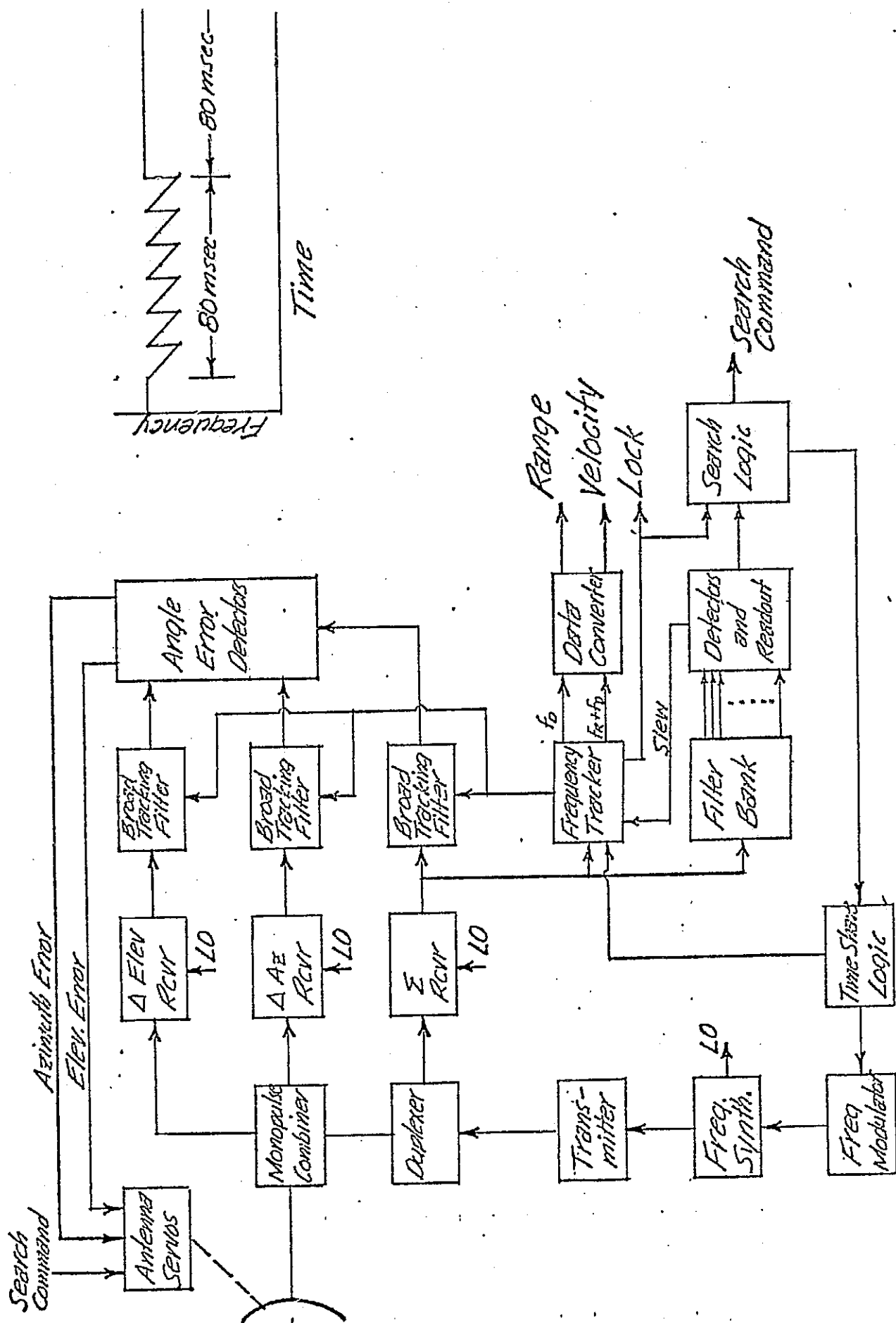
Figure 6.4-1 Functional Block Diagram of Pulse Doppler Radar

TABLE 6.4-1 CHARACTERISTICS OF CANDIDATE PULSE DOPPLER RADAR.

PERFORMANCE CHARACTERISTICS.

Detection range (P_D=0.99 for 1 m^2 Swerling I target)..... 19 km
Velocity capability... -38 to
                                                               +7.5 m/sec
Acquisition time... 60 seconds
Angular search coverage.. 80° cone
Accuracy, 3σ

	Bias	Random
Angle track[1]	0.24mR	0.15mR (at maximum range)
Angle rate[1]	0.09mR/sec	0.62mR/s (at maximum range)
Range:		
R >2 km	0	$\sqrt{(.005R)^2+(.57)^2+(.85V)^2}$
R <2 km	0	$\sqrt{(.005R)^2+(5.7)^2+(.85V)^2}$
Velocity	0	$\sqrt{(.03)^2+(.006V)^2}$

SYSTEM CHARACTERISTICS.

Operating frequency.. 15 gHz.
Antenna:
   Size... 1 m diameter
   Beamwidth (two-way)....................................... 1.0 degrees
   Gain.. 41.7 dB
   Scan program.. Spiral
Transmitter characteristics
   PRF... 4.8 kHz.
   Pulsewidth.. 100 μsec
   Peak power[2]... 10 watts
   Average power[2].. 5 watts

1. Not including glint effects.
2. A margin of 2 dB is included in transmitter power.

FREQUENCY AGILITY PROGRAM.

           Angle acquisition............................ 6 frequencies
                                                         75 mHz. apart
                                                         Step duration 1.5msec

           Tracking..................................... 6 frequencies
                                                         75 mHz. apart
                                                         Step duration 13msec

Receiver noise temperature........................ 1758°K

Doppler filter bank:
      Filter bandwidth............................ 267 Hz.
      Number of filters........................... 17

Frequency tracking filter bandwidth.............. 267 Hz.

Frequency modulation program
      Deviation:
           R > 2km................................ 2 mHz.
           R < 2km................................ 20 mHz.
      Time of linear sweep........................ 13 m/sec
      Time of retrace............................. .5 m/sec

6.4.1. PRF CONSIDERATIONS.

For the skin track mode the velocity limits of -38m/sec and +7.5 m/sec yield doppler shifts of -3.8 kHz. and +750 Hz. The PRF should then be greater than 4.55 kHz. to avoid velocity ambiguities. In the case of the cooperative mode the velocity limits are ±91 m/sec and the PRF must be greater than 18.2 kHz.

Considering first the cooperative mode, a minimum PRF of 20 kHz. will be selected. A fixed 20 kHz. PRF would result in blind ranges where the signal returns at the time the transmitter is on and the receiver is off as illustrated in Figure 6.4-2. It may be noted that at a range of 7.5 km and multiples, the received signal is completely eclipsed by the transmitter pulse.

To avoid blind ranges the PRF may be changed either in a regular or random manner. The first range hole at 7.5 km is completely filled by changing to a PRF of 30 kHz. as illustrated in the figure. For the cooperative mode the PRF will be dithered in a linear manner between the limits of 20 kHz. and 30 kHz. The dither rate must be such that the full PRF range is covered during the dwell time of the antenna beam and the target. For the skin track case and 1 search frame in 60 seconds the dwell time for a 0.5 m diameter antenna is 35.6 m/sec and for a 1 m diameter antenna it is 8.9 m/sec. The dither frequency, assuming a triangular function, should then be 14 Hz. for the 0.5 m diameter antenna and 5.6 Hz. for the 1 m diameter antenna.

To make most efficient use of the average transmitted power the transmit and receive duty ratios are made equal. To operate at a minimum range of 30 meters the receiver recovery time must be less than 0.2 microseconds. The duty ratio at a 30 kHz. PRF is then 0.497. For analysis purposes the duty ratio for transmitter and receiver will be assumed to be equal to 0.5

PRF = 20 kHz
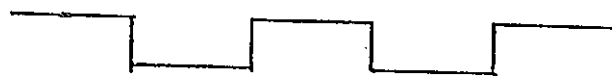
Transmitter
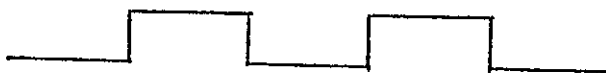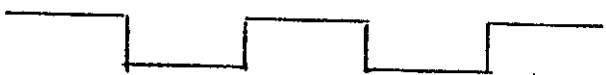
Receive   3.75 km

7.5 km

PRF = 30 kHz

Transmitter

Receive   3.75 km
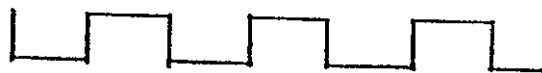
7.5 km

Figure 6.4-2 Transmit and Receive Functions

6.4.1.1   ECLIPSING/CONVERSION LOSS.

Only the power in the central spectral line of the received signal, P_c, is processed by the doppler filter. The other lines which are separated by the PRF fall well outside of the filter bandwidth. P_c is related to the peak received power, P_r, as follows:

$$P_c = P_r \tau_1^2 (PRF)^2$$

where τ_1 is the effective pulsewidth received after eclipsing by the transmitter on time. For example, at a range of 7.5 km the effective pulsewidth is about $17\eta sec$ at a PRF of 30 kHz. It decreases to zero as the PRF is varied to 20 kHz.

The the case of transmitter and receiver duty ratio equal to 0.5, the average factor between peak power and the power in the central spectral line, when integrated over a complete dither cycle, was computed as -10.8 dB. This factor will be referred to as the eclipsing/conversion loss factor, L_e, in later signal-to-noise ratio calculations.

The eclipsing/conversion loss term contains both a factor of 0.25 (6dB) representing the conversion peak power of a 50% duty ratio IF signal to the amount of power in the central spectral line, and the additional loss due to eclipsing which with PRF dither averages to 4.8 dB.

The eclipsing portion of the loss can be reduced to zero if the PRF is matched to the target range. However, as discussed previously, the PRF is constrained by the maximum doppler frequency to be encountered. The doppler frequency range corresponding to the skin track velocity limits -38m/sec to 7.5 m/sec is -3800Hz. to +750Hz. a PRF equal to the total frequency range above plus a margin of 250Hz. or a total of 4800Hz. is about the lowest value which can be used and resolve the velocity ambiguities.

A plot of the eclipsing loss, including the 6dB conversion factor, is given as a function of range for a PRF of 4800 Hz. in Figure 6.4-3. Two conclusions are drawn from the figure: (1) The average loss over the initial acquisition region is about 9 dB and (2) using the 4.8 kHz value for PRF it would be more efficient not to dither the PRF until the range has decreased to below 9 km.

The eclipsing/conversion loss can be expressed in terms of the PRF and Range as follows:

$$L_e = \left[\frac{2R}{c} (PRF) \right]^2 , \qquad R \leq \frac{c}{4PRF}$$

$$L_e = \left[1 - \frac{2R}{c} (PRF) \right]^2 , \qquad R > \frac{c}{4PRF}$$

It may be noted from the first expression that the loss increases as R^2 with decreasing range. Thus, the PRF could be held constant at 4.8 kHz in the skin track mode for ranges below 9 kHz as well since the peak signal from the target is increasing as $1/R^4$. However, since the dither capability must be incorporated for the cooperative mode anyway, one might as well obtain the extra SNR available and dither the PRF as the range decreases below 9 km. The PRF program would be the same as used in the cooperative mode.

Another possibility to minimize eclipsing is to set the PRF to an optimum value based on a-priori knowledge of target range and velocity. Assuming, for example, that the velocity is either unknown or is the maximum value of 38 m/sec and it is desired to minimize the eclipsing at a range of 21 km. Then the PRF can be made equal to two times 3.6 kHz (the optimum value at 21 km if velocity were not a constraint), or 7.2 kHz. At 21 km the
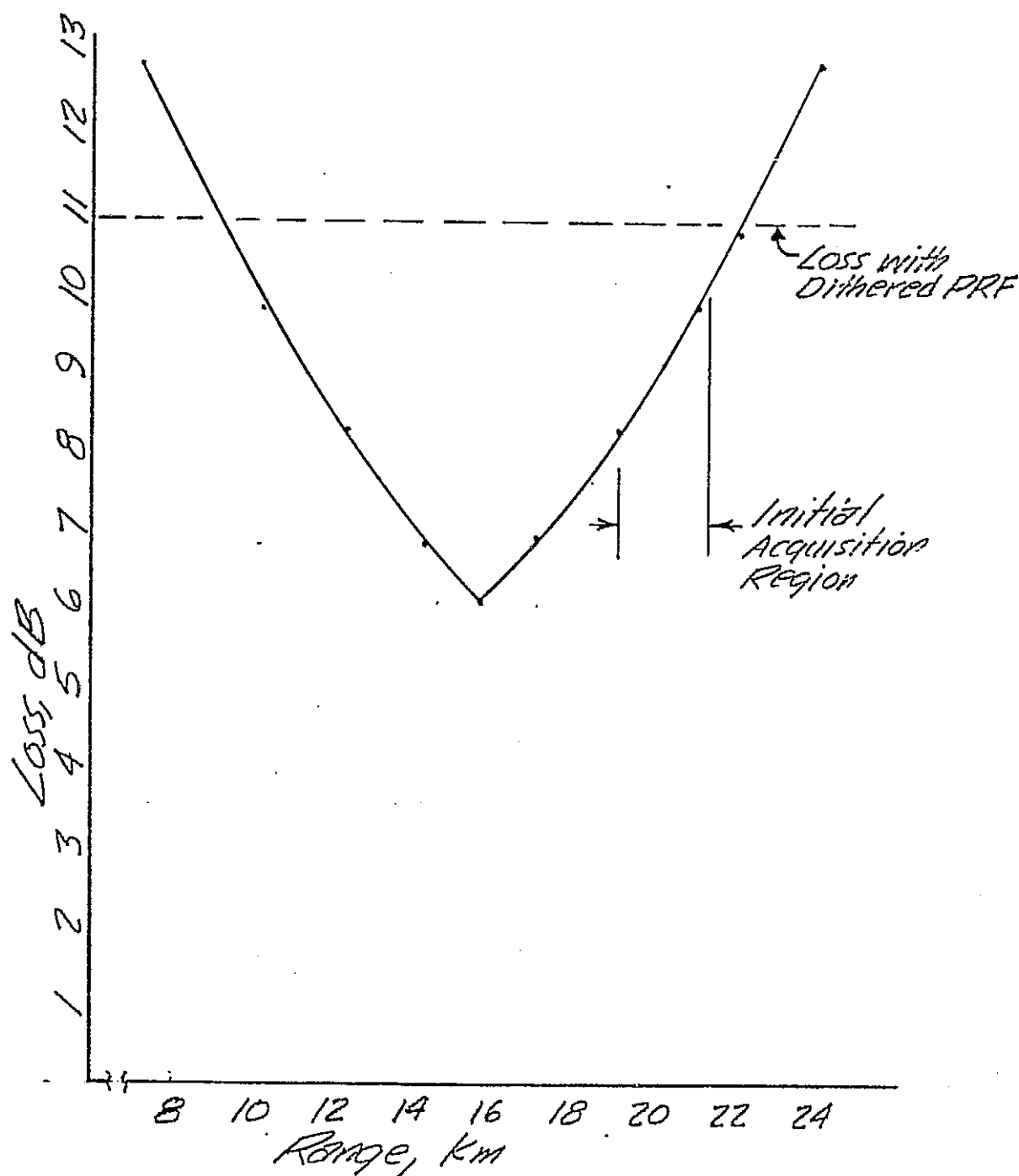
Figure 6.4-3 Combined Conversion and
Eclipsing Loss for PRF = 4.8 kHz

eclipsing is zero and the combined eclipsing/conversion loss is
6 dB.   If the uncertainty in the a-priori knowledge of range is
± 1 km the loss increases to 6.9 dB, if the uncertainty is ±2 km
the loss is 7.9 dB and if the uncertainty is ±3 km the loss is
8.9 dB.   Therefore, if a-priori range information is available
to an accuracy better than ±3 km we recommend that it be used to
set on the PRF for initial acquisition.   The PRF in this event
can be made equal to a multiple of the lowest optimum PRF to
minimize eclipsing; the higher the multiple the greater the
eclipsing loss due to a given error in the knowledge of range.

6.4.2.   SIGNAL AND NOISE CONSIDERATIONS.

The peak received signal power, P_r, is related to the radar
system parameters as follows:

$$P_r = \frac{P_t G^2 \lambda^2 \alpha}{(4\pi)^3 R^4 L_f L_s L_m}$$

where the symbols are as defined in Section 6.2.

The power in the central spectral line, P_c, which is that
processed by the system is related to the peak power through the
eclipsing/conversion loss term, L_e, as

$$P_c = P_r/L_e$$

The noise power in the doppler filter bandwidth is equal to
$k T_S B_T D_N$ where k is Boltzmanns constant, T_S is the system noise
temperature, B_T is the noise bandwidth of the doppler filter and
D_N is the duty ratio of the noise applied to the doppler filter.
In our case $D_N = 0.5$ since the IF amplifier is blanked when the
transmitter is on.

The net signal-to-noise ratio within the doppler filter may then be expressed:

$$SNR = \frac{P_t G^2 \lambda^2 \sigma}{(4\pi)^3 R^4 \; KT_S B_T D_N L_e L}$$

where the eclipsing loss L_e and the general loss terms, L, are expressed in ratios greater than unity.

6.4.3 SELECTION OF DOPPLER FILTER BANDWIDTH.

During initial angle acquisition the dwell time on the target is 4.4 msec (assuming 2 angle search frames) with a 1 meter diameter antenna, and 17.8 msec with a 0.5 meter antenna. If we consider initial acquisition on doppler alone before the range modulation is applied the frequency search interval is 4.6 KHz. for the skin track mode and 18.2 KHz. for the beacon track mode. We will first explore the feasibility of searching for the doppler signal with a frequency tracker while the angle search is in progress. To achieve a good compromise between false alarm rate and sensitivity during acquisition with the searching filter it has been found in practice desirable to follow the filter with a post detection time constant which is about 5 times longer than the reciprocal of the tracking filter bandwidth, B.

Allowing a dwell time of $\frac{5}{B}$ seconds for each of the $\frac{4.6 \text{ KHz}}{B}$ intervals the total search time, T_S, can be expressed:

$$T_S = \frac{2.3 \times 10^4}{B^2} \quad \text{seconds.}$$

For the 0.5 meter antenna dwell time of 17.8 msec, and assuming two frequency search frames in this period, the tracking filter bandwidth is equal to 1.1 KHz. For the case of the 4.4 msec

antenna dwell time the bandwidth must be 2.3KHz.

For the longest antenna dwell time considered the tracking filter bandwidth required to meet the acquisition time requirements is more than a factor of 10 greater than required to accomodate the dynamics of the signal. The transmitted power required for acquisition would be correspondingly larger for acquisition than required for tracking. To minimize the transmitted power requirements a filter bank will be used for acquisition, followed by a frequency tracker for accurate frequency measurements.

Even if a-priori velocity information is available for all missions it does not appear feasible to omit the filter bank. For example,if relative velocity is known within ±5 m/sec (a factor of 2.5 larger than the uncertainty indicated at a 19 km range for mission 3-B) the tracking filter width decreases to 750 Hz. for the longest antenna dwell time considered, which is still several times greater than needed for tracking.

The optimum bandwidth of the individual filters in the filter bank will be determined next. Assuming the filters consist of single tuned circuits the optimum half power bandwidth is equal to about 0.4 times the reciprocal of the pulsewidth. The missmatch loss of this filter to a rectangular pulse input is about 0.9 db. The loss to the actual signal form due to the antenna pattern will be somewhat less. For the 4.4 msec dwell time on target associated with the 1 meter diameter antenna, the optimum bandwidth is 91 Hz. For the 17.8 msec dwell time of the 0.5 meter antenna the optimum bandwidth is 22 Hz. If filters with these bandwidths were implemented to cover the 4.6 KHz doppler band a bank of 50 filters would be required for the 1 meter antenna and 207 filters for the 0.5 meter antenna. For preliminary system sizing purposes these values for bandwidth will be used. However, it is not

attractive hardware-wise to have so many filters and a trade-off
between transmitted power and numbers of filters can be made.
An alternate approach is to implement the filter bank with a
microcomputer using Fast Fourier Transform techniques.

The number of filters can also be reduced if a-priori
velocity information is available. Some examples of this are
given in Table 6.6-2

6.4.4. TARGET ACQUISITION.

Target acquisition in the uncooperative radar mode will be
considered in the following paragraphs.

We note that it is not feasible to use frequency agility on
a pulse-to-pulse basis with the high PRF radar considered since
several pulses are "in flight" to the target at a given time. The
feasibility of using frequency agility on groups of pulses will
be explored later.

Using a single transmitted frequency the target return is
assumed to follow Swerling 1 fluctuation statistics. For the case
of the filter bandwidth essentially matched to the dwell time of
the target during the antenna scan, the effective number of
pulses integrated is one. A false alarm time, t_F, of 10 minutes
will be used as before which results in a momentary hesitation
in the antenna scan program once each 10 minutes. The false
alarm number n^1 as discussed in the treatment of the non-coherent
pulse radar is equal to:

$$n^1 = \frac{t_F \, \alpha}{NT}$$

where t_F = false alarm time

α = ratio of range gate on time to $\frac{1}{PRF}$

N = number of pulses integrated

T = pulsewidth

6.95

TABLE 6.4-2

NUMBER OF DOPPLER FILTERS REQUIRED AS A FUNCTION OF A-PRIORI
VELOCITY INFORMATION.

A-priori velocity information	Velocity search range	Number of filters reqd	
		1 m antenna	0.5 m antenna
None			
• Beacon mode	±91 m/sec	200	827
• Skin track mode	-38 to -7.5 mSec	50	207
Sign (opening or closing)			
• Beacon mode	91 m/sec	100	414
• Skin track mode	38 m/sec	42	173
Value and sign within ±10m sec	±10 m/sec	22	91

In the case of the pulse doppler radar the pulsewidth,τ, becomes equal to the reciprocal of the doppler filter bandwidth, the receiver gate on time is equal to 0.5, N = 1 and the false alarm time per filter becomes equal to the total number of filters times the system false alarm time.

Using a system false alarm time of 10 minutes and the number of filters and filter bandwidths previously determined for the 0.5 meter and the 1.0 meter antenna the false alarm number, n^1, becomes equal to 1.4×10^6 for both antenna cases.

The signal-to-noise ratio required for acquisition for 2 scan frames in the acquisition period and a detection probability of 0.9 per scan is obtained from Fehlners treatment of Marcum's and Swerling's data on detection as before. The signal-to-noise ratio required is 21.1dB.

6.4.5. TRANSMITTED POWER REQUIRED FOR ACQUISITION.

The transmitted power required to achieve a given signal-to-noise ratio within a given doppler filter bandwidth is computed in Table 6.4-3. The peak transmitted power required was found to be:

$$P_t = 54.5 + 10\log SNR + 10\log B_T - 20\log G dBW$$

The parameters associated with the 1 meter and the 0.5 meter diameter antennas are tabulated below along with the peak transmitted power and average transmitted power required for acquisition.

Antenna size	Antenna gain	Filter 3 dB	Bandwidth noise	SNR required	Trans. Power Peak	Average
0.5 m	35.7 dB	22Hz.	35Hz.	21.1 dB	91.2 W	45.6 W
1.0 m	41.7 dB	91Hz.	143Hz.	21.1 dB	24.0 W	12.0 W

TABLE 6.4-3

COMPUTATION OF PEAK TRANSMITTED POWER REQUIRED FOR ACQUISITION FOR PULSE DOPPLER RADAR.

$$P_t = \frac{SNR(4\pi)^3 R^4 K T_s B_T D_N L_e L_M L_S L_F}{G^2 \lambda^2 \sigma}$$

Symbol	Parameter	Value	Value in db
SNR	Signal to noise ratio	SNR	$10 \log SNR$
$(4\pi)^3$		1984	33.0
R^4	(Range)^4	$(21.7 \times 10^3)^4$	173.6
K	Boltzmann's constant		-228.6
T_s	System noise temperature	1758°K	32.4
B_T	Noise bandwidth of doppler filter	B_T	$10 \log B_T$
D_N	Duty ratio of noise gate	0.5	-3.0
L_M	Microwave loss in transmit path	1.6 db	1.6
L_S	Scan loss	1.6 db	1.6
L_e	Eclipsing loss	9.0	9.0
L_F	Filter mismatch loss	0.9 db	0.9
G^2	(Antenna gain)^2	G^2	$-20 \log G$
λ^2	(Wavelength)^2	2×10^{-2}m	34.0
σ	Radar cross section	1m^2	0
P_t	Peak transmitter power		$54.5 + 10 \log SNR + 10 \log B_T$ $-20 \log G$

6.4.6. USE OF FREQUENCY AGILITY.

It appears feasible to use frequency agility with the pulse doppler, FM ranging radar by applying the frequency agility to groups of pulses.

During acquisition six frequency steps, as discussed previously in the case of the non-coherent pulse radar, would be programmed during the dwell time of the antenna beam on the target.

After angle acquisition the individual frequency steps would be made the same length/as the frequency modulation ramp time, or 13.3 milliseconds. A total of six frequency agility steps as considered previously would then take about 80 milliseconds. The time the frequency tracker dwells during the doppler or ranging measurement would be made equal to 80 milliseconds to average the measurement over the six frequency agility steps.

Considering initial target acquisition with frequency agility, the antenna would be programmed to scan the angular search area once in the 60 second search period. The dwell time of the antenna beam on target is then 8.9 msec for the 1 meter diameter antenna and 36 msec for the 0.5 meter diameter antenna. The duration of each frequency position is then about 1.5 msec for the 1 meter antenna and 6 msec for the 0.5 meter antenna.

To accomodate these six independent samples the doppler filter bandwidth must be increased to 267 Hz. for the 1 meter diameter antenna and 67 Hz. for the 0.5 meter antenna. In addition we note that at the maximum velocity of 38m/sec the doppler spread due to frequency agility is equal to 95Hz. Thus, the bandwidth in the case of the 0.5 m antenna will be increased to 100 Hz.

The signal-to-noise ratio required for acquisition with the six-step frequency agility is found as before by determining the frequency agility gain, $G(n_e)$, relative to the Swerling 1 case for n_e frequency states.[1]

1. Barton, D.K. Loc Cit.

$$10 \log G(n_e) = (1 - \frac{1}{n_e}) 10 \log L_f(1)$$

where $L_f(1)$ is the fluctuation loss for a fixed frequency.

In our case for a probability of detection of 0.99 the frequency agility gain is about 14 dB.

The signal-to-noise ratio required for acquisition is obtained by finding the SNR required for a detection probability of 0.99 per scan with 6 pulses integrated with a false alarm number of $\frac{1.4 \times 10^6}{6} = 2.3 \times 10^5$ for a Swerling case 1 fluctuation characteristic and subtracting the frequency agility gain from it. The result is as follows:

SNR (with frequency agility)=24.8dB-14dB=10.8dB.

Alternately, we note that since the number of frequency agile steps is equal to the number of independent samples during the time on target that a Swerling Class 2 detection model also applies. For these conditions the SNR required for acquisition using Swerling 2 statistics is 10.8 dB which agrees with the previous value.

The system parameters associated with the two antenna sizes are tabulated below along with the transmitted power required for acquisition using six-step frequency agility.

Antenna size	Antenna gain	filter 3 dB	Bandwidth noise	SNR required	Trans. Power Peak	Average
0.5 m	35.7 dB	100Hz	157 Hz	10.8 dB	38.9W	19.5W
1.0 m	41.7 dB	267Hz	419 Hz	10.8 dB	6.4W	3.1W

6.4.7. SYSTEM IMPLEMENTATION.

A block diagram of the candidate pulse doppler radar system with linear FM ranging is given in Figure 6.4-1.

The antenna is fed from a standard monopulse combiner. The transmitted energy is applied to the sum port and the sum received signal is also extracted from this port. Elevation and azimuth

received difference signals are obtained from two separate difference channel ports.

During initial acquisition the transmitter operates at a 50% duty ratio and without ranging frequency modulation applied. The received signal in the sum channel is applied to the sum receiver where it is converted to an IF frequency by mixing with a local ascillator signal off-set but coherent with the transmitted signal. A double conversion would be used; the first to an IF of about 10 MHz and the second to an IF of about 1 MHz. This allows filtering against PRF harmonics while providing an IF output compatible with operation of the filter bank and frequency tracker which follow. The bandwidth of the IF amplifier needs only to be broad enough to pass the received doppler plus ranging frequency band.

The 1 MHz IF signal is applied to the filter bank which for the case of a radar with a 1 meter diameter antenna consists of 51 filters each with a bandwidth of 91 Hz. One method of mechanizing the signal detection process is to follow each filter in the filter bank with a detector feeding two smoothing filters in parallel. One smoothing filter would have a long time constant, at least 10 times the reciprocal of the doppler filter width to develop a good estimate of the noise level out of the doppler filter. The other smoothing filter would have a time constant matched to the doppler filter bandwidth so that it responds promptly to the signal when the target is intercepted. The output of the two filters is fed to a coinicdence detector, biased off by the amount required to yield the desired false alarm time.

The advantage of the dual time constant acquisition approach is that it is adaptive and independent of the amplitude or shape of the noise spectrum or gain of the individual filter channels.

When the signal exceeds threshold in any filter in the bank the antenna search command is inhibited and the antenna scan is stopped. When the antenna scan is stopped the dual time constant acquisition system no longer functions and instead of comparing the short time constant smoothing filter output with that of the long time constant filter it is compared with a reference voltage derived from the broad band noise level. This less precise means of signal detection can be used after initial acquisition because the average signal-to-noise ratio in the doppler filter is relatively high.

After stopping the antenna scan the frequency tracker, which has a digital type VCO, is set on the frequency of the filter which responded in the doppler filter bank. If the antenna scan was stopped due to a false alarm in the filter bank, the frequency tracker will not acquire and after approximately one second the antenna search is resumed. (On the average one false alarm will be experienced in a 10 minute period.)

When the frequency tracker acquires, within one second after being set to the approximate frequency, a readout of velocity is made available and the angle tracking loops are activated.

The IF signals from the sum and difference receivers are applied to mixers along with a corresponding signal from the frequency tracker such that the IF signals are converted to a fixed frequency of about 16 KHz. (which is the loop reference frequency of the frequency tracker). A bandpass filter centered at 16 KHz. with a bandwidth about twice the frequency tracker bandwidth is used to extract the signal after mixing. The broad bandwidth minimizes differential phase shift between the sum and difference channels of the monopulse tracking loops.

The angle error is developed by comparing the difference channel outputs with the sum channel outputs by means of synchronous, or phase sensitive, detectors. The resulting error signals are used to drive the antenna to a monopulse null in each axis.

After the antenna has been driven to fine alignment with the target, the ranging mode is initiated by frequency modulating the transmitter. A linear triangular modulation is used such that the net signal frequency is the sum of the doppler shift and the range frequency as indicated below:

$$f = f_D + \frac{S2R}{C}$$

where the doppler frequency, f_D, is either plus or minus depending if the range is opening or closing.

To minimize the frequency search required, the slope of the frequency modulation function is selected as the minimum allowing the range frequency to be processed with an ample margin relative to the accuracy requirements. (bias error of 24m and random error of 91m for R >9 km and 0.01R or 30 m for R <9 km). A range scale factor of 1.0 Hz. per meter for ranges greater than 2 km and 10 Hz per meter for ranges less than 2 km was selected as a compromise between the two requirements.

During search and acquisition of the range signal the FM sawtooth function is repeated until acquisition occurs.

In absence of a-priori range information the frequency tracker is programmed to search upwards in frequency from the known doppler frequency an amount equivalent to 20 km of range, or 20 KHz.

The bandwidth of the frequency tracker must be wide enough to encompass at least three spectral lines of the ranging signal, which are 75 Hz apart, or 225Hz.

After acquisition of the range plus doppler signal the measured frequency is put into temporary storage, the transmitter resumes a fixed frequency mode and the tracker VCO is positioned to the last measured doppler frequency. If acquisition does not occur within 5 seconds during the range acquisition period the tracker is again set on frequency by noting which filter in the filter bank is responding.

After acquisition of both doppler and ranging signals the frequency tracker is time shared between these two functions, dwelling about 80 msec on each function. A separate tracking/holding register is used to control the VCO for doppler and range tracking. The output of the two tracking/holding registers is applied to the data converter where the frequency information is converted to digital signals representing velocity and range to the target.

6.4.8. ACCURACY OF VELOCITY AND RANGE MEASUREMENTS.

The measurement errors may be grouped into fixed random errors, which are random but relatively constant over the period of time the radar is in use and fluctuation errors which have periods of a few seconds or less.

VELOCITY MEASUREMENT ERROR.

A tabulation of velocity measurement errors is given in Table 6.4-4. A brief description of these errors is given in the following paragraphs. The net 3σ error is about $\sqrt{(.03)^2 + (.006V)^2}$ m/sec. At the maximum velocity for skin track of 38m/sec the 3σ error is 0.23 m/sec.

ERROR SOURCE	3 σ ERROR VALUE, METERS/SEC.	
	Fixed random	Fluctuating
Transmitter frequency, 10^{-3}%	Negligible	—
Frequency tracking	0.03	0.006V*
Data Processing	Negligible	Negligible
Total, rms	0.03	0.006V

$$\text{Net } 3 \, \sigma \text{ error} = \sqrt{(.03)^2 + (0.006V)^2}$$

* Assuming the use of frequency agility.

TABLE 6.4-4. VELOCITY MEASUREMENT ERROR.

TRANSMITTER FREQUENCY.

The amount of doppler shift is directly proportional to the transmitted frequency. Therefore, a given percentage uncertainty in transmitted frequency results in the same percentage velocity measurement error. Since this is a coherent system the transmitted frequency will be referenced to a crystal oscillator. The oscillator stability will be better than 1 part in 10^5 or 1×10^{-3}%. The resulting velocity measurement error is negligible.

FREQUENCY TRACKING.

Test data indicates that the error in measurement of average doppler frequency can be maintained less than 1 Hz (0.01 m/sec) under conditions of doppler spectrum widths up to the tracking filter bandwidth and signal-to-noise ratios as low as 3 dB. This will be taken as a 1σ value. The 3σ value is 0.03 m/sec.

We will next consider the fluctuation error, or noise at the tracker output after smoothing.

For the non-frequency agility case the spectral width of the central line is very narrow and RMS value of the fluctuations at the tracker output, σ_T, can be expressed as before by:

$$\sigma_T = \left[\frac{.078 \; B\,(1+\frac{1}{S/N})^2}{T \quad (1+S/N)^{1/2}} \right]^{1/2}$$

where the filter bandwidth, B, is equal to 225 Hz and the averaging time T equals 2 seconds.

At the signal-to-noise ratio required for acquisition in the filter bank the signal-to-noise ratio in the tracking filter

is about 16 dB for the case of the 1.0 meter antenna and 10.5 dB for the case of the 0.5 meter antenna. In either case the RMS noise is less than 1 Hz.

For the frequency agile case the fluctuation error will be about the same as developed previously for the coherent pulse radar in Section 6.3.6. The 1σ fluctuation error was found to be equal to 0.002V meters/sec where V is the velocity in meters. The 3σ error is equal to 0.006V m/sec.

RANGE MEASUREMENT ERROR

A tabulation of error sources in the range measurement is given in Table 6.4.5. A brief description of the errors is given in the following paragraphs.

The net 3 σ range error combining both fixed random and fluctuating errors is $(0.005R)^2 + (8)^2$ for R<2km and $(0.005R)^2 + (80)^2$ for R>2km. The relatively large error for R>2km is primarily due to fluctuation error caused by the doppler spectrum resulting from frequency agility. Itassumes the maximum velocity of 46 m/sec.

Slope Of Frequency Modulation.

The FM/CW radar altimeter used in the Apollo Landing Radar contained a linear frequency modulator with 20 MHz. deviation at X-band which had a maximum slope error of 0.6% over a wide temperature range. We will assume a value of 0.5% over the more restricted temperature in this application.

Quantization Errors Associated With FM/CW Ranging.

Linearly modulated FM ranging systems tend to exhibit a range quantizing error if there is no relative motion between the radar and target. The quantization is a consequence of the interruption of the range frequency waveform in mid-cycle at the end of the linear modulation period. If zero crossing frequency counters are used the quantization interval for a single axis crossing counter is equal to:

$$Q_R = \frac{C}{4\Delta F}$$

where ΔF is the frequency deviation.

The count jumps back and forth one as the range changes a quarter wavelength. It changes an average of one count as the range changes one quantization interval.

TABLE 6.4-5. RANGE MEASUREMENT ERROR.

ERROR SOURCE	3 σ ERROR VALUE, METERS			
	Fixed Random		Fluctuating	
	R<2km	R>2km	R<2km	R>2km
Slope of freq modulation	.005R	.005R	—	—
Quantization	0.38	3.8	—	—
Doppler compensation	0.3	3.0	0.06V	0.6V
Frequency tracking	0.3	3.0	0.06V	0.6V
Net 3σ error	$\sqrt{(.005R)^2+(.57)^2}$	$\sqrt{(.005R)^2+(5.7)^2}$	0.085V	0.85V

Combined error:

$$R < 2km, \quad \sqrt{(.005R)^2+(0.57)^2+(.085V)^2} \text{ meters}$$

$$R > 2km, \quad \sqrt{(.005R)^2+(5.7)^2+(0.85V)^2} \text{ meters}$$

6.110

The quantization effect can be observed, although reduced, if a frequency tracker is used to determine frequency rather than the simple zero counter. The quantization can be essentially eliminated from the data by placing a small amount of dither on the VCO of the frequency tracker using a dither frequency well above the response of the output data smoothing filter. This technique was used with excellent results in the radar altimeters used in the landing radars for both the Surveyor and Lunar Module spacecraft. The quantization error was reduced to values less than 10% of those computed for a zero crossing counter type processor.

Using these general values for the case of 20 mHz deviation, R<2km, the 0 to peak quantization noise will be less than 0.38 meters. For the 2 mHz deviation used for R>2km the 0 to peak quantization noise will be less than 3.8 meters.

DOPPLER COMPENSATION ERROR.

Since the doppler frequency is in effect subtracted from the range plus doppler frequency during the ranging mode in order to separate the range term, an error in the velocity measurement translates into an error in the range measurement. The 3σ velocity error is 0.03 m/sec random error plus a fluctuating error (with frequency agility) of 0.006V m/sec. The resulting equivalent 3σ range error is 3 meters fixed random plus 0.6V meters fluctuating at ranges greater than 2km and one tenth these values at ranges less than 2 km.

FREQUENCY TRACKING.

The fixed random tracking error will be less than 3 Hz, 3σ as discussed for the velocity measurements. This is equivalent to 3 meters for ranges greater than 2km and 0.3 meters for ranges less than 2 km.

Assuming the use of frequency agility the fluctuation error will be about the same as developed for the velocity measuring mode. This amounts to 0.6V meters, 3σ for R>2km and 0.06V meters 3σ for R<2km.

6.4.9. ANGLE TRACKING ACCURACY.

The analysis of angle tracking accuracy for the pulse doppler radar is similar to that given in Section 6.2.10 for the non-coherent pulse radar. Consequently, only a summary of the differences and the end results will be given in this section.

6.4.9.1. ANGLE TRACKING BIAS ERROR.

The angle tracking bias error will be about 0.24 mR for the 1.0 meter antenna and 0.48 mR for the 0.5 meter antenna.

6.4.9.2. ANGLE TRACKING FLUCTUATING ERROR.

The fluctuating error due to receiver noise in monopulse, doppler type radars is given by Barton[1] as follows:

$$\sigma_t = \frac{\alpha}{K_m \sqrt{\frac{SNR}{c} \frac{B}{\beta}}}$$

where
α = one way antenna beamwidth

K_m = constant   1.57

SNR = signal-to-noise ratio

B = IF bandwidth

c = $\frac{SNR+1}{SNR}$

β = servo bandwidth

The resulting RMS noise for the conditions associated with the 0.5 meter and the 1.0 meter antennas is tabulated below for operation at 19km range.

1. Barton, D.K. Radar System Analysis.

Antenna size	Beamwidth one way, Rad	SNR, dB	Tracker noise BW, Hz.	Servo noise BW, Hz.	RMS tracking noise, mR
0.5 m	0.049	10.6	270	0.79	0.50
1.0 m	0.024	13.0	419	1.57	0.21

The tracking data is smoothed with a time constant of 2 seconds prior to readout which reduces the RMS tracking noise to 0.16 mR in the case of the 0.5 meter antenna and 0.05 mR for the 1.0 meter antenna. The corresponding 3σ values are 0.48 mR for the 0.5 meter antenna and 0.15 mR for the 1.0 meter antenna.

The fluctuating error due to glint will be the same as developed for the non-coherent pulse radar or about 0.6 mR, 3σ after smoothing by the data output filter.

6.4.10   ANGLE RATE ACCURACY.

The determination of angle rate accuracy follows the material presented in Section 6.2.11 for the non-coherent pulse radar.

The bias error is essentially that due to the "hang off" of the rate gyro or about 0.09 mR/sec. The random error component of the gyro is also about 0.09 mR/sec, 3σ.

The noise on the rate output due to response of the rate measuring device to antenna jitter due to thermal noise and glint is determined in the same manner as in Section 6.2.11.

6.113

The results are summarized below.

Antenna size	Angle rate noise, mRad/sec, 3 σ	
	Due to thermal noise at 19km	Due to glint
0.5 meter	1.4	5.7
1.0 meter	0.61	8.1

Once again, the noise on the angle rate data due to low signal-to-noise ratio is largest near maximum range whereas the noise due to glint is largest at shorter ranges.

The total random error is given by the RSS of the error due to the gyro with the appropriate values above.

6.4.11 TRANSMITTER STABILITY REQUIREMENTS FOR PULSE DOPPLER RADAR.

The allowable FM and AM noise on the transmitter output is considerably higher for the pulse doppler radar in the Rendezvous Radar application than in applications where a high clutter environment exists.

Frequency modulation noise is of most importance in our application. It can create sidebands on the signal which lowers the power in the received carrier as well as increasing the fluctuation error at the output of the signal processor.

Treating first the power lost to sidebands, we can define the transmitted signal as

$$E_T = A(t) \cos\left(w_c t - \frac{\Delta w}{w_m} \cos w_m t\right)$$

where

$A(t)$ = Amplitude function

w_c = Carrier radian frequency

w_m = Modulating frequency

Δw = Peak frequency excursion.

The received echo signal is of the form

$$E_R = B(t) \cos\left[w_c\left(1 + \frac{2V}{c}\right)\left(t + \frac{2R}{c}\right)\right] - \frac{\Delta w}{w_m} \cos\left[w_m\left(\frac{1+2V}{c}\right)\left(t + \frac{2R}{c}\right)\right]$$

where

R = Range

V = Velocity

The major portion of the FM noise is generated in the common lower frequency stages of the Exciter/Local Oscillator. The noise is therefore highly correlated between the transmitter and local oscillator.

6.115

The difference frequency after mixing the received signal with the local oscillator is then of the form:

$$E_D = D(t) \cos\left[w_d t + \theta + \frac{2\Delta w}{w_m} \sin\left(\frac{w_m R}{c} \sin\left(w_m t + \frac{w_m R}{c}\right)\right)\right]$$

where

$$w_d = \frac{2V}{c} w_c = \text{doppler shift.}$$

This expression can be written in terms of Bessel functions as follows:

$$e(t) = \cos(\omega_d t + \theta)\left[J_0(u) + 2\sum_{n=1}^{\infty} J_{2n}(u) \cos 2n(\omega_m t + \phi)\right.$$
$$\left. - \sin(\omega_d t + \theta)\left[2\sum_{n=1}^{\infty} J_{2n-1}(u) \sin(2n-1)(\omega_m t + \phi)\right]\right.$$

where u = modulation index = $\frac{2\Delta w}{w_m} \sin \frac{w_m R}{c}$

The desired doppler shifted signal has the J_0 coefficient and the sidebands have the J_1, J_2, etc. coefficients.

A plot of the modulation index as a function of modulating frequency is given in Figure 6.4-4 for a maximum range of 22 km (the range at which acquisition must start for skin track to be acquired by a range of 19 km) and for a range of 560 km associated with the cooperative mode. A peak deviation of 100 Hz. was chosen for reference.

The loss in carrier power for modulating frequencies giving the highest modulation index is plotted in Figure 6.4-5 as a function of peak deviation of the frequency modulation. To
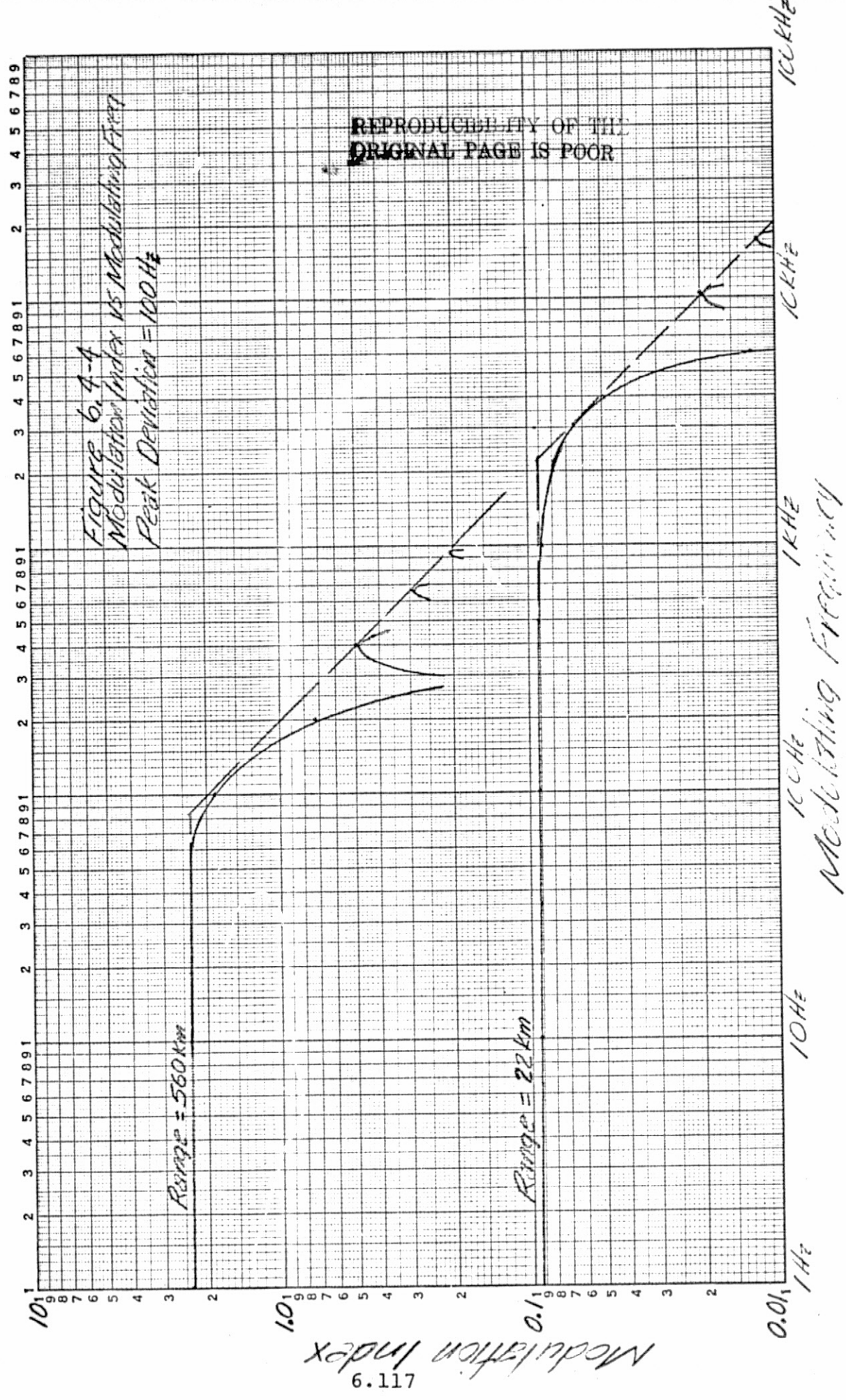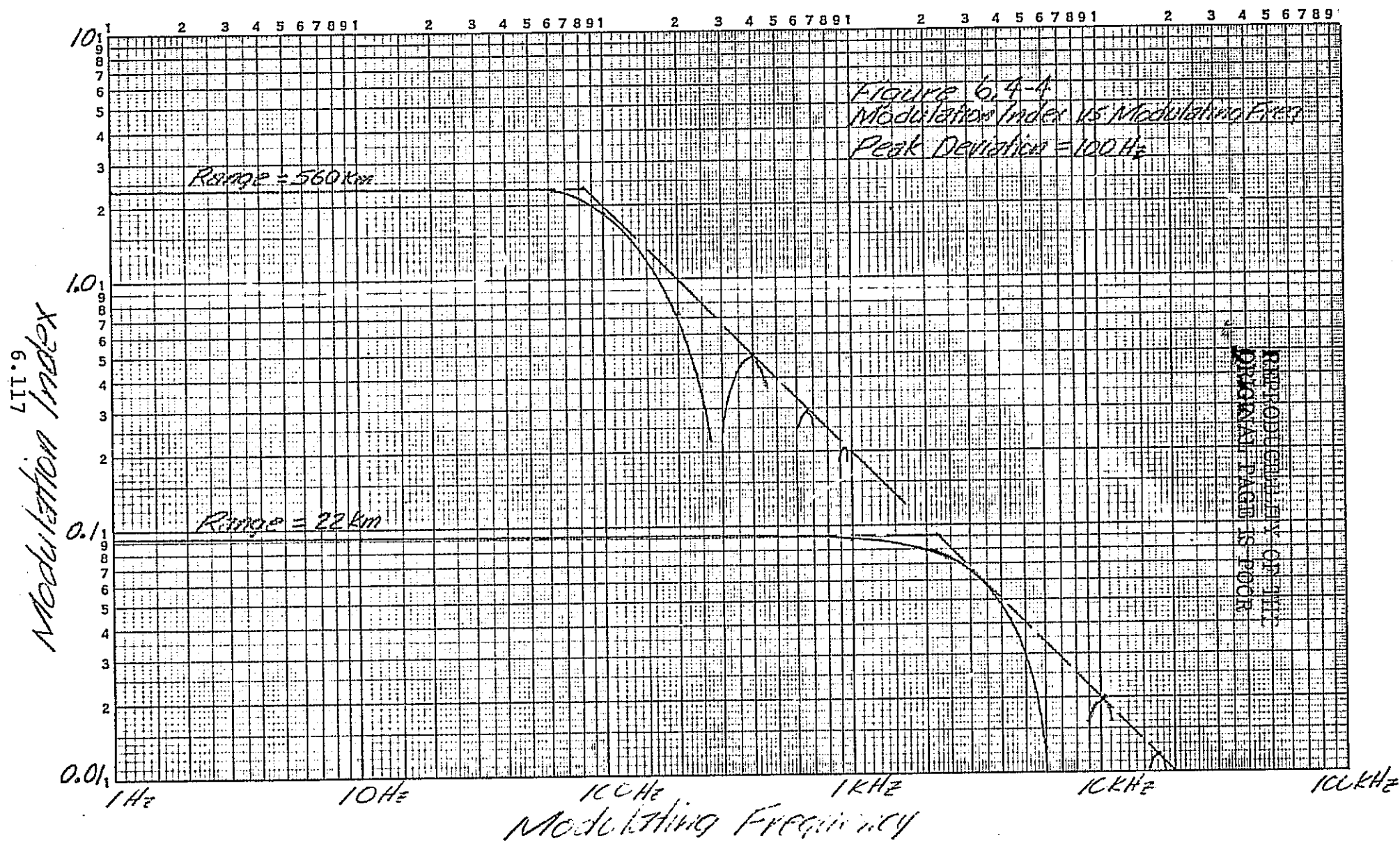
Figure 6.4-4
Modulation Index vs Modulating Freq.
Peak Deviation = 100 Hz

Modulating Frequency

Modulation Index

Range = 560 km

Range = 22 km

Figure 6.4-4
Modulation Index vs Modulating Freq
Peak Deviation = 100 Hz

Range = 560 km

Range = 22 km

Modulation Index

Modulating Frequency

Figure 6.4-5
Loss in Carrier Power
vs. Peak Deviation of FM
on Transmitter Signal

Range = 22 km
$f_m < 1$ kHz

Range = 560 km
$f_m < 53$ Hz

Peak Deviation

Loss in Carrier Power, dB
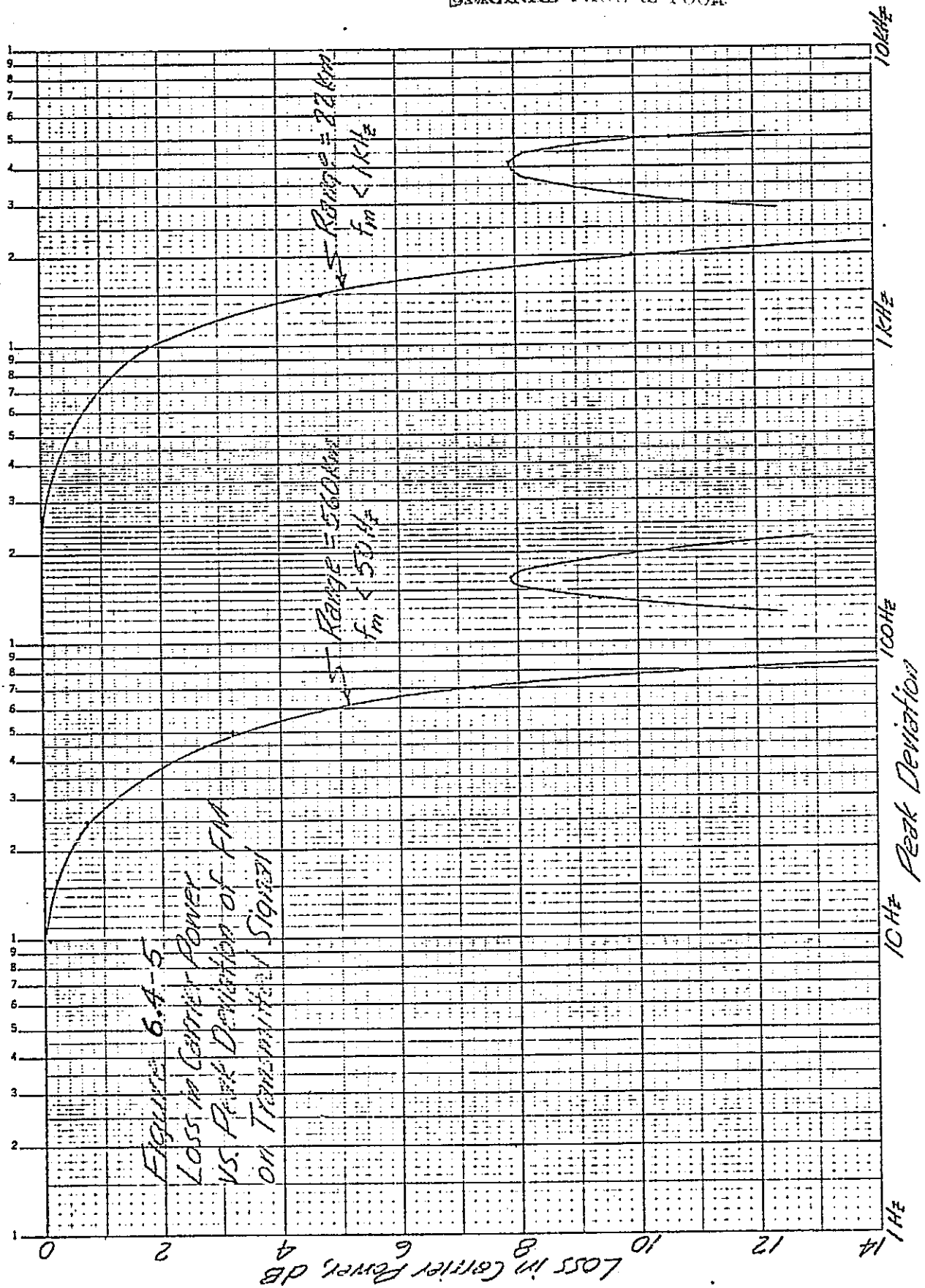
restrict the loss to 1 db for example the peak deviation should
be less than 27 Hz. (19 Hz. RMS) for the cooperative mode
(560 km range) and less than 700 Hz. (495 Hz. RMS) for the skin
track mode (22 km range). The value given for the cooperative
mode does not take into account FM noise which may be added by
the transponder.

The FM noise deviation for typical frequency multipliers at
X-band is in the order of 0.1 Hz. RMS in a 1 Hz. bandwidth over
a range of 10 Hz. to 100 KHz. from the carrier.[1] At a frequency
of 15 GHz. the noise would be about 1.5 times this value or
0.15 Hz. RMS in a 1 Hz. bandwidth.

For the skin track mode and a maximum range of 22 km, we
note from Figure 6.4-4 that modulating frequencies up to about
3 KHz are important. The total RMS deviation in the 0 to 3 KHz
band is then computed, based on a reference of 0.15 Hz RMS in
a 1 Hz. bandwidth, to be 8.2 Hz. This value is well below the
value of 495 Hz. RMS which results in a 1 db loss in carrier
power for the skin-track mode and the loss in signal due to FM
noise will be negligible. In the cooperative mode the round trip
loss due to FM noise will be about 0.2 dB.

6.5 OPERATION OF RENDEZVOUS RADAR IN THE COOPERATIVE MODE.

Operation of each of the three basic radar systems analyzed
previously for the skin track mode is treated for the cooperative
mode in this section. The specified operating limits for the
cooperative mode are 560 km to 30 m in range and ±91 m/sec in
velocity. At the maximum range (Mission I and II) the angular
search angle is 10 degrees by 10 degrees and the allowable
acquisition time is 5 minutes.

1.   "Microwave Power Sources", Microwave Journal, April, 1975.

6.5.1. NON COHERENT PULSE RADAR IN COOPERATIVE MODE.

A summary of system parameters of the non-coherent radar and transponder is given in Table 6.5-1   A functional block diagram of the transponder is given in Figure 6.5.-1.

The received signal is passed through the diplexer which provides at least 40 db of isolation to the transmitted signal. The signal is converted to an IF frequency of about 60 MHz. To accomodate the very wide dynamic range of the signal the IF amplifier which follows is designed to go into limiting once the peak signal to average noise ratio exceeds about 13 db.

A threshold detector which is referenced to the average noise level detects the presence of a pulse as it rises above the noise. When a given number of radar pulses is received in a fixed time period, the signal presence detector allows the trigger pulses from the threshold detector to pulse the modulator which in turn activates the transmitter. The pulse width received from the radar is monitored and when the radar switches to a 0.1 µsec pulse width the transponder pulse width is switched accordingly. Since the peak transmitter power required is relatively low an injection locked impatt solid state transmitter can be used.

6.5.1.1. SELECTION OF PRF.

An unambiguous range interval of 700 km rather than 560 km was selected to expand the range between first and second time around echo returns. A PRF of 214 Hz. is indicated for this range.

TABLE 6.5-1. CHARACTERISTICS OF NON COHERENT PULSE RADAR IN
COOPERATIVE MODE.

PERFORMANCE CHARACTERISTICS

Range for 0.99 probability of detection..... >560 km

Acquisition time............................ 5 minutes

Angular search coverage..................... 10°x10°sector

Accuracy, 3σ (at max range)

	Bias (Lag error)	Random
Range		30 m
Velocity	0. (?)	0.3 m/sec
Angle	0.24 mR	0.34 mR
Angle rate	0.09 mR/sec	7.2 mR/sec

RADAR CHARACTERISTICS (Different from skin track case)

Antenna size................................ 1 meter diameter

PRF

R > 40 km .... 214 Hz.

R < 40 km .... 3.7 KHz.

Pulsewidth .... 0.1 μsec

TRANSPONDER CHARACTERISTICS

Antenna gain .... 0 db

Peak transmitted power *(1m radar antenna)....... 4.0 watts

Pulse width .... 1.0μsec & 0.1μsec.

Average transmitted power (1μsec pulse width).... 8.6×10^{-4} watts

IF noise bandwidth .... 7.5 MHz.

Noise temperature 1670

* with 2dB margin added

6.121
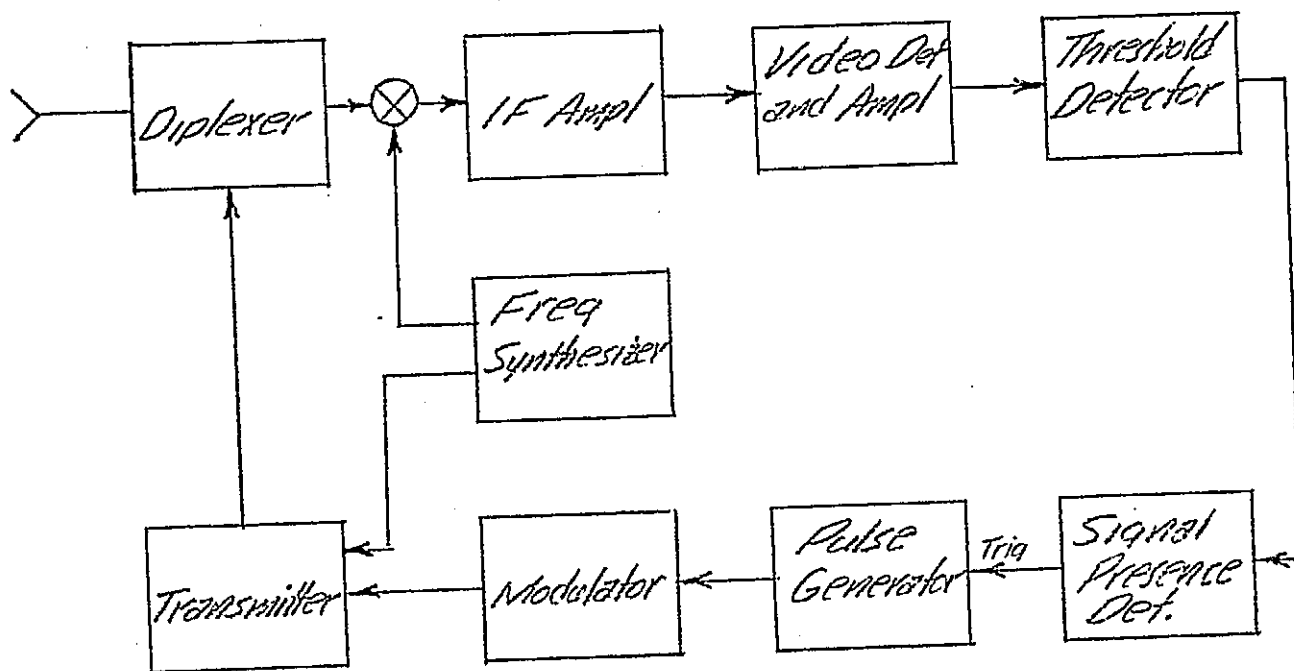
Figure 6.5-1   Functional Block Diagram
of Transponder for Noncoherent Pulse Radar

6.5.1.2. SELECTION OF ANTENNA SCAN FRAME TIME.

The optimum antenna scan program for the long range cooperative mode (Mission I and II) is determined in the following paragraphs. The specified allowable acquisition time is 5 minutes for 99% probability of detection. The specified search area is 10°x10°.

The antenna scan parameters are summarized in Table 6.5-2 for various antenna scan frame times considered. Also given are the associated signal-to-noise ratios required for acquisition. The signal-to-noise ratios required were taken from Fehlner[1] as before but for the case of a non-fluctuating target.

A false alarm time of one hour was assumed which implys that the antenna scan will momentary pause on the average once an hour and then resume scanning if signal presence is not confirmed. The 60 minute false alarm time, with a ratio of rangegate on time to $\frac{1}{PRF}$ of 0.84 results in a false alarm number, n', of $\frac{3 \times 10^9}{N}$ where N is the number of pulses integrated.

It is apparent from the table that the longer frame times require less signal-to-noise ratio for acquisition than the shorter frame times. Further, the signal-to-noise ratios indicated are generally below zero db. Consequently, range and range rate measurement accuracy will be the driving requirement for transmitted power from the transponder rather than acquisition considerations.

An antenna scan frame time of one minute which is used for the skin track mode with frequency agility appears reasonable with either the 0.5 meter or the 1.0 meter diameter antenna.

1. Fehlner, L.F. Marcum and Swerling's Data on Target Detection, John Hopkins University Report TG 451.

TABLE 6.5-2 ANTENNA SCAN PARAMETERS FOR COOPERATIVE MODE.

Antenna size, m	Two way B.W.,deg.	Frame time, min.	Single scan P_D	Scan rate, deg/sec	Dwell time,sec.	Number pulses received	SNR Req'd, db
0.5	2	5	.99	0.24	8.48	1814	−7.2
		2.5	.90	0.48	4.19	897	−6.6
		1	.60	1.23	1.63	349	−4.5
0.5	2	.5	.37	2.62	0.76	164	−3.0
1.0	1.0	5	.99	0.44	2.26	484	−3.5
		2.5	.90	0.9	1.10	236	−2.5
		1.0	.60	2.42	.413	88	−1.8
1.0	1.0	..5	.37	5.47	0.18	39	0.8

6.3.1.3. COOPERATIVE LINK CALCULATIONS.

The amount of peak transmitted power required from the transponder to produce a given signal-to-noise ratio in the radar receiver is calculated in Table 6.5-3. The radar receiver parameters are the same as developed previously for the non-coherent pulse radar. The resulting expression for peak transponder transmit power, P_b, is

$$P_b = 39.8 + 10 \log SNR - 10 \log G_r \text{ dBW.}$$

The peak transmit power required for the 0.5 meter and the 1.0 meter diameter radar antennas is tabulated below for a 6 db signal-to-noise ratio. This SNR yields adequate accuracy at maximum range.

Radar antenna size, meters	Antenna gain, db	SNR req'd. db	Peak transmit power	Average transmit power
0.5	35.7	6.0	10.2 watts	2.2×10^{-3} watts
1.0	41.7	6.0	2.5 watts	5.4×10^{-4} watts

TABLE 6.5-3 CALCULATION OF PEAK TRANSMITTED POWER REQUIRED BY TRANSPONDER FOR NON-COHERENT PULSE RADAR.

$$P_b = \frac{SNR(4\pi)^2 R^2 KT_s BL_b L_s L_f L_p}{G_r G_b \lambda^2}$$

Symbol	Parameter	Value	Value in db
SNR	Signal-to-noise ratio	SNR	$10 \log SNR$
$(4\pi)^2$	Constant	$(4\pi)^2$	22
R^2	$(Range)^2$	$(587\ km)^2$	115.4
K	Boltzmann's constant		-228.6
T_s	System noise temperature	$1758°K$	32.4
B	Receiver noise bandwidth	0.75 MHz.	58.8
L_b	Transponder transmit path loss	0.6 db	0.6
L_s	Scan loss	1.6 db	1.6
L_f	Filter miss-match loss	0.6 db	0.6
L_p	Polarization loss	3.0 db	3.0
G_r	Radar antenna gain	G_r	$-10 \log G_r$
G_b	Transponder antenna gain	0 db	0
λ^2	$(Wavelength)^2$	$(0.02m)^2$	34
P_b	Peak transmitted power		$39.8 + 10 \log SNR - 10 \log G_r$

6.5.1.4.   SIGNAL-TO-NOISE RATIO AT TRANSPONDER.

The transponder receiver will be configured with a 7.5 MHz. noise bandwidth to accomodate both the 1.0 and the 0.1 µsec radar pulsewidth and to minimize propagation delay errors. Modifying the results of the link calculation given in Table 6.5-2 for the increase in receiver bandwidth, and differences in microwave losses, the SNR in the beacon receiver can be expressed as follows:

$$10 \log SNR = 10 \log P_t + 10 \log G_r - 48.6 dB$$

A tabulation of SNR at maximum range for the cases of a 1 meter diameter radar antenna and a 0.5 meter antenna is given below.

Radar antenna size	Antenna gain	Radar peak transmit power	SNR at transponder
0.5 meter	35.7 db	5.4 kw	24.4 dB
1.0 meter	41.7 db	0.9 kw	22.6 dB

6.5.1.5   ACCURACY OF RANGE MEASUREMENT.

A tabulation of range measurement error for the cooperative mode is given in Table 6.5-4. Most of the errors within the radar are the same as described previously for the skin track mode. The remaining errors are briefly described in the following paragraphs.

The resultant error includes a deterministic component of 42.7 meters, (primarily due to lag in the range readout at 91 m/sec velocity), a fixed random component of 10.1m, 1σ and a fluctuating or noise term of 0.57m, 1σ. The total random error at maximum range is about 30.3 meters, 3σ.

TABLE 6.5-4   ERROR ANALYSIS OF NON-COHERENT RADAR IN COOPERATIVE
MODE AT   560 km RANGE.

Error Source	Deterministic error, meters	1σ error value, meters	
		Fixed random	Fluctuating
Radar errors			
Velocity lag (at 91m sec)	41		
Clock frequency (0.001%)		5.6	
Start pulse stability		0.2	
Propagation delay in receiver (1.0μsec pulsewidth)		8.3	
Gating & threshold delay		0.1	
Calibration		0.3	
Quantization (PRF=214)			0.14
Range tracker jitter (6db SNR)			0.3
Transponder errors			
Propagation delay in receiver		0.83	
Calibration		0.3	
Propagation delay in threshold detector and trigger circuits		0.1	
Noise bias (at 23db SNR)	1.7		
Delay in modulator and transmitter		0.9	
Jitter in threshold output due to noise			Negligible
Net error	42.7 m	10.1 m	0.57 m

Propagation Delay in Transponder Receiver.

Considering as before two synchronously tuned IF stages with a 7.5 MHz. noise bandwidth the propagation delay is about 0.19 µsec. The variation in delay from the calibrated value can vary about ±5% maximum or about 2.9% RMS. The error due to changes in the propagation delay is then equivalent to 0.83 m RMS.

Calibration Error.

A calibration error of 0.3 meters 1σ is assumbed as developed previously for the radar.

Propagation Delay in Threshold Detector and Trigger Circuits.

The nominal delay through these circuits is about 10 nsec with a variation of ±3nsec maximum. Assuming a uniform distribution of error the 1σ value is 1.7 nsec or about 0.12 meters.

Noise Bias.

A slight shift towards a lower range is incurred on the leading edge of the pulse due to addition of receiver noise. Skolnik[1] has developed an expression for the RMS value of this error, δT, as follows:

$$\delta T = \frac{t_r}{(2\ SNR)^{1/2}}$$

where t_r is the rise time of the pulse which is approximately equal to the reciprocal of the receiver bandwidth.

The 3 db bandwidth of the receiver is about 6.1 MHz. which yields a rise time of about 1.6×10^{-7} seconds.

The noise bias error at the signal-to-noise ratio at maximum range of about 20db is 11.3 nsec or 1.7 meters.

<u>Delay in Modulator and Transmitter.</u>

At the transmit power levels considered for the transponder, solid state transmitters are feasible. The variation in delay through a solid state modulator and transmitter is conservatively estimated to be ± 10ηsec. Assuming this error to be uniformly distributed the RMS value is 5.8ηsec or 0.9 meters.

<u>Jitter in Thresholding Time Due to Noise.</u>

The jitter in the time the signal detect threshold is crossed in the transponder will be of the same order of magnitude as the noise bias error treated previously. At 20 db signal-to-noise ratio at maximum range this term is equal to about two meters. A new independent value of the jitter will be obtained on each pulse, or at a 214 Hz. rate. After smoothing by the range tracker time constant of about 0.5 seconds the jitter is reduced to a negligible value (.003 meters RMS).

6.5.1.5.   ACCURACY OF RANGE RATE MEASUREMENT.

Range rate will be determined as before by taking range differences as a function of time. The analysis for the accuracy of the range rate measurement proceeds in the same manner as in the skin track case for the non-coherent radar.

The steady error in the velocity measurement will be neglibible using a digital implementation of the range tracker and differentiator. The 1σ value of the noise term is equal to about $0.77\sigma_R$ as before, where σ_R is the 1σ value of the range tracker jitter. Again using expressions for σ_R developed in the literature for a split gate tracker as representative, σ_R is equal to 0.3 meters at a 6 db signal-to-noise ratio and $1\mu sec$

pulsewidth. The 1σ value of noise on the range rate output is then 0.23 meters/sec.

The net error in measuring range rate is a fluctuating term with a 1σ value of 0.23 m/sec at maximum range. This error decreases as the range decreases.

6.5.1.6.   ACCURACY OF ANGLE MEASUREMENTS.

A bias error can be generated in the angle measurement due to phase errors in the monopulse combiner and IF stages. This bias error will be the same as developed previously for the skin track mode, or about 0.48 mR for the 0.5 meter antenna and 0.24 mR for the 1.0 meter antenna.

The fluctuating error due to thermal noise is developed in the same manner as in Section 6.2.10. The resulting 3σ error at a 6 dB signal-to-noise ratio at maximum range and a PRF of 214 Hz is 1.2 mR for the 0.5 meter antenna and 0.34 mR for the 1.0 meter antenna.

We assume that the glint from the transponder signal is negligible.

6.5.1.7.   ACCURACY OF ANGLE RATE MEASUREMENT.

The angle rate error will include a stand off error of .09 mR/sec plus a random error of 0.09 mR/sec in the gyro.

The angle rate noise due to jitter of the antenna due to thermal noise at a 6 dB signal-to-noise ratio is computed as in Section 6.2.11. The results indicate a 3σ value of noise on the angle rate data of 10.5 mR/sec for the 0.5 meter antenna and 7.2 mR/sec for the 1.0 meter antenna.

These values are appreciably above the 0.14mR allowable random error. In the case of the 0.5 meter antenna in order to reduce the noise to allowable random error, the transmitted power of the transponder would have to be increased from 10 W peak to about 56KW peak. Alternately, the data smoothing time may be able to be increased at the maximum range to decrease the noise on the data.

6.5.2. COHERENT PULSE RADAR IN COOPERATIVE MODE.

A summary of system parameters for the coherent pulse radar and transponder is given in Table 6.5.-5. A functional block diagram of a candidate transponder is given in Figure 6.5-2.

The received signal in the transponder passes through the diplexer, which has at least 40 db isolation to the transmitted signal, and is mixed with the local oscillator signal to generate a 60 MHz. IF signal. The IF amplifier is designed to limit once the signal exceeds about 13 db signal-to-noise ratio in the IF bandwidth. This provides a relatively constant 60 MHz. signal during the duration of the pulse. The IF signal is down converted to an IF frequency around 1 MHz. where the doppler shift is extracted by using either a frequency tracker or a phase lock loop. The smoothed doppler signal is up converted to a 60 MHz IF and then to a carrier frequency of 14.54 GHz. which is filtered and used to drive the transmitter.

A threshold detector senses the presence of a signal above a preset threshold. When some high percentage, say 90% of the radar pulses are received in a given time interval the signal presence detector actuates a gate which allows the trigger pulse to be applied to the modulator. The radar PRF can be coded to command a 1 ηsec pulse from the transponder at long ranges and 0.1 ηsec pulses at short ranges. This command would be decoded and the modulator set accordingly. The modulator pulses the solid state transmitter which in turn generates the transponded signal.

6.5.2.1. PRF CONSIDERATIONS.

In order to accomodate a velocity range of ±91 m/sec unambiguously, and assuming no a-priori velocity information, the PRF of the radar should be at least 18.2 KHz. A minimum value of

TABLE 6.5.-5.   CHARACTERISTICS OF COHERENT PULSE RADAR IN
               COOPERATIVE MODE.

PERFORMANCE CHARACTERISTICS

Range for 0.99 probability of detection....... >560 km

Acquisition time .... 5 minutes

Angular search coverage .... 10°x10° sector

Accuracy, 3σ (at max range)

	Bias (Lag error)	Random 30m
Range	(Lag error)	30m
Velocity	(Lag error)	0.3 m/sec
Angle	0.24mR	0.34 mR
Angle rate	0.09mR/sec	7.2 mR/sec

RADAR CHARACTERISTICS (Different from skin track case)

Antenna size.................................... 1.0 m diameter

PRF

        Acquisition................ 214 Hz.

        Track (dithered)........ 20-30 KHz.

Pulsewidth................... 0.1μsec

TRANSPONDER CHARACTERISTICS

Antenna gain .... 0 db

Peak transmitted power *(1 m radar antenna).... 4.0 watts

Pulsewidth .... 1.0 and 0.1μsec

Average transmitted power(1μsec pulsewidth).... 0.10 watts

IF noise bandwidth .... 7.5 MHz.

Noise temperature .... 1670°K

* with 2 dB margin added.
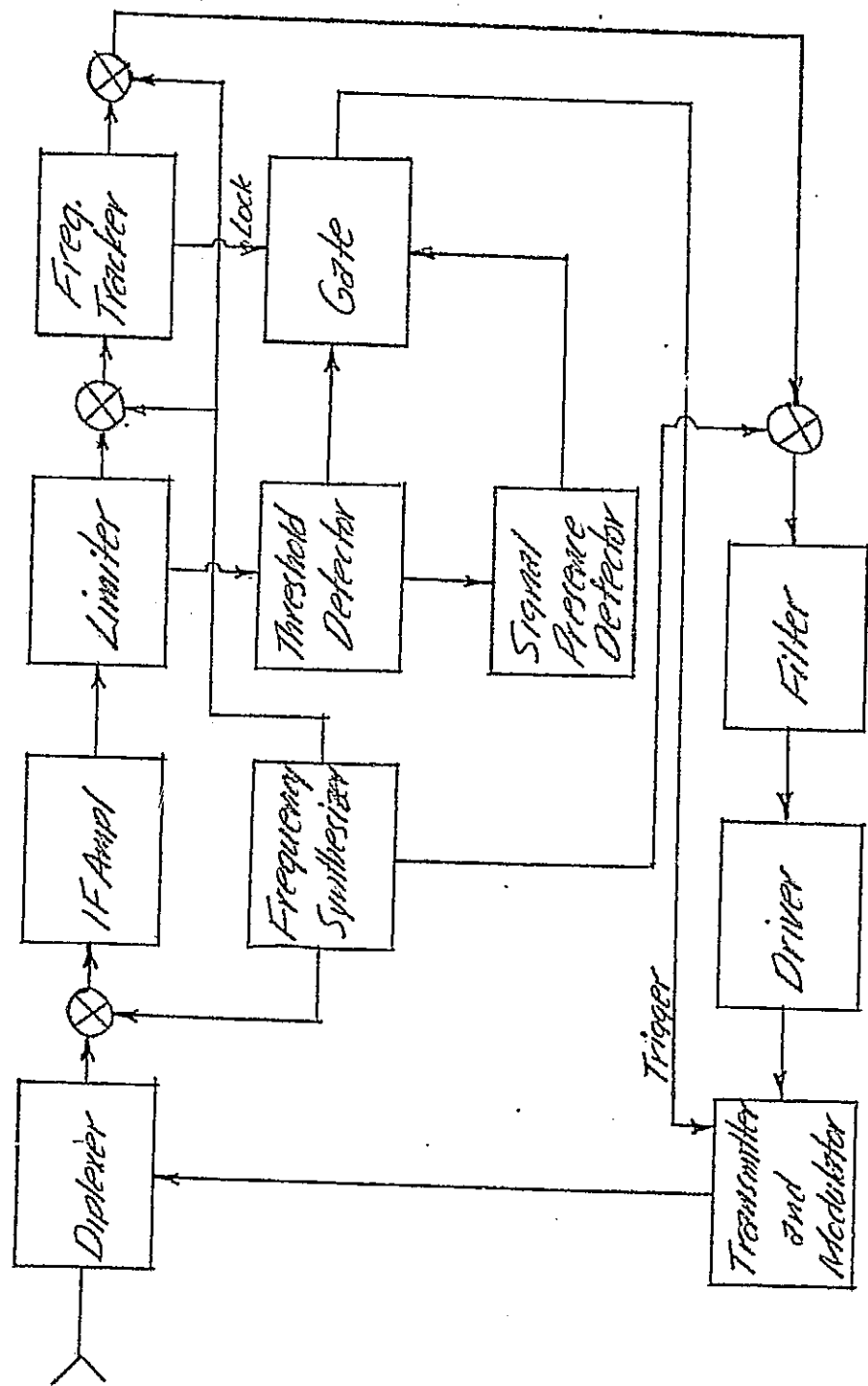
Figure 6.5-2 Functional Block Diagram of Transponder for Coherent Pulse Radar

6.135

19.2 KHz. will be assumed to provide some margin for filtering.

A PRF of 19.2 KHz. results in range ambiguities each 7.8 km. Consequently, some method of resolving the range ambiguities are required. The same approach as discussed previously for the coherent pulse radar in the skin track mode can be followed but using 3 values of PRF related through ratios of m_1, m_2 m_3 (all integers). The unambiguous range R_u may be expressed

$$R_u = \frac{m_2 \ m_3 \ C}{2 \ PRF}$$

Using ratios m_1, m_2, m_3 = 8,9, 10 and a minumum PRF of 19.2 KHz. the maximum unambiguous range is 703 Km.

The three values of PRF used by the radar would then be 19.2, 21.6 and 24.0 KHz. The range ambiguities would be resolved by the radar using an algorithm such as the Chinese remainder theorem.

An alternative way of obtaining unambiguous range is to perform initial target acquisition with a PRF of 214 Hz. as in the non-coherent radar case. After angle and range acquisition have been achieved the PRF would be switched to about 20 KHz to allow unambiguous doppler frequency measurement to be made. Once the range tracker has been locked to the signal it will continue to track the target at the proper range despite the ambiguities caused by the high PRF.

To avoid range holes, caused by the signal returning while the transmitter is pulsing, the PRF would be varied from 20 KHz. to 30 KHz. in a regular manner.

6.5.2.2. TRANSMITTED POWER REQUIRED FROM TRANSPONDER.

The peak power required from the transponder will be essentially the same as developed previously for the non-coherent transponder since the driving requirement on signal-to-noise ratio is measurement accuracy rather than on acquisition.

Transponding a 1μsec pulse at an average PRF of 25 KHz. the average power required from the transponder is tabulated below:

Radar Antenna Size	Peak Transmit Power	Average transmit power
0.5 m	10.2 watts	0.26watts
1.0 m	25 watts	0.063 watts

6.5.2.3. SIGNAL-TO-NOISE RATIO AT TRANSPONDER.

The peak power required for the coherent pulse radar in the skin track mode is 5.4 kw with the 0.5 meter antenna and 0.9 kw for the 1.0 meter antenna. In order to maintain the same peak transmitted power and about the same average power when the PRF is changed to an average value of 25 KHz. required for the cooperative mode, the pulsewidth must decrease to about 0.15 μsec. Since a pulsewidth of 0.1 μsec has previously been considered for the skin track mode when then the range decreases below 9 km, this same value will be used for the cooperative mode.

Using a two stage synchronously tuned IF filter with a noise bandwidth of 7.5 MHz. in the transponder and other parameters as considered previously, the signal-to-noise ratio in the transponder will be 24.4 dB for the 0.5 meter diameter radar antenna and 22.6 dB for the 1.0 meter antenna.

6.5.2.4. SIGNAL TO NOISE RATIO IN DOPPLER FREQUENCY TRACKER IN TRANSPONDER.

The signal-to-noise ratio within a doppler tracking filter bandwidth, B_t, can be expressed in terms of the IF signal-to-noise ratio as before by

$$SNR/_{Tracker} = SNR/_{IF} \frac{0.75 \; \tau (PRF)^2}{B_t}$$

Assuming a ΔV of 10 fps/sec^2 during the braking phase the one way rate of change of doppler frequency is 153 Hz/sec. In order to remain within the tracking filter bandwidth during this acceleration with a typical tracking loop time constant of about 0.1 seconds the one sided filter width should be about 16 Hz. which gives a total bandwidth of 32Hz. The equivalent noise bandwidth is about 39 Hz. With a pulsewidth of 0.1 µsec, an average PRF of 25 KHz. and a noise bandwidth of the tracking filter of 39 Hz. the signal-to-noiseratio in the tracking filter is about 0.8 db greater than in the IF bandwidth. Thus a signal-to-noise ratio in excess of 20 db will be available in the frequency tracker which affords a good operating margin over the value of 4 db SNR required for normal operation.

6.5.2.5. ACCURACY OF MEASUREMENTS.

The ranging accuracy will be essentially the same as previously determined for the non-coherent transponder case.

The velocity accuracy will be determined by the accuracy of the frequency trackers in the radar and transponder and the accuracy of the transmitted frequencies.

The largest error in the system will be due to the uncertainty in the fixed off-set between the received and transmit frequencies. We could time duplex the signals and retransmit the same frequency as received to eliminate the offset frequency. However, this would result in interference from skin return when the target is at short range. A separation of at least 200 MHz is desirable to allow discrimination of the skin track signal. In order to meet the velocity accuracy requirements the variation of the frequency reference in the transponder must be in the order of 10^{-7} over the operating period. This value is obtainable with a good quality aged crystal oscillator. This tolerance will result in a frequency uncertainty of 20 Hz in the 200 MHz offset frequency which corresponds to a velocity uncertainty of 0.2 m/sec. In addition, the error in the frequency tracker in the transponder and radar can be about 1 Hz (0.01 m/sec) each. The signal-to-noise ratio in the tracker bandwidth in the radar is about 4 db with a 6 db peak signal to average noise ratio in the IF bandwidth. The tracker noise at this SNR is about 2.9 Hz or 0.03 m/sec, 1σ. The SNR in the transponder frequency tracker bandwidth is about 20 db and the tracker noise is negligible.

The total velocity measurement error is then as follows:

ERROR SOURCE	3σ Value, m/sec.	
	Slowly varying	Fluctuating
Frequency offset	0.2	
Transponder tracker	0.01	
Radar tracker	0.01	
Radar tracker noise		0.09*
Net error	0.29 m/sec.	

*Decreases as SNR increases.

6.5.3. PULSE DOPPLER RADAR IN COOPERATIVE MODE.

A summary of system parameters for the pulse doppler radar and transponder in the cooperative mode is given in Table 6.5-6. A functional block diagram of a candidate transponder is given in Figure 6.5.-3.

6.5.3.1. TRANSPONDER OPERATION.

The signal received by the transponder passes through the diplexer and is converted to an IF frequency of about 60 MHz. The IF signal is amplified by an amplifier with about 20 db AGC range and applied to a limiting amplifier which is designed to limit and maintain a constant output at a level equivalent to the minimum expected signal at maximum range. This corresponds to about 6 db signal-to-noise ratio in the IF bandwidth.

The bandwidth of the IF amplifier is made slightly greater than 2 mHz at ranges greater than 2 km to pass the 2 mHz deviation of the linear frequency modulation on the radar signal. At ranges less than 2 km the radar deviation increases to 20 mHz and the transponder IF bandwidth is switched to 20 mHz upon detecting the change. The limiter maintains a nearly constant signal into the single sideband up converter over the wide dynamic range of the signal.

The amplified and filtered IF signal is up converted to about 14.76 GHz. by a single sideband, suppressed carrier up converter. The up converted signal is further cleaned up by passing through a microwave filter and then applied to the driver and transmitter. The transmitter can be a low power Gunn or Impatt solid state smplifier.

TABLE 6.5-6. CHARACTERISTICS OF PULSE DOPPLER RADAR IN COOPERATIVE MODE.

PERFORMANCE CHARACTERISTICS.

Range for 0.99 probability of detection .... >560 km

Acquisition time .... 5 minutes

Angular search coverage .... 10°x10° sector

Accuracy, 3σ (at maximum range)

	Bias	Random
Range	(Lag error)	$\sqrt{(.005R)+(68)^2}$
Velocity	(Lag error)	0.3 m/sec
Angle	0.24mR	0.17 mR
Angle rate	0.09mR/sec	2.0mR/sec

RADAR CHARACTERISTICS (Changes from skin track mode)

Antenna size........................ 1 meter diameter

Frequency modulation

    Deviation

        R < 2 km.................. 20 MHz

        2 km < R< 20 km .... 2 MHz

        R > 20 km .... 2 MHz.

    Duration of sweep

        R < 2 km .... 13 msec

        2 km < RL 20 km .... 13 msec

        R > 20 km .... 67 msec

TRANSPONDER CHARACTERISTICS

Antenna gain .... 0 db

Peak transmitted power .... 10 m W*

Duty ratio 0.5

IF bandwidth

    R > 2 km .... 2 MHz

    R < 2 km .... 20 MHz.

Noise temperature of receiver....... 1670°K

Transmit path losses............... 0.6 dB

*Results in a margin of about 5 dB relative to required value.
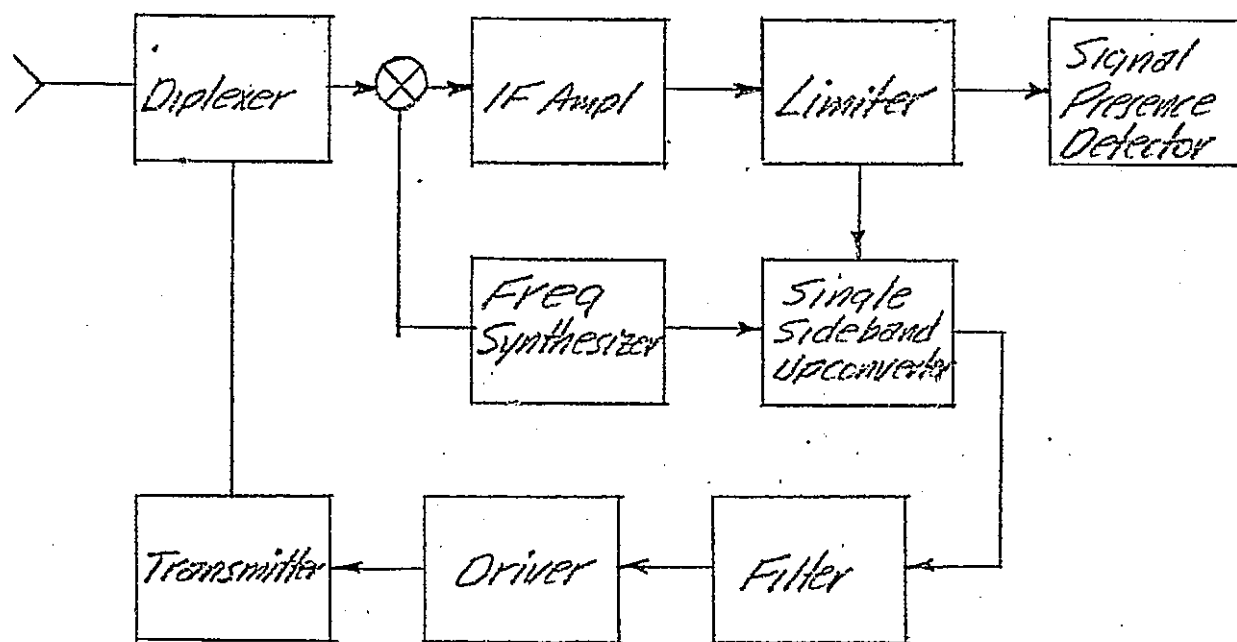
Figure 6.5-3 Functional Block Diagram of Transponder for Pulse Doppler Radar

6.5.3.2. SIGNAL-TO-NOISE RATIO AT TRANSPONDER

The peak signal to average noise ratio within the 2.4 MHz. IF noise bandwidth is computed in Table 6.5-7. The result is:

$$SNR = -43.4 + 10 \log P_t + 10 \log G_r$$

where P_t is the radar peak transmitted power and G_r is the radar antenna gain. The value of SNR for the two radar antenna sizes considered is given below:

RADAR ANTENNA SIZE	RADAR ANTENNA GAIN	RADAR PEAK POWER	TRANSPONDER SNR
0.5 meter	35.7 db	38.9 watts	3.2 db
1.0 meter	41.7 db	6.5 watts	6.4 db

6.5.3.3. TRANSMIT POWER REQUIRED OF TRANSPONDER.

Using the same values of filter bandwidth in the radar as determined for the skin track mode with frequency agility, 100 Hz for the 0.5 meter diameter antenna and 267 Hz. for the 1.0 meter antenna, the signal-to-noise ratio required for acquisition of a steady beacon signal with a false alarm rate of one hour is tabulated below.

ANTENNA SIZE	FRAME TIME	SINGLE SCAN P_d	BANDWIDTH (3 db)	DWELL TIME	NUMBER INDEPENDENT SAMPLES	SNR REQUIRED
0.5 m	1 min.	0.9	100 Hz.	1.63 sec	163	-4 db
1.0 m	1 min.	0.9	267 Hz.	0.41 sec	109	-2.8 db

It is apparent that the signal-to-noise ratio required for accurate tracking, about 4 db, will be the driving factor rather than signal-to-noise ratio required for acquisition.

TABLE 6.5-7.   SIGNAL-TO-NOISE RATIO AT TRANSPONDER

$$SNR = \frac{P_t G_r G_b \lambda^2}{(4\pi)^2 R^2 K T_s B L_m L_p}$$

SYMBOL	PARAMETER	VALUE	VALUE IN DB
P_t	Radar peak power	P_t	$10\log P_t$
G_r	Radar antenna gain	G_r	$10\log G_r$
G_b	Transponder antenna gain	0 db	0
λ^2	(Wavelength)^2	$(0.02 \text{ m})^2$	-34
$(4\pi)^2$	Constant	$(4\pi)^2$	-22
R^2	(Range)^2	$(587\text{km})^2$	-115.4
K	Boltzmann's constant		228.6
T_s	Transponder noise temperature	1670°K	-32.2
B	Receiver bandwidth	2.4 mHz	-63.8
L_R	Radar transmit path loss	1.6 dB	-1.6
L_p	Polarization loss	3.0 db	-3.0
SNR	Signal-to-noise ratio		$-43.4 + 10\log P_t + 10\log G_r$

Using a value of 4 dB for SNR required, the amount of peak transmitted power required from the transponder is computed in Table 6.5-8. The resulting peak transmitted power required is given below as a function of radar antenna size.

ANTENNA SIZE	DOPPLER TRACKER BANDWIDTH(noise)	ANTENNA GAIN	PEAK TRANS POWER REQ'D
0.5 meters	275 Hz	35.7 dB	0.011 watts
1.0 meters	320 Hz	41.7 dB	0.003 watts

At the maximum range, the peak signal power to average noise power ratio transmitted by the transponder is about 8.2 dB in a 2.4 mHz noise bandwidth for the 0.5 meter antenna case and 6.4 dB for the 1.0 meter antenna. Thus, the signal transmitted is greater than 80% of the total transmitted power or less than 1 dB below the total power transmitted.

The transmitted signal to noise ratio from the transponder of 6 to 8 dB in a 2.4 mHz bandwidth at maximum range results in a much greater signal to noise ratio within the bandwidth of the doppler tracking filter in the radar.

Converting from peak power to the amount of power in the central spectral line, and considering eclipsing as discussed for the case of skin track with the pulse doppler radar, the average signal to noise ratio within the tracking filter will be 10.8 dB less than if computed using peak power. The net effective signal to noise ratio within the radar tracking filter bandwidth is listed below:

TABLE 6.5-8.   CALCULATION OF PEAK POWER REQUIRED BY TRANSPONDER
FOR PULSE DOPPLER RADAR

$$P_b = \frac{SNR \ (4\pi)^2 R^2 K \ T_s \ BL_m L_p L_e D_n}{G_r G_b \lambda^2}$$

SYMBOL	PARAMETER	VALUE	VALUE IN DB
SNR	Signal-to-noise ratio	4 db	4
$(4\pi)^2$	Constant	$(4\pi)^2$	22
R^2	(Range)^2	$(587\text{km})^2$	115.4
K	Boltzmann's constant		-228.4
T_s	System noise temperature	1758°K	32.4
B_t	Tracker noise bandwidth	B_t	$10\log B_t$
L_m	Transponder transmit path loss	0.6 dB	0.6
L_p	Polarization loss	3.0 db	3.0
L_e	Eclipsing loss	10.8 db	10.8
D_n	Duty ratio of noise gate	0.5	-3.0
G_r	Radar antenna gain	G_r	$-10\log G_r$
G_b	Transponder antenna gain	0 db	0
λ^2	(Wavelength)^2	$(0.02\text{m})^2$	34
P_b	Peak transmit power		$-9.2+10\log B_t-10\log G_r$ dBW

RADAR ANTENNA SIZE	TRACKER BANDWIDTH (noise)	SNR OF TRANSPONDED SIGNAL IN 2.4 mHz BANDWIDTH	EFFECTIVE SNR OF TRANSPONDED SIGNAL
0.5 meters	275 Hz.	8.2 db	36.8 dB
1.0 meters	320 Hz.	6.4 db	34.4 dB

Since the transmitted power from the transponder will be sized to provide a 4 db signal to thermal noise ratio in the tracking filter, it is clear that thermal noise density is the dominant factor in determining signal-to-noise ratio in the radar at maximum range rather than the noise transmitted by the transponder.

6.5.3.4.   ACCURACY OF MEASUREMENTS.

The accuracy of the velocity measurement will be essentially the same as described for the coherent pulse system in the cooperative mode except the transponder frequency tracker is eliminated.   The net error will be about 0.29 m/sec, 3σ.

The accuracy of the range measurement is tabulated below:

ERROR SOURCE	σ Error Value, meters					
	Fixed random			Fluctuating		
	R<2km	2km <R<20km	R>20km	R<2km	2km<R<20km	R>20km
Slope of frequency modulation	0.005R	0.005R	0.005R			
Quantization	0.38 m	3.8 m	19.0 m			
Doppler compensation	0.3 m	3.0 m	15.0 m	negl.	negl.	44*
Frequency tracking	0.3m	3.0 m	15.0 m	negl.	negl.	44*

* At maximum range.   Decreases with increased SNR.

The parameters in the table are the same as discussed previously for the range accuracy of the pulse doppler radar in the skin track mode.

The combined errors are as follows:

$$R < 2\text{km}, \quad \sqrt{(.005R)^2+(0.57)^2}$$

$$2 < R \lessgtr 20\text{km}, \quad \sqrt{(.005R)^2+(5.7)^2}$$

$$R > 20\text{km}, \quad \sqrt{(.005R)^2+(68)^2}$$

6.5.3.5.   ACCURACY OF ANGLE MEASUREMENTS.

The bias errors will be the same as computed for the skin track mode, or about 0.48 mR for the 0.5 meter antenna and 0.24 mR for the 1.0 meter antenna.

The fluctuating error due to thermal noise is developed in the same manner as for the skin track mode. Based on a 4 dB signal-to-noise ratio the 3σ value of the noise on the angle data is 0.39 mR for the 0.5 meter antenna and 0.17 mR for the 1.0 meter antenna.

Once again we assume the glint on the transponded signal is negligible.

6.5.3.6.   ACCURACY OF ANGLE RATE DATA.

The errors in the angle rate data include a "hang off" error of 0.09 mR/sec and a random error of 0.09 mR/sec, 3σ in the rate gyro as discussed previously.

The noise on the angle rate data due to thermal noise in the receiver is computed in the same manner as for the skin track mode. The result, for a 4 dB signal-to-noise ratio at maximum range, is 3.3 mR/sec, 3σ for the 0.5 meter antenna and 2.0 mR/sec, 3σ for the 1.0 meter antenna.

Once again, these values exceed the 0.14 mR/sec stated allowance and either an increase in transponder transmitted power or an increase in data smoothing time is required to meet the specified values.

6.6 SYSTEM IMPLEMENTATION OF RECOMMENDED RENDEZVOUS RADAR.

6.6.1 RATIONALE FOR SELECTION OF RECOMMENDED RADAR.

A pulse doppler radar with linear FM ranging and frequency agility is recommended for the Rendezvous Radar application. The general form of the radar is described in Section 6.4 of the report. Other types considered were a non-coherent pulse radar and a coherent pulse radar which were analyzed in Sections 6.2 and 6.3.

The rationale for selection of the recommended radar is briefly summarized below:

- The peak transmitter power required is the lowest of the radar types considered.

- The relatively low peak transmitted power required minimizes breakdown problems and it can be provided by the communications TWT transmitter or by a solid state source.

- High velocity accuracy rather than high range accuracy is the driving requirement of the radar. The pulse doppler radar with FM ranging fits well with these requirements. (The pulse doppler radar inherently provides the most accurate velocity measurement of the systems considered.)

- The signal form of both the velocity intelligence and range intelligence is the same (frequency difference) which allows a common, time shared signal processor to be used for both velocity and range measurements.

6.6.2 SUMMARY OF CHARACTERISTICS OF PULSE DOPPLER RENDEZVOUS RADAR.

A summary of performance and system characteristics of the recommended Rendezvous Radar system is given in Table 6.6.1.

Table 6.6-1   PRINCIPAL CHARACTERISTICS OF PULSE DOPPLER
RENDEZVOUS RADAR.

PERFORMANCE CHARACTERISTICS

	Cooperative mode		Skin track mode	
Operating range	560km to 30 m		19km to 30m	
Target model	Transponder		$1m^2$ Swerling 1	
Acquisition time	300 seconds		60 seconds	
Probability of acquisition	0.99		0.99	
False alarm time (During acquisition)	10 minutes		10 minutes	
Angular search sector	5° cone (half angle)		40° cone (half angle)	
Relative velocity	±91 m/sec		-38,+7.5m/sec	
Accuracy, 3σ	Bias	Random	Bias	Random
Velocity, m/sec.	0.2	0.1m/sec	0	$\sqrt{(.03)^2+(.006V)^2}$
Range, meters				
R≤2km	0	$\sqrt{(.005R)^2+(.57)^2}$	0	$\sqrt{(.005R)^2+(.57)^2+(.085V)^2}$
2km<R<20km	0	$\sqrt{(.005R)^2+(5.7)^2}$	0	$\sqrt{(.005R)^2+(5.7)^2+(.85V)^2}$
20km<R<560km	0	$\sqrt{(.005R)^2+(68)^2}$	—	—
Angle, mr	0.24	0.17 R=560km 0.01 R=20km	0.24	0.6
Angle rate, mr/sec	0.09	2.0 R=560km 0.07 R=20km	0.09	8.1*

*Principally due to glint.

S Y S T E M   C H A R A C T E R I S T I C S

	Cooperative Mode	Skin Track Mode
Carrier Frequency	15 GHz	15 GHz
Antenna		
Size	1 meter	1 meter
Beam width (2 way)	1.0 degrees	1.0 degrees
Gain	40.6 dB	40.6 dB
Scan program	Spiral, 10° cone	Spiral, 80° cone
Scan frame time	1 minute	1 minute
Max search rate		110 deg/sec
Max tracking rate	5 deg/sec	5 deg/sec
Transmitter		
PRF	20 to 30 (Dithered)	4.8 for acquisitio 20 to 30 Dithered for track
Pulse width	25 to 17 n sec	
Duty cycle	50%	50%
Peak power	8.9 watts	8.9 watts
Average power	4.5 watts	4.5 watts
Frequency Agility Program		
Acquisition	none	6 frequencies 75 mHz. apart. dwell 1.5 m sec
Tracking	none	6 frequencies 75 mHz. apart. dwell 13 m sec
Frequency Modulation Program		
Deviation		
R< 2 km	20 mHz.	20 mHz.
R> 2 km	2 mHz.	2 mHz.
Time of Linear Sweep		
R< 20 km	13.3 m sec	13.3 m sec
R> 20 km	67 m sec	--
Time of retrace	0.5 m sec	0.5 m sec

	Cooperative Mode	Skin Track Mode
Doppler Scale Factor	100 Hz/m/sec	100 Hz/m/sec
Range Scale Factor		
R< 2 km	10 Hz/m	10 Hz/m
2 km< R< 20 km	1 Hz/m	1 Hz/m
20 km< R< 560 km	0.2 Hz/m	--
Receiver Noise Temperature	1858°k	1858°k
Doppler Filter Bank		
Filter bandwidth	267 Hz	267 Hz
Effective number of filters (FFT implementation)	69	18
Frequency Tracking Filter bandwidth	267 Hz	267 Hz
Data Smoothing Time		
Velocity	2 seconds	2 seconds
Range	2 second	2 second
Angle	2 second	2 second
Angle Rate	2 second	2 second

P H Y S I C A L   C H A R A C T E R I S T I C S

Weight

Antenna Assembly	10.6 kg
Boom Assembly	5.1 kg
Electronics Assembly	4.8 kg
Total Weight	20.5 kg

Size

Antenna Assembly	See Figure 5.5-7
Boom Assembly	See Figure 5.5-7
Electronics Assembly	25 x 17 x 18 cm

Power

Antenna Assembly

. Peak	100 watts
. Average during search	34 watts
. Average during track	13 watts

Boom Assembly	122 watts

Electronics Assembly

. During search	81 watts
. During track	71 watts

Total Power

. Peak	303 watts
. Average during search	237 watts
. Average during track	206 watts

ANTENNA CHARACTERISTICS

Frequency of operation   13.75 to 15.121gHz

Sum Pattern Characteristics (at 15gHz)
    Gain   41.6dB
    Beamwidth, one-way   1.4 degrees
    Minor lobe level below main lobe   17 dB
    VSWR   2:1 max

Difference Pattern Characteristics (at 15gHz)
    Gain   37.5 dB
    Beamwidth, one-way   1.1 degrees
    Minor lobe level below main lobe   15 dB
    VSWR   2:1 max

Transmitted Power Capability   100 watts peak or CW

Antenna Scan Coverage
    Azimuth   360°
    Elevation   320°

Scan Coverage During Acquisition   40° half angle cone

Scan Frame Period   60 seconds

Frequency Response   1 Hz.

6.6.3.   IMPLEMENTATION OF MAJOR ELEMENT OF THE RADAR LOCATED
         ON THE DEPLOYED ASSEMBLY.

A block diagram of that portion of the radar located
on the deployed assembly is given in Figure 6.6.-1.

A dedicated transmitter for the radar function is assumed
in this study. However, the communications TWT transmitter
could be used for the radar as well. The 50 watt transmitter
power level being considered for communications is adequate
for the radar, even using the 0.5 meter minimum size antenna.

Potential disadvantages of a combined transmitter are:

1.   The loss of both communications and rendezvous
capability should the transmitter fail.

2.   The requirement for a high voltage modulator, a
control grid in the tube to cut off the noise generated by
the tube during the radar receive cycle, or a fast action
switch at the transmitter to attenuate the transmitter noise
during the receive cycle.

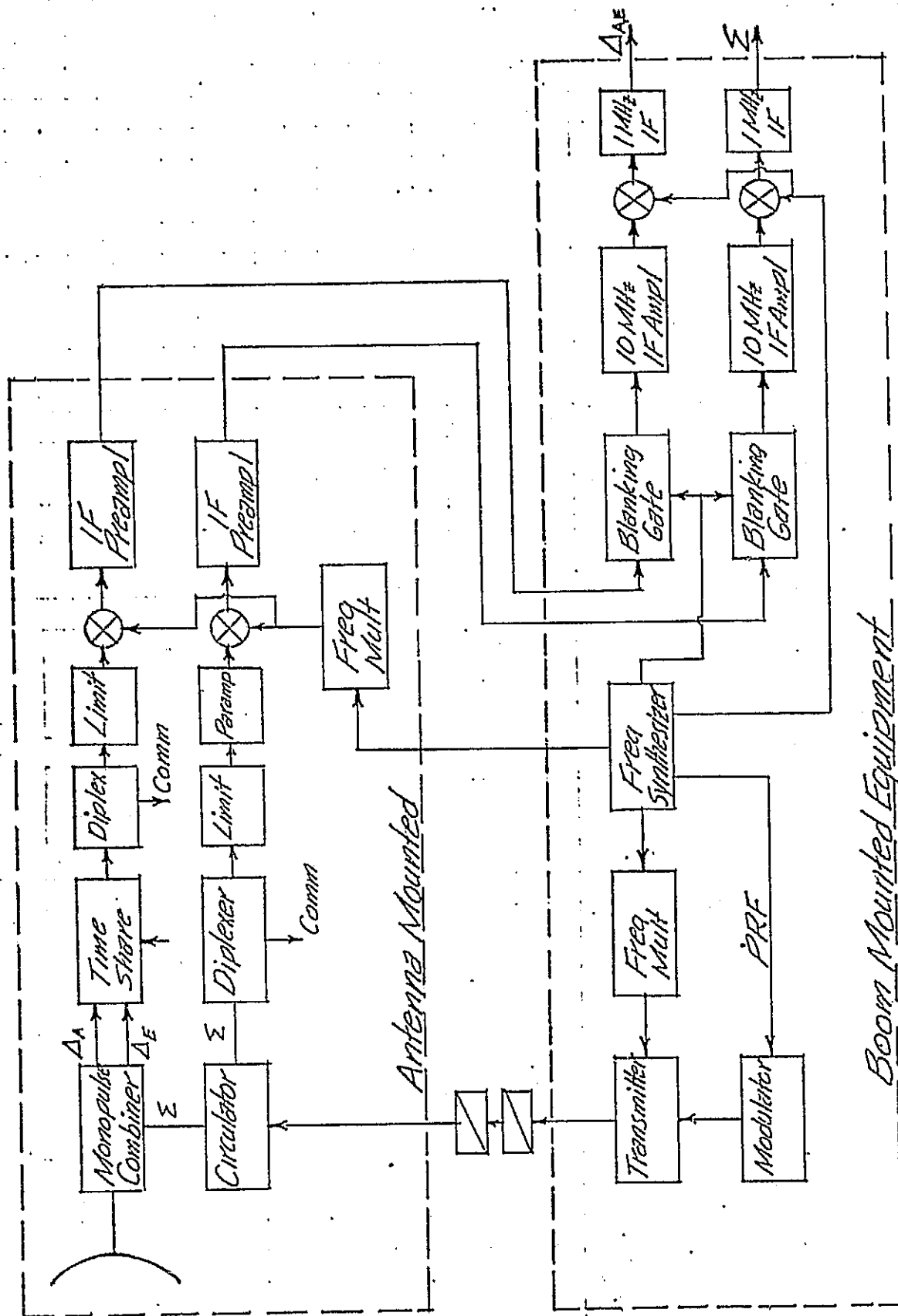The latter would introduce additional loss in the system.

Figure 6.6-1 Functional Block Diagram of Deployed Radar Equipment

6.6.3.1 MICROWAVE LOSSES AND SYSTEM NOISE TEMPERATURE

A tabulation of microwave losses for the transmit and receive paths indicated in Figure 6.6-1 are given below. The losses of major microwave components were taken from supplier catalogs.

Losses in transmit path

Waveguide & bends (1.5 meters)	0.6 db
Rotary joints (2)	0.2 db
Circulator	0.4 db
Monopulse Combiner	0.2 db
Transmitter Switch	0.2 db
	1.6 db

Losses in receive path

Waveguide	0.1 db
Monopulse Combiner	0.2 db
Circulator	0.4 db
Diplexer	0.3 db
Limiter	0.7 db
	1.7 db

The net microwave loss is about 3.3 db. The system noise temperature, Ts, becomes

$$Ts = Ta + Tr + Te$$

Where

Ta = Antenna noise temperature = $2.7^{\circ}k$

Tr = Transmission line noise temperature = $T (L-1)$

T = Physical temperature (assume $290^{\circ}k$)

L = Loss factor = 1.48 (1.7db)

Te = Receiver noise temperature = $To (NF-1)$

To = Reference temperature = $290^{\circ}k$

NF = Receiver noise figure = 5 (7db)

Then, $Ts = 1858^{\circ}k$

The parameters associated with the 1 meter and the 0.5 meter diameter antennas are tabulated below along with the peak transmitted power and average transmitted power required for acquisition using six step frequency agility.

| Antenna Size | Antenna Gain | Filter | Bandwidth | SNR Req'd | Trans. Power | |
		3 db	Noise		Peak	Avg.
0.5 m	34.6 db	100 H	157 H	8.2 db	33.9	17 W
1.0 m	40.6 db	267 H	419 H	8.2 db	5.6	2.8 W

6.6.3.2. TRANSMITTED POWER REQUIRED.

An updated calculation of transmitted power required, based on the implementation of system parameters shown in this section is given in Table 6.6-2. The peak transmitted power required was found to be

$$P_t = 56.1 + 10 \log SNR + 10 \log B_t - 20 \log G \text{ dBw.}$$

Table 6.6.-2.   COMPUTATION OF PEAK TRANSMITTED POWER REQUIRED
FOR OPERATION OF PULSE DOPPLER RADAR.

$$P_t = \frac{SNR(4\pi)^3 R^4 KT_s B_T D_N L_e L_M L_S L_F}{G^2 \lambda^2 \sigma}$$

Symbol	Parameter	Value	Value in dB
SNR	Signal-to-noise ratio	SNR	10 log SNR
$(4\pi)^3$	Constant	1984	33.0
R^4	(Range)^4	$(21.3 \times 10^3)^4$	173.1
K	Boltzmann's constant		-228.6
T_s	System noise temp. natural 1858°		32.7
B_T	Noise bandwidth of doppler filter	B_T	10 log B_T
D_N	Duty ratio of noise gate	0.5	-3.0
L_M	Microwave loss (transmit path)	1.6 dB	1.6
L_S	Scan loss	1.6 dB	1.6
L_e	Eclipsing/conversion loss	9.00dB	9.0
L_F	Filter mismatch loss	0.9 dB	0.9
G^2	(Antenna gain)^2	G^2	-20 log G
λ^2	(wavelength)^2	2×10^{-2}m	34.0
σ	Radar cross section	$1\ m^2$	0

P_t Peak transmitter power   54.3+10logSNR+10log B_T-20 log G.

6.6.3.4. TRANSMITTER IMPLEMENTATION.

Allowing a 2 dB margin for radar system degradation due to environment and aging, the peak transmitted power required is 62 watts for the 0.5 meter antenna and 10 watts for the 1 meter antenna. The average power is half of these values.

These peak and average power levels for the 1 meter antenna case are well within the state-of-the-art of solid state impatt diode transmitters. However, in the case of the 0.5 meter antenna it appears better to use a parametric amplifier in the receiver as discussed later which would reduce the required transmitted power by 5 dB to 19 watts which can be achieved with a solid state transmitter.

The Hewlett Packard 5082-0716 series of impatt diodes can generate about 7 watts of power at 15 gHz. at a pulse width of 10 μsec and 25% duty ratio.[1] The efficiency is about 11%. At a 50% duty ratio and pulse width of 104 μsec, which corresponds to a PRF of about 4.8 kHz. used during acquisition in the skin track mode, a power output in excess of 3 watts peak can be obtained. The efficiency is about 9%.

The desired peak power of 10 watts associated with the 1 meter antenna can be provided by 3 impatt devices operated in parallel. Allowing a loss of 0.2 dB for the power combiner the total output power of the impatt diodes is 10.5 watts. This requires each diode to provide 3.5 watts peak power.

---

1. "Silicon Double-Drift Impatt Diodes for Ulse Applications"; HP Application Note 961.

The transmitter would operate in an injection lock mode. a 400 MH bandwidth can be obtained with an injection lock gain of 10 dB. An imput drive power of about 1.0 watts peak is therefore required for the three injection locked impatt diodes. Allowing a power loss of 0.3 dB for the driver power divider, a total drive power of 1.1 watts peak is required. This drive signal would be provided by another impatt amplifier which in turn would be driven by a 110 milliwatt source. This power level can be readily furnished by a frequency multiplier driven by the frequency synthesizer.

The efficiency of the high level impatt stages will be about 9% and the lower power drive stage will have an efficiency of about 5%. Assuming an efficiency of 80% for the modulator, which consists of a pulsed current generator, the average dc input power required for the 10 watt transmitter is about 88 watts.

The size of the 8.9 watt transmitter and modulator will be about 12x12x10 cm. Its weight will be about 1 kg.

If a parametric amplifier is used in the receiver the transmitted power required for the 1 meter antenna is reduced to 3.2 watts peak. This power level can be obtained by one impatt diode driven by a second impatt diode. The driver impatt amplifier would provide about 0.3 watts peak power with an imput signal level of 30 milliwatts. The total dc input power would be about 29 watts. The size of the 3.2 watt transmitter and modulator would be about 6x12x10 cm. Its weight would be about 0.5 kg.

The estimated dc power, sizes and weight of the 19 watt peak power transmitter required with the 0.5 meter antenna and a parametric amplifier preamplifier is 190 watts, 16x12x10 cm and 1.5 kg respectively.

Since greater peak power and efficiency can be obtained from the impatt diodes when operated at 25% duty ratio, an investigation was made to determine the difference in peak power required if the system were operated at a 25% duty ratio rather than at 50%. Operation at 50% duty ratio had previously been found to be the most efficient usage of average transmitted power.

It was found, considering both eclipsing loss and receiver noise grating, that the net increase in peak power required to obtain the same performance at a 25% duty ratio as at 50% duty ratio is about a factor of 3. Therefore, operating at the 50% duty ratio is more favorable.

6.6.3.5. RECEIVER IMPLEMENTATION.

6.6.3.5.1. MONOPULSE CONFIGURATION.

Consideration was given to using a three channel monopulse receiver, $(\Sigma, \Delta_a, \Delta_e)$, a two channel receiver with one time shared difference channel $(\Sigma, \Delta_{a,e})$, and a single channel receiver where the difference channels are time shared and alternately added and subtracted from the sum channel $(\Sigma \pm \Delta_{a,e})$.

The single channel approach results in additional loss in the sum receiver channel of at least 1 dB and consequently it is not attractive for this application.

The feasibility of multiplexing the two difference channels to minimize hardware was considered. Phase multiplexing is not attractive for this application due to potential cross coupling between channels due to the finite isolation obtainable. Time division multiplexing appears feasible with the relatively low tracking rates encountered. The JSC defined requirements for the purpose of this study specify a maximum tracking rate of 5°/sec. Examination of the Mission 3-B rendezvous trajectory indicates a maximum line of sight rates of about 0.2°/sec at ranges greater than 1 km.

It appears reasonable then to time share the difference channels, keeping the time share rate at least an order of magnitude above the frequency response of the antenna positioning system. The time sharing would be accomplished by a solid state microwave switch which alternately applies the Δ_{EL} or the Δ_A signal to the receiver.

6.6.3.5.2. USE OF AN RF PREAMPLIFIER IN THE SUM CHANNEL.

Consideration was given to using a tunnel diode or a parametric pre-amplifier in the sum channel in the receiver to lower the receiver noise temperature. Neither pre-amplifier can operate effectively at the maximum return signal in excess of 0 dBm which is possible at the minimum range of 30 meters. An attenuator would be switched into the receive line at a range of about 0.3 km to limit the maximum power to about -30 dBm.

The noise figure obtainable from a tunnel diode amplifier at 156 Hz. is about 6 dB. This is close to that obtainable with a good quality diode mixer and no significant benefit is obtained.

Parametric amplifiers can provide noise figures better than 2 dB which is an improvement of 5 dB relative to a diode mixer. It does not appear desirable to use the communications parametric amplifier for the radar function because (1) it must be tuned from 13.8 gHz. to the radar frequency of about 15 gHz. and (2) the diplexer also must be tuned or switched.

If the communications transmitter is used for the radar, the signal-to-noise ratios will be adequate without a parametric amplifier, even for the minimum size 0.5 meter antenna.

In the case of the 1 meter diameter antenna the transmitter power requirement can readily be achieved with a solid state transmitter and the extra complexity of a parametric amplifier is not required. In the case of the 0.5 meter antenna the trade-off favor the use of a parametric amplifier rather than the larger transmitter.if a separate transmitter is used for the radar.

6.6.3.5.3. MIXERS.

Using a balanced Schottley diode type mixer such as the Hewlett Packard No. 5082-2724, and allowing 0.5 dB for mismatch and resistive loss of the diode holder, a mixer noise figure of 7 dB can be realized over a wide temperature range.

6.6.3.5.4. IF AMPLIFIERS.

A total gain of about 154 dB is required at intermediate frequency to raise a signal at zero dB SNR in 100 Hz. bandwidth referred to the mixer input to a level of 1 volt for the signal processing circuits. The total dynamic range in the skin track mode is the sum of the range variation (22km to 30 m) which causes a 115 dB change in signal level, and a radar cross section change from 1 m^2 to perhaps 100 m^2 which adds another 20 dB to the dynamic range. The total dynamic range required for the cooperative mode considering a range variation from 560 km to 0.03 km is 85 dB.

To avoid overloading the receiver, a 30 dB attenuator would be switched in the receive lines in front of the mixers at a range of about 300 meters to limit the maximum signal to about -20 dBm at the minimum range of 30 meters.

An IF pre-amplifier mounted on the back of the antenna along with the mixer provides about 30 dB gain. Its output remains linear over the 105 dB dynamic range of the signal at that point. The amplified 10 mHz. IF signal is fed over a transmission line to the 10 mHz. IF amplifier located on the boom.

The 10 mHz. IF amplifier has about 80 dB gain and 65 dB AGC range. The signal is down converted to 1 mHz. and further amplified by 44 dB. The 1 mHz. IF amplifier has an

AGC range of about 40 dB.

The gain and phase match of the two receiver channels to the output of the 1 mHz. amplifier will be within 1.5 dB and 10° respectively.

6.6.3.5.5. LOCAL OSCILLATOR.

The mixer diodes require a microwave local oscillator signal level of 1 milliwatt for best noise figure. The two balanced mixers require a total of 4 milliwatts which must be coherent with the transmitted signal. The local oscillator signal is generated by a frequency multiplier which accepts a signal near 100 mHz. from the frequency synthesizer and multiplies it to the LO frequency near 15 gHz.

6.6.3.6. PHYSICAL CHARACTERISTICS OF DEPLOYED EQUIPMENT.

A summary of weight and power requirements for the elements of the radar located on the antenna and on the boom is given in Table 6.6.-3. The use of a 1 meter diameter antenna was assumed in sizing the transmitter.

A summary of overall weight and power required by the deployed portion of the radar is given in Table 6.6.-4.

TABLE 6.6-3   PHYSICAL CHARACTERISTICS OF MAJOR ELEMENTS
OF DEPLOYED PORTION OF RENDEZVOUS RADAR

	Weight, kg	Power, watts
Elements Mounted on Antenna		
Monopulse Combiner	0.2	0
Circulator	0.15	0
Limiter	0.1	0
Switch (SPDT)	0.1	0.1
Balanced Mixers (2)	0.2	0
IF Preamplifiers (2)	0.1	0.4
Frequency Multiplier	0.15	5
Mounting Structure & Cover	0.5	--
Cabling & Connectors	0.2	--
	1.5	5.5
Elements on Boom		
Transmitter/Modulator	1.0	88
Freq. Multiplier	0.5	30
Freq. Synthesizer	0.2	1
10 MH 1F Ampl (Dual)	0.2	2
1 MH 1F Ampl (Dual)	0.1	1
Structure (Part of boom)	--	
Cabling & Connectors	0.2	--
	2.2	122

TABLE 6.6-4 PHYSICAL CHARACTERISTICS OF DEPLOYED EQUIPMENT.

Element	Weight, kg	Power, watts
Electronics & microwave on antenna	1.5	5.5
Electronics on boom	2.2	122
Antenna and feed	1.6	
Antenna gimbals including elevation and azimuth motors, rotary joints, waveguide and synchros	6.6	100 peak, 34 average during search
Boom structure	3.1	
Rate gyros (2)	0.91	6

### 6.6.4. IMPLEMENTATION OF MAJOR ELEMENTS OF ELECTRONICS ASSEMBLY.

A block diagram of the electronics assembly is given in Figure 6.6.-2. A detail description of the signal processing is given in Section 6.4.

6.6.4.1. VELOCITY AND RANGE MEASUREMENT.

The sum IF signal, at a frequency of about 1 mHz. plus doppler and ranging frequency, is applied to two mixers excited in quadrature from a 1 mHz. reference frequency. The I and Q outputs of the mixer are amplified and limited and applied to the frequency tracker and to a fast Fourier transform processor which functions as a filter bank. The digitizer for the FFT processor samples the hard limited doppler, or doppler plus range signal at rate twice the maximum signal frequency and provides an I and Q set of digital words to the FFT processor.

The FET processor is mechanized in software within a small micro-computer to function essentially as a bank of contiguous filters with 3 dB bandwidths of either 100 or 267 Hz. corresponding to the use of the 0.5 meter diameter antenna or the 1.0 meter antenna respectively. The presence of the signal is detected by the FFT processor which generates a "signal detected" signal which stops the antenna search program.

The antenna would be allowed to coast past the target where the search program is terminated. However, the antenna location at the instant of signal detection is placed into memory and the antenna is driven back to that location.

Figure 6.6-2 Block Diagram of Electronics Assembly
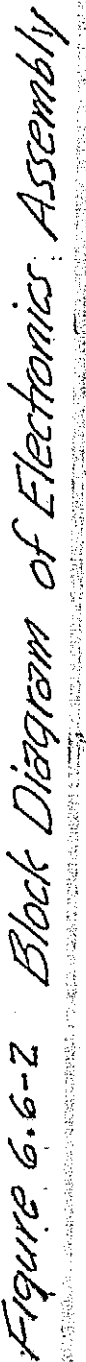
The frequency tracker is slewed to the signal frequency by a digital command from the FFT processor. After initialization of the velocity, range and angle measurements as described in Section 6.4, the tracker alternately tracks the doppler and the doppler plus range signal. Digital words representing these two quantities are applied to the data converter which is mechanized in software within the microcomputer. The computed range and velocity information is applied to a data formatting function within the microcomputer which provides target range, velocity, azimuth angle and angle rate, and elevation angle and angle rate in a format compatible with the space shuttle data systems.

6.6.4.2 ANGLE TRACKING

The 1 MH_z sum and difference signals are mixed with a sig-
nal from the frequency tracker which is maintained 5 KHz above
the doppler or doppler plus range frequency. The signal frequency
applied to the angle track circuits is then constant at 5 kHz.
The difference channel is demultiplexed and both the sum and dif-
ference signals are filtered by band pass filters centered at 5 KH
with a bandwidth of about 500 Hz . The filters are made about twice
the bandwidth of the doppler tracking filter to minimize phase shift.

The filter outputs are applied to phase sensitive detectors
which yield a dc output related to the angular displacement of
the target from the monopulse axis. The detector outputs are
filtered and applied as an error signal to the servo amplifiers
which drive the antenna positioner.

The antenna search program is generated in the microcomputer,
converted to an analog voltage by the digital to analog converters
and is applied to the servo amplifiers during the search mode.

6.6.4.3 PHYSICAL CHARACTERISTICS OF ELECTRONICS ASSEMBLY

A summary of estimated weight and power for the subassemblies and structure of the electronics assembly is given in table 6.6-5. The power supply is sized to provide power for the 10 watt peak power solid state transmitter.

The size of the electronics assembly is estimated at about 7500 cubic centimeters (25.4 x 16.6 x 17.8 cm). The weight is about 4.8 kg (10.6 pounds) and the power dissipated within the assembly is about 81 watts.

The total amount of regulated power required is about 20.7 watts for the electronics assembly and 119.5 watts for the deployed assembly for a total of 140.2 watts. An efficiency of 70% was assumed for the power supply which results in a power dissipation within the supply of 60 watts.

TABLE 6.6.5   PHYSICAL CHARACTERISTICS OF THE ELECTRONICS
               ASSEMBLY

Subassembly	Weight, kg	Power, watts
Angle Track	0.14	0.3
Servo Amplifiers (during search)	0.18	10
Synthesizer	0.14	1.0
Mixer Limiter & Digitizer	0.14	0.3
Frequency Tracker	0.28	0.3
Microcomputer	0.28	8
Synchro/Digital Converter	0.14	0.3
Buffer and Interface	0.14	0.5
Power Supply	2.27	60
Chassis & Interconnect	1.10	0
	4.81 kg	80.7